Quantum Chemical Simulations of Radical Cation Chemistry

Thesis submitted for the Degree of
Doctor of Philosophy
Department of Chemistry
September 2019

Jacqueline Tan Si Jia

Trinity College
University of Oxford

Contents

Abstract

The Diels-Alder (DA) reaction is among the most important and versatile methods in creating ring molecules, and factors governing stereoselectivity and rate have been widely studied. However, the chemoselectivity in products are often restricted, as electronic natures of the reactants (typically electron-rich diene and electron-poor dienophile) have to be matched.

On the other hand, in radical chemistry, the removal of a free election helps promote an entirely different chemical environment within the reactants. This has been experimentally shown to be imperative in forming a different set of products not predicted in neutral DA reactions using photochemistry or redox chemistry. Chapter 1 will encompass an overview of such reactions and also the different computational techniques applied in understanding this chemistry.

Using an emerging technique known as quasi-classical dynamics (QCD), coupled with Density Functional Theory (DFT), this thesis investigated the radical cation DA reaction of a small sample system (Chapter 2) to provide quantitative understanding to this observed phenomena, and discovered the existence of reactive intermediates that could not be predicted with Transition State Theory (TST). As these intermediates have exceptionally long lifetimes, they also describe the dynamical nature of forming different products via the same transition state, which provides a strong contrast against concerted reactions (Figure A.1). This has never been applied to the

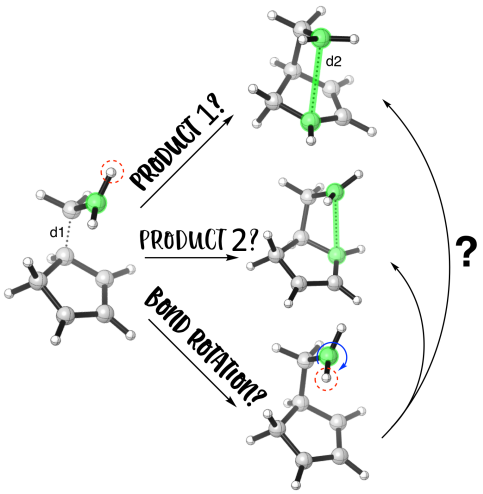

Figure A.1. Different products formed from the same 'dynamic intermediate'

study of radical cycloadditions before. In Chapter 3, the same techniques were applied to a larger DA system to predict product stereoselectivity, and kinetics rate theory provided evidence of reversibility from the neutral products.

The different chemical environment promoted from the removal of a single electron is revisited in Chapter 4 in the field of atropisomerism. In the radical cation systems chosen, we observed an unprecedented lowering of the energy barriers towards racemization. This effect also created a two-step mechanism, which was subsequently explained using Frontier Molecular Orbital (FMO) theory, and could allow better methods in isolating atropisomers.

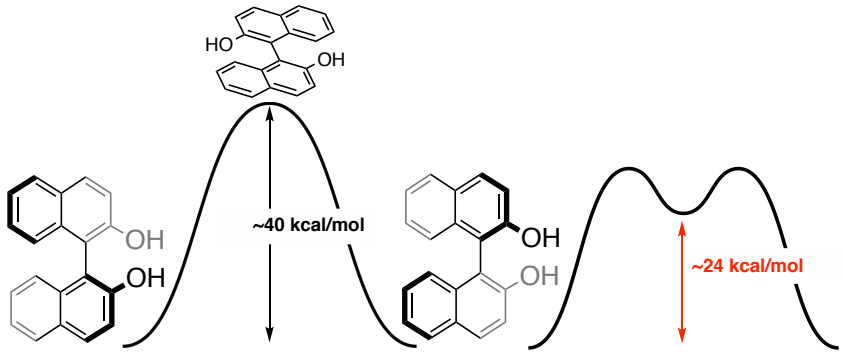

Figure A.2. Neutral atropisomerism versus radical cation atropisomerism

Once again, and lastly in Chapter 5, the aforementioned computational techniques (DFT and QCD) are utilized in understanding different reaction pathways in non-heme enzymes, this time with the addition of hybrid quantum mechanics/molecular mechanics (QM:MM). The selectivity between the radical rebound (RR) pathway and the desaturation pathway was revealed and these different pathways were observed under different timescales, which would facilitate better catalytic design that enables controlled selectivity.

Acknowledgements

I thank firstly, my main supervisor Prof. Robert Paton for being very helpful and understanding through the trials I've faced to get to this stage. He had endured my bad temper, my incessant tears, and also my constant badgering to writing and checking papers. Similarly to my other mentors Prof. John McGrady and Prof. Fernanda Duarte, for believing in me and allowing me to work remotely, a decision that really improved my mental and emotional state.

Despite the difficulties, my colleagues and friends at Oxford remained a constant joy by my side. I thank the dear friends I've made in Trinity College and at St. Ebbe's Church; for hammering in happy thoughts for me whenever I am moping around. I especially thank Kiran, Nod, Xing, and Alex for constantly reaching out and keeping me sane. My friendly lab neighbour Kiran was almost always my greatest comfort and I'm so happy and excited for her bright future.

It goes without saying that to be able to reach this stage of my life, the key people to thank are my family and my husband SJ. My family endured all the difficulties I threw at them, and I thank my brother and especially my sister for accepting me for who I am when I am at my ugliest. My parents showered me with love tirelessly and I know I have depleted their energies so much that I worry about them aging too quickly. I thank my husband for loving me back, and who have also imparted me the wonderful gift of forgiveness. Thank you for accepting all my flaws and returning all my frustration in love.

Last but not least, I thank God for bringing me through all these; both figuratively and literally. Thank You for giving me a wonderful family, for placing my husband in

my life, for pulling me through Oxford, for all the friends I've made, and for all the papers I've published. I truly truly would not have been able to accomplish all these without You.

Glossary

Å	angstrom(s), 10^{-10} m
aug	augmented
BINAM	1,1′-binaphthyl-2,2′-diamine
BINOL	1,1′-bi-2-naphthol
BM	BerkeleyMadonna
BOMD	Born-Oppenheimer Molecular Dynamics
cGTO	contracted Gaussian-type Orbital
CC	Coupled-Cluster
CCSD	Coupled-Cluster Single Double
CCSD(T)	Coupled-Cluster Single Double and Triple
Cp	Cyclopentadiene
CP	Car-Parinello
DA	Diels-Alder
DCM	Dichloromethane, CH_2Cl_2
DFT	Density Functional Theory
DLPNO	Domain-based Local Pair Natural Orbital
ECP	Effective Core Potential
EDG	Electron-donating group
EE	Electronic Embedding
ESR	Electron Spin Resonance
EWG	Electron-withdrawing group
FCI	Full Configuration Interaction
FMO	Frontier Molecular Orbital
GGA	Generalized Gradient Approximation
GTO	Gaussian-type Orbital
GS	Ground State
HF	Hartree-Fock
HK	Hohenberg-Kohn

HOMO	Highest Occupied Molecular Orbital
IRC	Intrinsic Reaction Coordinate
KS	Kohn-Sham
LCAO	Linear Combination of Atomic Orbitals
LDA	Local Density Approximation
LSDA	Local Spin Density Approximation
LUMO	Lowest Unoccupied Molecular Orbital
LYP	Lee-Yang-Parr
MD	Molecular Dynamics
MM	Molecular Mechanics
MO	Molecular Orbital
MP	Møller Plesset
ONIOM	Our own N-layered Integrated molecular Orbital and molecular Mechanics
PCM	Polarizable Continuum Model
PES	Potential Energy Surface
QCD	Quasi-classical Dynamics
QCI	Quadratic Configuration Interaction
QM	Quantum Mechanics
rt	room temperature
RMSD	Root Mean Square Deviation
RR	Radical Rebound
RRHO	Rigid Rotor Harmonic Oscillator
RS	Rayleigh-Schrödinger
SCF	Self-consistent Field
SCRF	Self-consistent Reaction Field
SD	Slater Determinant
SET	Single Electron Transfer
SMD	Solvent Model Based on Density
STO	Slater-type Orbital

TS	Transition State
TSS	Transition State Structure
TST	Transition State Theory
UFF	Universal Force Field
VRI	Valley-Ridge Inflection

Author's declaration

This thesis is an account of the work carried out by the author in the Department of Chemistry, University of Oxford, under the supervision of Professor Robert S. Paton. No part of this thesis has previously been submitted for a degree in this University or elsewhere. The work of other authors has been duly acknowledged in the text. A list of references is also given at the end of each chapter.

Publications and Awards

Publications describing work from this thesis

[1] Tan, J. S. J.; Hirvonen, V.; Paton, R. S. ***ACS Org. Lett.*** 20, 2821–2825 (2018). 'Dynamic Intermediates in the Radical Cation Diels-Alder Cycloaddition: Lifetime and Suprafacial Stereoselectivity'

[2] Tan, J. S. J. & Paton, R. S., ***Chem. Sci***. 10, 2285–2289 (2019). 'Frontier molecular orbital effects control the hole-catalyzed racemization of atropisomeric biaryls.'

[3] Fugard, A. J., Lahdenperä, A. S. K., Tan, J. S. J, Mekareeya, A., Paton, R. S., Smith, M. D., ***Angew. Chemie Int. Ed.*** 58, 2795–2798 (2019). 'Hydrogen-Bond-Enabled Dynamic Kinetic Resolution of Axially Chiral Amides Mediated by a Chiral Counterion.'

Awards

2018: Won a "Computers in Chemistry" Poster Award sponsored by Wiley at the 16th International Congress of Quantum Chemistry June 2018 held in Menton, France

2018: Won a Poster Award at the OxFEST Annual Conference 2018 - STEMpower Her: Together We Rise!

2017: Oxford Trinity College Graduate Prize for Distinction-level work in **1st year** Graduate study

Chapter 1: Overview of thesis

1.1 Introduction to Diels-Alder (DA)

The DA reaction allows the stereoselective formation of many cyclic molecules. Efficient thermal DA [4 + 2] cycloadditions typically require diene (4π electrons) and dienophile (2π electrons) components to be electronically matched. Conventionally, this would mean an electron-rich diene and an electron-poor dienophile. In contrast, radical cation DA reactions are not subject to the same convention due to higher levels of reactivity. In the following subsections, we will explore the importance of understanding such chemistry via various computational methods.

1.1.1 Normal and Inverse Demand DA Reactions

In a classic DA reaction, a conjugated diene and a dienophile react in a concerted approach. Otto Diels and Kurt Alder first described this reaction in 1928, in which the Nobel Prize in Chemistry was awarded to them in 1950[1]. This reactivity can be visualized using frontier molecular orbital (FMO) analysis to rationalize its productivity.

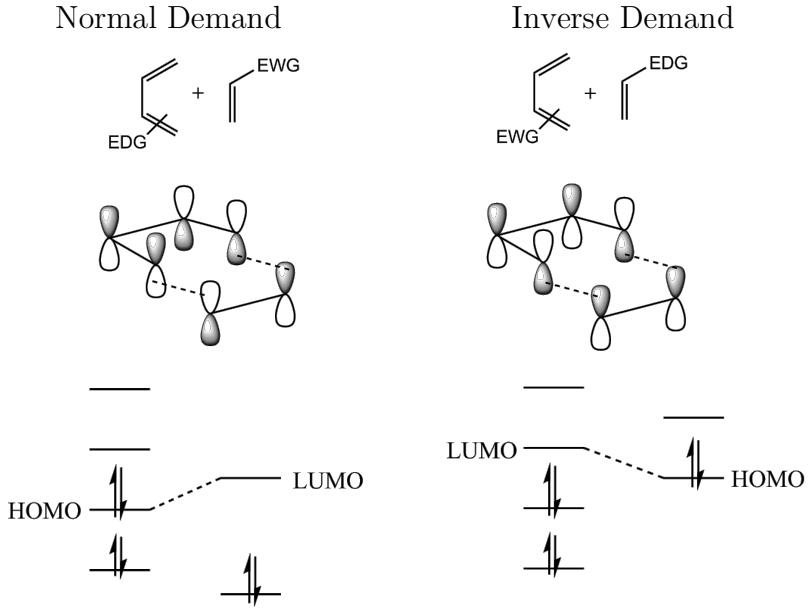

Figure 1.1. FMO analysis of neutral DA reaction

In a normal demand Diels-Alder reaction, the diene will be electron-rich due to the presence of electron-donating groups (EDGs) whilst the dienophile will be electron-poor due to electron-withdrawing groups (EWGs). This places the highest occupied molecular orbital (HOMO) of the diene at a higher energy level and the lowest occupied molecular orbital (LUMO) of the dienophile at a lower energy level, allowing the energy gap between these two orbitals to be small enough for overlap (**Figure 1.1**), thus decreasing the reaction temperature and time. Strategies to improve the reactivity of this reaction has been extensively explored by minimizing the energy gap between the HOMO and the LUMO[2] i.e. increasing the electron density in the diene or decreasing that of the dienophile.

Diene	Dienophile	Adduct	T_{DA} (°C)
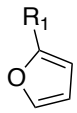	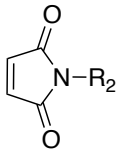	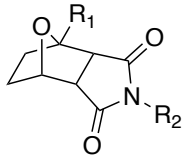	50 - 80
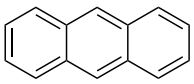	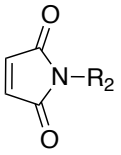	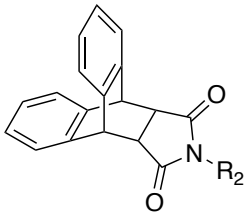	125
		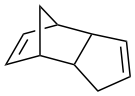	25 - 120
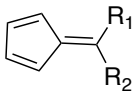	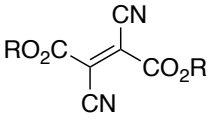	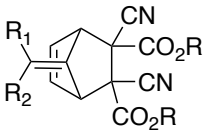	r.t.

Table 1.1. Examples of commonly used DA pairs and their reaction temperatures

Certain commonly used DA pairs like furan derivatives[3] (diene) and maleimide derivatives[4] (dienophile) were mainly studied as they could be carried out at low or

room temperatures. For example, Van Benthem and co-workers characterized a possible DA reaction between furan and maleimide in chloroform at 55°C in 48 h using ^{1}H-NMR.[5] However, by modifying the substituents on the diene and dienophile, the DA reactivity was tweaked and the reaction temperature dropped to 25°C.[6]

By screening the dienes, two additional families are added to the list of commonly used reactants: cyclopentadiene and anthracene (**Table 1.1**). In fact, for some of these examples, the diene and dienophile pairs are able to spontaneously form DA adducts at room temperature. For example, in cyclopentadiene-based adducts, a dynamic equilibrium could be observed at room temperature involving cyanofumarate derivatives.[7]

Conversely, in the inverse demand Diels-Alder reaction shown in **Figure 1.1**, the reaction occurs between an electron-poor diene and an electron-rich dienophile: the overlap now occurs between the LUMO of the diene and the HOMO of the dienophile.

The realisation that conjugated diene systems containing nitrogen are electron-poor steered towards the investigation of the inverse demand DA reaction. In the preparation of six-membered heterocyclic ring systems, its utility was demonstrated. Carboni and Lindsey first discovered the synthesis of pyridazines through the reaction of 1,2,4,5-tetrazines with dienophiles.[8] Electron-deficient heterocyclic azadienes like 1,2,4,5-tetrazines are widely employed in [4 + 2] cycloadditions,[9] acting as the 4π electron component, due to its synthetic accessibility, broad synthetic applications, and remarkable reactivity.[10]

In general, this type of inverse demand DA reactions proceed via three steps (**Figure 1.2**): (1) a [4 + 2] cycloaddition reaction; (2) a retro [4 + 2] cycloaddition with loss of

nitrogen to give a dihydro-1,2-diazine intermediate; and (3) aromatization of the resulting intermediate by elimination of an amine, alcohol, or thiol.

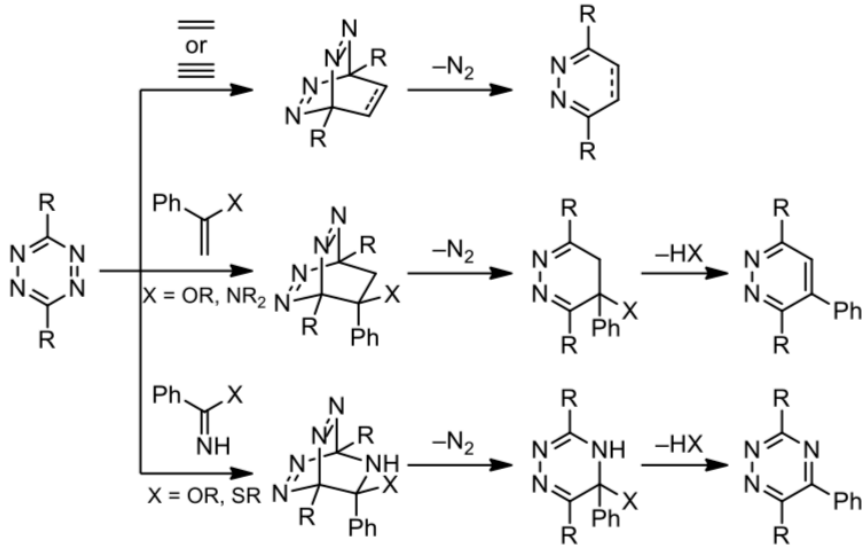

Figure 1.2. Inverse demand DA reactions of 1,2,4,5- tetrazines with dienophiles.

In both DA reaction types, the reactants have to be electronically matched. Many research groups took advantage of this intrinsic quality of the DA reaction and over the years, added substituents to the reactants for catalytic coordination to influence reactivity rate[11–13]. However, this electronic prerequisite also denotes this transformation's greatest limitation.

1.1.2 Radical Cation DA Reactions

The radical cation DA reaction creates a new pathway for reactants without the electronic prerequisite, and research groups began to explore this transformation with much success in the 1980s.

Photochemistry and redox chemistry are the experimental means primarily used to generate these radical cations. Light has always been known for its potential to catalyse chemical reactions via photocatalysis. Catalysts that are photoexcited can generate radical ion species from neutral starting materials through oxidative and

reductive single electron transfer (SET), and these species can in turn act as reactive intermediates for further synthesis.

In fact, the first report known to us came from Nathan Bauld's group in 1981, where they performed the dimerization of cyclohexadiene with the radical cation catalyst tris(p-bromophenyl)aminium hexachlorostibnate, for 15 minutes at 0 °C, giving rise to 70% yield (**Figure 1.2**)[14].

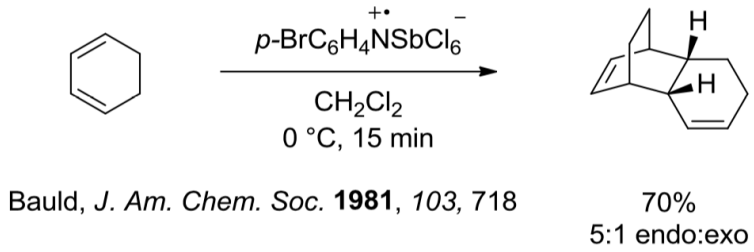

Figure 1.2. First report of radical cation DA by Bauld in 1981

This discovery is significant as under uncatalyzed circumstances, the thermal [4+2] cycloaddition of cyclohexadiene only gave 30% yield after a 20 h reaction at 200 °C. The report also mentioned that the endo product is favoured for the [4+2] cross-cycloaddition of cyclohexadiene and 2,4-dimethylhexadiene.

$$\mathbf{DP} + Ar_3N^{+\bullet} \rightleftharpoons Ar_3N^{\bullet\bullet} + \mathbf{DP}^{+\bullet} \qquad \text{[Initiation]}$$
$$\mathbf{DP}^{+\bullet} + \mathbf{D} \longrightarrow \mathbf{A}^{+\bullet}$$
$$\mathbf{A}^{+\bullet} + \mathbf{DP} \longrightarrow \mathbf{A} + \mathbf{DP}^{+\bullet} \qquad \text{[Propagation]}$$

DP = Dienophile, **A** = Cycloadduct, **D** = Diene

Figure 1.3. Proposed mechanism by Bauld group

They demonstrated a mechanism that starts by oxidising the dienophile with the radical cation catalyst to produce a radical cation intermediate. This intermediate then reacts with the diene to form a cyclic cation radical intermediate that is subsequently reduced to give the desired cyclohexene (**Figure 1.3**). Bauld group explored the reason for the dienophile being oxidised rather than the diene and using FMO theory, showed

that the [3 + 2] reaction between a radical cation diene with a neutral dienophile is symmetry forbidden[15].

Since the early works by Yoon,[16] MacMillan,[17] and Stephenson,[18] the usage of transition metal complexes in photocatalytic reactions has become fundamental in new reaction development for the field of synthetic organic chemistry.[19] From the work pioneered by Honda,[20] semiconductors have been studied as potential photocatalysts to induce SET at surfaces. Upon irradiation, the electron pair generated can act as both oxidant and reductant, even in the absence of sacrificial reagents that are generally needed to provide electrons/holes to facilitate homogeneous photocatalysts.[21]

An example of a semiconductor photocatalyst used for radical cation DA reactions is titanium dioxide (TiO_2), as described by Okada and co-workers[22] in **Figure 1.4**.

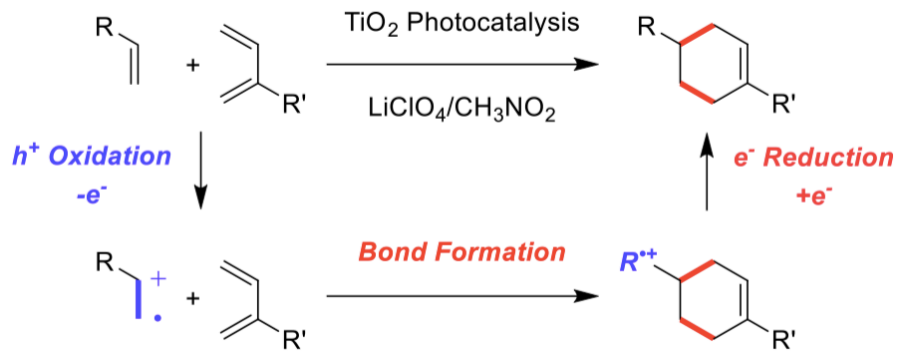

Figure 1.4. Radical cation DA cycloaddition by TiO_2 photocatalysis

In this figure, the reactions are believed to be first activated by hole oxidation of electron-rich alkenes, thereby generating highly reactive radical cation species, which are in turn trapped by unactivated alkene nucleophiles for subsequent bond formation. After bond formation, the excited electrons then reduce the resulting radical cation intermediates to complete the net redox-neutral reactions, producing the [4 + 2] cycloadducts.

Since then, many experimental and computational work had been done to investigate and understand the mechanistic details of the radical cation DA reaction[23–25]. A notable example by the Wiest group[26] closely examined three possible mechanisms of the radical cation DA system of 1,3-butadiene and ethylene using density functional theory (DFT) and quadratic configuration interaction (QCI) methods. It is predicted that the transition states (TSes) and intermediates of the neutral and the radical cationic pathway should be related to each other, with experimental support for this coming from finding the cyclohexane-1,4-diyl radical cation intermediate by electron spin resonance (ESR) after oxidation of 1,5 hexadiene[27]. An interesting feature that the radical cation DA reaction shares with many biradical reactions is the unusually flat potential energy surface (PES)[28–30]. It is therefore expected that analogous to biradical type reactions, the reaction outcome is dependent on dynamic effects in some cases.

1.1.3 Occurrence of dynamic effects

In fact, Carpenter's group first published a set of reports regarding trajectory calculations over PESes and their implications on the stereochemistry of biradical type reactions[29–31]. He proposed an alternative computational method using molecular dynamics (MD) and presented the idea of dynamic matching: where after crossing a TS, the momentum of atoms directs the selectivity from a shallow intermediate. He compared the kinetic model of transition state theory (TST) against this nonstatistical dynamic model for the cyclopropane stereomutation and concluded that predictions from TST alone cannot explain experimental findings[32,33]. With this, he also challenged the framework of concerted and stepwise mechanisms by explaining that instead of suggesting two different mechanisms occurring on two different parts of the PES, there

could be two different dynamic populations occupying the same space of the PES. In fact, for some symmetrical reactants, the trajectories do indicate unequal bond forming even though the time between formation of two bonds is shorter than a C−C vibrational frequency[34].

Building upon this, Singleton[35] described a combined experimental and computational study of hetero DA reaction of acrolein and methyl vinyl ketone via quasiclassical direct dynamics trajectories (**Figure 1.4**)[36–38]. They found that the results not only accurately predict the experimental ratio, but that non-statistical recrossing plays a substantial role.

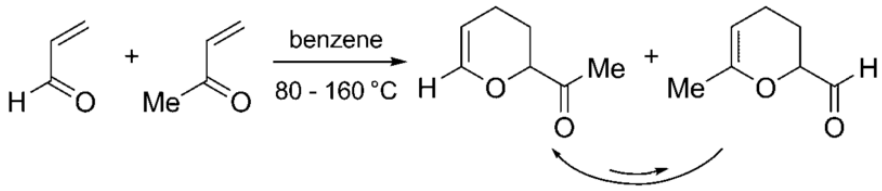

Singleton, D. A., **2009**, *Angew Chem Int Ed, 48*, 9156

Figure 1.4 Hetero DA reaction of acrolein and methyl vinyl ketone by Singleton

In 2000, Bauld and Gao studied the mechanism of the reaction between Cp to *cis*- and *trans*-anethole respectively[39]. They concluded that the dienophile was going through a stepwise mechanism when all four diastereomeric products were found in comparable amounts in the reaction mixture from *cis*-anethole and Cp. Nonetheless, no *cis*-products are found from the reaction of *trans*-anethole and Cp. They also asserted that an intermediate formed during the stepwise mechanism could undergo bond rotation at a comparable rate to cyclization.

In fact, the *cis*- product does isomerize to alleviate unfavorable eclipsing interactions between methyl and p-OMe phenyl groups (**Figure 1.5**). However, this raises

questions regarding the stability of the intermediate formed, and therefore more analysis in dynamics could be done to understand this product selectivity.

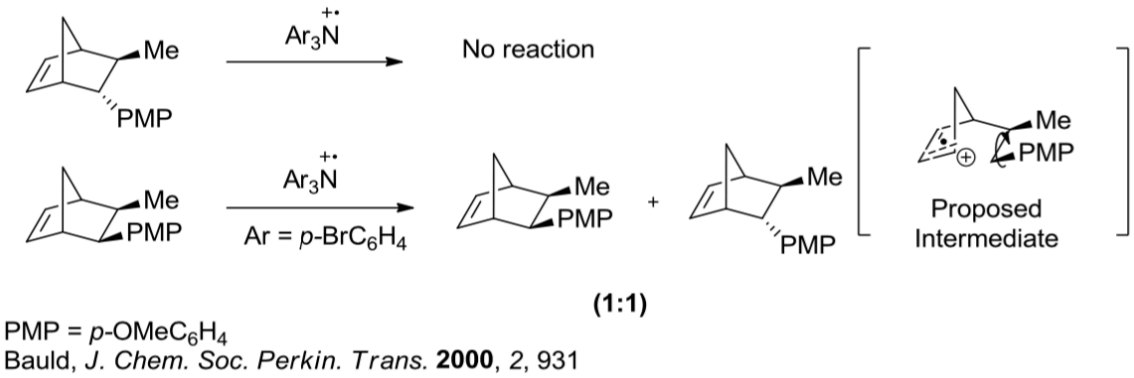

Figure 1.5 Radical cation DA between cis and trans-anethole with Cp

More recently in 2011, the radical cation DA reaction was done using a ruthenium polypyridyl photocatalyst by the Yoon lab (**Figure 1.6**)[40]. The desired cycloadducts were obtained in excellent yields with low loadings of $Ru(bpz)_3(BArF)_2$ photo-activated in air.

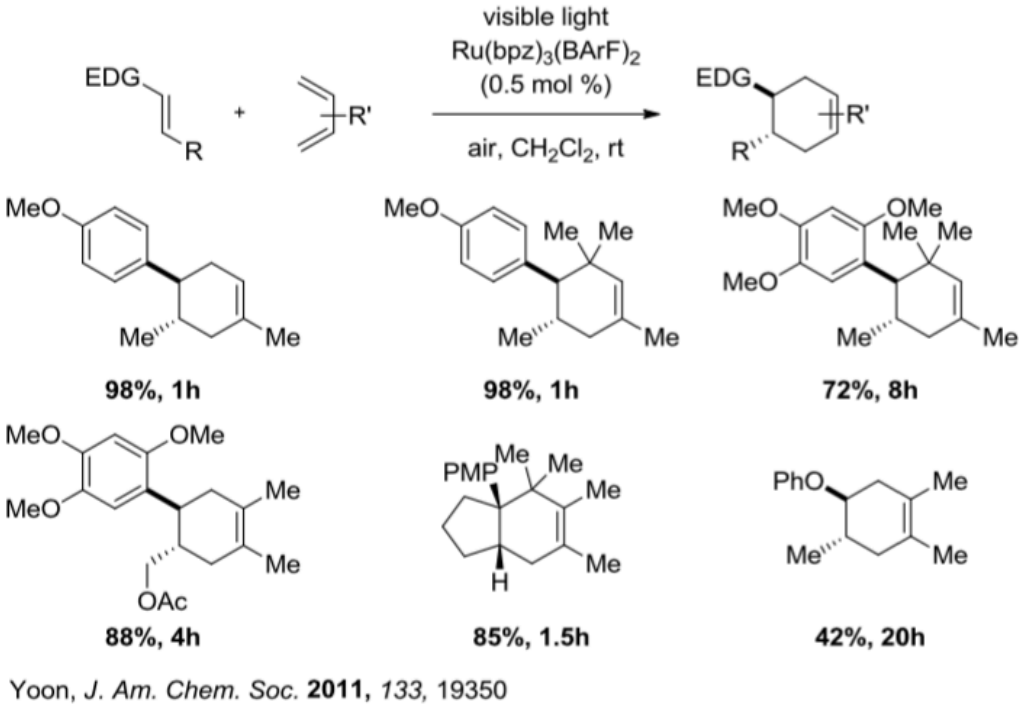

Figure 1.6 Photocatalytic radical cation DA reactions by $Ru(bpz)_3(BArF)_2$

Interestingly, this radical cation DA process reversed the overall regiochemical preference formed by the products of the neutral cycloaddition, which would not have proceeded under normal circumstances due to the use of two electron-rich reactants, i.e. the minor product in the neutral DA reaction is now the major product in the radical cation DA reaction[41]. The product selectivity here is hence not well understood and more research is necessary in describing the dynamics behind this phenomenon.

1.2 Principles of Computational Chemistry

Computational chemistry techniques are valuable for studying chemical phenomena in a cost and time efficient way than traditional experimental procedures. Due to the short-lived or unstable properties of intermediates and transition states, examination via observation might be challenging, and application of computational calculations and models can provide missing insight. A diverse selection of *in silico* approaches exist that is generally classified as empirical, semi-empirical, and *ab initio*.

Empirical methods, like molecular dynamics (MD), disregard electronic effects, but rely on parameterization from higher-level calculations and experimental data. *Ab initio* approaches, like the Hartree-Fock (HF) Method, depend exclusively on inputs from fundamental physical constants and by solving the electronic structure problem from first principles. Semi-empirical methods utilize a simplified version of Hartree-Fock Theory with adjustable empirical parameters, which will be the main technique used in this thesis. The fundamental theory underlying these techniques will be explained further in the subsections.

1.2.1 Quantum Mechanics (QM): The Schrödinger equation

QM-based methods are used to study the electronic effects of molecules. *Ab initio* calculations are computed from solutions to the electronic Schrödinger equation, while DFT calculations apply functionals of spatially dependent electron density.

It is necessary to solve the time-independent and non-relativistic Schrödinger Equation to understand electronic structure of atoms and molecules. We start with the time-dependent Schrödinger Equation that governs the time evolution of $\Psi(\mathbf{r},t)$, where the Hamiltonian operator, $\hat{\mathcal{H}}$, is composed of a sum of kinetic ($\hat{T}$) and potential ($\hat{V}$) energy terms. $\hat{\mathcal{H}}$ correspond to $-\frac{\hbar^2}{2m}\nabla^2$ in the position basis, while $\hat{V}$ defines the specific system to give equation 1.1.

$$[-\frac{\hbar^2}{2m}\nabla^2 + V(\mathbf{r},t)]\Psi(\mathbf{r},t) = i\hbar\frac{\partial}{\partial t}\Psi(\mathbf{r},t) \tag{1.1}$$

If the potential term is independent of time (i.e. $V(\mathbf{r},t) \longrightarrow V(\mathbf{r})$), the total wavefunction $\Psi(\mathbf{r},t)$ can in general be separable into the space and time component:

$$\Psi(\mathbf{r},t) = \psi(\mathbf{r})\phi(t) \tag{1.2}$$

Substituting equation 1.2 into 1.1, we obtain the familiar time-independent Schrödinger Equation:

$$[-\frac{\hbar^2}{2m}\nabla^2 + V(\mathbf{r})]\psi(\mathbf{r}) = E\psi(\mathbf{r}) \tag{1.3}$$

The wave function is then described as $\psi(\mathbf{r})$, the quantum state of the entire system of particles, and the square modulus of the wave function $|\psi^2|$ is a probability density. For the lowest energy of the system, the related eigenfunction of $\hat{\mathcal{H}}$ corresponds to the ground state.

1.2.2 The Hartree-Fock (HF) Theory

The molecular $\hat{\mathcal{H}}$ consists of 5 terms:

$$\hat{\mathcal{H}} = -\sum_i \frac{\hbar^2}{2m_e}\nabla_i{}^2 - \sum_I \frac{\hbar^2}{2m_I}\nabla_I{}^2 - \sum_i \sum_I \frac{e^2 Z_I}{4\pi\varepsilon_0 r_{iI}} + \sum_{i<j} \frac{e^2}{4\pi\varepsilon_0 r_{ij}} + \sum_{I<J} \frac{e^2 Z_I Z_J}{4\pi\varepsilon_0 r_{IJ}} \quad (1.4)$$

The first two terms of equation 1.4 corresponds to the sum of kinetic energies of the electrons ($\hat{T}_e$) and the nuclei ($\hat{T}_N$) respectively. The third term corresponds to the electrostatic potential energy (attractive) between positively charged nuclei and electrons ($\hat{V}_{Ne}$), whereas the last two terms are the electron-electron repulsion and nuclear-nuclear repulsion energies. All lower case i and j run over the electrons, while upper case I and J run over nuclei.

The first step to reduce the complexity of the problem is to invoke the Born-Oppenheimer approximation. A qualitative way to explain the approximation is to note that the nuclear timescale is much longer than the electronic timescale; as such, the nuclear wavefunction can be separated from the electronic one. Hence, the second term of equation 1.4 can be dropped and the electronic wavefunction at fixed nuclei coordinates can be evaluated (equation 1.5). The last term in the same equation also becomes a constant under the approximation, which has no effect on the electronic wavefunction and adds a constant to the associated eigenvalue:

$$\hat{\mathcal{H}}_{elec} = -\sum_i \frac{\hbar^2}{2m_e}\nabla_i{}^2 - \sum_i \sum_I \frac{e^2 Z_I}{4\pi\varepsilon_0 r_{iI}} + \sum_{i<j} \frac{e^2}{4\pi\varepsilon_0 r_{ij}} + \sum_{I<J} \frac{e^2 Z_I Z_J}{4\pi\varepsilon_0 r_{IJ}} \quad (1.5)$$

We cannot ignore the existence of the spin of an electron, and therefore include it as:

$$\chi_i = \psi_i \alpha_i \quad (1.6)$$

Here, the spin-orbital, χ_i, of electron i is represented as a product of the spatial wavefunction, ψ_i, and the spin wavefunction, α_i.

From quantum statistics, electrons are indistinguishable fermions (spin 1/2 particles), and the implication of this further constrains the acceptable wavefunction to be antisymmetric with respect to the change in coordinates of two electrons. The easiest way to construct such a wavefunction is to cast it in the form of a Slater determinant (SD). We represent this SD by Ψ_{HF} in equation 1.7, known as the HF wavefunction. This simplest antisymmetrization approach assumes that each electron "moves" in the mean field of all other electrons. However, in reality, each electron can "sense" the presence of other electrons within its vicinity and tries to avoid them. This is known as electron correlation, which is absent in HF theory. Electron correlation can be formally defined as $E_{correlation} = E_{exact} - E_{HF}$ at the complete basis set limit. This concept will be expanded upon in a later section.

$$\Psi_{HF} = \frac{1}{\sqrt{N!}} \begin{vmatrix} \chi_1(\mathbf{r}_1, \omega_1) & \chi_2(\mathbf{r}_1, \omega_1) & \cdots & \chi_N(\mathbf{r}_1, \omega_1) \\ \chi_1(\mathbf{r}_2, \omega_2) & \chi_2(\mathbf{r}_2, \omega_2) & \cdots & \chi_N(\mathbf{r}_2, \omega_2) \\ \vdots & \vdots & \ddots & \vdots \\ \chi_1(\mathbf{r}_\mathrm{N}, \omega_N) & \chi_2(\mathbf{r}_\mathrm{N}, \omega_N) & \cdots & \chi_N(\mathbf{r}_\mathrm{N}, \omega_N) \end{vmatrix} \tag{1.7}$$

In equation 1.7, $\frac{1}{\sqrt{N!}}$ is the normalization constant, where N is the number of electrons, and $\mathbf{r}_\mathrm{i}$ and ω_i correspond to the spatial and spin cordinate respectively. In order to obtain the expectation value of E_{elec}, with the above wavefunction, the following integral 1.8 has to be evaluated:

$$E_{HF} = \iint \Psi_{HF}^{*} \hat{\mathcal{H}}_{elec} \Psi_{HF} d\mathbf{r}_1 d\mathbf{r}_2 \cdots d\mathbf{r}_\mathrm{N} d\omega_1 d\omega_2 \cdots d\omega_N \tag{1.8}$$

The approximate electronic ground state energy evaluated use a single determinant is known as the HF energy, E_{HF}, which is expressed in full in equation 1.9.

Expanding equation 1.8 using equations 1.7 and 1.5, 5 terms emerge: kinetic term, electron-nuclear attraction term, coulomb term J_{ab}, exchange term K_{ab}, and nuclear-

nuclear repulsion term V_{NN}. The former two terms are one-electron terms, which can be combined to give h_a in equation 1.10, while the third and fourth terms are two-electron terms described in equations 1.11 and 1.12 respectively. The last term in equation 1.13, V_{NN}, as mentioned previously, is a constant term and does not affect the electronic wavefunctions.

$$E_{HF} = \sum_a^N h_a + \sum_{a<b}^N (J_{ab} - K_{ab}) + V_{NN} \tag{1.9}$$

$$h_a(\mathbf{r_i}) = \sum_I \int \psi_a^*(\mathbf{r_i})(-\frac{\hbar^2}{2m_e}\nabla_i{}^2 - \frac{e^2 Z_I}{4\pi\varepsilon_0 r_{iI}})\psi_i(\mathbf{r_i})d\mathbf{r_i} \tag{1.10}$$

$$J_{ab}(\mathbf{r_i}, \mathbf{r_j}) = \iint \psi_a^*(\mathbf{r_i})\psi_a(\mathbf{r_i})\frac{e^2}{4\pi\varepsilon_0 r_{ij}}\psi_b^*(\mathbf{r_j})\psi_b(\mathbf{r_j})d\mathbf{r_i}d\mathbf{r_j} \tag{1.11}$$

$$K_{ab}(\mathbf{r_i}, \mathbf{r_j}) = \iint \psi_a^*(\mathbf{r_i})\psi_b(\mathbf{r_i})\frac{e^2}{4\pi\varepsilon_0 r_{ij}}\psi_b^*(\mathbf{r_j})\psi_a(\mathbf{r_j})d\mathbf{r_i}d\mathbf{r_j} \tag{1.12}$$

$$V_{NN} = \sum_{I<J}\frac{e^2 Z_I Z_J}{4\pi\varepsilon_0 r_{IJ}} \tag{1.13}$$

Having an expression for E_{HF} and Ψ_{HF} in terms of one-electron spatial wavefunctions, it is possible to construct an *ansatz* (educated guess) in equation 1.14, ψ_a^{trial}, using linear combination of atomic orbitals (LCAO), to approximate ψ_a.

$$\psi_a^{trial} = \sum_{\mu=1}^{N_{basis}} C_{\mu a}\phi_\mu \tag{1.14}$$

ϕ_μ represent the arbitrary basis functions that mimic atomic orbitals that are predefined, while $C_{\mu a}$ are the associated coefficients to be determined. The equation is now transformed to another problem: to determine the optimal set of $C_{\mu a}$, for a given basis set, which will give the best estimate of the exact ground state Ψ_{HF} and ground state E_{HF}.

Fortunately, since the eigenfunctions of $\widehat{\mathcal{H}}_{elec}$ span the complete space, and ψ_a^{trial} can be expressed as the linear combination of eigenfunctions, and a simple mathematical

manipulation show that $\langle \psi_a^{trial} | \widehat{\mathcal{H}}_{elec} | \psi_a^{trial} \rangle \geq \langle \psi_a^{ground} | \widehat{\mathcal{H}}_{elec} | \psi_a^{ground} \rangle$. Thus, for a given basis set, the best set of $C_{\mu a}$ is the one that minimizes the energy. This is also commonly known as the variational theorem.

By introducing pre-defined basis functions, the Hartree-Fock problem can now be rewritten as the Roothan-Hall equation:

$$\mathbf{FC} = \mathbf{SC}\varepsilon \tag{1.15}$$

where **F** is the Fock matrix with matrix elements defined as the following:

$$F_{\mu\nu} = h_{\mu\nu} + \sum_{\lambda\sigma}^{N_{basis}} P_{\mu\nu}[(\mu\nu|\lambda\sigma) - \frac{1}{2}(\mu\lambda|\nu\sigma)] \tag{1.16}$$

The one-electron term cast in terms of the chosen basis set is:

$$h_{\mu\nu} = \sum_I \int \phi_\mu^*(\mathbf{r_i}) \left(-\frac{\hbar^2}{2m_e}\nabla_i{}^2 - \frac{e^2 Z_I}{4\pi\varepsilon_0 r_{iI}}\right)\phi_\nu(\mathbf{r_i}) d\mathbf{r_i} \tag{1.17}$$

P is the density matrix with matrix elements:

$$P_{\mu\nu} = \sum_a^{occupied} C_{\mu a}\, C_{a\nu} \tag{1.18}$$

The four-center-two-electron terms are defined as:

$$(\mu\nu|\lambda\sigma) = \iint \phi_\mu(\mathbf{r_i})\, \phi_\nu(\mathbf{r_i}^*)\, \frac{e^2}{4\pi\varepsilon_0 r_{ij}} \phi_\lambda(\mathbf{r_j})\phi_\sigma(\mathbf{r_j}^*) d\mathbf{r_i} d\mathbf{r_j} \tag{1.19}$$

and **S** is the overlap matrix elements corresponding to:

$$S_{\mu\nu} = \int \phi_\mu^*(\mathbf{r_i})\, \phi_\nu(\mathbf{r_i}) d\mathbf{r_i} \tag{1.20}$$

Finally, upon solving equation 1.15 self-consistently with an initial guess for **C**, ε is the diagonal matrix corresponding to the eigenvalues of ψ_a (orbital energies), and the a^{th} column of **C** corresponds to ψ_a in terms of a linear combination of ϕ_α. Ψ_{HF} is easily obtained with ψ_a evaluated, while the closed-shell E_{HF} can be expressed as:

$$E_{HF} = 2\sum_a^{N/2} h_{aa} + \sum_{ab}^{N/2}(2J_{ab} - K_{ab}) \tag{1.21}$$

where each spatial orbital, ψ_a, is doubly occupied.

1.2.3 Basis Sets and Effective Core Potentials

Due to the close likeness of hydrogenic wavefunctions, the Slater functions, $e^{-\alpha r}$ (where α is an exponent coefficient), appear to be a clear choice for the user-defined basis sets. However, the four-center-two electron $(\mu\nu|\lambda\sigma)$ integral has no analytical solutions when constructed with Slater functions (or Slater-type orbitals (STOs)). Computer programs will have to resort to numerical integration techniques, which is incredibly inefficient.

The use of Gaussian functions $e^{-\alpha r^2}$, on the other hand, allows the analytical evaluation of $(\mu\nu|\lambda\sigma)$, which speeds up the calculations tremendously. This results in the widespread use of the latter in the vast majority of quantum chemical calculations.

In the cartesian form, the normalized Gaussian-type orbitals (GTOs) can be expressed as the following:

$$\phi_\alpha = \left(\frac{2\alpha}{\pi}\right)^{\frac{3}{4}}\left[\frac{(8\alpha)^{i+j+k} i!j!k!}{(2i)!(2j)!(2k)!}\right]^{\frac{1}{2}} x^i y^j z^k e^{-\alpha(x^2+y^2+z^2)} \tag{1.22}$$

α in equation 1.22 governs the width of the GTO, while $i + j + k$ relates to the orbital angular momentum, l. For example, a d_{xy} orbital will have $i = 1$, $j = 1$ and $k = 0$.

Two of the limitations of GTOs are that firstly, they cannot reproduce the "cusp" condition at the nuclei ($\frac{d\phi_\alpha}{dr}$ at nuclei is 0 instead of a finite value), and secondly, it falls off too quickly with respect to STOs. To retain the mathematical convenience while at the same time reproduce the latter as closely as possible, a linear combination of GTOs can be constructed to fit an STO. This is commonly known in literature as contracted GTOs (cGTOs), shown in equation 1.23:

$$\phi^{cGTO} = \sum_{\alpha=1}^{M} c_\alpha \phi_\alpha \tag{1.23}$$

where M is the number of primitive GTOs used to construct a particular cGTO. For example, the rudimentary STO-3G basis set uses an M value of 3.

Basis sets like STO-3G are known as single-ζ (zeta) basis set because only one cGTO is used to describe a particular orbital, like the 1s orbital of oxygen. To create more flexibility for the electrons to relax, it is typical that we use multiple-ζ basis sets in standard calculations. So if atomic orbitals are described by two basis functions, such a basis set is known as a double-ζ basis set.

As the core electrons are much less involved in chemical bonding, given the poor cost-to-accuracy ratio, the increase in flexibility brought about by multiple-ζ basis sets is rather unnecessary. Hence, split-valence basis sets are developed for popular Pople and Dunning classes. For a Pople basis set, such as 6-311G, the first number, 6, represents the number of primitive GTOs used to construct the cGTO for core electrons, and the number of digits after the dash symbol represents the number of basis functions used to describe the valence electrons. In this case, 3 basis functions are used: 1 cGTO with M = 3 and 2 other primitive GTOs. For Dunning basis sets, the number of "ζ" can be easily seen from the name of the basis set; cc-pVDZ, cc-pVTZ and cc-pVQZ correspond to double, triple and quadruple- ζ respectively.

To further add flexibility, polarized functions, with angular momentum higher than the atomic orbital it is describing, are introduced. This is usually important even for simple molecules in predicting the correct molecular geometries. In the example of the ammonia molecule, a basis set containing just *s* and *p*-type basis functions will produce a planar optimal geometry instead of the correct pyramidal one. Adding polarized *d*-orbitals can eliminate this problem. In the Pople basis sets, polarization functions are

represented with *, while the Dunning basis sets are polarized by default (the "p" in cc-pVXZ).

In order to describe non-covalent interactions and anions accurately, diffused functions, represented by "+" and "aug" in Pople and Dunning basis sets respectively, are added. These functions have small exponents, α, so that they decay more slowly with r.

Different philosophies have been adopted to parameterize the exponents, α, and the coefficients, c_α. For Pople basis sets, a test set consisting atoms and molecules was chosen and the optimal α and c_α values minimize E_{HF}. For the correlation consistent Dunning basis set, α and c_α values are optimized to reproduce correct results, for a different set of atoms and molecules, in post-HF methods that include electron correlation.[42,43]

For larger atoms, a huge basis set size is required to reasonably describe all the electrons. This considerably increases computational time, as all quantum chemical methods scale at least with $O(N_{basis}^4)$. Additionally, core electrons of atoms with large nuclear charge travel at a considerable fraction of the speed of light, making relativistic effects non-negligible. To address these two problems, effective core potentials (ECPs) could be used to replace the core electrons of large atoms. ECPs are classified as either small-core (covers all electrons up to 2 shells below valence shell) or large-core (covers all electrons up to the shell below valence shell). The former is typically more accurate as sub-valence electrons are vital in chemical bonding involving large atoms. ECPs are usually assembled using Gaussian functions just like GTOs, and the parameterization normally involves minimizing the difference between the energies of atoms and

molecules evaluated using all-electron high level relativistic calculations and the same quantities evaluated using a non-relativistic framework with ECPs.[44]

1.2.4 Density Functional Theory (DFT)

Two of the most cited papers in scientific literature are the Hohenberg-Kohn (HK) theorems in 1964[45] and Kohn-Sham (KS) approach in 1965.[46] Together, they form the underlying theory for the DFT approach. The two HK theorems state that, firstly, the external potential V_{ext}, uniquely determines the ground state density ρ_0, and hence the electronic Hamiltonian $\widehat{\mathcal{H}}_{elec}$, ground state wavefunction Ψ_0, and all other physical properties. Secondly, the density ρ, that minimizes the ground state energy, E_0, is the ground state density, ρ_0.

In the molecular sense, V_{ext} in the first HK theorem corresponds to the potential created by the electric field of the static nuclei, and hence their position. In other words, there is only one ground state density corresponding to a particular nuclear configuration, in which all other physical properties can be determined. Electronic energy can hence be expressed in terms of a functional of density, $E[\rho]$.

The second HK theorem provides a means for the trial density to become closer to ρ_0, i.e. the variational theorem of DFT. However, some constraints have to be applied just like the HF case. Firstly, the trial density, $\tilde{\rho}(\mathbf{r})$, must be non-negative at all $\mathbf{r}$, and secondly $\int \tilde{\rho}(\mathbf{r})\, d\mathbf{r} = N$, where N is the number of electrons.

Based on the wavefunction theory presented in Section **1.2.1** and **1.2.2**, E_0 can be re-expressed as:

$$E_0 = \langle \Psi_0 | \hat{T}_e | \Psi_0 \rangle + \langle \Psi_0 | \hat{V}_{ee} | \Psi_0 \rangle + \langle \Psi_0 | \hat{V}_{Ne} | \Psi_0 \rangle + V_{NN} \qquad (1.24)$$

where $\hat{V}_{ee}$ is the potential energy operator stemming from electron-electron interaction.

Equation 1.24 can then be described in terms of ρ as:

$$E_0[\rho] = E_T[\rho] + \iint \frac{e^2\rho(\mathbf{r_i})\rho(\mathbf{r_j})}{4\pi\varepsilon_0 r_{ij}} d\mathbf{r_i} d\mathbf{r_i} + E_{XC}[\rho] - \sum_I \frac{e^2\rho(\mathbf{r_i})}{4\pi\varepsilon_0 r_{Ii}} d\mathbf{r_i} + V_{NN} \quad (1.25)$$

where $E_T[\rho]$ and $E_{XC}[\rho]$ are the kinetic and exchange-correlation energies respectively. Since the first three terms in equation 1.25 are independent of V_{ext}, they are often labelled collectively as the universal functional, $F[\rho]$. There are, however, no known functional forms of $E_T[\rho]$ and $E_{XC}[\rho]$ for molecular systems.

To partly tackle the problem, Kohn and Sham introduced the concept of fictitious non-interacting KS orbitals expressed in equation 1.26, in which the sum of squared of the occupied orbitals recover the exact ground state density. Since this philosophy is to reproduce the exact ground state density, electron correlation is inherently included.

$$\rho_0(\mathbf{r}) = \sum_a^N |\phi_a^{KS}(\mathbf{r})|^2 \quad (1.26)$$

Hence, $E_T[\rho]$ can now be expressed in terms of orbitals, similar to the HF case:

$$E_T[\rho] = -\int \phi_a^{*KS}(\mathbf{r}) \frac{\hbar^2}{2m} \nabla^2 \phi_a^{KS}(\mathbf{r}) d\mathbf{r} \quad (1.27)$$

After the introduction of KS orbitals, the final problem would be to obtain a good approximation of $E_{XC}[\rho]$.

Historically, the first attempt to approximate $E_{XC}[\rho]$ is the local density approximation (LDA) or the local spin density approximation (LSDA). In LDA or LSDA, the $E_{XC}[\rho]$ is further decomposed into the exchange energy $E_X[\rho]$, and correlation energy $E_C[\rho]$. Using results from the Thomas-Fermi-Dirac model, $E_X[\rho]$ has a $\rho^{\frac{3}{4}}$ dependence,[47] while interpolation of quantum Monte-Carlo simulations by Vosko, Wilk and Nusiar gave sophisticated analytical solutions for $E_C[\rho]$.[48] The next advancement was the generalized gradient approximation (GGA), in which both ρ and $\nabla\rho$ enter the E_{XC}

expression explicitly. Instead of $\nabla\rho$, the reduced density gradient, s (dimensionless quantity) is a more common parameter used in GGA functionals:

$$s = \frac{|\nabla\rho|}{\rho^{4/3}} \tag{1.28}$$

Similarly, GGAs are often expressed as a sum of exchange and correlation parts. One of the most popular pioneer GGA $E_X[\rho, s]$ is the B88 function by Axel Becke, obtained by fitting exact exchange energies of rare gas atoms.[49] For $E_C[\rho, s]$, the Lee-Yang-Parr (LYP) functional is arguably the most widely used in the 1980−90s, parameterized using correlation methods.[50] Both functionals each contain one empirical parameter. Since DFTs only differ in E_{XC}, it is traditionally named by its exchange functional followed by the correlation function (if separable). For example, if E_X = B88 and E_C = LYP, the DFT is named B-LYP or BLYP.

Although GGAs offer significant improvements over LDAs, they are still in general far from reliable in predicting chemical phenomena within chemical accuracy. Rather than developing E_X purely as a functional of ρ and its derivatives, it is also possible to include some percentage of HF exchange, E_X^{HF}, as derived from HF theory. These functionals are known as hybrid-GGAs. Undoubtedly, the most revolutionary hybrid-GGA is the B3LYP functional[51] as expressed below:

$$E_{XC}^{B3LYP} = (1-a)E_X^{LSDA} + aE_X^{HF} + bE_X^{B88} + (1-c)E_C^{LSDA} + cE_C^{LYP} \tag{1.29}$$

where a, b, and c in equation 1.29 are the optimized parameters with values of 0.20, 0.72 and 0.81 respectively.

B3LYP has achieved unprecedented success in reproducing a wide range of experimental data. For example, the mean unsigned error for the B3LYP calculated

results with reference to the G2 data set is about 2 kcal/mol. Moreover, it has also shown promise in tackling challenging problems in open-shell transition metal chemistry.[52]

Beyond hybrid-GGAs, there are meta-GGAs that include kinetic energy density or even higher derivatives of the density, or hybrid-meta-GGAs and double-hybrid GGAs, which include virtual orbitals. The Truhlar group from Minnesota, and the Head-Gordon group from Berkeley are two of the most successful DFT development groups.

In terms of reproducing accurate ΔGs and $\Delta G^{\ddagger}$s for chemical reactions, the Minnesota functionals developed by the Truhlar group have enjoyed widespread popularity. These functionals are usually highly parametrized to fit experimental data.[53] In light of developing a universal functional, Yu et al. had reported the MN15 functional that gave excellent results for both single and multi-reference systems, non-covalent interactions, bond lengths and electronic excitations.[54]

The Head-Gordon group, on the other hand, is renowned for their "B97" series of functionals. Many of them contain long-range correction for exchange, whereby the HF exchange is not a fixed percentage but varies with distance between two electrons. These functionals are prefixed by ω. Recently, Mardirossian et al. have developed the ωB97M−V functional using a combinatorial approach, which performs well with an augmented quadruple-ζ basis set in non-covalent energies, isomerization energies, thermochemistry and barrier heights for main group elements.[55]

1.2.5 Post-HF methods

A more systematic and general way to introduce electron correlation is through the inclusion of more Slater determinants in the trial wavefunction and to optimize them.

The most rigorous, but intractable method, for a given basis set, is the full configuration interaction (FCI). FCI generates all possible determinants exhaustively and solve for their corresponding weights. Two main classes of post-HF methods are the Møller Plesset (MP) perturbation theory and the Coupled-Cluster (CC) Theory.

Inspired by the Rayleigh-Schrödinger (RS) perturbation theory for single electron systems, Christian Møller and Milton Plesset extended the former theory to a multielectron system in 1934.[56] Similar to the RS theory, MP theory can also be truncated at an arbitrary order. For example, the most commonly used 2nd order MP perturbation theory is known as MP2, but in general, an nth order MP theory, is known as MPn. Without evaluating the MP2 wavefunction, the electronic energy at MP2 level, E_{MP2} can be expressed in terms of occupied and virtual molecular orbitals as shown here:

$$E_{MP2} = E_{HF} + \sum_i^{occ} \sum_{j>i}^{occ} \sum_a^{virt} \sum_{b>a}^{virt} \frac{[(ij|ab)-(ia|jb)]^2}{\varepsilon_i+\varepsilon_j-\varepsilon_a-\varepsilon_b} \quad (1.30)$$

where indices i and j correspond to occupied orbitals and a and b correspond to virtual orbitals. ε_x corresponds to orbital energies of orbital x. Expanding the second term in terms of basis functions and their associated coefficients, it is proven that the computational complexity of MP2 theory is about $O(N_{basis}^5)$.

Due to the slow convergence of MPn theory and the sharp increase in computational complexity, MP3 $[O(N_{basis}^6)]$, MP4 $[O(N_{basis}^7)]$ and higher truncations are seldom used today with the development of Coupled-Cluster theory, which has a better accuracy-to-cost ratio. The Coupled-Cluster ansatz is given as the following:

$$\Psi_{CC} = e^{\hat{\mathbf{T}}}\Psi_{HF} \quad (1.31)$$

where $\hat{\mathbf{T}}$ is the cluster operator, which can be truncated at any arbitrary order:

$$\hat{\mathbf{T}} = \hat{\mathbf{T}}_1 + \hat{\mathbf{T}}_2 + \hat{\mathbf{T}}_3 + \cdots \tag{1.32}$$

The term $\hat{\mathbf{T}}_i$ in the cluster operator generates a complete set of determinants that correponds to i electronic excitations. For example, the explicit form of $\hat{\mathbf{T}}_2$ is:

$$\hat{\mathbf{T}}_2 = \sum_{i<j}^{occ} \sum_{a<b}^{virt} t_{ij}^{ab} \Psi_{ij}^{ab} \tag{1.33}$$

where t_{ij}^{ab} are corresponding double excitation amplitudes of doubly excited wavefunction, Ψ_{ij}^{ab}, with occupied orbitals i and j replaced by virtual orbitals a and b. The commonly employed CCSD (CC Single Double), truncates the cluster operator at the second term, and scales with $O\left(N_{basis}^6\right)$. The next level of complexity, CCSDT (Triple), scales basis with $O\left(N_{basis}^8\right)$, which is computationally intractable for the majority of systems. In 1989, Raghavachari et al. introduced a perturbative approach, CCSD(T), in treating the triple excitation term, lowering the computation complexity to $O\left(N_{basis}^7\right)$.[57]

CCSD(T) has since been established as the "gold-standard" for solving single-reference quantum chemistry problems, and widely used as a benchmark. More recently, Frank Neese and co-worker have developed the Domain-based Local Pair Natural Orbital CCSD(T) (DLPNO-CCSD(T)), which exhibits linear scaling with respect to system size for large molecules.[58] This development provides an opportunity to replace DFT single-point calculations with a more robust DLPNO-CCSD(T) approach at almost the same cost.[59] Currently, the analytical gradients are available for DLPNO-CCSD,[60] and a more widespread use of DLPNO-CCSD(T) would be expected when the corresponding analytical gradients are developed.

1.2.6 Molecular Mechanics (MM)

The general potential energy function used in MM force fields is a summation describing the different contributions from bonded and non-bonded interactions terms:

$$U_{total} = U_{bond} + U_{angle} + U_{dihedral} + U_{vdW} + U_{Coulomb} \quad (1.34)$$

The harmonic bond potential U_{bond} is represented as:

$$U_{bond} = \sum_{bonds} k_b (r - r_0)^2 \quad (1.35)$$

with k_b as the stretching constant, r as the bond length between two bonded atoms, and r_0 as the bond length for the minimum energy configuration of the molecule.

The harmonic potential term, U_{angle}, illustrates the energy according to the oscillations between three bonded atoms about a bond angle:

$$U_{angle} = \sum_{angles} k_\theta (\theta - \theta_0)^2 \quad (1.36)$$

with k_θ as the angle force constant, θ as the valence angle between the three bonded atoms, and θ_0 as the reference angle.

The $U_{dihedral}$ term is defined as the contribution from the torsional rotation of four atoms around a bond., Due to the nature of the internal rotation barriers, which are relatively lower than in other interactions, deviations in dihedral angles are large. Furthermore, the torsional potential goes via a $360°$ rotation and it is therefore common to model this using a Fourier series:

$$U_{dihedral} = \sum_{dihedrals} k_\phi (1 + \cos(n\phi - \delta)) \quad (1.37)$$

with the phase angle represented as δ and the other terms given by the parameter files: ϕ as the dihedral angle between four bonded atoms, k_ϕ as the dihedral angle force constant, and n as the multiplicity.

The final two terms, U_{vdW} and $U_{Coulomb}$, are the non-bonded interactions that represent energetic effects due to van der Waals attraction, steric repulsion, and electrostatic interactions.

U_{vdW} is characterized using the Lennard-Jones potential which describes the Pauli repulsion due to the short-range interaction of the electron clouds from both atoms (r^{12} term) and the long-range attractive dispersion forces from dipole-induced dipole interactions(r^6 term):

$$U_{vdW} = 4\varepsilon[\left(\frac{\sigma}{r_{ij}}\right)^{12} - \left(\frac{\sigma}{r_{ij}}\right)^{6}] \tag{1.38}$$

with r_{ij} as the distance between atoms i and j, σ as the minimum energy difference, and ε as the depth of the potential well.

The electrostatic interaction is lastly accounted for by the $U_{Coulomb}$ term. This stems from the unequal charge distribution in a molecule, and is modelled by labelling point charges for each atom that will sum to the formal charge of the molecule:

$$U_{Coulomb} = \frac{q_i q_j}{\varepsilon r_{ij}} \tag{1.39}$$

with q_i and q_j as the atomic charges for atoms i and j, and ε as the permitivitty of free space.

1.2.7 Quantum Mechanics/Molecular Mechanics (QM/MM)

Using **O**ur own **N**-layered **I**ntegrated molecular **O**rbital and molecular **M**echanics (ONIOM),[61] QM and MM approaches are combined to deal with large and complex molecular systems, like reactions in protein environments, at a reduced computational cost relative to pure QM. The entire molecular system is divided into two parts: the model system and the environment system. The "model" part, usually small, represents

the chemically important part, where the atoms are directly involved with the reaction, and is treated with the accurate but expensive QM method. The remaining environment part is then treated with the less accurate, but more efficient MM method. The energy of the combined system could be calculated in two different ways. Firstly, in the "additive" scheme of QM/MM,[62] the total energy $E_{QM/MM}$, is a sum of the energy of the model part by QM method (E_{QM}), the energy of the environment part by MM method (E_{MM}), and the interactions (E_{QM-MM}) between the QM model system and the MM environment system:

$$E_{QM/MM} = E_{QM} + E_{MM} + E_{QM-MM} \tag{1.40}$$

Secondly, for the "subtractive" scheme of ONIOM,[63] the total energy E_{ONIOM} of the whole ("real") system is evaluated as the QM energy of the "model" part ($E_{QM,model}$) plus the MM energy of the whole "real" system ($E_{MM,real}$) minus the MM energy of the model part ($E_{MM,model}$).

$$E_{ONIOM} = E_{QM,model} + E_{MM,real} - E_{MM,model} \tag{1.41}$$

It is necessary to create link atoms in cases where the covalent bond crosses between different layers of the QM and MM regions; all dangling bonds are capped off with a hydrogen atom.

To account for the electronic polarization of the QM layer by the MM layer, an electronic embedding (EE) is often used. The wavefunction of the QM layer is solved with an external electric field generated from the partial charges of the MM layer, hence this resulting charge density of the QM layer accounts for the anisotropy of charge distribution in the MM layer.

1.2.8 Implicit Solvation Model

In the aforementioned section of QM/MM, EE was described as electronic polarization by partial charges. For implicit solvation models, the idea is essentially the same, except that a dielectric constant is applied around the system of interest in this case. Hence, this approach of modelling solvation is defined as the self-consistent reaction field (SCRF) method. The total solvation free energy ($\Delta G_{solvation}$), is then calculated as the sum of the free energy of the cavity created around the system (ΔG_{cav}), dispersion effects (ΔG_{disp}), repulsive interactions (ΔG_{rep}), and electrostatic interactions (ΔG_{elec}).

1.2.9 Quasi-classical Dynamics (QCD)

QCD, or direct dynamics,[64,65] is a subclass of MD in which the forces used to propagate these MD trajectories are calculated on the fly using either DFT or any other wavefunction methods. In other words, the functional form of the potential energy surface in question is not known a priori, unlike the case for classical MD. Standard propagation methods such as the velocity verlet[66], leap-frog and predictor-corrector algorithms can be used calculate the phase space properties of the next time step. The challenge lies in generating initial positions and velocities to kick start the propagation of the trajectory. For simulating chemical reactions, the sampling process begins with the optimized TS structure and its associated eigenvectors of the Hessian matrix. Initial coordinates and velocities are generated from the normal mode sampling procedure described below. Under the harmonic approximation, the partition function Z_i, corresponding to vibrational mode i is:

$$Z_i = \sum_{n=0}^{\infty} e^{\left(-\frac{nhv_i}{k_B T}\right)} = \left(1 - e^{\left(-\frac{hv_i}{k_B T}\right)}\right)^{-1} \quad (1.42)$$

where n is the vibrational state of the ith mode, and v_i is the vibrational frequency of that mode.

The probability of the n_i^{th} state of vibrational mode i being occupied is:

$$P(n_i) = \frac{e^{(-\frac{n_i h v_i}{k_B T})}}{Z_i} = e^{\left(-\frac{n_i h v_i}{k_B T}\right)}\left(1 - e^{\left(-\frac{h v_i}{k_B T}\right)}\right) \tag{1.43}$$

If the sampling process results in the n_i^{th} state of vibrational mode i being occupied, the normal mode amplitude, $A(n_i)$, can be calculated with the following formula:

$$A(n_i) = \frac{\sqrt{2E(n_i)}}{(2\pi v_i)} \tag{1.44}$$

The transition state geometry is then displaced by:

$$\boldsymbol{Q}(\boldsymbol{n_i}) = A(n_i)\cos(2\pi R) \times \boldsymbol{Q_i} \tag{1.45}$$

where $\boldsymbol{Q_i}$ is the unit vector corresponding to the vibrational mode i, while R is a random number from 0 to 1.

Obtaining the corresponding velocity is then straightforward:

$$\dot{\boldsymbol{Q}}(\boldsymbol{n_i}) = -(\boldsymbol{2\pi v_i})\boldsymbol{A}(\boldsymbol{n_i})\boldsymbol{sin}(\boldsymbol{2\pi R}) \times \boldsymbol{Q_i} \tag{1.46}$$

These steps will be repeated for all 3N-7 vibrational modes (leaving out the imaginary mode) and all $\boldsymbol{Q}$s and $\dot{\boldsymbol{Q}}$s from all modes will be linearly combined and transformed into the respective cartesian coordinates to obtain the initial structure and velocity for the direct dynamics procedure.

References

1. Diels, O. & Alder, K. Synthesen in der hydroaromatischen Reihe. *Justus Liebig's Ann. der Chemie* **460**, 98–122 (1928).
2. Houk, K. N. Generalized frontier orbitals of alkenes and dienes. Regioselectivity in Diels-Alder reactions. *J. Am. Chem. Soc.* **95**, 4092–4094 (1973).
3. Eggelte, T. A., de Koning, H. & Huisman, H. O. Diels-Alder reaction of furan with some dienophiles. *Tetrahedron* (1973).
4. Gandini, A. The furan/maleimide Diels–Alder reaction: A versatile click–unclick tool in macromolecular synthesis. *Prog. Polym. Sci.* **38**, 1–29 (2013).
5. Canadell, J., Fischer, H., De With, G. & Van Benthem, R. A. T. M. Stereoisomeric effects in thermo-remendable polymer networks based on diels-alder crosslink reactions. *J. Polym. Sci. Part A Polym. Chem.* (2010).
6. Kamahori, K., Tada, S., Ito, K. & Itsuno, S. Optically active polymer synthesis by Diels-Alder polymerization with chirally modified Lewis acid catalyst. *Macromolecules* (1999).
7. Bartlett, P. D. & Wu, C. Reactions of Tetracyanoethylene (TCNE) with the Three Isodicyclopentadiene Isomers. *J. Org. Chem.* (1984).
8. Carboni, R. A. & Lindsey, R. V. Reactions of Tetrazines with Unsaturated Compounds. A New Synthesis of Pyridazines. *J. Am. Chem. Soc.* (1959).
9. Boger, D. L. Diels-alder reactions of heterocyclic azadienes: Scope and application. in *Scientia Pharmaceutica* (1990).
10. Mayer, S. & Lang, K. Tetrazines in Inverse-Electron-Demand Diels-Alder Cycloadditions and Their Use in Biology. *Synth.* (2017).

11. Evans, D., Miller, S. & Lectka, T. Bis (oxazoline) copper (II) complexes as chiral catalysts for the enantioselective Diels-Alder reaction. *J. Am. Chem. Soc.* **12**, 6460–6461 (1993).

12. Nakashima, D. & Yamamoto, H. Design of chiral N-triflyl phosphoramide as a strong chiral Brønsted acid and its application to asymmetric Diels-Alder reaction. *J. Am. Chem. Soc.* **128**, 9626–9627 (2006).

13. Ahrendt, K. A., Borths, C. J. & Macmillan, D. W. C. New Strategies for Organic Catalysis: The First Highly Enantioselective Organocatalytic Diels-Alder Reaction. *J. Am. Chem. Soc.* **122**, 4243–4244 (2000).

14. Bellvile, D. J., Wirth, D. D. & Bauld, N. L. The Cation-Radical Catalyzed Diels-Alder Reaction. *J. Am. Chem. Soc.* 718–720 (1981).

15. Bellville, D. J. & Bauld, N. L. Selectivity Profile of the Cation Radical Diels-Alder Reaction. *J. Am. Chem. Soc.* **104**, 2665–2667 (1982).

16. Ischay, M. A., Anzovino, M. E., Du, J. & Yoon, T. P. Efficient visible light photocatalysis of [2+2] enone cycloadditions. *J. Am. Chem. Soc.* **130**, 12886–12887 (2008).

17. Nicewicz, D. A. & Macmillan, D. W. C. Merging Photoredox Catalysis with Organocatalysis. *Science* (2008).

18. Narayanam, J. M. R., Tucker, J. W. & Stephenson, C. R. J. Electron-transfer photoredox catalysis: Development of a tin-free reductive dehalogenation reaction. *J. Am. Chem. Soc.* (2009).

19. Twilton, J. *et al.* The merger of transition metal and photocatalysis. *Nature*

Reviews Chemistry (2017).

20. Fujishima, A. & Honda, K. Electrochemical photolysis of water at a semiconductor electrode. *Nature* (1972).

21. Vamvasakis, I., Liu, B. & Armatas, G. S. Size Effects of Platinum Nanoparticles in the Photocatalytic Hydrogen Production Over 3D Mesoporous Networks of CdS and Pt Nanojunctions. *Adv. Funct. Mater.* (2016).

22. Nakayama, K., Maeta, N., Horiguchi, G., Kamiya, H. & Okada, Y. Radical Cation Diels-Alder Reactions by TiO 2 Photocatalysis. *Org. Lett.* (2019).

23. Mattay, J., Gersdorf, J. & Mertes, J. A new type of electron acceptor for Diels-Alder reactions via radical cations. *J. Chem. Soc. Chem. Commun.* 1088 (1985).

24. Groenewold, G. S., Gross, M. L. & Croenewold, G. S. Reaction of the vinyl methyl ether cation radical and 1,3-butadiene: a two-step cycloaddition. *J. Am. Chem. Soc.* **106**, 6569–6575 (1984).

25. Mlcoch, J. & Steckhan, E. Electrochemically induced [4+2] cycloadditions - a mechanistic interpretation of the cation radical Diels-Alder reaction based on preparative results. *Tetrahedron Lett.* **28**, 1081–1084 (1987).

26. Haberl, U., Wiest, O. & Steckhan, E. Ab initio studies of the radical cation Diels-Alder reaction. *J. Am. Chem. Soc.* **121**, 6730–6736 (1999).

27. Williams, F. Inverted Potential-energy Surfaces in the Radical-cation Cope Rearrangements of Hexa-1,5-diene and Semibullvalene. *J. Chem. Soc. Faraday Trans.* **90**, 1681–1687 (1994).

28. Doubleday, C., Bolton, K. & Hase, W. L. Direct Dynamics Quasiclassical

Trajectory Study of the Thermal Stereomutations of Cyclopropane. *J. Phys. Chem. A* **102**, 3648–3658 (1998).

29. Carpenter, B. K. Dynamic Matching: The Cause of Inversion of Configuration in the [1,3] Sigmatropic Migration? *J. Am. Chem. Soc.* **117**, 6336–6344 (1995).

30. Carpenter, B. K. Dynamic Behavior of Organic Reactive Intermediates. *Angew. Chemie Int. Ed.* **37**, 3340–3350 (1998).

31. Carpenter, B. K. Trajectories through an intermediate at a fourfold branch point. Implications for the stereochemistry of biradical reactions. *J. Am. Chem. Soc.* **107**, 5730–5732 (1985).

32. Hrovat, D. A., Fang, S., Borden, W. T. & Carpenter, B. K. Investigation of Cyclopropane Stereomutation by Quasiclassical Trajectories on an Analytical Potential Energy Surface. *J. Am. Chem. Soc.* **7863**, 5253–5254 (1997).

33. Doubleday, C., Bolton, K. & Hase, W. L. Direct Dynamics Study of the Stereomutation of Cyclopropane. *J. Am. Chem. Soc.* **119**, 5251–5252 (1997).

34. Black, K., Liu, P., Xu, L., Doubleday, C. & Houk, K. N. Inaugural Article: Dynamics, transition states, and timing of bond formation in Diels-Alder reactions. *Proc. Natl. Acad. Sci.* **109**, 12860–12865 (2012).

35. Wang, Z., Hirschi, J. S. & Singleton, D. A. Recrossing and dynamic matching effects on selectivity in a diels-alder reaction. *Angew. Chemie - Int. Ed.* **48**, 9156–9159 (2009).

36. Hase, W. L., Song, K. & Gordon, M. S. Direct dynamics simulations. *Comput. Sci. Eng.* **5**, 36–44 (2003).

37. Lin, H. & Truhlar, D. G. QM/MM: What have we learned, where are we, and where do we go from here? *Theor. Chem. Acc.* **117**, 185–199 (2007).

38. Kamerlin, S. C. L., Cao, J., Rosta, E. & Warshel, A. On unjustifiably misrepresenting the evb approach while simultaneously adopting it. *J. Phys. Chem. B* **113**, 10905–10915 (2009).

39. Bauld, N. L. & Gao, D. Approaching a possible stepwise/concerted mechanistic crossover point in the cation radical cycloadditions of cis- and trans-anethole. *J. Chem. Soc. Perkin Trans. 2* 931–934 (2000).

40. Lin, S., Ischay, M. A., Fry, C. G. & Yoon, T. P. Radical Cation Diels–Alder Cycloadditions by Visible Light Photocatalysis. *J. Am. Chem. Soc.* **133**, 19350–19353 (2011).

41. Moeller, K. D. Intramolecular anodic olefin coupling reactions: Using radical cation intermediates to trigger new umpolung reactions. *Synlett* 1208–1218 (2009).

42. Wilson, A. K., Woon, D. E., Peterson, K. A. & Dunning, T. H. Gaussian basis sets for use in correlated molecular calculations. IX. The atoms gallium through krypton. *J. Chem. Phys.* (1999).

43. Dunning, J., Peterson, K. A. & Wilson, A. K. Gaussian basis sets for use in correlated molecular calculations. X. The atoms aluminum through argon revisited. *J. Chem. Phys.* (2001).

44. Dolg, M. & Cao, X. Relativistic Pseudopotentials: Their Development and Scope of Applications. *Chem. Rev.* (2012).

45. Hohenberg, P. & Kohn, W. Inhomogeneous electron gas. *Phys. Rev.* (1964).

46. Kohn, W. & Sham, L. J. Self-consistent equations including exchange and correlation effects. *Phys. Rev.* (1965).

47. Dirac, P. A. M. Note on Exchange Phenomena in the Thomas Atom. *Math. Proc. Cambridge Philos. Soc.* (1930).

48. Vosko, S. H., Wilk, L. & Nusair, M. Accurate spin-dependent electron liquid correlation energies for local spin density calculations: a critical analysis. *Can. J. Phys.* (1980).

49. Becke, A. D. Density-functional exchange-energy approximation with correct asymptotic behavior. *Phys. Rev. A* **38**, 3098–3100 (1988).

50. Lee, C., Yang, W. & Parr, R. G. Development of the Colle-Salvetti correlation-energy formula into a functional of the electron density. *Phys. Rev. B* **37**, 785–789 (1988).

51. Stephens, P. J., Devlin, F. J., Chabalowski, C. F. & Frisch, M. J. Ab Initio Calculation of Vibrational Absorption and Circular Dichroism Spectra Using Density Functional Force Fields. *J. Phys. Chem.* **98**, 11623–11627 (1994).

52. Edition, S., Koch, W. & Holthausen, M. C. Wolfram Koch , Max C . Holthausen A Chemist ' s Guide to. *Neural Networks* (2001).

53. Yu, X., Zhu, H. & Zeng, Y. A DFT study of Lp…π/halogen bond competition in complexes of perhalogenated alkenes with oxygen/nitrogen containing simple molecules. *Int. J. Quantum Chem.* (2016).

54. Yu, H. S., He, X., Li, S. L. & Truhlar, D. G. MN15: A Kohn-Sham global-

hybrid exchange-correlation density functional with broad accuracy for multi-reference and single-reference systems and noncovalent interactions. *Chem. Sci.* (2016).

55. Mardirossian, N. & Head-Gordon, M. ω B97M-V: A combinatorially optimized, range-separated hybrid, meta-GGA density functional with VV10 nonlocal correlation. *J. Chem. Phys.* (2016).

56. Møller, C. & Plesset, M. S. Note on an approximation treatment for many-electron systems. *Phys. Rev.* (1934).

57. Raghavachari, K., Trucks, G. W., Pople, J. A. & Head-Gordon, M. Reprint of: A fifth-order perturbation comparison of electron correlation theories. *Chem. Phys. Lett.* (2013).

58. Riplinger, C., Sandhoefer, B., Hansen, A. & Neese, F. Natural triple excitations in local coupled cluster calculations with pair natural orbitals. *J. Chem. Phys.* (2013).

59. Liakos, D. G. & Neese, F. Is It Possible to Obtain Coupled Cluster Quality Energies at near Density Functional Theory Cost? Domain-Based Local Pair Natural Orbital Coupled Cluster vs Modern Density Functional Theory. *J. Chem. Theory Comput.* (2015).

60. Datta, D., Kossmann, S. & Neese, F. Analytic energy derivatives for the calculation of the first-order molecular properties using the domain-based local pair-natural orbital coupled-cluster theory. *J. Chem. Phys.* (2016).

61. Chung, L. W. *et al.* The ONIOM Method and Its Applications. *Chem. Rev.* **115**,

5678–5796 (2015).

62. Senn, H. M. & Thiel, W. QM/MM Methods for Biomolecular Systems. *Angew. Chemie Int. Ed.* **48**, 1198–1229 (2009).

63. Maseras, F. & Morokuma, K. IMOMM: A new integratedab initio + molecular mechanics geometry optimization scheme of equilibrium structures and transition states. *J. Comput. Chem.* **16**, 1170–1179 (1995).

64. Pratihar, S., Ma, X., Homayoon, Z., Barnes, G. L. & Hase, W. L. Direct Chemical Dynamics Simulations. *J. Am. Chem. Soc.* **139**, 3570–3590 (2017).

65. Jamieson, C. S., Ohashi, M., Liu, F., Tang, Y. & Houk, K. N. The expanding world of biosynthetic pericyclases: cooperation of experiment and theory for discovery. *Nat. Prod. Rep.* (2019).

66. Swope, W. C., Andersen, H. C., Berens, P. H. & Wilson, K. R. A computer simulation method for the calculation of equilibrium constants for the formation of physical clusters of molecules: Application to small water clusters. *J. Chem. Phys.* **76**, 637–649 (1982).

Chapter 2: Radical Cation Diels-Alder Cycloaddition with Cyclopentadiene and Ethylene

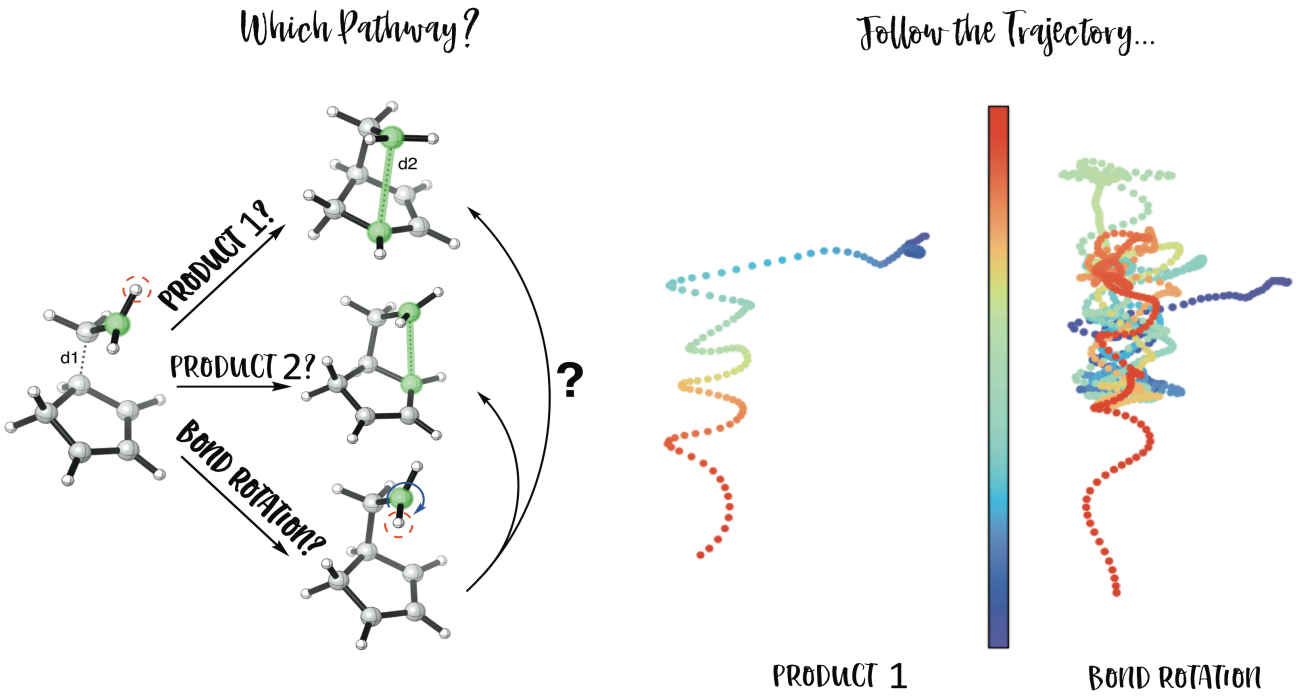

Chapter Overview

In this chapter, we apply quasi-classical trajectory calculations to study the mechanism of the radical cation Diels-Alder cycloaddition reaction. This approach relies on a description of the potential energy surface, and its gradients, computed by quantum chemistry (i.e., DFT), while also including the effects of vibrational energy and its redistribution throughout the reacting species. In contrast to a more conventional representation of the reaction coordinate that is dependent upon the assumptions of transition state theory (TST), we have been able to characterize intermediates according to their expected lifetime(s) for the first time. As these intermediates have exceptionally long lifetimes, they also describe the dynamical nature of forming different products via the same transition state, which provides a strong contrast

against "concerted" reactions. In certain cases, remarkably long lifetimes (>1000 fs) were found which led to a loss of alkene stereochemistry[1], which would correspond to erosion in the observed levels of stereoselectivity for this class of reactions.

[1] **Tan, J. S. J.; Hirvonen, V.; Paton, R. S.** ***ACS Org. Lett.*** **2018, 20 (10), 2821–2825. 'Dynamic Intermediates in the Radical Cation Diels-Alder Cycloaddition: Lifetime and Suprafacial Stereoselectivity'**

2.1 Introduction

2.1.1 Overview of DA reactions

The thermal Diels-Alder (DA) [4+2] reaction is among the most important and versatile methods in creating ring molecules, and factors governing stereoselectivity and rate have been widely studied,[2–5] with it being recognized with a Nobel Prize in the 1950s.[6] However, the chemoselectivity in products are often restricted, as electronic natures of the reactants (typically electron-rich diene and electron-poor dienophile) have to be matched. In the conventional sense of electron demand, this necessitates the use of electron-rich dienes and electron-poor dienophiles, and in the inverse sense these electronic characteristics are swapped. However, the DA cycloaddition of two electron-rich or two electron-poor reactants is a much more challenging reaction to accomplish. On the other hand, in radical chemistry, the removal of a single electron helps promote an entirely different chemical environment within the reactants[7–13] with much higher reactivity.

Experimentally, this has been demonstrated via photochemistry or redox chemistry for the reactions of mismatched electron-rich diene and dienophile partners, which would be challenging to react when using a conventional DA cycloaddition. Furthermore, this has been shown to give rise to the formation of complementary, regioisomeric products than those expected to be formed in neutral DA reactions.[14,17] For example, in **Scheme 2.1**, Yoon has pioneered the use of ambient sunlight and low catalyst loadings, to give a nearly 98% yield of the product with an opposite regiochemical preference from that of a neutral DA reaction.[14,15]

Scheme 2.1. Proposed mechanism by Yoon, where the cycloadduct was formed in 98% yield after just 1 hour of irradiation with a household fluorescent light bulb at ambient temperature.[14]

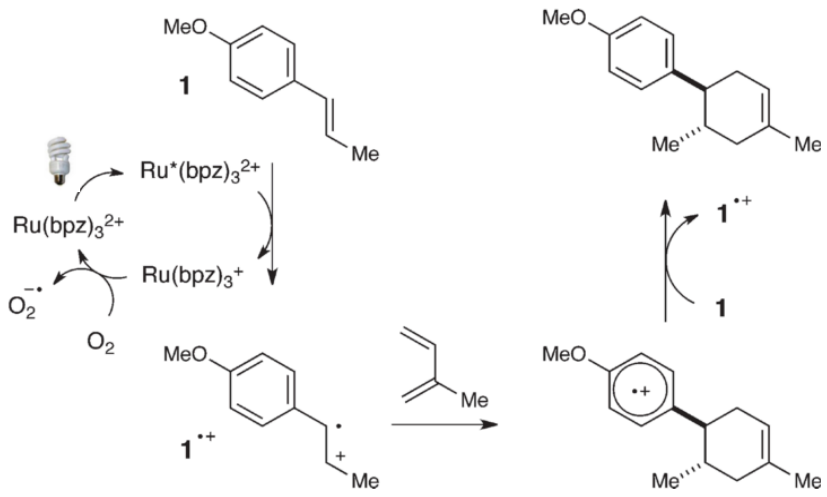

The classical (i.e., closed-shell) DA cycloaddition is widely accepted to occur via a concerted, single-step mechanism. This is supported by experimental observations of the complete transfer of alkene stereochemistry into the DA-adduct and by numerous computational and theoretical studies, notably from Houk and co-workers.[18–20] However, since the 1990s, the mechanism of DA cycloadditions of radical cations has proven to be more contentious. The involvement of both concerted and stepwise mechanistic pathways have been invoked to explain varying degrees of stereoselectivity observed in product formation. For example, while the reactions of trans-alkenes often occur with complete stereochemical integrity, the reactions of cis-alkenes tend to give a mixture of diastereomeric DA-adducts. Important theoretical contributions from Wiest[21] have recognized that the synchronous C_s-symmetric transition structure is not stable towards a pseudo-Jahn-Teller distortion, hence lying significantly higher in energy (19 kcal/mol) than the stepwise pathways. Nevertheless, differences in levels of suprafacial

stereoselectivity have driven mechanistic speculation on the possibility that both stepwise and concerted pathways can take place (**Scheme 2.2**).

Scheme 2.2. Cation Radical Diels–Alder cycloadditions (*cis*- and *trans*-anethole to cyclopenta-1,3-diene).[22]

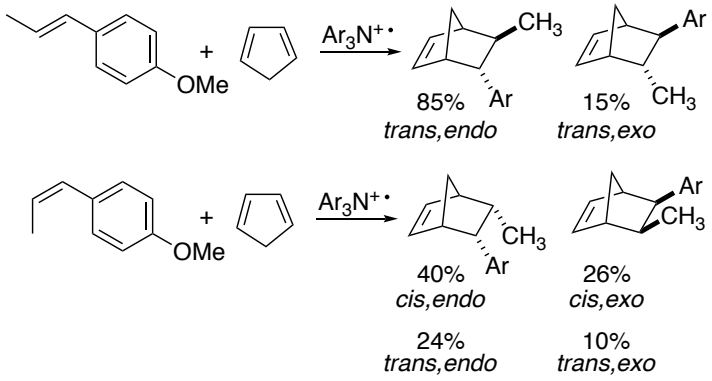

In the radical cation DA reactions of cyclopentadiene and anethole shown in **Scheme 2.2**, Bauld observed exclusive formation of the *trans*-adducts from *trans*-anethole, whereas the *cis*-diastereomer gives a mixture of all four *cis*- and *trans*-cycloadducts.[11,22] In the case of a stepwise mechanism, these results are consistent with the second C–C bond forming step (i.e., ring-closure) occurring much faster (1000-fold) than bond rotation for *trans*-alkene, while bond rotation becomes competitive for *cis*-alkene. The (less-likely) idea of a mechanistic continuum has also been alternatively proposed, with *trans*- and *cis*-isomers reacting via concerted and stepwise pathways, respectively.[18] The experimental picture suggests that there is a subtle competition between ring-closing steps and the interconversion between acyclic conformations via bond-rotations. Given the expected rates of these processes, they are extremely difficult to study via experimental means (e.g., NMR spectroscopy). In contrast, computational chemistry provides a tool to study the reactive intermediates and transition structures involved in

these processes. We set out to study this competition between bond rotation and cyclization in the radical cation DA reactions using computational tools, with the intention of addressing the outstanding stereochemical conundrums, and therefore provide useful predictions for product formation in radical cation DA cycloadditions. Given the relatively small activation barriers involved for these processes, we were aware that some of the conventional assumptions employed regarding energy redistribution along the reaction coordinate could not be taken for granted, which led us to adopt approaches based on the dynamics of individual reacting molecules, as is described in the following paragraphs.

2.1.2 Understanding bifurcating reactions

Often, organic reactions and their rates are explained in the framework of transition state theory (TST), formulated by Eyring in the 1930s (**Equation 2.1**).[23] It describes how reaction rate constants depend on the curvature of the potential energy surface (PES).

$$\mathrm{k} = \kappa \frac{k_B T}{h} e^{\frac{-\Delta G}{RT}} \qquad \textbf{(2.1)}$$

Eyring's equation shows how the rate constant k is related to the temperature T and the Gibbs free energy of activation $G^{\dagger}$. If the rate constant has been determined experimentally, Eyring's equation can be used to calculate Gibbs free energies of activation to estimate the activation barrier required for bond formation.

Despite the usefulness and many successful applications of TST, it is inherently a statistical model for which the central assumption is that all excess energy is distributed equally between all vibrational modes, and that the redistribution of energy

occurs faster than any chemical event. Expressed differently, each intermediate species has a long enough lifetime such that it is able to come into equilibrium with the surroundings (e.g., solvent), and that there is also an equilibration of energy between the various vibrational modes.

However, this assumption fails for reactions involving intermediates whose lifetimes are shorter than the timescales involved for energy redistribution. An example where this could be anticipated to occur is a reaction proceeding upon a flat potential energy surface, like that expected in the radical cation DA reaction.[21] For example, consider the case of a shallow intermediate between two transition states (TSs). After passing the first TS, if there is a very small barrier to the second TS, the intermediate can proceed straight through to the products.[24] This is not possible in statistical theory, because any additional energy is distributed between all vibrational modes; but in reality some molecules may have excess energy localized in the vibrational modes along the reaction coordinate, which helps the reaction to proceed without passing directly through the expected TS structure. In effect, the atoms' momentum gained in the first elementary step carries the reacting species through to the second energy barrier, without sufficient time available to allow heat to be lost (i.e., equilibration with the surrounding solvent) or for energy redistribution between vibrational modes.

As a consequence of TST being a statistical rate theory, the lifetimes of different chemical species and the associated rate constants of elementary reaction steps are uniquely defined by "static" descriptions of molecules and their energies. Such a picture lacks any description of the dynamical nature of said phenomenon, i.e., the time evolution. The momenta of particles are omitted as well. One other fundamental

assumption (so-called "no recrossing") behind TST is that each molecule passes through the TS only once. This is to say that once the reacting molecule(s) reach the dividing surface in phase-space (the transition state), they always carry on towards the products without ever returning back to the reactant side. This is not always the case, and recrossing is known to occur in several reactions.[20,25–28] In a dynamic sense, recrossing means that the trajectories do not cross over the saddle point (i.e., a successful reaction) but rather follow the reaction path back to reactants. This reality means that rate constants estimated by TST always provide an upper limit for the true rate of reaction, since the effect of this behavior is to reduce the overall number of successful trajectories. In the context of predicting the selectivities of organic reactions, it is typically assumed that these effects are relatively small, and may even cancel favorably, however, this is not always the case and these effects can give rise to material differences in selectivity between experiment and theory.

An additional problem with TST relates to reactions with bifurcating energy surfaces, where one TS structure leads to many different products (shown in **Figure 2.1**).[29] This occurs when two successive TSs are connected by a valley-ridge inflection point (VRI) instead of a local minimum, with this reaction mechanism being known as a "two-step no intermediate" mechanism. After passing through the VRI, the reaction paths are separated into two or more products, in which the product ratio cannot be predicted either qualitatively or quantitatively, according to TST.[30] Tantillo's group has explored extensively on these bifurcations in rearrangement reactions and they found that product distribution can be controlled with noncovalent interactions, but that

nonetheless, trajectory calculations are required to account for the levels of selectivity.[31–33]

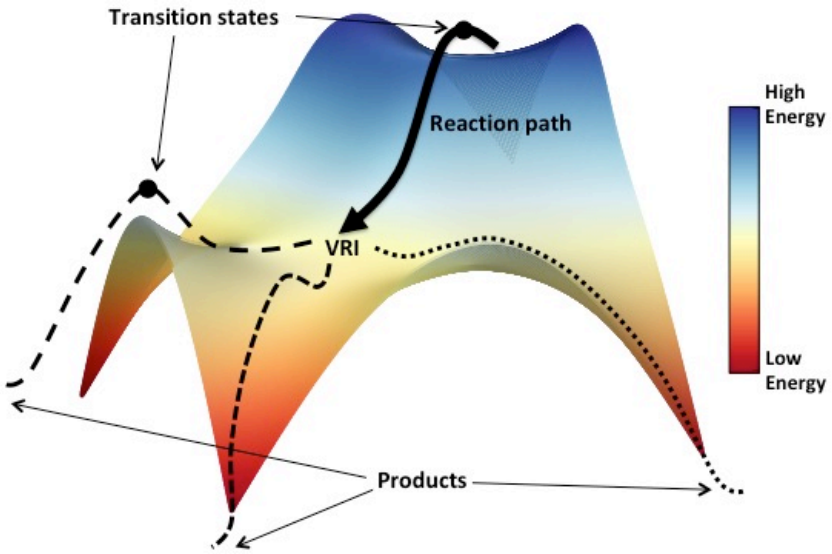

Figure 2.1. Bifurcating energy surfaces with a valley-ridge inflection point (VRI)

For this reason, one method to obtain a clearer description of chemical reactions is to couple DFT calculations (which will provide the theoretical basis for the PES of the reaction) with so called "direct" dynamics simulations.[34] In these simulations, the molecular energies and their derivatives are obtained from quantum chemical calculations, while the quasiclassical trajectories are calculated by the numerical integration of Newton's equations of motion.[35] Quasi-classical dynamics (QCD) calculations avoids the computationally expensive procedure of calculating the whole PES, and have since become a powerful tool in understanding selectivity for cases which cannot be accurately (or sometimes, even at all!) predicted with TST.[32,33,36,37] Recent studies from Houk had also shed light on the synchronicity and mechanisms of DA and ambimodal [6+4]/[4+2] cycloadditions and how different substituents and solvents influence these reactions.[34,35,38,39]

2.2 Methodology

To explore the degree of concert and stereoselectivity in the radical cation DA reaction, DFT calculations were performed with *Gaussian09*[40] using Truhlar's M06-2X hybrid meta GGA functional[41] and Pople's 6-31G(d) split valence basis set[42] to characterize the PES and to perform QCD simulations. Due to the extreme flatness of the PES of this reaction, coupled with low barrier pathways for several competing pathways, this study makes for an ideal candidate. Starting with ethylene and cyclopentadiene, we focus on events following the dynamic bottleneck, to understand the competition between C–C rotation and the formation of cycloadducts.

From benchmarking studies performed by Houk *et al.*[38,43], the M06-2X functional has been proven to yield accurate energetics specifically for cycloaddition reactions. When compared against G3B3[44], an expensive composite ab initio method derived for predicting activation energies with high accuracies, M06-2X methods were found to give small errors for activation enthalpies. By comparing M06-2X against benchmark values for the binding energies of 1744 non-covalent dimers, a root mean square deviation (RMSD) of 0.43 kcal/mol was calculated. Using a similar comparison of the barrier heights for 206 reactions, including pericyclic transformations and hydrogen transfers, gave an RMSD of 2.57 kcal/mol.[45] The B3LYP functional has also been used previously for studying quasi-classical trajectories of DA reactions, but due to systematic errors in treating π *vs.* σ bonds[46] and a lack of dispersion interactions, B3LYP activation barriers were calculated to give several kcal/mol higher than the M06-2X with the same basis set. The relative computational costs between M06-2X and B3LYP calculations are of the same order of magnitude.

Stationary points were optimized with default optimization criteria, tight self-consistent field (SCF) convergence and ultrafine grid for the numerical integration of the exchange-correlation energy and potential used in DFT calculations. Recently, this has been found to be very important for avoiding noise associated with numerical integration.[47] This effect is largely seen in the final Gibbs energy values, due to the errors in calculating the entropies of low frequency vibrations. There is expected to be a much smaller effect of this in the propagation of dynamics trajectories, which use the energy and its first derivative. Solvation by dichloromethane (CH_2Cl_2) has been employed via an implicit Solvent Model Based on Density Model (SMD).[48] Additionally, high-precision harmonic frequencies for vibrational modes were computed from the Hessian. All transition state structures (TSSs) were verified by intrinsic reaction coordinate (IRC) calculations connecting them to relevant ground state structures. Reported energies are zero-point corrected electronic energies at 298.15K, using a quasi-rigid rotor harmonic oscillator (RRHO) treatment of vibrational entropies introduced by Grimme,[49] unless otherwise stated. All spin density plots have been generated at 0.05 isovalue using *IQmol* [50]and molecular images produced using *Cylview*.[51]

The frequencies taken from the transition state optimizations were processed by *Progdyn*, an external script by Singleton,[52] at 298.15K, to give a randomized set of 150 starting structures with initial velocities, where the displacements represent that of a Boltzmann distribution. Trajectories were then propagated from these displaced starting structures using Born-Oppenheimer molecular dynamics[53,54] (BOMD) in Gaussian09 and Gaussian16, with the SMD/M06-2X gradient being calculated on the

fly at each time-step.[55] These trajectories were set to run at a stepsize of 2.5fs for 1200 steps (step lengths of 0.5 amu½ · Bohr), with force constants updated every 99 steps, alongside the ReadStop option to stop the run as soon as a C-C bond formation criterion is reached (bond lengths <1.6 Å). These settings were chosen to ensure conservation of total energy and momentum. Some trajectories were also ran using the random seed generator keyword *IOp(1/44)* with and without solvent, which gave rise to the formation of the 4-membered ring structure and the bond rotation structure, and these are not observed when running trajectories generated from *Progdyn*. We tentatively assign the origins of this behavior to the extra stabilization of charge-separated intermediates in solvent, which is a more realistic representation of the true reaction conditions.

These parameters were justified through comparison against trajectories propagated with shorter step lengths of 0.1 amu½ · Bohr (approximately 0.7 fs per step) and force constants updated every 10 steps. These calculations took more than 5 times longer to run, while the results were quantitatively indistinguishable from those described above (**Figure 2.2** and **2.3**).

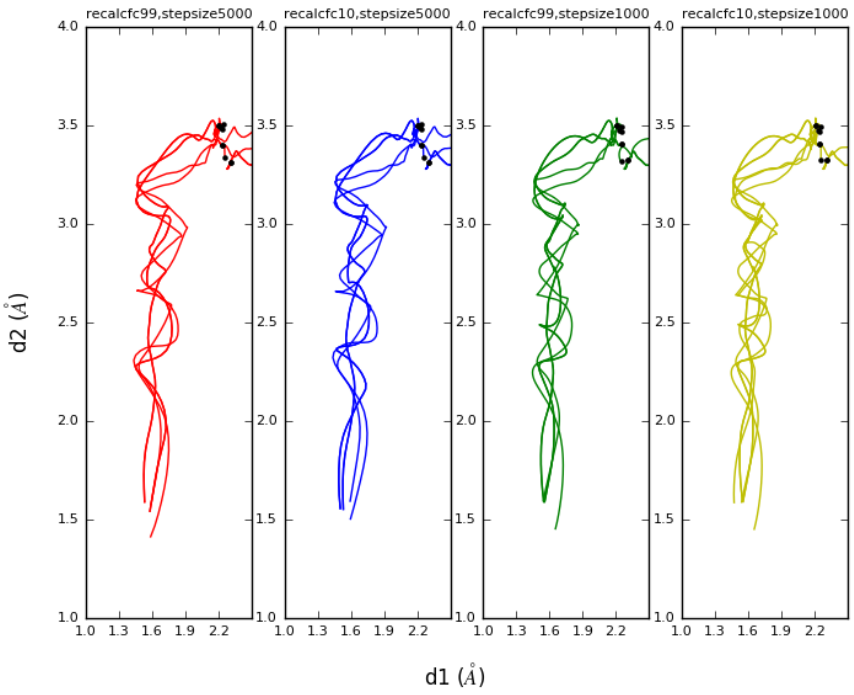

Figure 2.2. Comparison of 10 trajectories with different stepsize and recalcfc conditions (bond lengths *d1* and *d2*)

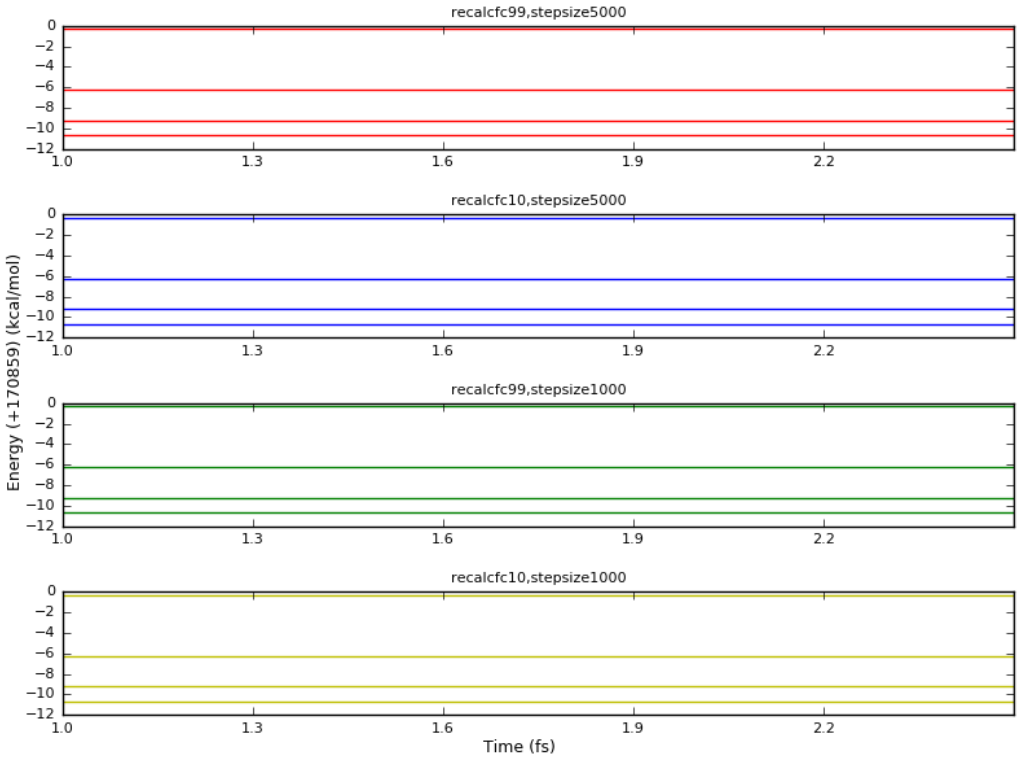

Figure 2.3. Comparison of 10 trajectories with different stepsize and recalcfc conditions (total energy conservation)

2.3 Results

2.3.1 DFT calculations

We computed pathways for the neutral and radical cation DA reactions of cyclopentadiene and ethylene (**Scheme 2.3**).[21] The reaction between cyclopentadiene **1** and ethylene **2** is a well-known example of a neutral DA reaction, resulting in the formation of norbornene **3**. Important contributions from Houk revealed the absence of diradical intermediates in neutral DA reactions such as this,[56,57] and therefore, a single transition structure exists in which bond formation is concerted. The computed activation energy in DCM solvent is high, which meant that the reaction requires elevated temperatures for product formation[8,20]. Both C1─C2 and C3─C4 bond lengths in structure **TS** are 2.23 Å.

Scheme 2.3(a) Concerted, neutral DA and **(b)** stepwise, radical cation DA reaction of ethylene and cyclopentadiene are shown at SMD-M06-2X/6-31G(d) level with Gibbs energies quoted in kcal/mol

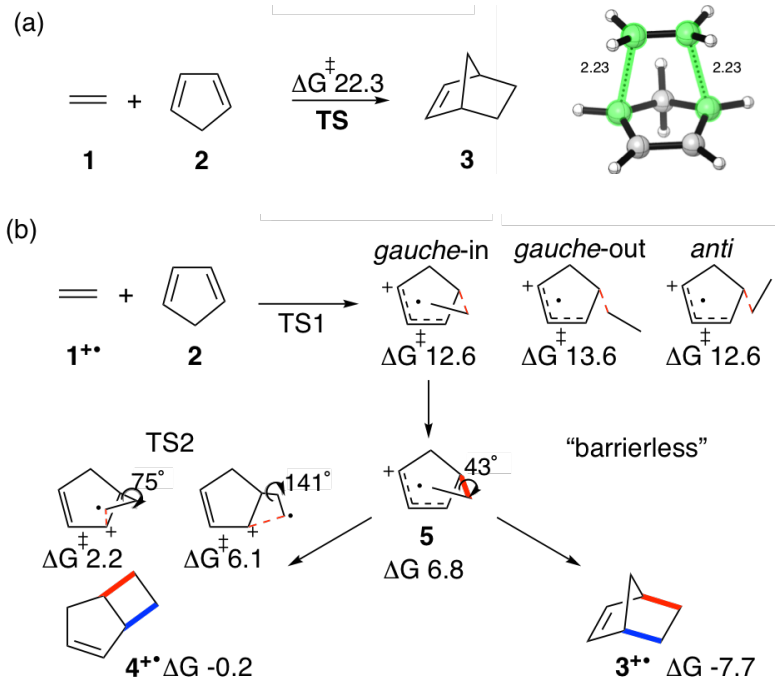

Consistent with earlier computational results for different substrates[10], we discover that the radical cation DA reaction is stepwise (**Scheme 2.3(b)**), with the intervention of an acyclic intermediate $\mathbf{5}^{+\bullet}$. This overall barrier is much lower compared to the neutral reaction, giving support that radical cation reactions can help to promote reaction reactivity. Cyclization of this intermediate can form the DA adduct $\mathbf{3}^{+\bullet}$ or four-membered bicyclo[3.2.0]hept-2-ene $\mathbf{4}^{+\bullet}$. We located three TSs ('*anti*', '*gauche-in*' and '*gauche-out*') on the PES corresponding to the first elementary step, and they differ by the rotation about the forming C─C bond. The most stable of these is *gauche-in*. Starting from the acyclic intermediate, PES scans revealed essentially no barrier toward the formation of the DA cycloadduct; no saddle point could be found. Two distinct TSs were traced corresponding to the formation of the competing 4-membered cycloadduct, and the energetically lower one lies 2.2 kcal/mol above the intermediate, due to a smaller dihedral angle. We also examined the rotation of the exocyclic C─C bond of $\mathbf{5}^{+\bullet}$, a process which would result in the loss of suprafacial stereoselectivity, and the barrier height for this rotation is 0.4 kcal/mol.

With barriers of ~0, 0.4 and 2.2 kcal/mol with respect to 6-membered ring formation, C─C rotation or 4-membered ring formation, the fate of $\mathbf{5}^{+\bullet}$ is finely balanced. As the PES is extremely flat in this region, non-TST behavior is likely to be observed. Following the IUPAC definition of an intermediate being 'a molecular entity with a lifetime substantially longer than a molecular vibration (comparable to a local potential energy minimum of depth greater than room temperature (rt))',[58] it is then questionable if $\mathbf{5}^{+\bullet}$ does indeed exist long enough to be considered a *bona fide*

intermediate. To address these concerns, we turned to quasi-classical trajectory calculations to compare both neutral and radical cationic systems and to understand the potential role of non-statistical dynamic effects in the radical cation DA reaction.

2.3.2 QCD simulations

Taking the harmonic frequencies and normal modes of **TS** and *gauche-in* **TS1**, a total of 150 initial coordinates and momenta were created using Singleton's *Progdyn* and simulated using BOMD. These structures represent a Boltzmann distribution about the TS dividing surface (**Figure 2.4**).

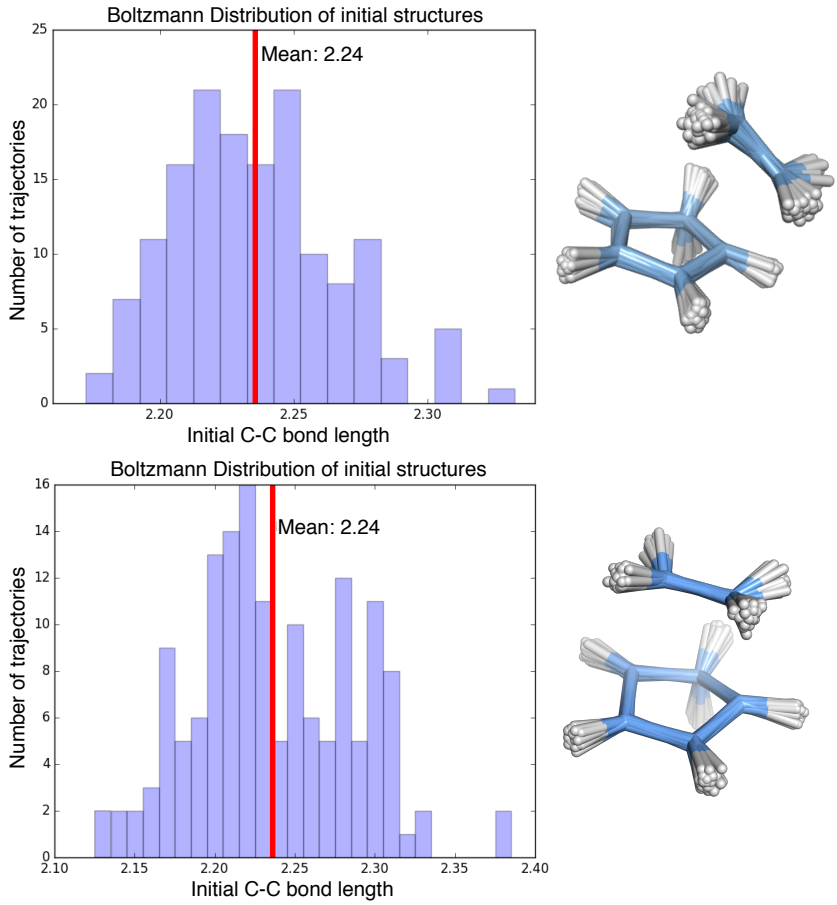

Figure 2.4. Distributions of forming C─C bond lengths for 150 initial structures. Above: radical cation TS, below: neutral TS.

The trajectories were propagated in both forward and reverse directions until either the reactants are separated by >5 Å or a cycloadduct is formed (both forming C─C bond lengths <1.6 Å). Quasi-classical trajectories are plotted in **Figure 2.5** (LHS). Out of the 150 trajectories initiated, 142 (red and brown lines) led to the formation of DA cycloadduct **3** and 8 (blue lines) recrossed back to reactants.

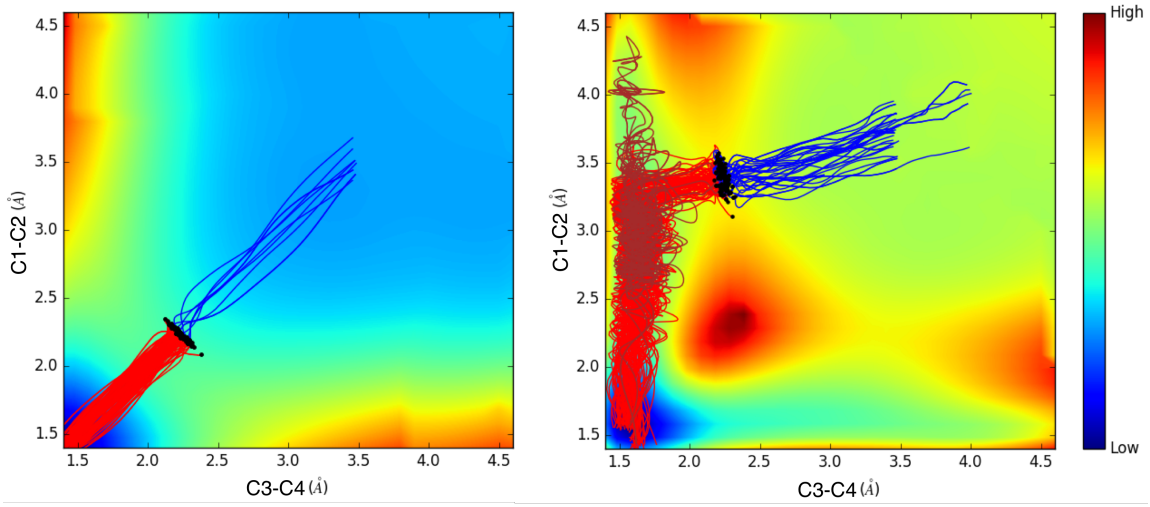

Figure 2.5. Energy contour plots (kcal/mol) for neutral (LHS) and radical cation (RHS) DA reactions, with the results of 150 trajectory simulations. Blue paths recrossed, red and brown paths formed the cycloadducts. Black dots are starting structures.

Comparing with the 150 corresponding radical cation trajectories, the extent of recrossing was more significant. 110 trajectories led to DA cycloadduct $\mathbf{3}^{+\bullet}$, while none proceeded directly to $\mathbf{4}^{+\bullet}$. A small number (4) of trajectories "roamed" for an appreciably longer time (>1000 fs). 40 trajectories recrossed back to reactants, which showed that in asynchronous reactions, recrossing could be significant.[59]

The degree to which these reactions may be considered as either stepwise or concerted can be observed through the time gaps between the two C─C bond formations. Houk

had previously presented the concept of "dynamic concert"[20] to designate reactions for which this time gap is smaller than the lifetime of a C—C bond stretch (30-60 fs). Reactions with a larger time gap could be characterized as dynamically stepwise. In our reaction, we also used the timescale of C—C bond rotation as a key quantity in governing suprafacial stereoselectivity. As the rotational barrier for the ethyl radical is extremely small (0.4 kJ/mol)[60], a suitable lower bound for the half-life of this rotation may be estimated from the TST pre-exponential factor at rt as 130 fs. With our computed barrier of 0.4 kcal/mol, we obtained a value of 220 fs. Hence, for time gaps substantially longer than these values, we expect that C—C rotation to become competitive with cyclization.

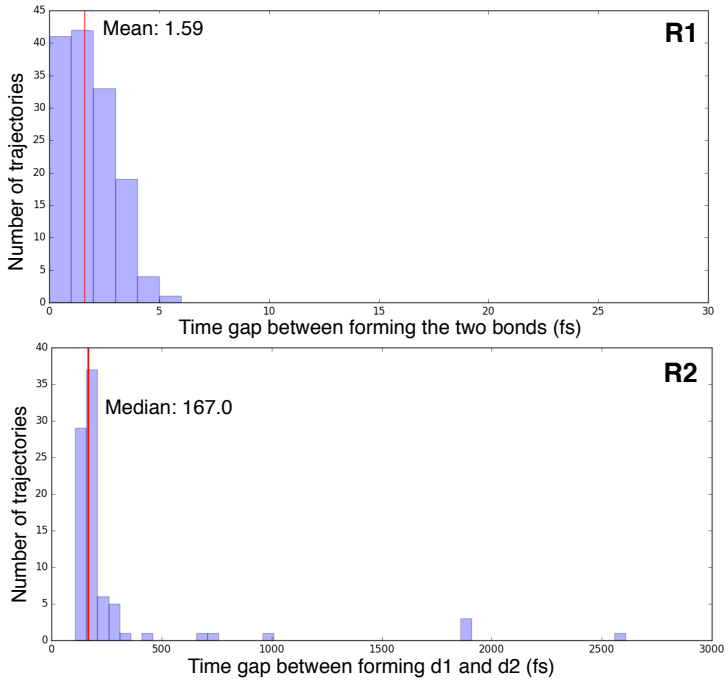

Figure 2.6. Time gaps between C—C bond formation for neutral DA and radical cation DA reactions. Note the extended x-axis of the latter.

By applying a 1.6 Å cutoff for C—C bond formation, the time gap between formation of the first and second bond is shown for both systems in **Figure 2.6**. For the neutral reaction, the bond formation times ranged from 30 to 130 fs, and the average times to form both bonds are around 50 fs (**Figure 2.7**) with an average time gap less than 2 fs (**Figure 2.8**). This reaction is dynamically concerted.

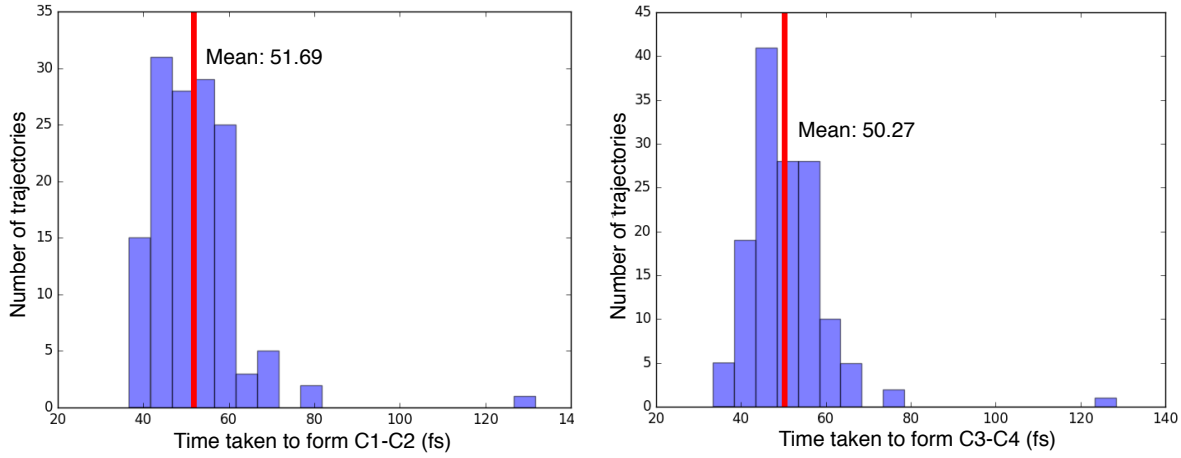

Figure 2.7. C1—C2 and C3—C4 bond forming distances for 142 trajectories

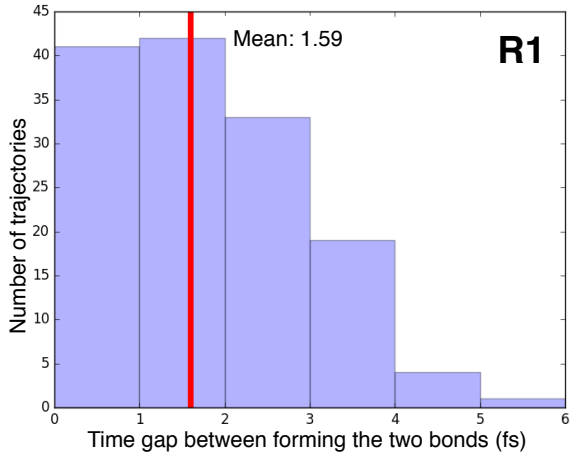

Figure 2.8. Timegap between forming two bonds for 142 trajectories

In contrast, the radical cation DA reaction gave a much greater time gap (**Figure 2.6**) with longer bond formation times and more extreme outliers that take much larger times to cyclize. Consequently, this reaction is dynamically stepwise. The median time

gap between C─C bond formation is ~167 fs. Almost 10% of the trajectories take a long time (>350 fs) for bond rotation to occur between forming the first C─C bond (*d1*) and the second C─C bond (*d2*), with 4 trajectories taking more than 1000 fs to form *d2* (~3%). **Figure 2.9** shows a range of bond formation times between 200 fs and 2700 fs for *d2*, with the average time taken for cyclization given as ~365 fs.

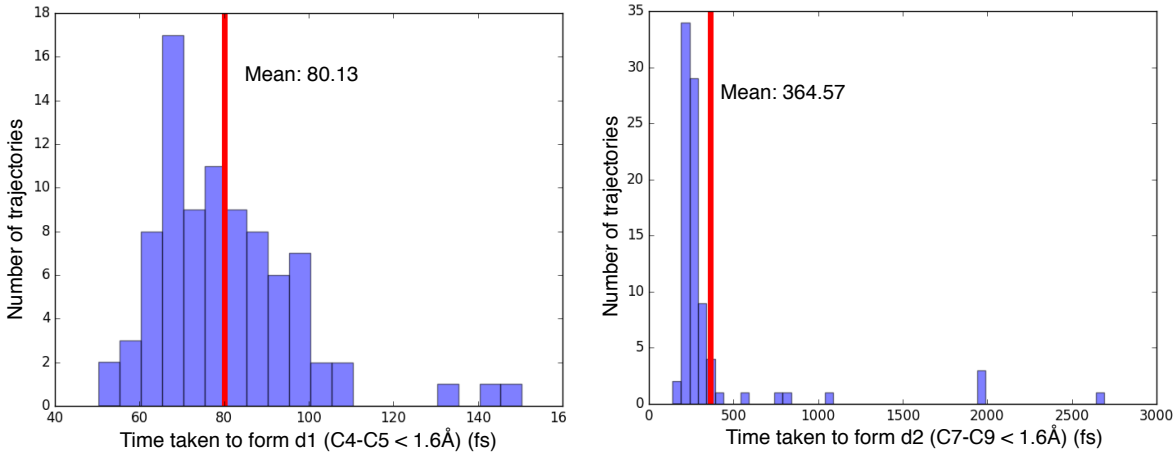

Figure 2.9. C5─C6 and C7─C9 bond forming distances (*d1* and *d2*)

The median timegap between *d1* and *d2* is also estimated in **Figure 2.10** as ~210 fs, which gave a clear indication of an intermediate, congruent with IUPAC Gold Book's definition.[58]

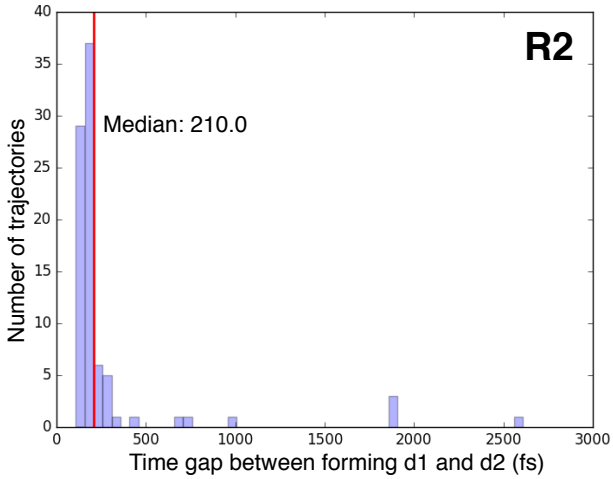

Figure 2.10. Timegap between *d1* and *d2* for 110 trajectories

Given the lack of a discernible barrier for cyclization of intermediate $\mathbf{5}^{+\bullet}$, the dynamically stepwise nature of the radical cation DA found from these trajectories is somewhat unexpected. However, as the changes in bonding are clearly dynamically separated, these results reiterate Singleton's discovery of "*dynamic intermediates*" for which the energetic definition (the exit barrier is less than RT) takes less importance.[61] Consistent with the higher barrier of 2.2 kcal/mol towards the 4-membered cycloadduct $\mathbf{4}^{+\bullet}$, this product is absent from the trajectories. The large time gap undoubtedly allows for several C—C bond stretching vibrations (30-60 fs), but we also did observe C—C bond rotation occurring in those trajectories that extended beyond 1000 fs.

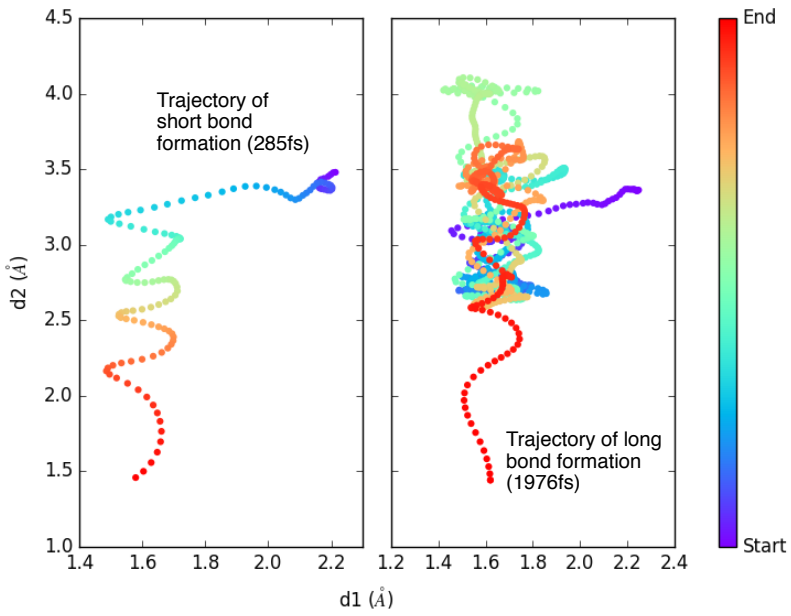

Figure 2.11. Radical cation DA adduct $\mathbf{3}^{+\bullet}$ formation. Comparison of short (LHS) and long (RHS) trajectories.

For the radical cation DA reaction, we compare the results of a typical trajectory (time gap 285 fs) with a much longer (1976 fs) in **Figure 2.11**. In the shorter trajectory, *d1* forms reasonably quickly, and the system then undergoes a series of vibrations as

motion occurs along *d2* towards cycloadduct $\mathbf{3}^{+\bullet}$. In this second stage, the shortening of the second C—C bond is continuous and no significant amount of time is spent in the acyclic conformation. The motion along the two C—C forming coordinates is hence uncorrelated. As shown in **Figure 2.5**, this shape of trajectory is most commonly observed. However, for the longer trajectory, the second C—C bond is formed while most of the time is being spent in the acyclic conformation. There are thus two distinct types of trajectories: those which cyclization occur almost immediately after the first bond is formed, taking around 170 fs on average, and those in which the acyclic intermediate is present for > 500 fs.

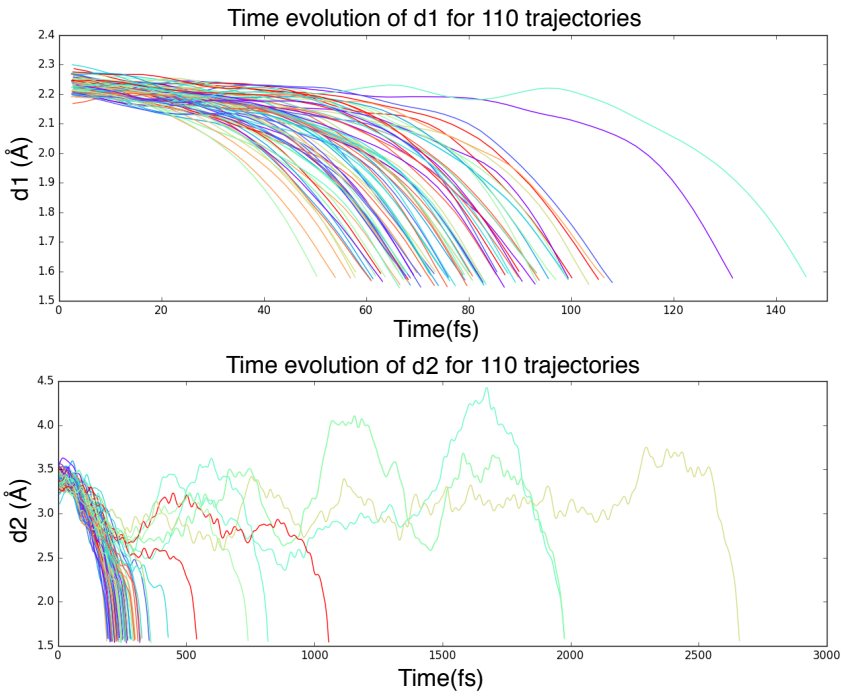

Figure 2.12. Comparison of time evolutions of *d1* and *d2*

A closer investigation of the time evolutions of *d1* and *d2* in **Figure 2.12** showed clearly that *d1* is formed readily for all trajectories, while *d2* formation is more erratic and the long trajectories displayed large changes in the *d2* bond, where the carbons

associated with forming *d2* are actually moving away from each other during the trajectory. It is in these distinctive trajectories that we measure C—C bond rotation. With distance-based criteria, we were able to identify which trajectories underwent C—C bond rotation prior to cyclization. **Scheme 2.4** provides an extension to the radical cation DA mechanism regarding bond rotation and it is clear that measuring the H8-C8 distance of the product is one method in differentiating between trajectories that led to bond rotation. This rotation will represent a loss in stereochemistry for systems with unique side groups, hence providing insight into stereochemical control.

Scheme 2.4. Bond rotation from INT, Gibbs energies quoted in kcal/mol

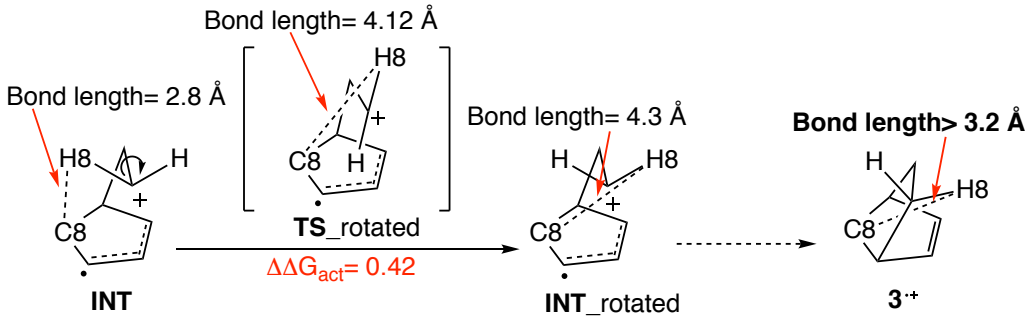

The cut-off for this distance in non-rotated products is defined as 3.2Å (**Figure 2.13**); if H8—C8 bond length > 3.2Å, it indicates that H8 is now on the other side of the C—C bridge. This was the case for all 4 long trajectories > 1000 fs. This is to be expected in light of the above value for the rotation half-life of 220 fs. In shorter trajectories, the second bond would already begin to form, preventing this rotation.

The normal bond formation trajectory is compared against the long trajectory in **Figure 2.14**. Similar to **Scheme 2.4**, on the left trajectory, the product showed a H8—C8 bond distance of ~2.8 Å, indicating that the product retains its stereochemistry due to the normal bond formation of *d2*. However, the right trajectory is more

convoluted due to bond rotation, resulting in the product having a H8—C8 bond distance of ~3.3 Å, demonstrating that H8 has flipped to the other side. The TS structure for bond rotation also gave a H8—C8 distance of 4.12 Å, which is well depicted on the right trajectory as *d2* increases to >4 Å.

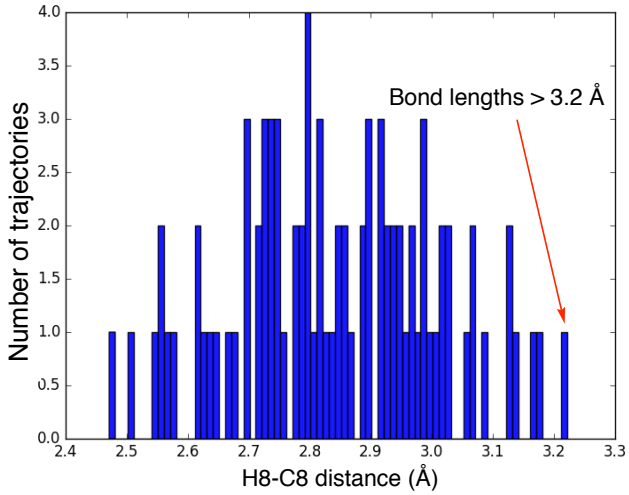

Figure 2.13. Scan of H8—C8 distances, showing a trajectory with bond rotation

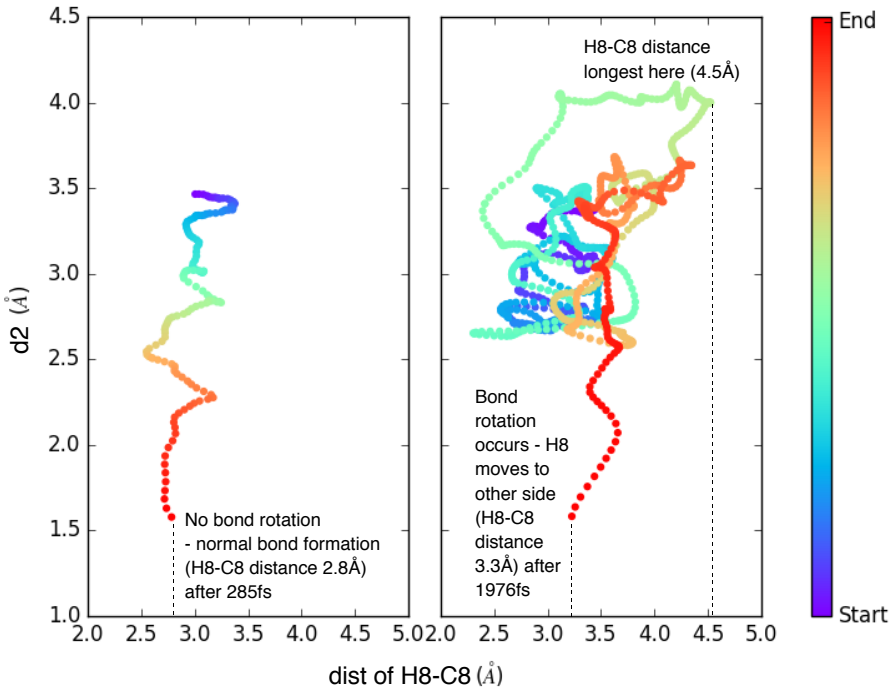

Figure 2.14. Comparison of stereoretentive trajectory (LHS) with one undergoing alkene rotation (RHS).

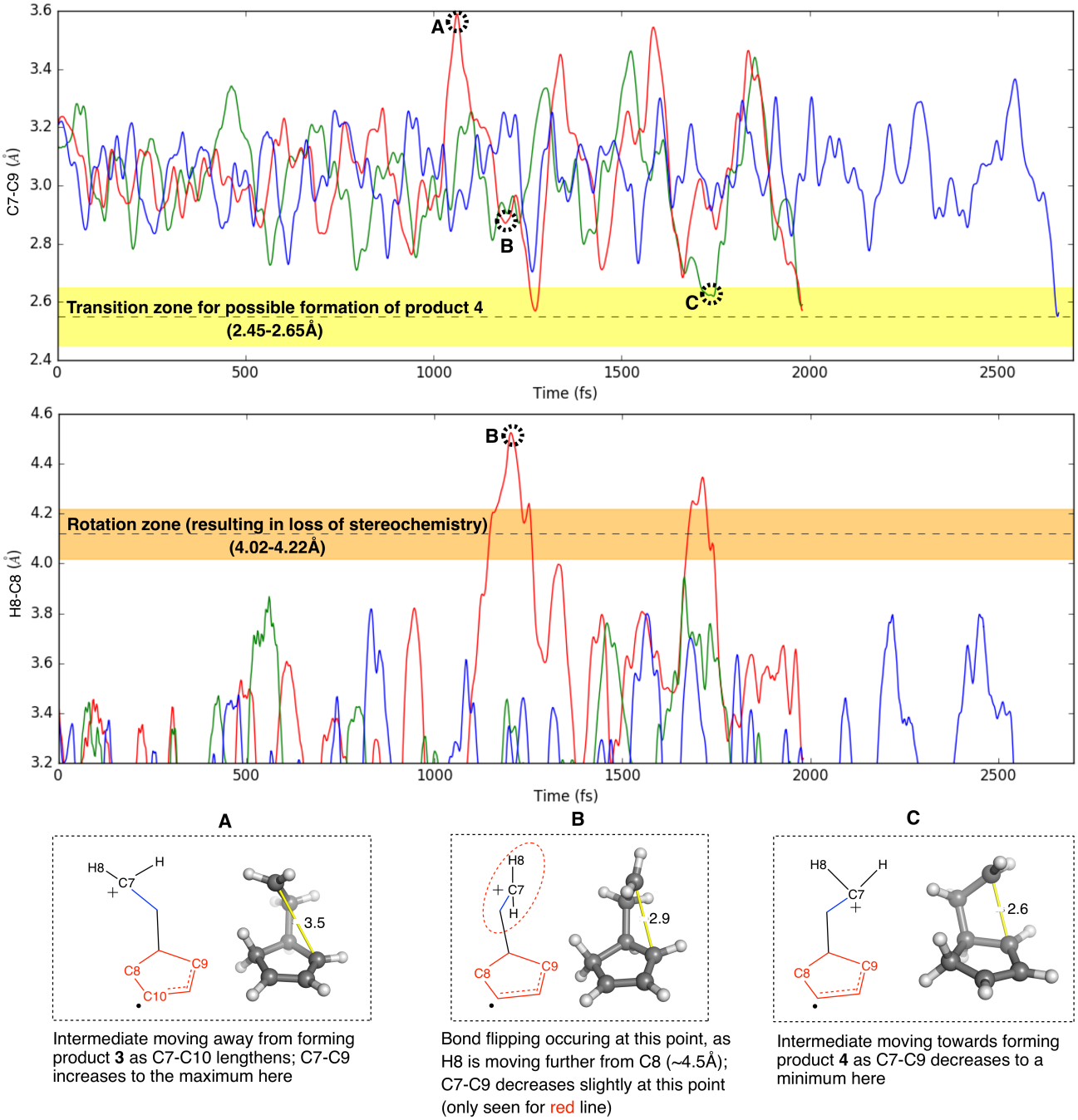

Figure 2.15. Top graph: C7—C9 distance versus time (transition zone for product $4^{+\bullet}$), bottom graph: H8—C8 distance versus time (rotation zone)

Despite not having any product 4 formation from the QCD simulations, the long trajectories display a possibility of forming the transition state leading up to product $4^{+\bullet}$, as seen in **Figure 2.15**. Three of the long trajectories are shown here, with the red line depicting bond rotation. The transition zone described in the top graph of **Figure**

2.15 is arbitrarily defined as the transition state bond length found from DFT calculations, which is 2.55 ± 0.10Å. This zone is also a region that includes more than 96% of the initial transition state geometries. Hence, the range of structures formed within this zone is considered possible TS geometries.

The top graph also drew a parallel with bond rotation in the bottom graph of H8-C8 bond distance against time. The rotation zone is arbitrarily defined as the rotation bond length found from DFT calculations, at 4.1 ± 0.1 Å, where H8 starts to get further from C8. It appeared that when the H8–C8 distance reaches a maximum, the intermediate could actually move away from forming product $\mathbf{3}^{+\bullet}$; with a possibility for product $\mathbf{4}^{+\bullet}$ formations as C7─H9 length decreases.

3% of trajectories experienced a loss of stereoselectivity and this would be experimentally measurable, as they lie in between the two extremes of *cis*- (34% rotation) and *trans*-anethole (0% rotation). It is possible that increasing the rotational barrier will help suppress the loss of stereoselectivity even with long, wandering trajectories (and vice-versa). The hypothesis of different mechanisms for these substrates is therefore superfluous.

2.4 Conclusion

Despite not finding a TS2 in terms of forming product **3** with DFT, quasi-classical simulations do show that the intermediate structure exists for a lifetime longer than a molecular vibration, which will allow for bond rotation and possibly formation of other stereoisomers. In fact, QCD do not differentiate between the 3 starting TS1es when forming product **3** or **4**. This is a key difference between DFT and quantum dynamics, as static energetics would only allow the formation of one product from the TS.

The time gap between formations of each C─C bond is longer than a molecular vibration (167 ± 42 fs for 90% of trajectories, excluding the long ones), but too short for C─C bond rotation to occur, which was found only after 1000 fs in trajectories. Compared with neutral DA reactions calculated at the same level with solvent, this time gap is 2 orders of magnitude longer in radical cation DA reactions. The "long tail" of trajectories up to 3000 fs would allow for loss of stereochemistry via rotation. This timescale is ~1000 fs, hence the reaction is dynamically stepwise.

Furthermore, recrossing can contribute substantially to the overall frequency of asynchronous and stepwise cycloadditions,[52] which is also seen in these simulations: 27% of all trajectories recross back to reactants, while only 5% of trajectories recross in the neutral DA reaction. TST doesn't account for this behaviour and the effects of recrossing to reactions are largely hidden. Direct dynamics simulations are a way to illustrate how important this effect actually is.

These simulations are therefore useful when researching reactions leading to the formation of different stereoisomers. Singleton et al found that TST fails to describe the selectivity in alkene hydroboration reactions,[59] which led to the discussion of what

actually controls selectivity. Further investigation in this field is currently ongoing with a statistically significant amount of trajectories to test if this conservation of stereochemistry is actually true in other radical cation DA reactions, or if a larger amount of trajectories lose their orientations.

In the next chapter, the dienophile is changed to a bigger molecule, and a combination of methods involving DFT and dynamics will be used to explore and contrast the differences in reactivity by this change.

References

1. Tan, J. S. J., Hirvonen, V. & Paton, R. S. Dynamic Intermediates in the Radical Cation Diels-Alder Cycloaddition: Lifetime and Suprafacial Stereoselectivity. *Org. Lett.* **20**, 2821–2825 (2018).

2. Bear, B. R., Sparks, S. M. & Shea, K. J. The Type 2 Intramolecular Diels–Alder Reaction: Synthesis and Chemistry of Bridgehead Alkenes. *Angew. Chemie Int. Ed.* **40**, 820–849 (2001).

3. Nicolaou, K. C., Snyder, S. A., Montagnon, T. & Vassilikogiannakis, G. The Diels-Alder reaction in total synthesis. *Angew. Chemie - Int. Ed.* **41**, 1668–1698 (2002).

4. Stocking, E. M. & Williams, R. M. Chemistry and Biology of Biosynthetic Diels–Alder Reactions. *Angew. Chemie Int. Ed.* **42**, 3078–3115 (2003).

5. Takao, K., Munakata, R. & Tadano, K. Recent Advances in Natural Product Synthesis by Using Intramolecular Diels-Alder Reactions. *Chem. Rev.* **105**, 4779–4807 (2005).

6. Diels, O. & Alder, K. Synthesen in der hydroaromatischen Reihe. *Justus Liebig's Ann. der Chemie* **460**, 98–122 (1928).

7. Bellville, D. J., Bauld, N. L., Pabon, R. & Gardner, S. a. Theoretical analysis of selectivity in the cation radical Diels-Alder. *J. Am. Chem. Soc.* **105**, 3584–3588 (1983).

8. Bauld, N. L., Bellville, D. J., Pabon, R., Chelsky, R. & Green, G. Cation-Radical Pericyclic Reactions. *J. Am. Chem. Soc.* **105**, 2378–2382 (1983).

9. Pabon, R. A. & Bauld, N. L. Mechanisms of hole-catalyzed reactions: ab initio

theoretical reaction paths for olefin cation radical/olefin cycloaddition. *J. Am. Chem. Soc.* **106**, 1145–1146 (1984).

10. Wiest, O., Steckhan, E. & Grein, F. Selectivity in Radical-Cation Diels-Alder Reactions of Indole and Electron-Rich Dienes: A Semiempirical Approach. *J. Org. Chem.* **57**, 4034–4037 (1992).

11. Bauld, N. L. & Yang, J. Stereospecificity and mechanism in cation radical Diels-Alder and cyclobutanation reactions. *Org. Lett.* **1**, 773–774 (1999).

12. Valley, N. A. & Wiest, O. Methyl substituent effects in radical cation Diels-Alder reactions. *J. Org. Chem.* **72**, 559–66 (2007).

13. Sevov, C. S. & Wiest, O. Selectivity in the electron transfer catalyzed Diels-Alder reaction of (R)-alpha-phellandrene and 4-methoxystyrene. *J. Org. Chem.* **73**, 7909–7915 (2008).

14. Lin, S., Ischay, M. A., Fry, C. G. & Yoon, T. P. Radical Cation Diels–Alder Cycloadditions by Visible Light Photocatalysis. *J. Am. Chem. Soc.* **133**, 19350–19353 (2011).

15. Lin, S., Padilla, C. E., Ischay, M. A. & Yoon, T. P. Visible light photocatalysis of intramolecular radical cation Diels-Alder cycloadditions. *Tetrahedron Lett.* **53**, 3073–3076 (2012).

16. Okada, Y., Yamaguchi, Y., Ozaki, A. & Chiba, K. Aromatic "Redox Tag"-Assisted Diels-Alder Reactions by Electrocatalysis. *Chem. Sci.* **7**, 6387–6393 (2016).

17. Saettel, N. J., Wiest, O., Singleton, D. A. & Meyer, M. P. Isotope effects and

the mechanism of an electron-transfer-catalyzed Diels-Alder reaction. *J. Am. Chem. Soc.* **124**, 11552–11559 (2002).

18. Chen, J. S., Houk, K. N. & Foote, C. S. Theoretical study of the concerted and stepwise mechanisms of triazolinedione Diels-Alder reactions. *J. Am. Chem. Soc.* (1998).

19. Houk, K. N., Lin, Y. T. & Brown, F. K. Evidence for the concerted mechanism of the Diels-Alder reaction of butadiene with ethylene. *J. Am. Chem. Soc.* **108**, 554–556 (1986).

20. Black, K., Liu, P., Xu, L., Doubleday, C. & Houk, K. N. Inaugural Article: Dynamics, transition states, and timing of bond formation in Diels-Alder reactions. *Proc. Natl. Acad. Sci.* **109**, 12860–12865 (2012).

21. Haberl, U., Wiest, O. & Steckhan, E. Ab initio studies of the radical cation Diels-Alder reaction. *J. Am. Chem. Soc.* **121**, 6730–6736 (1999).

22. Bauld, N. L. & Gao, D. Approaching a possible stepwise/concerted mechanistic crossover point in the cation radical cycloadditions of cis- and trans-anethole. *J. Chem. Soc. Perkin Trans. 2* 931–934 (2000).

23. Eyring, H. The Activated Complex in Chemical Reactions. *J. Chem. Phys.* **3**, 107–115 (1935).

24. Vinet, L. & Zhedanov, A. A 'missing' family of classical orthogonal polynomials. *J. Phys. A Math. Theor.* **44**, 085201 (2011).

25. Truhlar, D. G. & Garrett, B. C. Variational Transition-State Theory Gi. **235**, 440–448 (1980).

26. Mann, D. J. & Hase, W. L. Ab initio direct dynamics study of cyclopropyl radical ring-opening. *J. Am. Chem. Soc.* **124**, 3208–3209 (2002).

27. Sun, L., Hase, W. L. & Song, K. Trajectory studies of SN2 nucleophilic substitution. 8. Central barrier dynamics for gas phase Cl- + CH3Cl. *J. Am. Chem. Soc.* **123**, 5753–5756 (2001).

28. Hase, W. L., Kakhiani, K., Lourderaj, U., Hu, W. & Birney, D. Cyclohexane isomerization. Unimolecular dynamics of the twist-boat intermediate. *J. Phys. Chem. A* **113**, 4570–4580 (2009).

29. Ess, D. H. *et al.* Bifurcations on Potential Energy Surfaces of Organic Reactions. *Angew. Chem. Int. Ed.* **47**, 7592–7601 (2008).

30. Carpenter, B. K., Harvey, J. N. & Orr-Ewing, A. J. The Study of Reactive Intermediates in Condensed Phases. *J. Am. Chem. Soc.* **138**, 4695–4705 (2016).

31. Hare, S. R. & Tantillo, D. J. Cryptic post-transition state bifurcations that reduce the efficiency of lactone-forming Rh-carbenoid C–H insertions. *Chem. Sci.* **8**, 1442–1449 (2017).

32. Hare, S. R. & Tantillo, D. J. Dynamic behavior of rearranging carbocations - Implications for terpene biosynthesis. *Beilstein J. Org. Chem.* **12**, 377–390 (2016).

33. Hare, S. R., Pemberton, R. P. & Tantillo, D. J. Navigating Past a Fork in the Road: Carbocation-**π** Interactions Can Manipulate Dynamic Behavior of Reactions Facing Post-Transition-State Bifurcations. *J. Am. Chem. Soc.* **139**, 7485–7493 (2017).

34. Hase, W. L., Song, K. & Gordon, M. S. Direct dynamics simulations. *Comput. Sci. Eng.* **5**, 36–44 (2003).

35. Paranjothy, M., Sun, R., Zhuang, Y. & Hase, W. L. Direct chemical dynamics simulations: Coupling of classical and quasiclassical trajectories with electronic structure theory. *Wiley Interdiscip. Rev. Comput. Mol. Sci.* **3**, 296–316 (2013).

36. Carpenter, B. K., Harvey, J. N. & Orr-Ewing, A. J. The Study of Reactive Intermediates in Condensed Phases. *J. Am. Chem. Soc.* **138**, 4695–4705 (2016).

37. Hare, S. R. & Tantillo, D. J. Cryptic post-transition state bifurcations that reduce the efficiency of lactone-forming Rh-carbenoid C–H insertions. *Chem. Sci.* **8**, 1442–1449 (2017).

38. Yu, P. *et al.* Mechanisms and Origins of Periselectivity of the Ambimodal [6 + 4] Cycloadditions of Tropone to Dimethylfulvene. *J. Am. Chem. Soc.* **139**, 8251–8258 (2017).

39. Grayson, M. N., Yang, Z. & Houk, K. N. Chronology of CH $\cdot\cdot\cdot$ O Hydrogen Bonding from Molecular Dynamics Studies of the Phosphoric Acid-Catalyzed Allylboration of Benzaldehyde. *J. Am. Chem. Soc.* **139**, 7717–7720 (2017).

40. Schmid, M. *et al.* References. *Cytogenet. Genome Res.* **138**, 341–367 (2012).

41. Lin, H. & Truhlar, D. G. QM/MM: What have we learned, where are we, and where do we go from here? *Theor. Chem. Acc.* **117**, 185–199 (2007).

42. Hehre, W. J., Ditchfield, R. & Pople, J. A. Self-Consistent Molecular Orbital Methods. 12. Further extensions of Gaussian-type basis sets for use in molecular-orbital studies of organic-molecules. *J. Chem. Phys.* **56**, 2257–2261

(1972).

43. Lan, Y., Zou, L., Cao, Y. & Houk, K. N. Computational methods to calculate accurate activation and reaction energies of 1,3-dipolar cycloadditions of 24 1,3-dipoles. *J. Phys. Chem. A* **115**, 13906–13920 (2011).

44. Baboul, A. G., Curtiss, L. A., Redfern, P. C. & Raghavachari, K. Gaussian-3 theory using density functional geometries and zero-point energies. *J. Chem. Phys.* **110**, 7650–7657 (1999).

45. Mardirossian, N. & Head-Gordon, M. How Accurate Are the Minnesota Density Functionals for Noncovalent Interactions, Isomerization Energies, Thermochemistry, and Barrier Heights Involving Molecules Composed of Main-Group Elements? *J. Chem. Theory Comput.* **12**, 4303–4325 (2016).

46. Pieniazek, S. N., Clemente, F. R. & Houk, K. N. Sources of error in DFT computations of C-C bond formation thermochemistries: $\pi \rightarrow \sigma$ transformations and error cancellation by DFT methods. *Angew. Chemie - Int. Ed.* **47**, 7746–7749 (2008).

47. Bootsma, A. N. & Wheeler, S. Popular Integration Grids Can Result in Large Errors in DFT-Computed Free Energies. *ChemRxiv* (2019).

48. Mennucci, B., Cancès, E. & Tomasi, J. Evaluation of Solvent Effects in Isotropic and Anisotropic Dielectrics and in Ionic Solutions with a Unified Integral Equation Method: Theoretical Bases, Computational Implementation, and Numerical Applications. *J. Phys. Chem. B* **101**, 10506–10517 (1997).

49. Grimme, S. Supramolecular Binding Thermodynamics by Dispersion-Corrected

Density Functional Theory. *Chem. - A Eur. J.* **18**, 9955–9964 (2012).

50. Ghosh, D. *et al.* Effective fragment potential method in Q-CHEM: A guide for users and developers. *J. Comput. Chem.* **34**, 1060–1070 (2013).

51. Legault, C. Y. CYLview User Manual. *Comput. Programs Biomed.* **18**, 99–108 (2010).

52. Ussing, B. R., Hang, C. & Singleton, D. A. Dynamic effects on the periselectivity, rate, isotope effects, and mechanism of cycloadditions of ketenes with cyclopentadiene. *J. Am. Chem. Soc.* **128**, 7594–7607 (2006).

53. Helgaker, T., Uggerud, E. & Jensen, H. J. A. Integration of the classical equations of motion on ab initio molecular potential energy surfaces using gradients and Hessians: application to translational energy release upon fragmentation. *Chem. Phys. Lett.* **173**, 145–150 (1990).

54. Uggerud, E. & Helgaker, T. Dynamics of the reaction CH2OH+ -> CHO+ + H2. Translational energy release from ab initio trajectory calculations. *J. Am. Chem. Soc.* **114**, 4265–4268 (1992).

55. Gaussian 16, Revision A.03, M. J. Frisch, G. W. Trucks, H. B. Schlegel, G. E. Scuseria, M. A. Robb, J. R. Cheeseman, G. Scalmani, V. Barone, G. A. Petersson, H. Nakatsuji, X. Li, M. Caricato, A. V. Marenich, J. Bloino, B. G. Janesko, R. Gomperts, B. Mennu, 2016. Gaussian 16. *Gaussian, Inc. Wallingford CT,* (2016).

56. Houk, K. N., Loncharich, R. J., Blake, J. F. & J, W. L. J. Substituent Effects and Transition Structures for Diels-Alder Reactions of Butadiene and

Cyclopentadiene with Cyanoalkenes. *J. Am. Chem. Soc.* **84**, 9172–9176 (1989).

57. Houk, K. N., Li, Y. & Evanseck, J. D. Transition Structures of Hydrocarbon Pericyclic Reactions. *Angew. Chem. Int. Ed.* **31**, 682–708 (1992).

58. intermediate. in *IUPAC Compendium of Chemical Terminology* **1077**, 3096 (IUPAC, 2014).

59. Oyola, Y. & Singleton, D. A. Dynamics and the failure of transition state theory in alkene hydroboration. *J. Am. Chem. Soc.* **131**, 3130–3131 (2009).

60. Yamada, K., Kawashima, Y. & Tachikawa, M. Accurate prediction of hyperfine coupling constants in muoniated and hydrogenated ethyl radicals: Ab initio path integral simulation study with density functional theory method. *J. Chem. Theory Comput.* **10**, 2005–2015 (2014).

61. Yu, P. *et al.* Mechanisms and Origins of Periselectivity of the Ambimodal [6 + 4] Cycloadditions of Tropone to Dimethylfulvene. *J. Am. Chem. Soc.* **139**, 8251–8258 (2017).

Appendix

I. Absolute energies and Cartesian coordinates of transition structures

R1	M06-2X/6-31G(d) in dichloromethane (SMD)					
	E/au	ZPE/au	H/au	T.qh-S/au	qh-G(T)/au	imag. ν
Ethene	-78.539256	0.051656	-78.483622	0.025503	-78.509126	-
Cp	-194.013473	0.093663	-193.914729	0.031683	-193.946412	-
CPX	-272.557058	0.146792	-272.400713	0.042567	-272.443280	-
TS	-272.527576	0.149173	-272.371424	0.036340	-272.407764	-491.44
PDT	-272.606637	0.154786	-272.445732	0.034626	-272.480358	-

R2	M06-2X/6-31g* in dichloromethane (SMD)					
	E/au	ZPE/au	H/au	T.qh-S/au	qh-G(T)/au	imag. ν
ethene radical	-78.271647	0.049609	-78.218105	0.02619	-78.244295	-
cp	-194.013473	0.093663	-193.914729	0.031683	-193.946412	-
ethene	-78.539256	0.051656	-78.483622	0.025503	-78.509126	-
cp radical	-193.796372	0.09344	-193.697679	0.032679	-193.730358	-
CPX_gauche-in	-272.341202	0.146517	-272.184882	0.043731	-272.228612	-
CPX_anti	-272.341346	0.146609	-272.184989	0.043571	-272.22856	-
CPX_gauche-out	-272.341185	0.146509	-272.184891	0.043677	-272.228568	-
TS1_gauche-in	-272.335328	0.147551	-272.179659	0.039741	-272.2194	281.32
TS1_anti	-272.335909	0.148078	-272.179862	0.039477	-272.219339	-219.63
TS1_gauche-out	-272.334313	0.148063	-272.178278	0.03947	-272.217749	-260.52
TS_rotated	-272.343657	0.147473	-272.188493	0.038694	-272.227187	-165.48
INT_gauche-in	-272.343824	0.14775	-272.187641	0.040208	-272.227849	-
INT_anti	-272.344263	0.147855	-272.18796	0.040239	-272.2282	-
INT_gauche-out	-272.344429	0.147682	-272.188204	0.040474	-272.228678	-
INT_rotated	-272.343824	0.147735	-272.187649	0.040229	-272.227878	-
TS2a	-	-	-	-	-	-
TS2b	-272.342458	0.148575	-272.186573	0.037855	-272.224428	-198.00
TS2c	-272.337296	0.148869	-272.181208	0.037695	-272.218903	-222.21
PDT **(3)**	-272.606637	0.154786	-272.445732	0.034626	-272.480358	-
PDT **(4)**	-272.593386	0.153446	-272.433293	0.035886	-272.46918	-

uM062x/6-31G(d) opt=(ts, noeigen, calcfc) freq SCRF(SMD, solvent=dichloromethane) SCF=(tight, nosym) Int=UltraFine

(neutral DA)

TS

C	-0.45894	1.15406	0.36191
C	-1.18026	0.70334	-0.73981
C	-1.18039	-0.70341	-0.73962
C	-0.45915	-1.15404	0.36226
H	-0.38931	2.19217	0.67059
H	-1.55996	1.32982	-1.54022
H	-1.56030	-1.33004	-1.53981
H	-0.39011	-2.19207	0.67119
C	-0.36074	0.00018	1.32366
H	0.50664	0.00021	1.98471
H	-1.27049	0.00040	1.94611
C	1.61026	0.69015	-0.33759

H	2.04152	1.23868	0.49497
H	1.54620	1.24053	-1.26996
C	1.61039	-0.69031	-0.33774
H	2.04231	-1.23916	0.49433
H	1.54643	-1.24038	-1.27031

(radical cation DA)

TS1_gauche-in

C	0.02159	0.26963	-1.02967
C	0.63930	1.24673	-0.22023
C	1.49569	0.62014	0.70954
C	1.49369	-0.73633	0.47330
H	-0.46098	0.49141	-1.97454
H	0.45763	2.31271	-0.29534
H	2.06168	1.12929	1.47925
H	2.04384	-1.47984	1.03808
C	0.66056	-1.05374	-0.72047
H	-0.02646	-1.89281	-0.58658
H	1.32137	-1.32305	-1.55995
C	-2.05382	0.18268	-0.20738
H	-2.37663	-0.45648	-1.02460
H	-2.20824	1.25091	-0.32986
C	-1.82231	-0.34607	1.02544
H	-1.80798	-1.41928	1.18940
H	-1.61241	0.28889	1.88091

TS1_anti

C	-0.10996	-0.06660	0.83114
C	0.76221	-1.12091	0.47902
C	1.80202	-0.63067	-0.34783
C	1.67087	0.72952	-0.46886
H	-0.75617	-0.11053	1.69903
H	0.63575	-2.15240	0.78731
H	2.58006	-1.23794	-0.79283
H	2.31384	1.38200	-1.04765
C	0.51354	1.21466	0.33797
H	-0.15632	1.88078	-0.21373
H	0.87709	1.78736	1.20452
C	-1.58143	-0.55252	-0.64974
H	-1.65387	-1.62304	-0.48216
H	-0.96230	-0.22690	-1.48217
C	-2.55775	0.27122	-0.15292
H	-3.28308	-0.09224	0.56792
H	-2.59198	1.32466	-0.41293

TS1_gauche-out

C	0.05793	-0.21942	0.82407
C	-0.38137	1.08600	0.51677
C	-1.51971	1.03144	-0.31932
C	-1.87533	-0.28296	-0.50018
H	0.67473	-0.45290	1.68342
H	0.10467	1.99335	0.85771
H	-2.02550	1.89151	-0.73938
H	-2.69630	-0.64258	-1.10927
C	-0.97544	-1.17578	0.28180
H	-0.58836	-2.02251	-0.29218
H	-1.52572	-1.60592	1.13303
C	1.63846	-0.54273	-0.58989
H	1.01258	-0.30223	-1.44568
H	1.71811	-1.59158	-0.31889
C	2.61125	0.32787	-0.17832
H	2.64675	1.34879	-0.54575
H	3.34429	0.03750	0.56737

TS_rotated

C	0.25705	0.18147	-0.82905
C	-0.46366	-1.07456	-0.53913
C	-1.58980	-0.87872	0.24447
C	-1.68044	0.47986	0.50670
H	0.24815	0.33157	-1.91875
H	-0.12451	-2.04078	-0.90570
H	-2.27304	-1.64369	0.58883
H	-2.46939	0.94260	1.09354
C	-0.58702	1.24246	-0.11532
H	-0.03540	1.80553	0.65141
H	-1.00561	2.00041	-0.79314
C	1.73579	0.09534	-0.38084
H	2.21239	1.05800	-0.61559
H	2.24085	-0.64909	-1.01032
C	1.88041	-0.24590	1.06068
H	2.86812	-0.32114	1.49851
H	1.02453	-0.28311	1.72607

TS2b

C	-0.28299	0.50006	0.71987
C	0.21758	-0.90634	0.70581
C	1.43100	-1.02893	0.03011
C	1.76719	0.21665	-0.45703
H	-0.24591	0.89800	1.74281
H	-0.28496	-1.71221	1.23441
H	2.00366	-1.93928	-0.08964
H	2.68303	0.44001	-0.99744
C	0.72988	1.23116	-0.17600
H	0.28411	1.55351	-1.13071
H	1.16137	2.13318	0.27274
C	-1.72883	0.42258	0.19687
H	-2.06373	1.40527	-0.16349
H	-2.39229	0.12091	1.01038

C	-1.72462	-0.61213	-0.88291	H	-1.45352	2.24192	-0.41159
H	-1.10046	-0.47051	-1.75995	H	-2.73536	0.02804	-1.01333
H	-2.49998	-1.36716	-0.93947	C	-1.13650	-1.12884	0.09833
				H	-1.02729	-1.93004	-0.64028
TS2c				H	-1.77723	-1.52647	0.89934
C	0.18617	-0.57662	0.64444	C	1.35270	-0.75619	-0.36618
C	-0.02601	0.90500	0.62509	H	0.92153	-0.84983	-1.36716
C	-1.13166	1.23917	-0.16280	H	1.91881	-1.67342	-0.15399
C	-1.79638	0.07288	-0.46886	C	2.20113	0.47142	-0.30282
H	0.46178	-0.94208	1.63653	H	2.58005	0.93037	-1.20876
H	0.53701	1.61324	1.22406	H	2.67752	0.74729	0.63193

II. Sample input BOMD calculation

#uM062X/6-31G(d) SCRF(SMD, solvent=dichloromethane) geom=crowd
BOMD=(readstop, maxpoints=1200, recalcfc=99, rtemp=300, stepsize=5000, readvelocity)

Cartesian coordinates from Progdyn

1 2
C 0.0145210 0.2909864 -1.0524406
C 0.5999745 1.2405723 -0.2479957
C 1.4751708 0.6362996 0.7170793
C 1.4852997 -0.7388993 0.4832679
H -0.4949639 0.5142388 -2.0020842
H 0.4703332 2.3464140 -0.2796783
H 2.2617704 1.0545169 1.4393743
H 2.1406690 -1.4819730 1.0958411
C 0.6286538 -1.0884536 -0.6510167
H -0.0105365 -1.9420100 -0.5633474
H 1.3059457 -1.4597696 -1.4403721
C -2.0706620 0.1591107 -0.2202373
H -2.3271523 -0.5010115 -1.0523393
H -2.2531421 1.2846768 -0.3329432
C -1.7534548 -0.3020682 0.9969079
H -1.6185565 -1.4074336 1.2331893
H -1.4237454 0.3263452 1.7553934

2 #stopping conditions for reaction
1, 1, 1, 1, 1, 1, 1, 1, 1, 1, 1, 2, 2, 2, 2, 2, 2
1, 1, 1, 1, 1, 1, 1, 1, 1, 1, 1, 1, 1, 1, 1, 1, 1
0, 0, 0, 0, 0, 1, 1, 12, 6.50
0, 0, 0, 0, 0, 0, 4, 15, 2.75
#initial velocities for propagation (from Progdyn)
-813263976000.000000 4448598084000.000000 7342840512000.000000
-2665204668000.000000 -6483938328000.000000 5611869648000.000000
-3441297636000.000000 1138430916000.000000 -7698298860000.000000
-163464588000.000000 -2650778676000.000000 475687296000.000000
20012671728000.000000 -34173460440000.000000 -3220144956000.000000
2394661752000.000000 39887566236000.000000 -10535636412000.000000

-15542932104000.000000 -6184352916000.000000 -35304471972000.000000
-11900522592000.000000 27420074640000.000000 -20743962624000.000000
4159025135999.999512 -1898250984000.000000 -2563921080000.000000
6147298332000.000000 46595922408000.000000 4524099048000.000000
-1923192180000.000000 2996272188000.000000 26427179016000.000000
4440691836000.000000 -4808522880000.000000 8488341540000.000000
-26883545220000.000000 -4147509744000.000000 -32896760148000.000000
14965183296000.000000 3159964332000.000000 3416060088000.000000
805050792000.000000 6157929960000.000000 -5391918252000.000000
-10929562308000.000000 -33499645956000.003906 -7263756864000.000000
-4349711772000.000000 7673294160000.000000 32625179999.999996

III. Usage of Progdyn script

First step: **Python extractout.py**. Run this command in the "out.txt" directory, which contains all the Gaussian output files.
Second step: **./sampling.sh**

extractout.py:

```
import glob

lookup1 = 'Input orientation:'
lookup2 = 'Harmonic frequencies (cm**-1), IR intensities (KM/Mole), Raman scattering'

filename= ' *.out'
for out in glob.glob(filename):
        NUM_1=1
        NUM_2=1

        with open(out) as myFile:
                for num, line in enumerate(myFile, 1):
                        if lookup1 in line: NUM_1=num
                        if lookup2 in line: NUM_2=num

        fileout=open(out+'.txt','w')
        with open(out) as myFile:
                for num, line in enumerate(myFile, 1):
                        if num >= NUM_1 and num <= NUM_2 : fileout.write(line)
                        if num > NUM_2 : break
```

sampling.sh:

```
mkdir g09_NC
for i in {1..150}       #to generate 160 geoPlusVel files
do
        if (test -f ./out.txt/TS_NC.out.txt) then
                sh g09.sh ./out.txt/TS_NC.out.txt
                mv geoPlusVel ./g09_NC/geoPlusVel_1$i
```

```
        fi
done
```

g09.sh:

```
mkdir used
origdir=./
randdir=~/bin
proggramdir=~/program/
#freqfile=$1
# B1B1B1B1B1B1B1B1B1B1B1B1B1B1B1B1B1B1B1B1B1B1B1B1B1B1B1B1B1B1B1B1B1B1 generate geoPlusVel and first input file
echo 3 > runpointnumber
$randdir/randgen > temp811
# the next 8 lines would have to be changed to use low-precision modes
awk '/A A A A A/,/Harmonic frequencies/ {print}' $freqfile > temp401
awk '/Frequencies --/ {print $3;print $4;print $5;print $6;print $7}' temp401 > tempfreqs
awk '/Reduced masses/ {print $4;print $5;print $6;print $7;print $8}' temp401 > tempredmass
awk '/Force constants/ {print $4;print $5;print $6;print $7;print $8}' temp401 > tempfrc
mv tempfreqs tempfreqs_1
mv tempfrc tempfrc_1
python revisefreq.py
awk '/0/ && ((length($1) < 2) && ($1 < 4)) {print}' temp401 > tempmodes
awk '/has atomic number/ {print}' $freqfile > tempmasses
awk '/Input orientation:/,/tional const/ {if ( $2 < 50 && $2 > 0) print}' $freqfile > tempstangeos
awk -f $proggramdir/proggenHP ' $freqfile > geoPlusVel

if (test -f isomernumber) then
        cp isomernumber temp533
        awk 'BEGIN {getline;i=$1+1;print i,"----trajectory isomer number----"}' temp533 > isomernumber
        rm temp533
else
        echo "1 ----trajectory isomer number----" > isomernumber
fi
```

revisefreq.py:

```
import sys
import os
from numpy import *
import numpy as np
datain=np.genfromtxt('tempfreqs_1')
datain1=np.genfromtxt('tempfrc_1')
fileout=open('./tempfreqs','w')
fileout1=open('./tempfrc','w')
num=len(datain)
for i in range(0,num):
```

```
        if datain[i]<100 and datain[i]>0 :
                datain1[i]=datain1[i]*(100/datain[i])*(100/datain[i])
                datain[i]=100
        fileout1.write(str(datain1[i])+'\n')
        fileout.write(str(datain[i])+'\n')
fileout.close()
fileout1.close()
```

Chapter 3: Radical Cation Diels-Alder Cycloaddition with Cyclopentadiene and Anethole

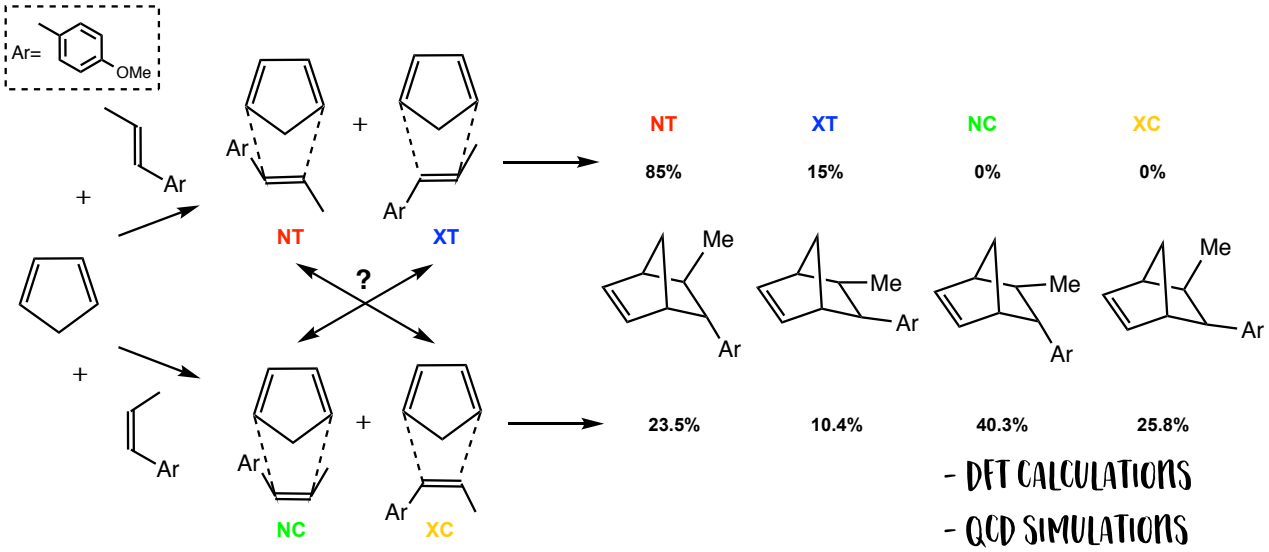

Radical cation DA reaction of *cis*- and *trans*-anethole to Cp (NT=endo trans, XT=exo trans, XC=exo cis, NC=endo cis)

Chapter Overview

Synthetic radical chemistry, often supported by electron transfer via photoredox catalysis, has captured the attention of chemists in recent years. However, despite its successful methodology in many areas of research, product stereoselectivity has not been clearly understood. In this Chapter, the stereoselectivity of the radical cation Diels-Alder reaction of Cp and anethole is fully investigated with an intense study of Density Functional Theory (DFT) calculations, Quasi-classical dynamics (QCD) simulations and kinetics rate theory. Combinatorial employment of these methods was able to provide evidence of reversibility from neutral products based on the reactants used.

3.1 Introduction

3.1.1 Overview of combinatorial efforts in radical cation DA reactions

As mentioned in Chapter 2, in standard DA reactions, reactivity is most often optimal between an electron-rich diene and an electron-poor dienophile. However, this electronic prerequisite also represents the greatest limitation of the reaction. Instead, the radical cation DA reaction creates a new pathway for reactants without this electronic prerequisite, and research groups began to explore this transformation with much success in the 1980s.[1–4] In fact, the first report known to us came from Bauld's group in 1981 (**Scheme 3.1**), where they performed the dimerization of cyclohexadiene with 3-5% of the radical cation catalyst tris(p-bromophenyl)aminium hexachlorostibnate, for 15 minutes at 0 °C, giving rise to 70% yield.[5]

Scheme 3.1. First report of radical cation DA by Bauld in 1981

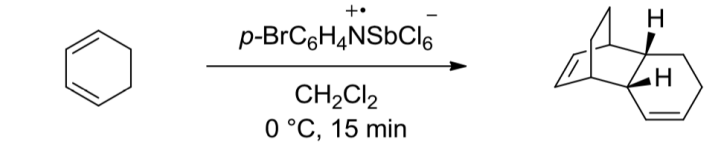

Bauld, *J. Am. Chem. Soc.* **1981**, *103,* 718 70%
5:1 endo:exo

This discovery is significant, as compared against uncatalysed circumstances, the thermal [4+2] cycloaddition of cyclohexadiene only gave 30% yield after a 20h reaction at 200 °C. Bauld also explored the reason for the dienophile being oxidised rather than the diene and using frontier molecular theory (FMO) theory, showed that the [3+2] reaction between a radical cation diene with a neutral dienophile is symmetry forbidden.[6]

Since then, much experimental and computational work had been done to investigate and understand the mechanistic details of the radical cation DA reaction.[7–12] A notable example by the Wiest group[13] closely examined three possible mechanisms of the radical cation DA system of 1,3-butadiene and ethylene using DFT and quadratic CI (QCI) methods. It is

predicted that the transition states (TSs) and intermediates of the neutral and the radical cationic pathway should be related to each other, with experimental support for this coming from finding the cyclohexane-1,4-diyl radical cation intermediate by electron spin resonance (ESR) after oxidation of 1,5 hexadiene.[14]

Scheme 3.2. Proposed mechanism for radical cation DA cycloaddition by visible light photo catalysis

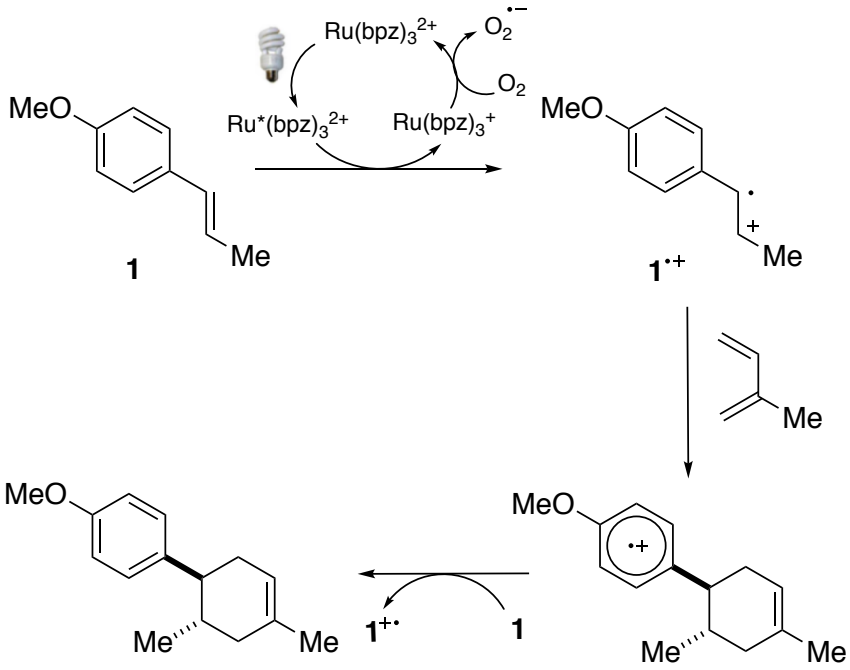

More recently, the use of photoredox catalysis has allowed for new methodology in C—H activation[15] and increasingly, DA-type reactions.[16,17] Specifically, the radical cation DA reaction of anethole 1 was performed using a ruthenium polypyridyl photocatalyst by the Yoon lab (**Scheme 3.2**).[9] The desired cycloadducts were obtained in excellent yields with low loadings of $Ru(bpz)_3(BArF)_2$ photo-activated in air. Interestingly, this radical cation DA process reversed the overall regiochemical preference formed by the products of the neutral cycloaddition, which would not have proceeded under normal circumstances due to the use of two electron-rich reactants, i.e. the minor product in the neutral DA reaction is now the major product in the radical cation DA reaction. The product selectivity here is

not well understood and additional research is necessary to describe the dynamic factors behind such a product distribution.

3.1.2 Introducing dynamics into the picture

Carpenter first published a set of reports regarding trajectory calculations over PESs and their implications on the stereochemistry of biradical type reactions.[18–20] He proposed an alternative computational method using molecular dynamics (MD) and presented the idea of dynamic matching: where after crossing a TS, the momentum of atoms directs the selectivity from a shallow intermediate. He compared the kinetic model of transition state theory (TST) against this nonstatistical dynamic model for the cyclopropane stereomutation and concluded that predictions from TST alone cannot explain experimental findings.[21,22] With this, he also challenged the framework of concerted and stepwise mechanisms by suggesting that instead of two different mechanisms occurring on two different parts of the PES, there could be two different dynamic populations occupying the same space of the PES.

Building upon this, Singleton's group[23] described a combined experimental and computational study of hetero DA reaction of acrolein and methyl vinyl ketone via QCD trajectories[24–26]. They found that the results not only accurately predict the experimental ratio, but that non-statistical recrossing also plays a substantial role. Recent attention has focused on dynamics in reactions where regioselectivity is not properly understood[27–29] and are essential even in exploring C—H activation reactions.[30] In Chapter 2, a sample radical cation DA system with an essentially flat PES has also been studied using both DFT and QCD methods to investigate the role of dynamic intermediates in product stereoselectivity,

and found that carbocation lifetimes that exceed 1000 fs meant a loss of stereochemical information.[31]

3.1.3 Model of interest

In 2000, Bauld and Gao studied the mechanism of the reaction at 0°C between Cp to *cis*- and *trans*-anethole, respectively (**Scheme 3.3**)[32]. They concluded that the dienophile was going through a stepwise mechanism when all four diastereomeric products were found in comparable amounts in the reaction mixture from *cis*-anethole and Cp. However, no *cis*-products are found from the reaction of *trans*-anethole and Cp. They also asserted that an intermediate formed during the stepwise mechanism could undergo bond rotation at a comparable rate to cyclization.

Scheme 3.3. Radical cation DA between *cis*- and *trans*-anethole with Cp

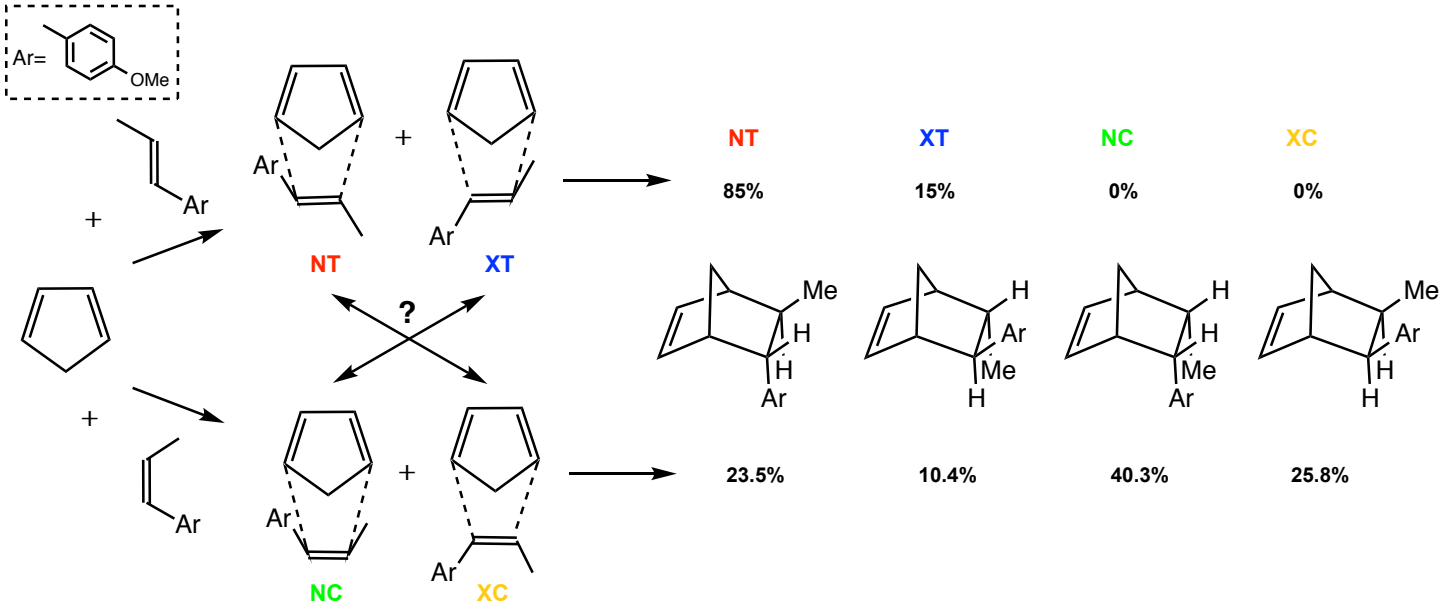

Nonetheless, this raises questions regarding the stability of the intermediate formed, which would allow time for rotation in this radical cation DA reaction, and therefore to be rigorous, this Chapter aims to perform a complete analysis combining DFT calculations, QCD simulations and kinetics to understand this product selectivity.

3.2 Methodology

3.2.1 DFT and QCD

To ascertain the use of the DFT methods mentioned in the methodology, benchmarking against coupled cluster (CC) methods were used. CC methods like CCSD(T) have been shown to be very successful in calculating ground-state energies when using a large basis set, and has been widely acclaimed as the "gold standard" method for its outstanding accuracy.[33] However, the poor linear scaling meant that optimization demands high computational time when using CCSD(T) and hence its single point calculations are used as a benchmark against DFT and Complete Basis Set (CBS) methods.[34] Conclusive evidence showed that uM06-2X results correlate best to CCSD(T) results, with CBS-4M scaling poorly. Henceforth, DFT calculations are carried out using uM06-2X/6-311+G(d,p)//uM06-2X/6-31G(d).[35,36] To these calculations were carried out using the Gaussian 09 D01 suite of programs.[37] All structures have been fully optimized and confirmed as minima by vibrational analysis. All MOs have been generated at 0.02 and 0.05 au isosurfaces using the Gaussview software. Spin density plots are also generated at 0.05 isovalues using IQmol.[38] Solvation in dichloromethane is employed via the Polarizable Continuum Model (PCM) using the integral equation formalism variant (IEF-PCM) within Gaussian.[39] Additionally, high-precision frequencies for vibrational modes were calculated for the simulations. All transition states were verified with intrinsic reaction coordinate (IRC) calculations.[40] Energies in the report are zero-point corrected electronic energies, unless otherwise stated.

The frequencies taken from the transition state optimizations were processed by Progdyn, an external script by Singleton,[41] at 298.15K, to give a randomized set of 150 starting structures with initial velocities, where the displacements represent that of a Boltzmann

distribution. These structures were then calculated using the Born-Oppenheimer molecular dynamics[42] (BOMD) model in Gaussian09 to give 150 forward and 150 reverse trajectories. Similarly, they were run at uM06-2X/6-31G(d) with solvent to minimize computational time. These trajectories were set to run at a stepsize of about 1.2 fs for about 15000 steps (step lengths of 0.7 amu½ · Bohr), with force constants updated every 97 steps, alongside the ReadStop option to stop the run as soon as a C—C bond formation criterion is reached (bond lengths <1.6 Å). All preparation and analysis was automated through Python and bash scripts.

3.2.2 Marcus-Hush Theory and BerkeleyMadonna

When transferring ions from the gas to liquid phase, the standard states in experiment are chosen at 1 atm and 1 molar solution. Hence, computer simulated results have to be corrected by subtracting 1.9 kcal/mol to each of the products due to the net change in the number of species.[43–45]

$$\Delta G_{ET}^{\ddagger} = \frac{\lambda_0}{4}\left(1 + \frac{\Delta G_r}{\lambda_0}\right)^2 \tag{3.1}$$

$$\lambda_0 = \left(332\frac{kcal}{mol}\right)\left[\frac{1}{2a_1} + \frac{1}{2a_2} - \frac{1}{R}\right]\left[\frac{1}{\varepsilon_{op}} - \frac{1}{\varepsilon}\right] \tag{3.2}$$

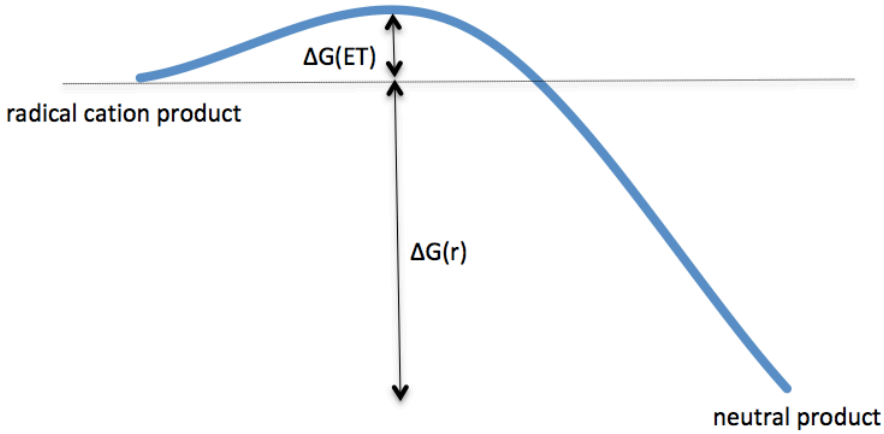

Figure 3.1 Marcus-Hush Theory of Electron Transfer (a_1 is the radius of the first sphere, a_2 is the radius of the second sphere, and R is the total distance of their separation)

The mechanistic analysis of oxygen-mediated photoredox DA reaction done by Dang et al.[46] provided a possible estimation of the required activation free energy for the single electron transfer (SET) step of radical cation reactions using the Marcus-Hush theory of Electron Transfer (**Figure 3.1**)[47–49]. This is essential for understanding the ease of reducing the radical cation product to its neutral state. The concept of Marcus-Hush theory lies in determining the probability of electron transfer from donor to acceptor. Hence, primarily the distance between donor and acceptor is one controlling factor. Also necessary are the Gibbs activation energy ΔG_r and the reorganization energy (λ_0) stemming from molecular rearrangement energy as the charge transfer is distributed throughout the donor and acceptor in the medium.

BerkeleyMadonna (BM),[50,51] a differential equation solver, was used to resolve the kinetics of the DA reactions. BM is a mathematical modelling software package, developed for the purpose of modelling and visualisation of chemical reactions.

3.3 Results

3.3.1 DFT calculations

The neutral DA reaction with the symmetrical diene Cp was first investigated for comparison. In this concerted reaction, two stereoisomers, as shown in **Figure 3.2** (NT/XT and NC/XC) are formed for each *trans*- and *cis*-anethole reaction respectively. The *cis*- values are all corrected for easy comparison due to *cis*-anethole being 1.7 kcal/mol higher in energy. Unsurprisingly, the endo formation proceeds via the TS with slightly lower energy due to stabilizing secondary orbital effects[4].

Name	ΔG(NT)	ΔG(XT)	ΔG(NC)	ΔG(XC)
TS	31.7	32.5	34.7	36.3
PRD	-6.5	-5.6	-3.8	-4.3

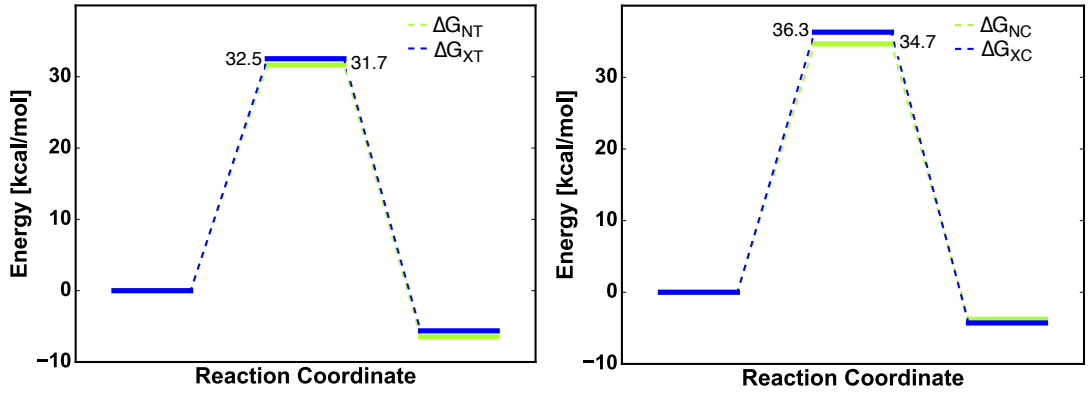

Figure 3.2 Energy profiles of four regioisomers formed in neutral DA reaction (PRD=product) in kcal/mol

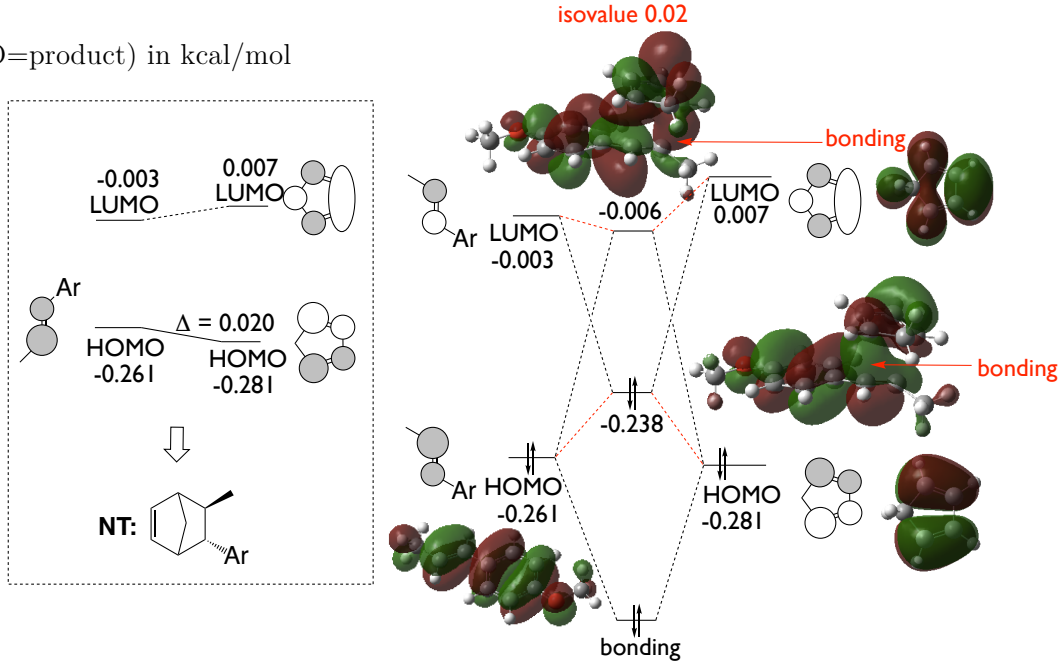

Figure 3.3 Detailed FMO analysis of neutral DA system with Cp and *trans*-anethole

With FMO analysis, it can be seen that both *cis*- and *trans*-anethole reactions with Cp predict high activation barriers for the neutral DA reaction to occur. The formation of NT is given in **Figure 3.3** to show the concerted asynchronous manner of formation.

As previously seen in a simpler system,[31] the radical cation reaction now allows for a stepwise pathway. In **Figure 3.4**, the energy profiles for the *trans*- system are drawn, with endo formation giving the lower activation energy. Compared to the neutral DA system, the activation energies for both stereoisomers have decreased, suggesting a more energetically feasible reaction. It should also be mentioned that consistent with experimental data, no *cis*- products are formed despite this stepwise reaction as the TS for rotation has a much higher activation barrier (ΔG=28.4kcal/mol in **Scheme 3.5**). Taking the TS1 values of NT and XT (which is the rate-limiting step) and calculating the %ee (enantiomeric excess) via Eyring's equation gave a NT:XT=95:5% ratio, compared to the experimental ratio of 85:15.

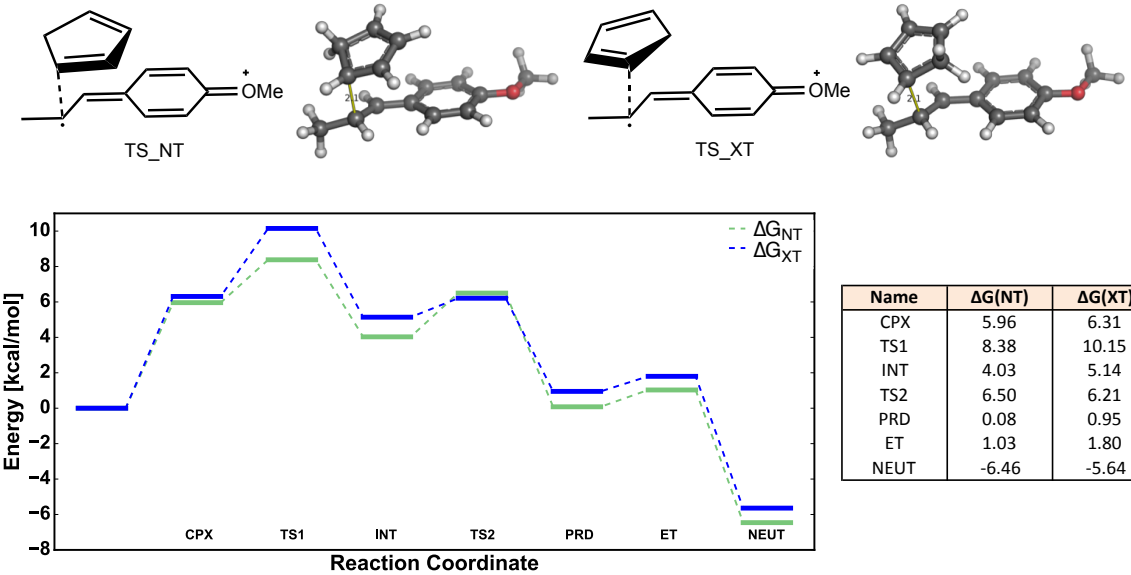

Name	ΔG(NT)	ΔG(XT)
CPX	5.96	6.31
TS1	8.38	10.15
INT	4.03	5.14
TS2	6.50	6.21
PRD	0.08	0.95
ET	1.03	1.80
NEUT	-6.46	-5.64

Figure 3.4 Energy profile diagram of NT and XT in radical cation DA reaction (CPX=complex, INT=intermediate, PRD=product, ET=electron transfer, NEUT=neutral product)

In contrast to **Figure 3.3**, the FMO analysis for this radical cation reaction in **Figure 3.5** showed that the SOMO of anethole overlaps well with the HOMO of Cp as these two orbitals have a smaller energy gap. The presence of one bonding orbital and one anti-bonding orbital instead of two bonding orbitals also imply a stepwise asynchronous manner of reaction in radical cations.

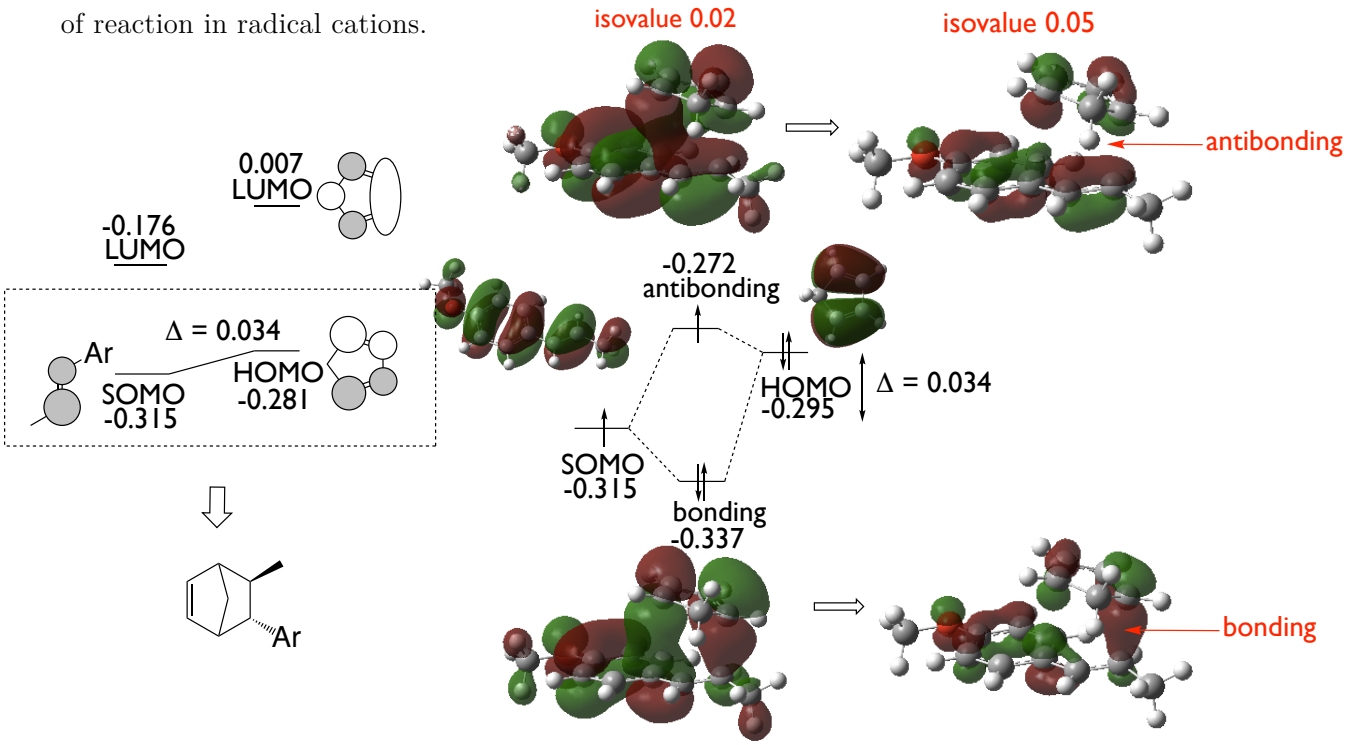

Figure 3.5 FMO analysis of radical cation DA system with Cp and *trans*-anethole

With this analysis of the *trans*-anethole and Cp reaction, the same is done for the *cis*-reaction, with similar results achieved. Despite the *trans*- reaction not forming any *cis*-products, this is not true for the *cis*- reaction. The experimental results show that rotated products are formed as the ratio of the products are NC:XT:XC:NT=40.3:10.4:25.8:23.5. There are 3 plausible hypotheses to explain this result: 1. The starting material *trans*-anethole radical cation underwent rotation to form *cis*-anethole. 2. The *cis*- intermediate underwent rotation to give a *trans*- intermediate (**Scheme 3.4**). 3. Reversibility of *cis*-products to *trans*- products.

Scheme 3.4 Conversion due to bond rotation before second bond formation

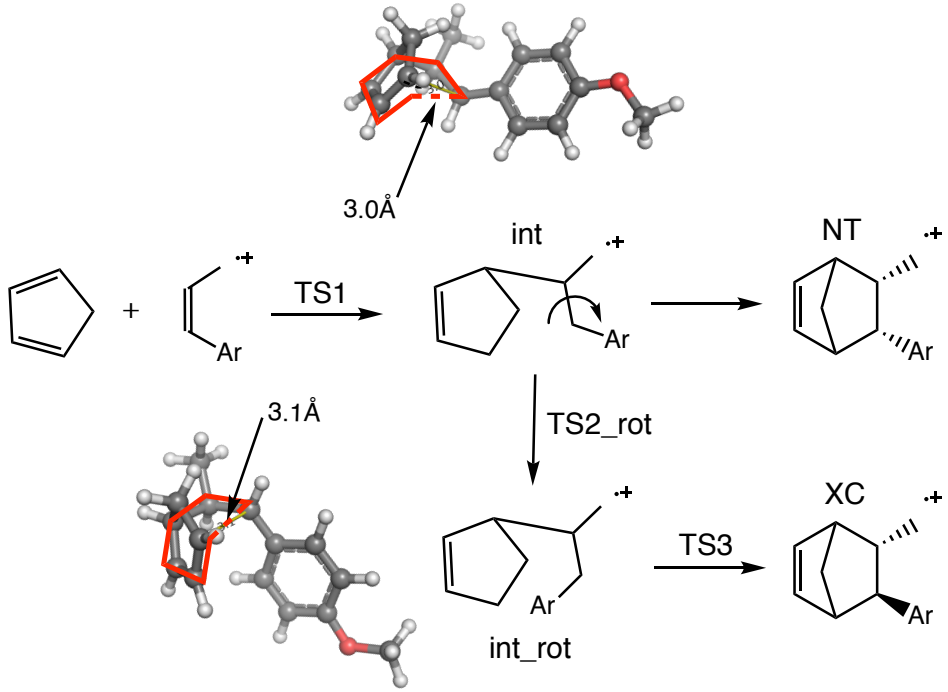

For hypothesis 1, the rotation barrier of *cis*-anethole is also calculated via DFT and given in **Scheme 3.5**. Occurring at nearly 24kcal/mol, this rotation is unlikely to happen at room temperature and hence this hypothesis is ruled out.

Scheme 3.5 Conversion of *trans*-anethole (TA) to *cis*-anethole (CA) and vice versa

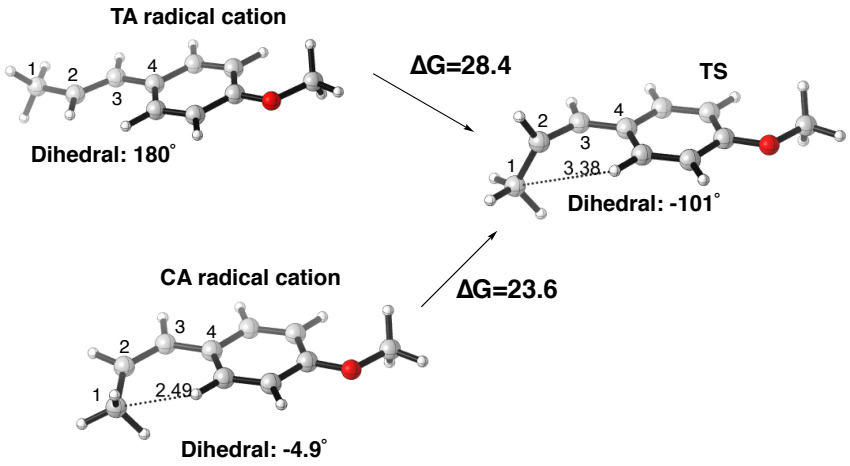

On a related note, it seems that with the aid of Cp, it is possible for *cis*-anethole to rotate easier (energy barrier lowered by almost 4kcal/mol) via collision. This potential mechanism in **Scheme 3.6** shows the transition state where the Cp comes into close proximity with

cis-anethole, resulting in electronic repulsion that pushes the flexible C—C arm on *cis*-anethole to form the more stable *trans*-anethole.

Scheme 3.6 Rotation barrier resulting from collision between Cp and *trans*-anethole

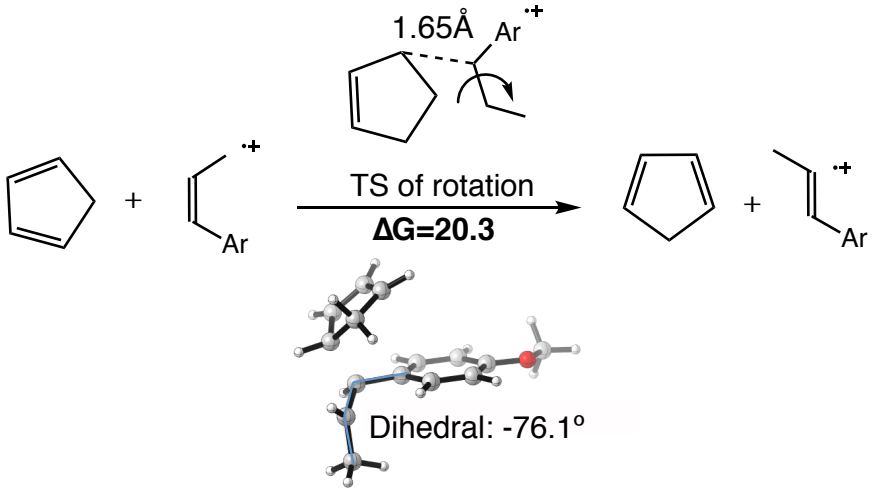

This collision does not form new bonds as Cp is separated after the transition state to release *trans*-anethole. However, this energy barrier is still relatively higher than the energy values tabulated for the mechanistic profiles in **Figure 3.6**, rendering this collisional pathway unlikely to occur since it is diffusion and entropy controlled.

The energy profiles of these mechanisms are examined in detail in **Figure 3.7**. All the *cis*-energies are corrected to be relative to the *trans*- values (shifted upwards by 1.68kcal/mol). As the rotated barriers have comparatively smaller energies compared to the first rate-limiting step, it is possible for rotation to be competitive in *cis*- reactions.

To calculate the theoretical yield for the *cis*- system, TST is once again employed by firstly comparing the ΔG values of the rate-limiting step for NC and XC, and secondly comparing the four possible routes of product formation. The areas highlighted in red on **Figure 3.7** are magnified in **Figure 3.8** and the theoretical results gave an overestimation of NC and XC and an underestimation of NT and XT.

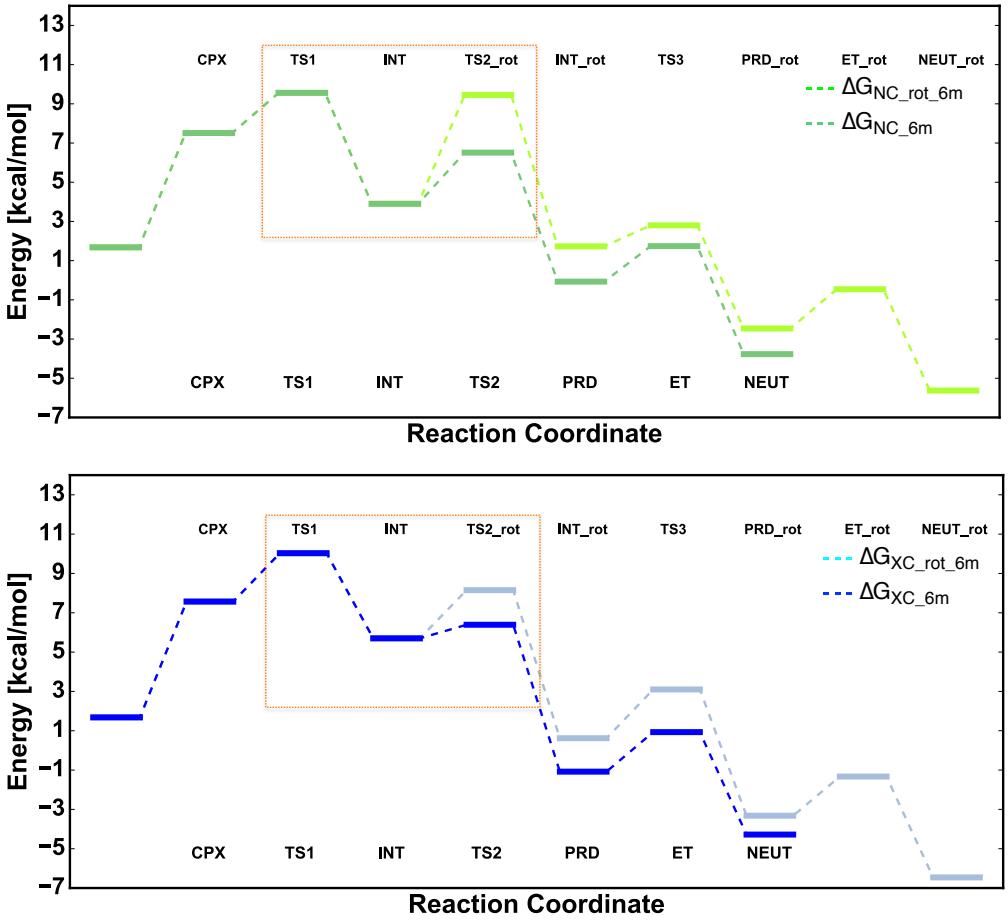

Name	ΔG(NC)	ΔG(XC)
CPX	7.51	7.57
TS1	9.56	10.03
INT	3.90	5.70
TS2	6.51	6.39
PRD	-0.07	-1.08
ET	1.74	0.93
NEUT	-3.77	-4.28
TS2_rot	9.45	8.15
INT_rot	1.73	0.62
TS3	2.80	3.10
PRD_rot	-2.46	-3.32
ET_rot	-0.46	-1.33
NEUT_rot	-5.63	-6.46

Figure 3.7 Top diagram shows the energy profiles of NC (and its rotated product XT) and bottom diagram shows the energy profiles of XC (and its rotated product NT), the red highlighted areas are magnified in **Figure 3.8**

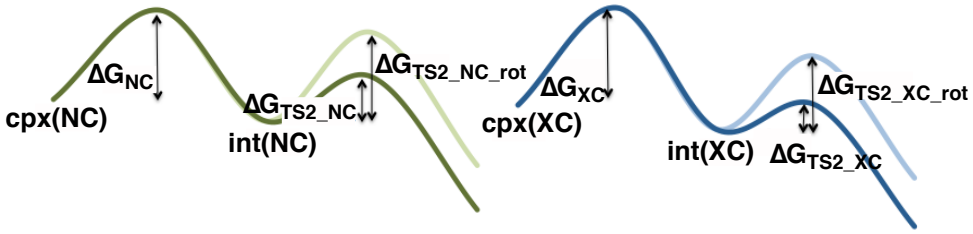

Product	ΔG/kcal/mol	Calc. %	Exp. %
NC	6.51	68.7	40.3
XC	6.39	29.3	25.8
NT	8.15	1.5	23.5
XT	9.45	0.5	10.4

Figure 3.8 Theoretical yield vs. Experimental yield of products in *cis*- system

This result, which gives a clear indication of a dynamic reaction with some reversibility happening within the reaction, does not yet differentiate between hypotheses 2 or 3.

Interconversion could occur at the intermediate stage, or a more complex interplay of thermodynamics and kinetics could allow interconversion to occur at the product stage. This differentiation would be explained in the next Section with a rigorous analysis of QCD and kinetics calculations.

3.3.2 QCD simulations

With this stepwise nature, it is possible that the intermediate (INT) in both *trans*- and *cis*-reactions exist for a long time before the second bond forms with TS2. QCD simulations provide an estimate of this time, which is useful to understand the likelihood of other side-reactions. To reduce computational time, the pathways for the major product reactions are focused on NT and NC. 150 structures of the NT reaction pathway were propagated from the transition state region of TS1 to produce these QCD trajectories. This distribution of initial trajectories follows a Boltzmann distribution when plotted against the initial *d1* (first forming bond) bond lengths (**Figure 3.9**).

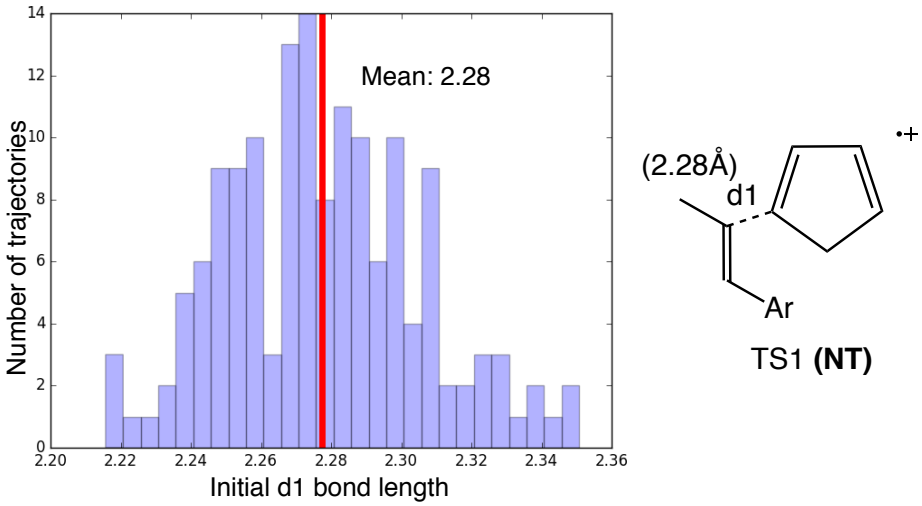

Figure 3.9 Boltzmann distribution of 150 starting trajectories of TS1 of NT

Amongst the 150 trajectories, 114 gave the product NT. One such example trajectory is given in **Figure 3.10(a)**, starting from purple and ending in red. It shows the stepwise formation of the product.

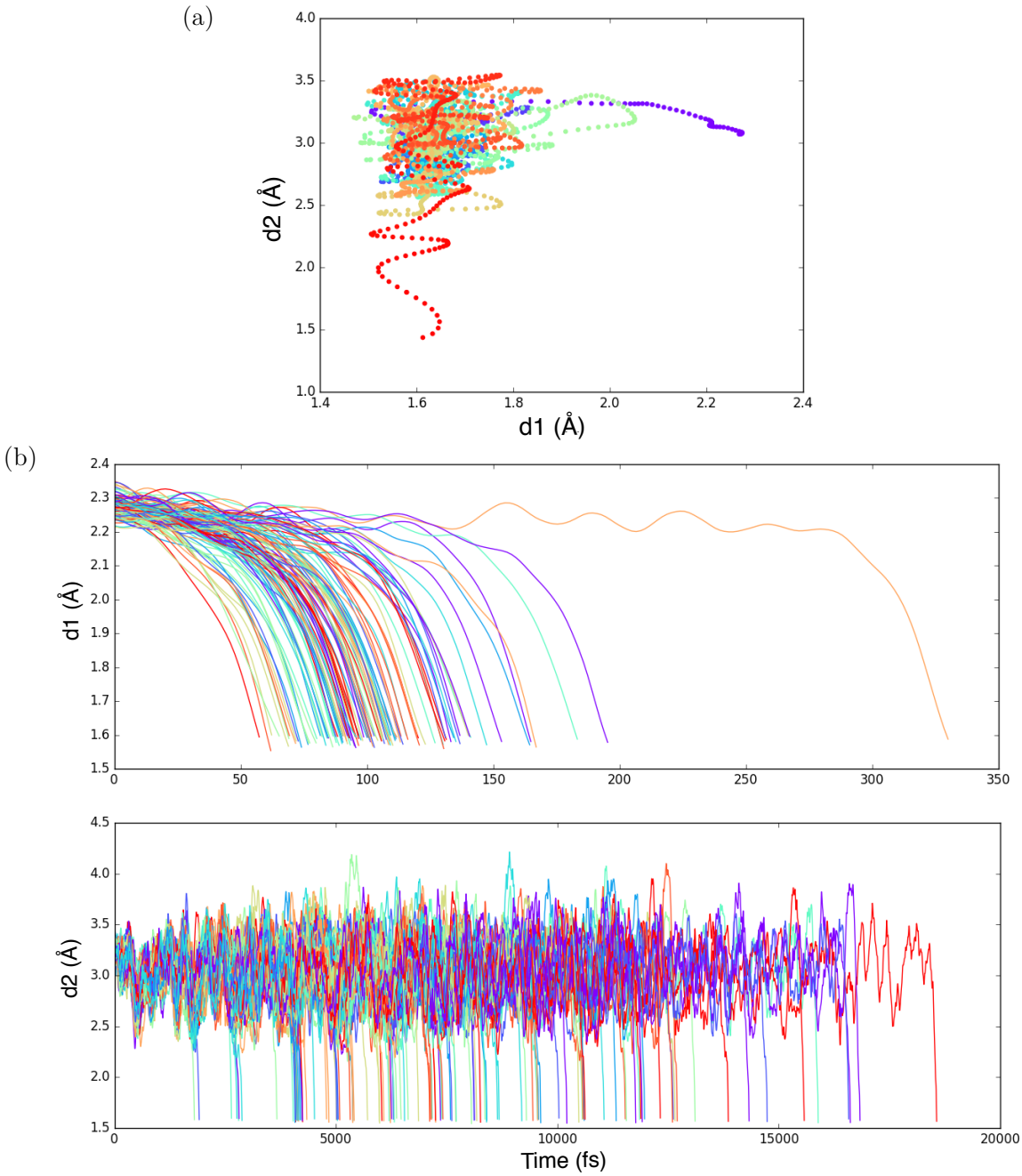

Figure 3.10(a) Example trajectory showing total trajectory time ~15000 fs **(b)** Time evolutions of *d1* and *d2* in fs of the NT trajectories

Figure 3.10(b) also gave the time evolutions of *d1* and *d2* formations for the 114 trajectories, with *d2* taking much longer to form (2000-20000 fs). This showed that the intermediate (>60 fs) exists for a long time on average. With such a long timegap between *d1* and *d2* formations, it seems plausible for rotation to occur before *d2* is formed, or that

some other side reactions could occur. In fact, of the 150 trajectories ran, 2 trajectories actually produced a 4-membered ring structure (4mring in **Scheme 3.7**). Tracing back to DFT, the transition state structure TS2_4m was not found with uM062X, which may indicate a flat PES, hence giving rise to the possibility of forming the 4-membered ring intermediate in dynamics. It is feasible, however, for this structure to undergo [1,3] sigmatropic shift to give the NT product in the end. But this low possibility does not suggest a competitive pathway and hence in the case of NT, the QCD simulations showed that forming product NT is still the main pathway from TS1.

Scheme 3.7 Sigmatropic shift mechanism for 4-membered ring structure to NT product

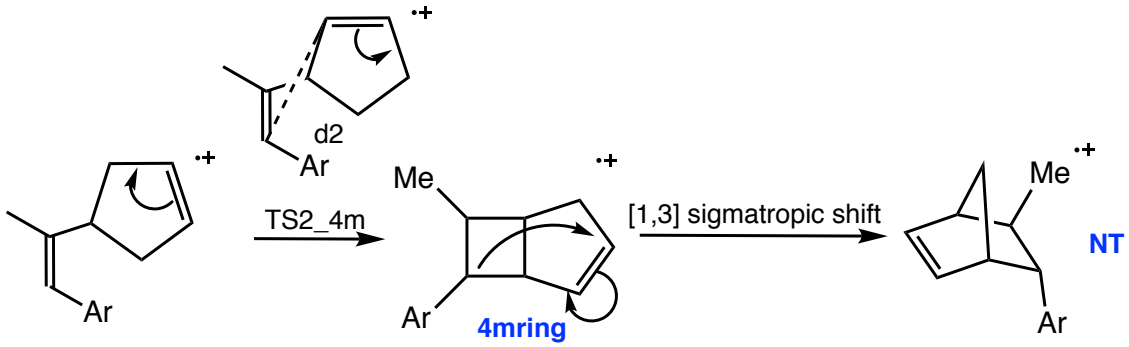

Similarly, QCD simulations were conducted for the NC reaction pathway to understand formation times and to investigate possible side reactions. The NC reaction pathway was chosen, as it was the major product formed for the *cis*- reaction. 150 trajectories representing a Boltzmann distribution (**Figure 3.11**) were ran from the transition state region TS1 of NC reaction, of which 65 gave the product NC while 84 trajectories recrossed. This amount of recrossing is more than twice that of the QCD simulations of NT, which could also represent a higher probability for the NC pathway to have side reactions and hence form other products other than NC.

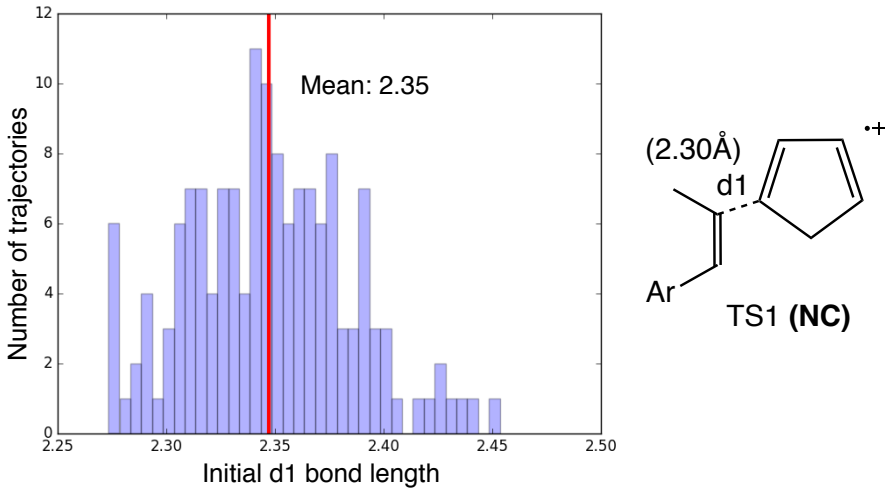

Figure 3.11 Boltzmann distribution of 150 starting trajectories of TS1 of NC

This higher number of recrossing could also be attributed to the shorter transition state structure bond length for NT shown in the NCI plot in **Figure 3.12**.

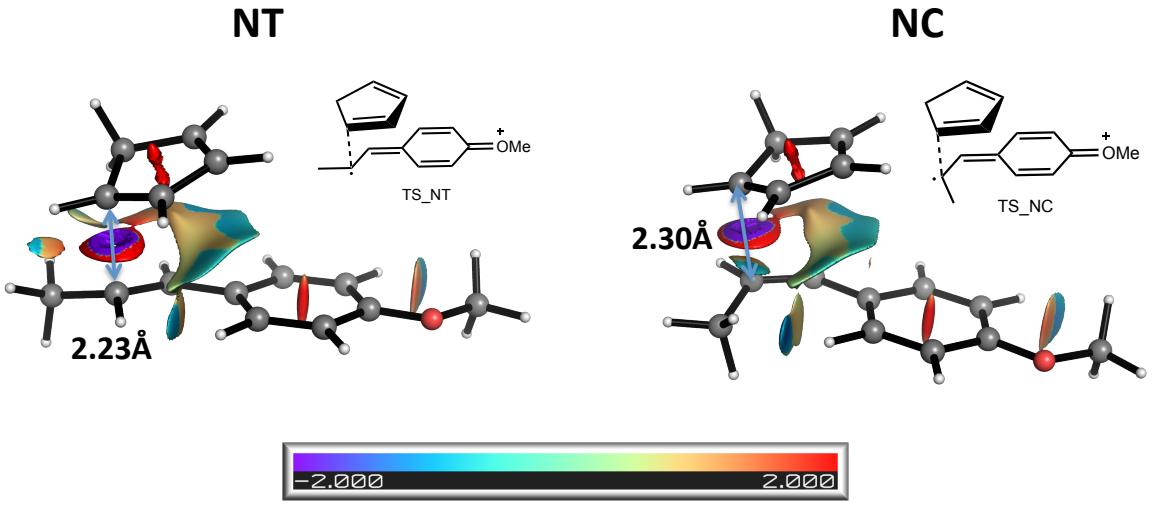

Figure 3.12 NCI plots of TS1 of NT and NC

The NCI plots show similar interactions happening between Cp and *trans*-/*cis*-anethole, but the reason for NT having a shorter bond length could be sought by comparing the activation barriers in **Figure 3.4** and **Figure 3.7**. Based on Hammond's postulate, as the activation barrier for TS1 of NC is lower (7.9kcal/mol if not corrected to *trans*- values), the TS structure is of an earlier TS stage, and hence more reactant-like, giving it a slightly longer bond length as compared to NT's more product-like TS1 that has a higher

activation barrier (8.4kcal/mol). This reasoning supports the notion that more NT products are formed in the first place, but it is also necessary to explain the product distribution of the radical cation *cis*- reaction.

Once again, looking at the time evolutions of forming d1 and d2 in the NC reaction pathway, it is possible to see that the intermediate exists for ~7000 fs on average, similar to the NT case previously.

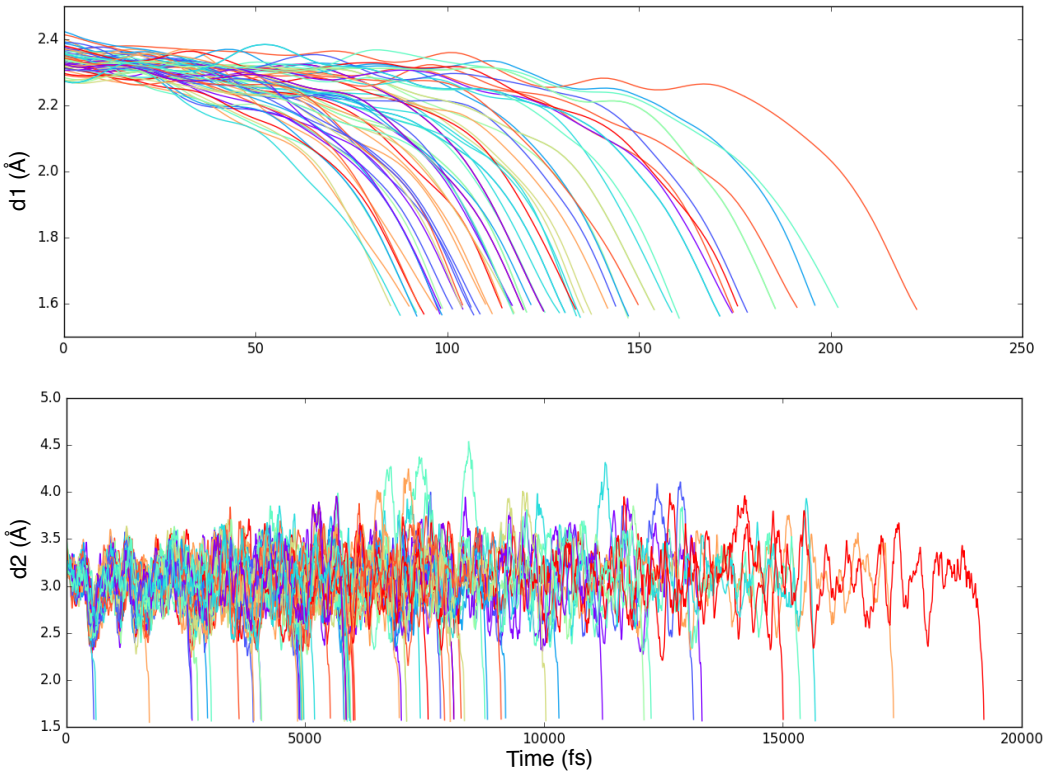

Figure 3.13 Time evolutions of *d1* and *d2* in fs of the NC trajectories

The first bond *d1* forms over a time range <250 fs while *d2* forms after nearly 20000 fs, hence it is similarly possible for the intermediate to stay long enough for side reactions to occur in this stepwise reaction. Despite this, nothing was seen in the 65 trajectories that formed product NC, and only 1 other trajectory formed an XT 4-membered ring (analogous to the case of NT). Likewise, TS2_4m was not found with uM062X, explaining the possibility of 4-membered ring formation in dynamics.

Scheme 3.8 Sigmatropic shift mechanism for 4-membered ring structure to XT product

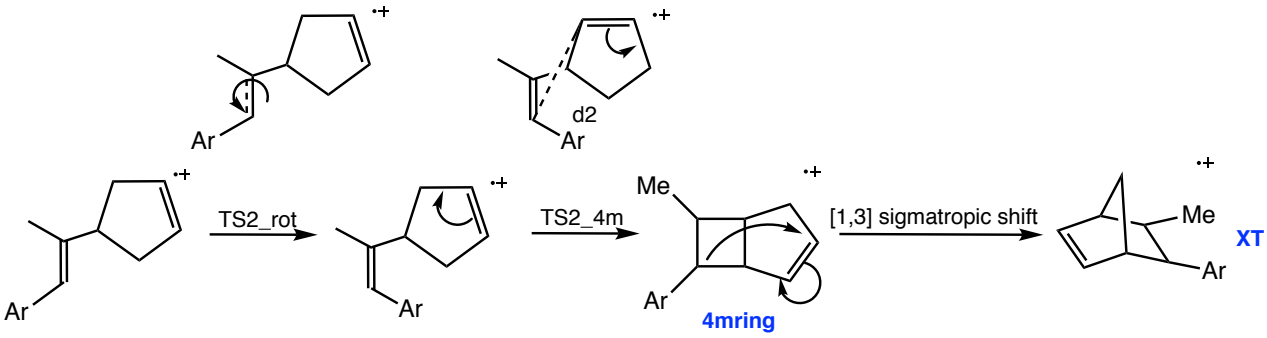

This XT 4-membered ring (**Scheme 3.8**) may in the end also undergo sigmatropic shift to give the XT product, which represents one source of side-products but this reaction is not competitive enough to explain the occurrence of all other products. The large amount of time that the intermediate existed for meant that the radical is extremely stable, possibly due to the delocalization of the radical within the aryl ring. From the 150 trajectories ran at the associated timescales (~20000 fs or 20 ps), it is shown that the conversion mechanism (hypothesis 2) proposed in **Scheme 3.4** is unlikely to occur. In the next Section, this phenomenon and hypothesis 3 are further investigated with kinetic studies.

3.3.3 Kinetics calculations

By putting all the energy values calculated via DFT in **Figure 3.4** (*trans*-) and **Figure 3.7** (*cis*-) into BerkeleyMadonna (BM), it is possible to calculate the product distribution against time and track the changes occurring to the reactants, intermediates and products over time. This helped to give a clearer picture of the thermodynamics of the system as the reaction evolved.

Figure 3.14 shows this product distribution of the NT and XT neutral products, of which the neutral NT product actually reached 96% at its highest point (kinetics), but over time tapers off to about 82% (thermodynamics). Since QCD results did not show rotation

occurring at the intermediate, another plausible reason would be hypothesis 3, where the neutral products are reversibly formed, which was portrayed in **Figure 3.14**.

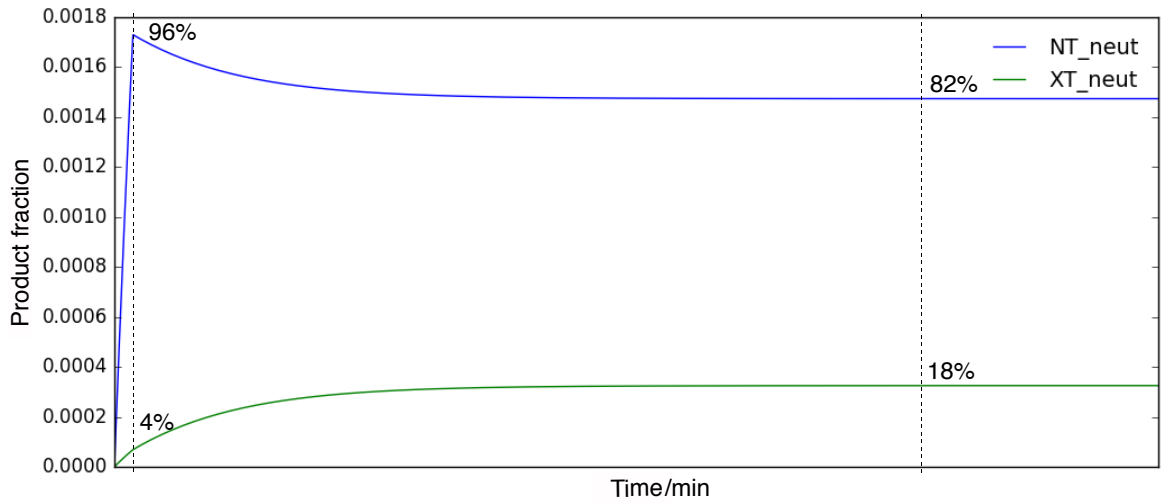

Figure 3.14 Kinetics versus thermodynamics of the NT and XT neutral products

Similarly, in the *cis*- system, **Figure 3.15** shows that the ratio of the neutral products do change over time, and on the timescales of <1 minute (~25 seconds), there is a spike in the amount of NC and XC products (due to kinetics) before they revert to XT and NT products due to thermodynamics. The experimental results obtained by Bauld were taken when the reactions were quenched after 2 minutes. This could be a limitation of QCD: the trajectories (ran in femtoseconds) could not be run that long (in minutes) computationally, and hence the conversion mechanism was not observed during the simulations.

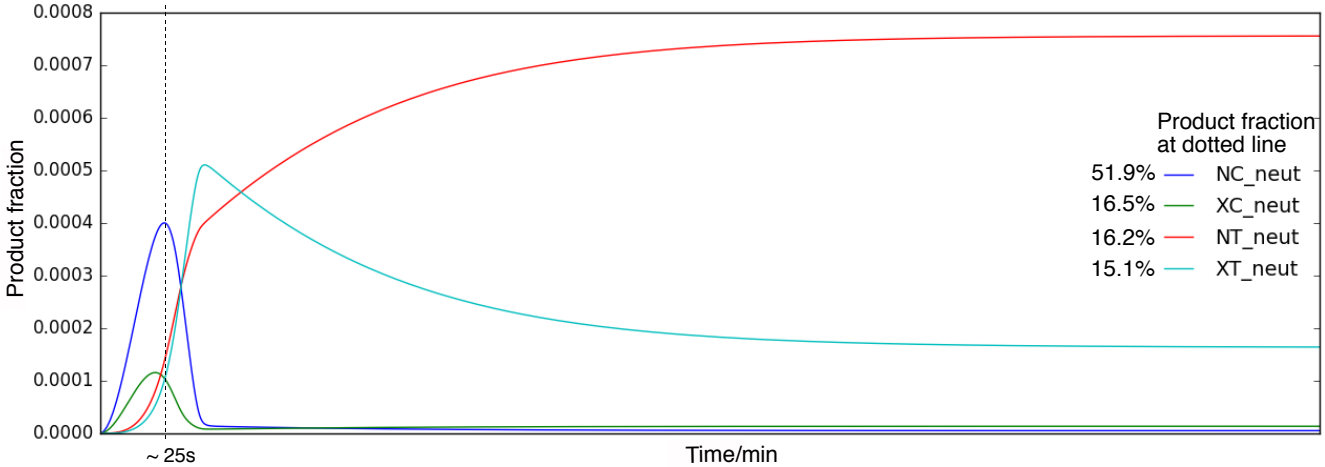

Figure 3.15 Kinetics versus thermodynamics of the NC, XC, NT and XT neutral products

At the point marked by the dotted line, the ratio of products are calculated as NC:XT:XC:NT=51.9:15.1:16.5:16.2, which gave a similar trend to the experimental distribution between the products where NC and XC are the most formed. Comparing with the theoretical yield (of NT and XT) given in **Figure 3.8**, this result is even closer to the experimental yield.

Compared to the BM results for the *trans-* reaction in **Figure 3.14**, the BM results for the *cis-* reaction shows much more reversibility and change. This is not surprising when comparing the DFT energies in **Figure 3.7**. To reverse the *cis-* product, the product NEUT has to cross the energy barrier of electron transfer ET, which is calculated to be 4-5kcal/mol. This is compared against the *trans-* product, where NEUT_rot crosses over ET_rot at 7-8kcal/mol, making it harder for reversibility to occur for the *trans-* products. However, as seen from both **Figures 3.14** and **3.15**, given enough time, the *trans-* products are predominantly the products of the reaction due to thermodynamic stability. This would mean that the results reported in Bauld's paper possibly represent product distribution under kinetic control, over a timescale measured in minutes.

3.4 Conclusion

From this analysis, it was possible to draw several conclusions. Firstly, the starting materials, *trans*- or *cis*-anethole, are highly unlikely to undergo rotation. Secondly, the intermediate existing in this stepwise reaction is thought to undergo rotation, but none of the QCD simulations actually exhibit this behaviour. Nonetheless, this hypothesis for rotation cannot be entirely ruled out unless more trajectories are run and at longer timescales except that this would be computationally difficult to achieve. Thirdly, it is described that the likelihoods of sigmatropic shift and collisional rotation could be used to explain, to a limited extent, rotation in the reaction. Therefore, some of the explanation lies in the reversibility from the neutral products as shown from the combined reliance of kinetics and dynamics. Despite the limitation of QCD in this scenario, the rate of recrossing gave a clear idea of the reversibility of the reactions. This is vastly important in the current state of chemistry as dynamics is becoming widely possible in understanding reactivity not previously done before, and with the addition of kinetic rate theory, this computational method will help to predict and explain product distribution over longer timescales with higher accuracy.

References

1. Valley, N. A. & Wiest, O. Methyl substituent effects in radical cation Diels-Alder reactions. *J. Org. Chem.* **72**, 559–66 (2007).

2. Sevov, C. S. & Wiest, O. Selectivity in the electron transfer catalyzed Diels-Alder reaction of (R)-alpha-phellandrene and 4-methoxystyrene. *J. Org. Chem.* **73**, 7909–7915 (2008).

3. Yang, Z. *et al.* Influence of water and enzyme SpnF on the dynamics and energetics of the ambimodal [6+4]/[4+2] cycloaddition. *Proc. Natl. Acad. Sci.* **115**, 848–855 (2018).

4. Levandowski, B. J. & Houk, K. N. Hyperconjugative, Secondary Orbital, Electrostatic, and Steric Effects on the Reactivities and Endo and Exo Stereoselectivities of Cyclopropene Diels-Alder Reactions. *J. Am. Chem. Soc.* **138**, 16731–16736 (2016).

5. Bellvile, D. J., Wirth, D. D. & Bauld, N. L. The Cation-Radical Catalyzed Diels-Alder Reaction. *J. Am. Chem. Soc.* 718–720 (1981).

6. Bellville, D. J. & Bauld, N. L. Selectivity Profile of the Cation Radical Diels-Alder Reaction. *J. Am. Chem. Soc.* **104**, 2665–2667 (1982).

7. Paton, R. S. *et al.* Origins of stereoselectivity in the trans Diels-Alder paradigm. *J. Am. Chem. Soc.* **132**, 9335–9340 (2010).

8. Okada, Y., Yamaguchi, Y., Ozaki, A. & Chiba, K. Aromatic "Redox Tag"-Assisted Diels-Alder Reactions by Electrocatalysis. *Chem. Sci.* **7**, 6387–6393 (2016).

9. Lin, S., Ischay, M. A., Fry, C. G. & Yoon, T. P. Radical Cation Diels–Alder Cycloadditions by Visible Light Photocatalysis. *J. Am. Chem. Soc.* **133**, 19350–

19353 (2011).

10. Lin, S., Padilla, C. E., Ischay, M. A. & Yoon, T. P. Visible light photocatalysis of intramolecular radical cation Diels-Alder cycloadditions. *Tetrahedron Lett.* **53**, 3073–3076 (2012).

11. Stevenson, S. M., Higgins, R. F., Shores, M. P. & Ferreira, E. M. Chromium photocatalysis: accessing structural complements to Diels–Alder adducts with electron-deficient dienophiles. *Chem. Sci.* **8**, 654–660 (2017).

12. Higgins, R. F. *et al.* Detection of an Energy-Transfer Pathway in Cr-Photoredox Catalysis. *ACS Catal.* **8**, 9216–9225 (2018).

13. Haberl, U., Wiest, O. & Steckhan, E. Ab initio studies of the radical cation Diels-Alder reaction. *J. Am. Chem. Soc.* **121**, 6730–6736 (1999).

14. Williams, F. Inverted Potential-energy Surfaces in the Radical-cation Cope Rearrangements of Hexa-1,5-diene and Semibullvalene. *J. Chem. Soc. Faraday Trans.* **90**, 1681–1687 (1994).

15. Margrey, K. A., Czaplyski, W. L., Nicewicz, D. A. & Alexanian, E. J. A General Strategy for Aliphatic C-H Functionalization Enabled by Organic Photoredox Catalysis. *J. Am. Chem. Soc.* **140**, 4213–4217 (2018).

16. Karkas, M. D., Matsuura, B. S. & Stephenson, C. R. J. Enchained by visible light-mediated photoredox catalysis. *Science* **349**, 1285–1286 (2015).

17. Morse, P. D., Nguyen, T. M., Cruz, C. L. & Nicewicz, D. A. Enantioselective counter-anions in photoredox catalysis: The asymmetric cation radical Diels-Alder reaction. *Tetrahedron* **74**, 3266–3272 (2018).

18. Carpenter, B. K. Dynamic Matching: The Cause of Inversion of Configuration in the [1,3] Sigmatropic Migration? *J. Am. Chem. Soc.* **117**, 6336–6344 (1995).

19. Carpenter, B. K. Dynamic Behavior of Organic Reactive Intermediates. *Angew. Chemie Int. Ed.* **37**, 3340–3350 (1998).

20. Carpenter, B. K. Trajectories through an intermediate at a fourfold branch point. Implications for the stereochemistry of biradical reactions. *J. Am. Chem. Soc.* **107**, 5730–5732 (1985).

21. Hrovat, D. A., Fang, S., Borden, W. T. & Carpenter, B. K. Investigation of Cyclopropane Stereomutation by Quasiclassical Trajectories on an Analytical Potential Energy Surface. *J. Am. Chem. Soc.* **7863**, 5253–5254 (1997).

22. Doubleday, C., Bolton, K. & Hase, W. L. Direct Dynamics Study of the Stereomutation of Cyclopropane. *J. Am. Chem. Soc.* **119**, 5251–5252 (1997).

23. Wang, Z., Hirschi, J. S. & Singleton, D. A. Recrossing and dynamic matching effects on selectivity in a diels-alder reaction. *Angew. Chemie - Int. Ed.* **48**, 9156–9159 (2009).

24. Hase, W. L., Song, K. & Gordon, M. S. Direct dynamics simulations. *Comput. Sci. Eng.* **5**, 36–44 (2003).

25. Lin, H. & Truhlar, D. G. QM/MM: What have we learned, where are we, and where do we go from here? *Theor. Chem. Acc.* **117**, 185–199 (2007).

26. Kamerlin, S. C. L., Cao, J., Rosta, E. & Warshel, A. On unjustifiably misrepresenting the evb approach while simultaneously adopting it. *J. Phys. Chem. B* **113**, 10905–10915 (2009).

27. Blümel, M. *et al.* Rearrangement of Hydroxylated Pinene Derivatives to Fenchone-Type Frameworks: Computational Evidence for Dynamically-Controlled Selectivity. *J. Am. Chem. Soc.* **140**, 9291–9298 (2018).

28. Hare, S. R. & Tantillo, D. J. Cryptic post-transition state bifurcations that reduce the efficiency of lactone-forming Rh-carbenoid C–H insertions. *Chem. Sci.* **8**, 1442–1449 (2017).

29. Hare, S. R. & Tantillo, D. J. Post-transition state bifurcations gain momentum – current state of the field. *Pure Appl. Chem.* **89**, 679–698 (2017).

30. Carlsen, R., Wohlgemuth, N., Carlson, L. & Ess, D. H. Dynamical Mechanism May Avoid High-Oxidation State Ir(V)–H Intermediate and Coordination Complex in Alkane and Arene C–H Activation by Cationic Ir(III) Phosphine. *J. Am. Chem. Soc.* **140**, 11039–11045 (2018).

31. Tan, J. S. J., Hirvonen, V. & Paton, R. S. Dynamic Intermediates in the Radical Cation Diels-Alder Cycloaddition: Lifetime and Suprafacial Stereoselectivity. *Org. Lett.* **20**, 2821–2825 (2018).

32. Bauld, N. L. & Gao, D. Approaching a possible stepwise/concerted mechanistic crossover point in the cation radical cycloadditions of cis- and trans-anethole. *J. Chem. Soc. Perkin Trans. 2* 931–934 (2000).

33. Řezáč, J., Šimová, L. & Hobza, P. CCSD[T] Describes Noncovalent Interactions Better than the CCSD(T), CCSD(TQ), and CCSDT Methods. *J. Chem. Theory Comput.* **9**, 364–369 (2013).

34. Montgomery, J. A., Frisch, M. J., Ochterski, J. W. & Petersson, G. A. A complete

basis set model chemistry. VII. Use of the minimum population localization method. *J. Chem. Phys.* **112**, 6532–6542 (2000).

35. Becke, A. D. Density-functional exchange-energy approximation with correct asymptotic behavior. *Phys. Rev. A* **38**, 3098–3100 (1988).

36. Lee, C., Yang, W. & Parr, R. G. Development of the Colle-Salvetti correlation-energy formula into a functional of the electron density. *Phys. Rev. B* **37**, 785–789 (1988).

37. Frisch, M. J. *et al.* Gaussian 09, Revision D.01. *Gaussian Inc Wallingford CT* (2009).

38. Gilbert, A. T. B. IQmol molecular viewer.

39. Mennucci, B., Cancès, E. & Tomasi, J. Evaluation of Solvent Effects in Isotropic and Anisotropic Dielectrics and in Ionic Solutions with a Unified Integral Equation Method: Theoretical Bases, Computational Implementation, and Numerical Applications. *J. Phys. Chem. B* **101**, 10506–10517 (1997).

40. Fukui, K. The Path of Chemical Reactions - The IRC Approach. *Acc. Chem. Res.* **14**, 363–368 (1981).

41. Ussing, B. R., Hang, C. & Singleton, D. A. Dynamic effects on the periselectivity, rate, isotope effects, and mechanism of cycloadditions of ketenes with cyclopentadiene. *J. Am. Chem. Soc.* **128**, 7594–7607 (2006).

42. Helgaker, T., Uggerud, E. & Jensen, H. J. A. Integration of the classical equations of motion on ab initio molecular potential energy surfaces using gradients and Hessians: application to translational energy release upon fragmentation. *Chem.*

Phys. Lett. **173**, 145–150 (1990).

43. Yu, H. *et al.* A Combined Experimental and Theoretical Study of Ion Solvation in Liquid N -Methylacetamide. *J. Am. Chem. Soc.* **132**, 10847–10856 (2010).

44. Grossfield, A., Ren, P. & Ponder, J. W. Ion Solvation Thermodynamics from Simulation with a Polarizable Force Field. *J. Am. Chem. Soc.* **125**, 15671–15682 (2003).

45. Jensen, J. H. Predicting accurate absolute binding energies in aqueous solution: thermodynamic considerations for electronic structure methods. *Phys. Chem. Chem. Phys.* **17**, 12441–51 (2015).

46. Yang, Y., Liu, Q., Zhang, L., Yu, H. & Dang, Z. Mechanistic Investigation on Oxygen-Mediated Photoredox Diels–Alder Reactions with Chromium Catalysts. *Organometallics* **36**, 687–698 (2017).

47. Marcus, R. A. Electrostatic Free Energy and Other Properties of States Having Nonequilibrium Polarization. I. *J. Chem. Phys.* **24**, 979–989 (1956).

48. Marcus, R. A. On the Theory of Oxidation-Reduction Reactions Involving Electron Transfer. I. *J. Chem. Phys.* **24**, 966–978 (1956).

49. Hush, N. S. Adiabatic theory of outer sphere electron-transfer reactions in solution. *Trans. Faraday Soc.* **57**, 557 (1961).

50. Fontecave-Jallon, J. & Baconnier, P. Berkeley-Madonna Implementation of Ikeda's Model. in *2007 29th Annual International Conference of the IEEE Engineering in Medicine and Biology Society* 582–585 (IEEE, 2007).

51. Macey, R., George, O. & Zahnley, T. Berkeley Madonna. (2009).

Appendix

I. Analysis of the reaction mechanism

	M06-2X/6-31g* in gas phase						6-311+g** in DCM
Fig. 3.2	E/au	ZPE/au	H/au	T.qh-S/au	qh-G(T)/au	imag. ν	E/au
CA radical cation	-463.080655	0.197625	-462.871523	0.04753	-462.919053		-463.182308
TA radical cation	-463.086881	0.196219	-462.879408	0.047236	-462.926644		-463.188529
TS	-463.039401	0.194912	-462.833107	0.047331	-462.880438	-480.88	-463.142016

	M06-2X/6-31g* in gas phase						6-311+g** in DCM
Scheme 3.6	E/au	ZPE/au	H/au	T.qh-S/au	qh-G(T)/au	imag. ν	E/au
TS of rotation	-656.998724	0.292244	-656.690372	0.057538	-656.74791	-93.36	-657.23291

	M06-2X/6-31g* in gas phase						6-311+g** in DCM
Fig. 3.4	E/au	ZPE/au	H/au	T.qh-S/au	qh-G(T)/au	imag. ν	E/au
Cp	-194.004693	0.094034	-193.905599	0.031648	-193.937247		-194.061306
trans anethole rad	-463.009101	0.196496	-462.80066	0.048626	-462.849286		-463.188488
CPX_NT	-657.032637	0.292026	-656.723246	0.060292	-656.783538		-657.261285
TS1_NT	-657.028771	0.292782	-656.719816	0.057719	-656.777535	-218.73	-657.25725
INT_NT	-657.040572	0.295302	-656.729432	0.056834	-656.786266		-657.26687
TS2_NT	-657.039225	0.29605	-656.728325	0.054833	-656.783158	-196.15	-657.265465
PRD_NT	-657.051845	0.298076	-656.738931	0.054782	-656.793713		-657.275854
NEUT_NT	-657.326491	0.298669	-657.013317	0.053472	-657.066788		-657.506424
CPX_XT	-657.031871	0.291988	-656.722412	0.060569	-656.782981		-657.260588
TS1_XT	-657.027571	0.293261	-656.718368	0.057134	-656.775503	-202.39	-657.254891
INT_XT	-657.040326	0.295656	-656.728866	0.05686	-656.785725		-657.264909
TS2_XT	-657.040341	0.296057	-656.729505	0.054658	-656.784163	-88.67	-657.266359
PRD_XT	-657.050452	0.298037	-656.737439	0.05516	-656.792598		-657.274457
NEUT_XT	-657.325082	0.298757	-657.011822	0.053484	-657.065306		-657.505201

	DLPNO-CCSD(T)/aug-cc-pVTZ	CBS-4M	
Fig. 3.4	E/au	E/au	G/au
Cp	-193.7485057	-121604.1063	-121584.8508
trans anethole rad	-462.689049	-290389.5777	-290360.8532
NEUT_NT	-656.4784714	-412004.206	-411969.7806
NEUT_XT	-656.477484	-412003.625	-411969.0307

	M06-2X/6-31g* in gas phase						6-311+g** in DCM
Fig. 3.7	E/au	ZPE/au	H/au	T.qh-S/au	qh-G(T)/au	imag. ν	E/au
cis- anethole rad	-463.002658	0.197473	-462.793574	0.047801	-462.841374		-463.181844
CPX_NC	-657.026539	0.293307	-656.716252	0.059296	-656.775549		-657.254951
TS1_NC	-657.022159	0.293422	-656.712594	0.057669	-656.770263	-181.04	-657.250658
INT_NC	-657.035269	0.295162	-656.724199	0.056954	-656.781153		-657.26687
TS2_NC	-657.033813	0.296005	-656.722943	0.054797	-656.77774	-184.91	-657.260001
PRD_NC	-657.047886	0.298885	-656.734365	0.054265	-656.78863		-657.272146
NEUT_NC	-657.323114	0.299205	-657.009475	0.053317	-657.062793		-657.50271
TS2_rot_NC	-657.027293	0.294889	-656.717208	0.055683	-656.772891	-43.26	-657.252657
INT_rot_NC	-657.040326	0.295655	-656.728867	0.056861	-656.785727		-657.264908
TS3_NC	-657.040341	0.296053	-656.729508	0.054661	-656.784169	-87.24	-657.266341
PRD_rot_NC	-657.050452	0.298037	-656.737439	0.05516	-656.792599		-657.274459
NEUT_rot_NC	-657.325083	0.298756	-657.011826	0.053476	-657.065302		-657.505201
CPX_XC	-657.025828	0.292649	-656.715946	0.060076	-656.776022		-657.254844
TS1_XC	-657.023432	0.294133	-656.713531	0.056766	-656.770297	-191.7	-657.251229
INT_XC	-657.034502	0.296085	-656.722768	0.056443	-656.779212		-657.260299
TS2_XC	-657.034153	0.296613	-656.722871	0.054393	-656.777264	-128.47	-657.259555
PRD_XC	-657.04695	0.298334	-656.733806	0.05465	-656.788457		-657.272146
NEUT_XC	-657.323742	0.299278	-657.010158	0.052898	-657.063057		-657.504223
TS2_rot_XC	-657.028502	0.294582	-656.718574	0.056043	-656.774618	-57.46	-657.254988
INT_rot_XC	-657.040573	0.295303	-656.729431	0.056833	-656.786265		-657.26687
TS3_XC	-657.039225	0.29605	-656.728326	0.054833	-656.783159	-196.12	-657.265219
PRD_rot_XC	-657.051845	0.29808	-656.738928	0.05478	-656.793708		-657.275856
NEUT_rot_XC	-657.326491	0.298667	-657.013318	0.053477	-657.066795		-657.506424

	DLPNO-CCSD(T)/aug-cc-pVTZ	CBS-4M	
Fig 3.7	E/au	E/au	G/au
cis- anethole rad	-462.6864558	-290388.6145	-290358.5879
NEUT_NC	-656.4747779	-412001.2756	-411966.9543
NEUT_XC	-656.4757942	-412001.8234	-411967.6464

II. Absolute energies and Cartesian coordinates of transition structures

Fig. 3.2

TS

C	0.76845	-1.32139	-0.18063
C	-0.54003	-0.96886	-0.27137
C	-0.92930	0.41646	-0.19696
C	0.09376	1.41069	-0.02311
C	1.41058	1.06632	0.06850
C	1.76160	-0.30972	-0.01223
H	1.09786	-2.35317	-0.23237
H	-1.31037	-1.72306	-0.40215
H	-0.20291	2.45442	0.03354
H	2.17279	1.82392	0.19864
O	2.99098	-0.74691	0.05964
C	4.07991	0.17732	0.23033
H	3.96481	0.72084	1.17096
H	4.97556	-0.43953	0.25832
H	4.12266	0.86691	-0.61577
C	-2.24179	0.80414	-0.28933
H	-2.44656	1.87869	-0.21646
C	-3.37562	-0.09575	-0.45327
H	-3.80343	-0.16378	-1.45133
C	-4.22117	-0.43475	0.73555
H	-4.89558	-1.26009	0.49594
H	-3.60365	-0.71915	1.59361
H	-4.83735	0.42250	1.04503

Scheme 3.6

TS of rotation

C	1.11563	-2.08573	0.99277
C	1.25962	-2.58250	-0.29660
C	2.23382	-1.82145	-0.92950
C	2.63819	-0.69217	-0.10440
H	0.36475	-2.41207	1.70745
H	0.68867	-3.39074	-0.73581
H	2.59212	-1.98442	-1.94289
H	3.68211	-0.39763	-0.22050
C	2.17611	-1.10147	1.29966
H	1.86583	-0.29443	1.96406
H	2.99561	-1.64406	1.79879
C	-1.94097	-0.21837	-0.97394
C	-0.57341	-0.12004	-1.18636
C	0.28811	0.45513	-0.24241
C	-0.28235	0.92796	0.95597
C	-1.63919	0.82781	1.19393
C	-2.48539	0.25883	0.22833
H	-2.57310	-0.65317	-1.73871
H	-0.16495	-0.48817	-2.12661
H	0.34713	1.42471	1.69090
H	-2.08396	1.20650	2.10772
O	-3.78548	0.21695	0.54354
C	-4.70482	-0.27225	-0.42246
H	-4.50749	-1.32474	-0.65249
H	-5.68948	-0.17611	0.03099
H	-4.66125	0.32507	-1.33912
C	1.75428	0.62601	-0.54858
H	1.86929	0.70784	-1.63903
C	2.39400	1.81233	0.09924
H	3.08667	1.66994	0.92191
C	2.14200	3.16996	-0.45528
H	1.06716	3.35390	-0.58235
H	2.55043	3.94722	0.19300
H	2.60049	3.29051	-1.44795

Fig. 3.4

TS1_NT

C	-1.64325	1.91988	-0.98187
C	-1.11052	2.04007	0.26982
C	-1.97333	1.38960	1.20445
C	-3.00963	0.76131	0.52707
H	-1.21451	2.30629	-1.89913
H	-0.18568	2.54391	0.52350
H	-1.82619	1.37100	2.27904
H	-3.91671	0.41261	1.00737
C	-2.96941	1.23288	-0.90612
H	-3.76617	1.98065	-1.04458
H	-3.13092	0.46762	-1.67009
C	2.34658	-0.37726	-1.05477
C	1.03580	-0.72803	-1.27952
C	0.10143	-0.87580	-0.21799
C	0.56882	-0.65155	1.11030
C	1.86871	-0.29567	1.34843
C	2.77875	-0.15549	0.27049
H	3.03327	-0.27863	-1.88649
H	0.69818	-0.90165	-2.29789
H	-0.10449	-0.77745	1.95199
H	2.24511	-0.13004	2.35202
O	4.01254	0.18167	0.61032
C	5.01188	0.30875	-0.40140
H	4.74230	1.09835	-1.10882
H	5.92516	0.57801	0.12438
H	5.14807	-0.64247	-0.92368
C	-1.23564	-1.22619	-0.52334
H	-1.46409	-1.38735	-1.57730
C	-2.28976	-1.34317	0.37959
H	-2.05929	-1.38295	1.44091

C	-3.57098	-2.01331	-0.03428
H	-3.84274	-1.76841	-1.06501
H	-3.43368	-3.09970	0.02299
H	-4.40468	-1.75936	0.62323

TS2_NT

C	-2.00787	-1.18349	1.27836
C	-1.77158	-1.99441	0.13975
C	-2.57040	-1.53702	-0.87416
C	-3.25983	-0.29220	-0.43114
H	-1.49299	-1.28344	2.22846
H	-1.02594	-2.77703	0.06863
H	-2.60749	-1.92727	-1.88587
H	-4.20043	-0.06910	-0.93722
C	-3.32611	-0.49417	1.09338
H	-4.13665	-1.18965	1.34746
H	-3.45984	0.41829	1.67679
C	2.51628	0.48700	0.96321
C	1.18046	0.74671	1.15078
C	0.21488	0.51838	0.12795
C	0.67774	-0.01555	-1.11268
C	2.00325	-0.28804	-1.30910
C	2.94475	-0.03527	-0.27824
H	3.22571	0.68379	1.75762
H	0.84430	1.14838	2.10323
H	-0.02719	-0.21088	-1.91406
H	2.37546	-0.68957	-2.24514
O	4.19978	-0.32120	-0.57556
C	5.22673	-0.08904	0.39017
H	5.05202	-0.69327	1.28489
H	6.15257	-0.39617	-0.09092
H	5.27368	0.97260	0.64826
C	-1.14168	0.79423	0.38991
H	-1.34262	1.28144	1.34493
C	-2.23069	0.90830	-0.63514
H	-1.81471	0.83417	-1.64318
C	-2.95509	2.25486	-0.50891
H	-3.42742	2.36256	0.47254
H	-2.25894	3.08627	-0.64406
H	-3.73270	2.33681	-1.27282

TS2_rot_NT

C	-3.52304	-1.58174	0.89343
C	-3.66103	-1.79746	-0.46938
C	-3.59054	-0.59096	-1.15551
C	-3.32749	0.54074	-0.20794
H	-3.52227	-2.34983	1.65766
H	-3.79565	-2.76785	-0.93373
H	-3.69952	-0.46330	-2.22670
H	-4.02815	1.36808	-0.36124
C	-3.50442	-0.11039	1.18870
H	-4.46632	0.18577	1.62968
H	-2.73538	0.18124	1.91284
C	2.57783	-1.14385	0.01636
C	1.21368	-1.10412	-0.09753
C	0.49305	0.12731	-0.23346
C	1.25928	1.34192	-0.27511
C	2.61697	1.31522	-0.17166
C	3.29795	0.07519	-0.01535
H	3.09129	-2.09080	0.12556
H	0.64932	-2.03248	-0.07613
H	0.75756	2.29099	-0.41279
H	3.21678	2.21762	-0.20829
O	4.60341	0.16445	0.08546
C	5.39703	-1.01696	0.24427
H	5.27646	-1.67240	-0.62224
H	6.42443	-0.66652	0.30727
H	5.12042	-1.53692	1.16510
C	-0.88565	0.05148	-0.34642
H	-1.28860	-0.95948	-0.38198
C	-1.89924	1.14350	-0.41788
H	-1.89154	1.50897	-1.45745
C	-1.65066	2.33828	0.52833
H	-1.18521	2.02288	1.46636
H	-1.02621	3.11026	0.07637
H	-2.60701	2.80914	0.77094

TS3_NT

C	-1.95215	-1.35770	0.94138
C	-2.98879	-1.93228	0.17033
C	-3.86485	-0.93213	-0.17326
C	-3.30958	0.37689	0.27301
H	-1.08995	-1.89316	1.32494
H	-3.03415	-2.96532	-0.15322
H	-4.75430	-1.04160	-0.78421
H	-4.04766	1.15948	0.45687
C	-2.43012	-0.03948	1.46473
H	-3.04831	-0.20295	2.35705
H	-1.63413	0.66292	1.71987
C	2.50332	-0.86559	-0.68291
C	1.16469	-0.90974	-0.98698
C	0.23407	0.05535	-0.49606
C	0.75081	1.07777	0.35974
C	2.08000	1.12600	0.67919
C	2.97991	0.16186	0.16019
H	3.17738	-1.60971	-1.08894
H	0.79720	-1.70019	-1.63607
H	0.09303	1.83430	0.76584

H	2.48355	1.89758	1.32560
O	4.24202	0.30834	0.52255
C	5.22676	-0.60677	0.03994
H	5.27793	-0.57062	-1.05194
H	6.16912	-0.27072	0.46659
H	5.00352	-1.62206	0.37980
C	-1.11816	-0.09970	-0.87600
H	-1.27961	-0.92551	-1.56454
C	-2.26309	0.87804	-0.82747
H	-2.75829	0.79874	-1.80137
C	-1.94996	2.35940	-0.59209
H	-1.77550	2.58964	0.46259
H	-1.08328	2.68637	-1.17219
H	-2.80979	2.95460	-0.90952

TS1_XT

C	-1.55503	2.05012	0.21229
C	-2.59661	1.99101	-0.66583
C	-3.53578	1.01636	-0.20289
C	-3.02834	0.37826	0.92509
H	-0.68143	2.68645	0.12935
H	-2.70715	2.58075	-1.56760
H	-4.47957	0.78214	-0.68297
H	-3.63003	-0.22528	1.59639
C	-1.82225	1.15462	1.37874
H	-0.96017	0.56515	1.70392
H	-2.12064	1.77093	2.24150
C	2.40197	0.22729	-1.03256
C	1.07774	-0.02236	-1.31266
C	0.22449	-0.68834	-0.39201
C	0.79451	-1.11962	0.84250
C	2.10947	-0.87792	1.13433
C	2.93418	-0.19950	0.20218
H	3.02243	0.73900	-1.75795
H	0.66412	0.30286	-2.26361
H	0.19159	-1.67282	1.55624
H	2.56071	-1.20942	2.06317
O	4.19055	-0.02164	0.57894
C	5.10351	0.63116	-0.30265
H	4.77514	1.65501	-0.50445
H	6.05606	0.64451	0.22235
H	5.20011	0.07056	-1.23689
C	-1.12531	-0.92002	-0.76050
H	-1.39620	-0.63641	-1.77769
C	-2.14558	-1.43769	0.03526
H	-1.88303	-1.79653	1.02954
C	-3.36075	-2.07108	-0.58495
H	-3.60950	-1.60378	-1.54123
H	-3.15164	-3.13040	-0.77211
H	-4.23249	-2.02341	0.07253

TS2_XT

C	1.86645	-1.69343	0.38453
C	2.99228	-1.77411	-0.46220
C	3.81838	-0.71129	-0.17890
C	3.13287	0.19021	0.79016
H	1.01765	-2.36868	0.36319
H	3.14166	-2.51218	-1.24123
H	4.76384	-0.49305	-0.66246
H	3.79492	0.79521	1.41192
C	2.19601	-0.78387	1.52550
H	1.32990	-0.31772	2.00067
H	2.75159	-1.34473	2.28874
C	-2.53216	-0.44636	-0.96665
C	-1.18524	-0.36461	-1.22358
C	-0.28531	0.31049	-0.34827
C	-0.83650	0.91373	0.82389
C	-2.17499	0.83501	1.09377
C	-3.04461	0.15403	0.20512
H	-3.18644	-0.96198	-1.65885
H	-0.78671	-0.82442	-2.12425
H	-0.19554	1.45878	1.50901
H	-2.60992	1.29316	1.97513
O	-4.31852	0.14002	0.55655
C	-5.27533	-0.50872	-0.28193
H	-5.04435	-1.57403	-0.37158
H	-6.23391	-0.37744	0.21488
H	-5.29968	-0.03764	-1.26873
C	1.08569	0.32947	-0.67419
H	1.33874	-0.07229	-1.65403
C	2.14522	1.15077	-0.01365
H	1.69717	1.79773	0.74588
C	2.89738	2.01672	-1.02875
H	3.32525	1.40257	-1.82750
H	2.23143	2.75221	-1.48628
H	3.71168	2.55616	-0.53595

TS2_rot_XT

C	-3.74528	-1.83316	-0.28451
C	-3.32665	-1.62485	1.01467
C	-3.04184	-0.27561	1.22430
C	-3.28252	0.52128	-0.03503
H	-4.03854	-2.78735	-0.70603
H	-3.22862	-2.39919	1.76694
H	-2.76102	0.16972	2.17202
H	-4.03243	1.30553	0.12092
C	-3.80897	-0.53751	-1.04066
H	-3.22746	-0.56599	-1.97237

H	-4.84035	-0.31772	-1.34346
C	2.53821	-1.13630	-0.11665
C	1.17652	-1.06655	-0.24084
C	0.46975	0.18103	-0.25039
C	1.25036	1.38207	-0.13837
C	2.60711	1.32587	-0.02744
C	3.27326	0.06943	-0.00744
H	3.03941	-2.09609	-0.10770
H	0.60313	-1.98557	-0.32808
H	0.76362	2.34731	-0.15793
H	3.21585	2.22005	0.04630
O	4.57891	0.13046	0.11313
C	5.35726	-1.07155	0.14592
H	5.23399	-1.62619	-0.78789
H	6.38837	-0.74292	0.25177
H	5.06857	-1.68510	1.00308
C	-0.90945	0.12287	-0.37666
H	-1.30114	-0.88256	-0.52986
C	-1.95246	1.20181	-0.43934
H	-2.01478	1.52637	-1.49364
C	-1.69669	2.43989	0.43618
H	-1.28926	2.16310	1.41352
H	-1.02113	3.15545	-0.03465
H	-2.64120	2.96510	0.59961

TS3_XT

C	-2.07140	-1.68995	0.49909
C	-1.95909	-0.84162	1.62876
C	-2.79993	0.22377	1.44280
C	-3.38557	0.14827	0.07361
H	-1.49814	-2.59862	0.34584
H	-1.26734	-0.98093	2.45086
H	-2.94000	1.05161	2.12926
H	-4.34481	0.65196	-0.05512
C	-3.35901	-1.36664	-0.19715
H	-3.40212	-1.64388	-1.25221
H	-4.18569	-1.86196	0.32861
C	2.51344	-0.76118	-0.78738
C	1.19256	-0.85783	-1.15144
C	0.18474	-0.01203	-0.59947
C	0.59425	0.93446	0.38916
C	1.90343	1.03098	0.77181
C	2.88633	0.19376	0.18422
H	3.25112	-1.41071	-1.24218
H	0.90248	-1.59152	-1.89927
H	-0.13928	1.57670	0.85836
H	2.23049	1.74193	1.52268
O	4.12062	0.37986	0.61625
C	5.18326	-0.41189	0.08310
H	5.27792	-0.24707	-0.99383
H	6.08247	-0.07154	0.59166
H	5.01229	-1.47096	0.29526
C	-1.14236	-0.19172	-1.04193
H	-1.24329	-0.95617	-1.81149
C	-2.32211	0.74385	-0.95696
H	-2.81636	0.65367	-1.93141
C	-2.06060	2.23348	-0.71681
H	-1.86214	2.47012	0.33098
H	-1.22137	2.59404	-1.31741
H	-2.94887	2.80015	-1.00905

Fig. 3.7

TS1_NC

C	-1.87713	-2.18646	-0.02959
C	-1.49709	-1.58221	-1.19256
C	-2.39479	-0.50166	-1.46881
C	-3.29568	-0.36495	-0.42712
H	-1.38922	-3.03128	0.44215
H	-0.65606	-1.86590	-1.81336
H	-2.35941	0.12131	-2.35569
H	-4.20014	0.23182	-0.47435
C	-3.13555	-1.55845	0.47980
H	-3.97531	-2.24697	0.29376
H	-3.14430	-1.35159	1.55340
C	2.36857	-0.40431	1.01302
C	1.07824	-0.22875	1.45282
C	0.12468	0.54435	0.73063
C	0.55350	1.13476	-0.49487
C	1.83294	0.96014	-0.95018
C	2.76224	0.19367	-0.20349
H	3.06585	-0.99248	1.59674
H	0.77100	-0.68742	2.38899
H	-0.12893	1.73573	-1.08041
H	2.17541	1.40270	-1.87926
O	3.97111	0.09619	-0.73086
C	4.98109	-0.64455	-0.04510
H	4.68125	-1.69101	0.06168
H	5.86850	-0.57518	-0.67015
H	5.17875	-0.20148	0.93502
C	-1.18103	0.64724	1.27172
H	-1.33532	0.07360	2.18430
C	-2.30526	1.31434	0.79244
H	-3.15536	1.26867	1.47053
C	-2.35556	2.46260	-0.18388
H	-2.07558	2.18960	-1.20216
H	-3.36507	2.87625	-0.22090
H	-1.67997	3.25956	0.14766

TS2_NC

C	2.07142	-1.68989	0.49918
C	1.95920	-0.84148	1.62881
C	2.80003	0.22388	1.44275
C	3.38560	0.14829	0.07352
H	1.49818	-2.59858	0.34606
H	1.26749	-0.98074	2.45096
H	2.94016	1.05177	2.12914
H	4.34483	0.65197	-0.05530
C	3.35901	-1.36663	-0.19714
H	4.18571	-1.86193	0.32862
H	3.40208	-1.64395	-1.25217
C	-2.51346	-0.76123	-0.78732
C	-1.19258	-0.85791	-1.15136
C	-0.18475	-0.01210	-0.59942
C	-0.59426	0.93443	0.38917
C	-1.90345	1.03098	0.77180
C	-2.88635	0.19375	0.18422
H	-3.25114	-1.41077	-1.24211
H	-0.90249	-1.59164	-1.89916
H	0.13928	1.57667	0.85836
H	-2.23050	1.74196	1.52264
O	-4.12064	0.37990	0.61623
C	-5.18329	-0.41186	0.08308
H	-5.01235	-1.47092	0.29529
H	-6.08251	-0.07146	0.59158
H	-5.27790	-0.24709	-0.99387
C	1.14235	-0.19180	-1.04188
H	1.24326	-0.95628	-1.81142
C	2.32208	0.74381	-0.95702
H	2.81627	0.65359	-1.93149
C	2.06055	2.23344	-0.71692
H	1.86211	2.47012	0.33086
H	2.94878	2.80011	-1.00922
H	1.22128	2.59395	-1.31751

TS2_rot_NC

C	3.74528	-1.83316	-0.28451
C	3.32665	-1.62485	1.01467
C	3.04184	-0.27561	1.22430
C	3.28252	0.52128	-0.03503
H	4.03854	-2.78735	-0.70603
H	3.22862	-2.39919	1.76694
H	2.76101	0.16972	2.17202
H	4.03243	1.30553	0.12092
C	3.80897	-0.53751	-1.04066
H	4.84035	-0.31772	-1.34345
H	3.22746	-0.56599	-1.97237
C	-2.53821	-1.13630	-0.11665
C	-1.17652	-1.06655	-0.24084
C	-0.46975	0.18103	-0.25039
C	-1.25036	1.38207	-0.13837
C	-2.60711	1.32587	-0.02744
C	-3.27326	0.06943	-0.00744
H	-3.03941	-2.09609	-0.10770
H	-0.60313	-1.98557	-0.32808
H	-0.76362	2.34731	-0.15793
H	-3.21585	2.22005	0.04630
O	-4.57891	0.13046	0.11313
C	-5.35726	-1.07155	0.14591
H	-5.06857	-1.68511	1.00308
H	-6.38837	-0.74292	0.25177
H	-5.23399	-1.62619	-0.78789
C	0.90945	0.12287	-0.37666
H	1.30114	-0.88256	-0.52987
C	1.95246	1.20181	-0.43934
H	2.01478	1.52637	-1.49364
C	1.69670	2.43989	0.43617
H	1.28926	2.16310	1.41352
H	2.64120	2.96510	0.59960
H	1.02113	3.15545	-0.03466

TS3_NC

C	-1.86674	-1.69413	0.38429
C	-2.99241	-1.77428	-0.46266
C	-3.81829	-0.71127	-0.17929
C	-3.13277	0.18986	0.79009
H	-1.01800	-2.36945	0.36281
H	-3.14189	-2.51219	-1.24181
H	-4.76359	-0.49269	-0.66299
H	-3.79484	0.79466	1.41202
C	-2.19602	-0.78448	1.52524
H	-2.75171	-1.34521	2.28852
H	-1.32978	-0.31857	2.00042
C	2.53218	-0.44591	-0.96688
C	1.18528	-0.36394	-1.22383
C	0.28538	0.31090	-0.34827
C	0.83660	0.91366	0.82414
C	2.17507	0.83468	1.09404
C	3.04464	0.15395	0.20516
H	3.18645	-0.96131	-1.65927
H	0.78673	-0.82337	-2.12468
H	0.19566	1.45850	1.50945
H	2.60999	1.29242	1.97562
O	4.31852	0.13962	0.55665
C	5.27532	-0.50885	-0.28205
H	5.29975	-0.03737	-1.26866
H	6.23389	-0.37784	0.21485

H	5.04427	-1.57411	-0.37214
C	-1.08557	0.33014	-0.67424
H	-1.33872	-0.07149	-1.65410
C	-2.14517	1.15091	-0.01327
H	-1.69724	1.79758	0.74658
C	-2.89753	2.01722	-1.02794
H	-3.32561	1.40333	-1.82677
H	-3.71168	2.55656	-0.53478
H	-2.23165	2.75281	-1.48540

TS1_XC

C	1.77475	-1.85688	0.80608
C	2.71472	-2.17971	-0.12858
C	3.66217	-1.11278	-0.21815
C	3.25739	-0.05798	0.59730
H	0.92081	-2.46046	1.09058
H	2.74854	-3.09137	-0.71226
H	4.54233	-1.10977	-0.85145
H	3.91191	0.75422	0.89468
C	2.12930	-0.55916	1.45956
H	1.28249	0.12170	1.59311
H	2.53140	-0.76058	2.46488
C	-2.34476	-0.73669	-0.78337
C	-1.03702	-0.58812	-1.18344
C	-0.20225	0.45567	-0.69341
C	-0.78486	1.37615	0.22880
C	-2.08613	1.24022	0.63423
C	-2.88663	0.18282	0.13937
H	-2.94448	-1.54641	-1.18075
H	-0.61896	-1.29396	-1.89623
H	-0.21393	2.21544	0.60244
H	-2.54200	1.93910	1.32689
O	-4.12868	0.14664	0.59493
C	-5.01608	-0.87265	0.13605
H	-4.63539	-1.86189	0.40676
H	-5.96025	-0.68747	0.64332
H	-5.15414	-0.79984	-0.94658
C	1.13124	0.50368	-1.17765
H	1.35642	-0.24429	-1.93589
C	2.21536	1.30236	-0.80624
H	3.04537	1.27072	-1.50747
C	2.17939	2.53405	0.06060
H	1.54079	3.29647	-0.40120
H	1.79903	2.33966	1.06714
H	3.18012	2.95965	0.15587

TS2_XC

C	1.95186	-1.35789	0.94105
C	2.98880	-1.93233	0.17026
C	3.86490	-0.93209	-0.17292
C	3.30939	0.37687	0.27334
H	1.08939	-1.89333	1.32403
H	3.03434	-2.96533	-0.15340
H	4.75463	-1.04146	-0.78347
H	4.04738	1.15951	0.45742
C	2.42978	-0.03982	1.46485
H	1.63389	0.66254	1.72039
H	3.04809	-0.20375	2.35700
C	-2.50332	-0.86530	-0.68330
C	-1.16472	-0.90937	-0.98750
C	-0.23404	0.05556	-0.49637
C	-0.75073	1.07784	0.35962
C	-2.07989	1.12601	0.67917
C	-2.97983	0.16192	0.16013
H	-3.17742	-1.60928	-1.08951
H	-0.79729	-1.69965	-1.63684
H	-0.09294	1.83436	0.76573
H	-2.48340	1.89750	1.32571
O	-4.24188	0.30824	0.52274
C	-5.22659	-0.60703	0.04036
H	-5.00286	-1.62235	0.37983
H	-6.16884	-0.27139	0.46758
H	-5.27831	-0.57060	-1.05148
C	1.11824	-0.09964	-0.87614
H	1.27961	-0.92527	-1.56492
C	2.26320	0.87806	-0.82734
H	2.75865	0.79885	-1.80112
C	1.94992	2.35940	-0.59193
H	1.08294	2.68621	-1.17167
H	1.77587	2.58964	0.46283
H	2.80951	2.95474	-0.90975

TS2_rot_XC

C	3.52325	-1.58164	0.89341
C	3.66103	-1.79746	-0.46940
C	3.59039	-0.59101	-1.15561
C	3.32748	0.54075	-0.20808
H	3.52266	-2.34967	1.65770
H	3.79559	-2.76788	-0.93371
H	3.69921	-0.46342	-2.22683
H	4.02811	1.36810	-0.36154
C	3.50463	-0.11027	1.18858
H	2.73568	0.18139	1.91281
H	4.46658	0.18594	1.62941
C	-2.57787	-1.14385	0.01649
C	-1.21371	-1.10414	-0.09734
C	-0.49306	0.12727	-0.23336
C	-1.25929	1.34188	-0.27515

C	-2.61698	1.31520	-0.17173
C	-3.29797	0.07519	-0.01536
H	-3.09133	-2.09079	0.12574
H	-0.64936	-2.03251	-0.07583
H	-0.75755	2.29094	-0.41286
H	-3.21678	2.21760	-0.20845
O	-4.60345	0.16447	0.08536
C	-5.39707	-1.01692	0.24424
H	-5.12050	-1.53682	1.16512
H	-6.42447	-0.66648	0.30718
H	-5.27647	-1.67244	-0.62221
C	0.88563	0.05142	-0.34628
H	1.28859	-0.95955	-0.38162
C	1.89920	1.14346	-0.41785
H	1.89137	1.50896	-1.45742
C	1.65064	2.33823	0.52840
H	1.02634	3.11030	0.07638
H	1.18502	2.02284	1.46634
H	2.60702	2.80896	0.77117

TS3_XC

C	2.00811	-1.18336	1.27848
C	1.77190	-1.99440	0.13995
C	2.57064	-1.53700	-0.87402
C	3.25990	-0.29204	-0.43114
H	1.49327	-1.28330	2.22860
H	1.02636	-2.77713	0.06891
H	2.60777	-1.92734	-1.88570
H	4.20046	-0.06884	-0.93725
C	3.32624	-0.49386	1.09340
H	3.45987	0.41867	1.67673
H	4.13689	-1.18921	1.34751
C	-2.51635	0.48704	0.96318
C	-1.18052	0.74674	1.15073
C	-0.21493	0.51823	0.12796
C	-0.67777	-0.01593	-1.11258
C	-2.00329	-0.28842	-1.30899
C	-2.94480	-0.03541	-0.27820
H	-3.22578	0.68399	1.75753
H	-0.84437	1.14856	2.10312
H	0.02717	-0.21144	-1.91391
H	-2.37548	-0.69013	-2.24495
O	-4.19984	-0.32132	-0.57552
C	-5.22682	-0.08882	0.39010
H	-5.27362	0.97287	0.64799
H	-6.15267	-0.39591	-0.09100
H	-5.05226	-0.69291	1.28494
C	1.14162	0.79419	0.38985
H	1.34256	1.28150	1.34483
C	2.23058	0.90828	-0.63525
H	1.81456	0.83396	-1.64326
C	2.95479	2.25496	-0.50921
H	2.25849	3.08625	-0.64434
H	3.42721	2.36280	0.47218
H	3.73229	2.33697	-1.27321

III. Sample input BOMD calculation

#uM062X/6-31g* SCRF(SMD,solvent=dichloromethane)
BOMD=(readstop,maxpoints=15000,recalcfc=99,rtemp=300,stepsize=5000,readvelocity)
geom=crowd

Cartesian coordinates from Progdyn

1 2
C -1.5528953 2.0162175 -0.8276371
C -1.0348541 2.0197040 0.4009109
C -1.9271454 1.2793221 1.2583837
C -2.9881206 0.7909390 0.5471377
H -1.2071193 2.4819040 -1.7673799
H -0.0591082 2.3948781 0.7660675
H -1.7608233 1.2500315 2.3915125
H -3.9297118 0.4413397 0.9291123
C -2.8200032 1.2804965 -0.8560507
H -3.6408504 1.9799041 -0.9047548
H -2.8755129 0.4055764 -1.6745433
C 2.3078357 -0.3006704 -1.0463274
C 0.9201895 -0.6438506 -1.2943906
C 0.0578045 -0.8330738 -0.2135734
C 0.5842074 -0.7448016 1.1238509
C 1.8872712 -0.4751228 1.3676675
C 2.7773143 -0.2306895 0.2495606
H 3.1488295 -0.2192206 -1.9025538
H 0.5379752 -0.8844415 -2.3240631
H -0.0127347 -0.8259555 1.9897537
H 2.3766412 -0.6528348 2.3738916
O 4.0214386 0.1099786 0.6230557
C 4.9192507 0.4082938 -0.4656288
H 4.4940539 1.2195438 -1.1060784
H 5.8874823 0.7192651 0.1391228
H 5.0760179 -0.5364802 -1.1633247
C -1.2933437 -1.2213065 -0.5481121
H -1.4541673 -1.3004900 -1.6787263
C -2.3036564 -1.4045850 0.2946532
H -2.1818176 -1.5759812 1.3269549
C -3.6472502 -1.9215835 -0.2405730
H -3.8750757 -1.5148926 -1.2234043
H -3.4323586 -2.9798201 -0.2215503
H -4.4773563 -1.5306172 0.3958676

2 #stopping conditions for reaction
1, 1, 1, 1, 1, 1, 1, 1, 1, 1, 1, 2, 2, 2, 2, 2, 2, 2, 2, 2, 2, 2, 2, 2, 2, 2, 2, 2, 2, 2, 2, 2, 2, 2, 2
1, 1, 1, 1, 1, 1, 1, 1, 1, 1, 1, 1, 1, 1, 1, 1, 1, 1, 1, 1, 1, 1, 1, 1, 1, 1, 1, 1, 1, 1, 1, 1, 1, 1, 1
0, 0, 0, 0, 0, 1, 4, 29, 6.50
0, 0, 0, 0, 0, 0, 1, 27, 2.75
3539744712000.000000 118307952000.000000 8427647592000.000000

-97706196000.000000 654874416000.000000 1117278792000.000000
2091832344000.000000 4802193648000.000000 -5738787684000.000000
2778162408000.000000 6268649184000.000000 -2806617492000.000000
-7124482008000.000000 8218560672000.000000 18922403304000.000000
-28460386584000.000000 -20491751196000.000000 -21188665260000.000000
-5125968792000.000000 13756564584000.000000 41390473068000.000000
-27144366732000.000000 1297095660000.000000 -8169276276000.000000
-3965126256000.000000 -2403705780000.000000 10969352856000.000000
25716870900000.000000 -26368268472000.000000 -16397849412000.000000
-14011353216000.000000 8015480172000.000000 -5433608628000.000000
4735869012000.000000 -4170111876000.000000 231884856000.000000
-1135827252000.000000 2295685476000.000000 -963281592000.000000
-2613194892000.000000 -3322000080000.000000 400620276000.000000
5800010832000.000000 5150740644000.000000 -5712370020000.000000
-4846958676000.000000 4904747316000.000000 -3160800468000.000000
6240516912000.000000 -6491701692000.000000 6716908044000.000000
-1756970460000.000000 14235294780000.000000 12400621884000.000000
-19557633816000.000000 -16424441712000.000000 -23352759864000.000000
-1927515744000.000000 -28482777036000.000000 4640321952000.000000
1660285620000.000000 9835986384000.000000 -58392658296000.000000
-33503652000.000000 -1386255276000.000000 -4930619904000.000000
-5984728092000.000000 -4113201708000.000000 4752216000000.000000
-31622435964000.000000 -4959265500000.000000 -21183383844000.000000
26641954836000.000000 -2861442612000.000000 12537107856000.000000
-18925197480000.000000 14863132368000.000000 13084226568000.000000
1349460000.000000 484445556000.000000 -2234001924000.000000
-9402090012000.000000 5972762880000.000000 24471583920000.000000
-3046117536000.000000 -7261851744000.000000 -197740872000.000000
18805249008000.000000 31972274208000.000000 -34631991072000.000000
4573833264000.000000 -2017770804000.000000 -997647840000.000000
-4417634592000.000000 5787177732000.000000 16461226404000.000000
16602300540000.001953 49442981364000.000000 -13513159044000.000000
-14545818756000.000000 15467177124000.000000 6639946488000.000000

Chapter 4: Computational studies of atropisomeric molecules

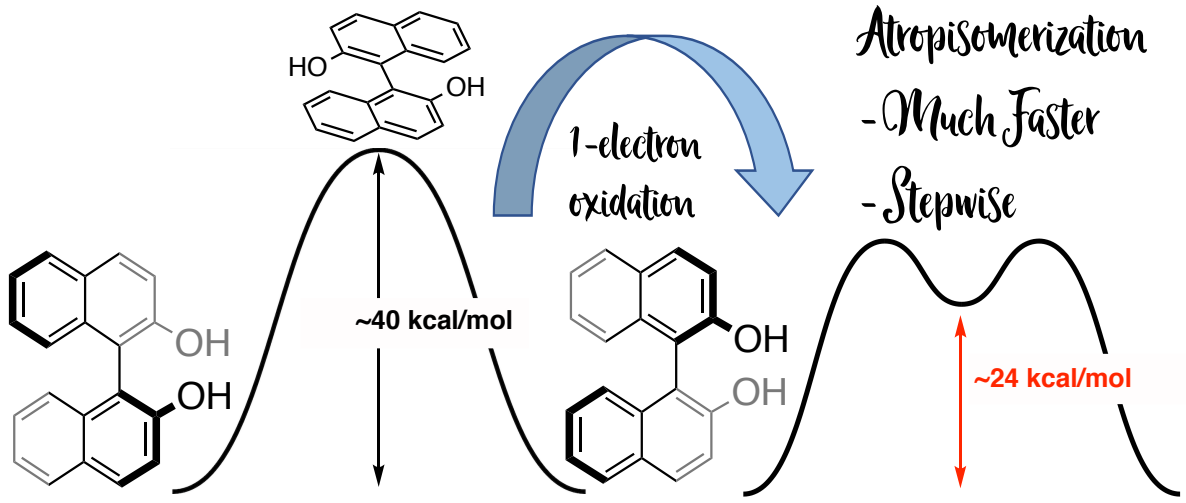

Chapter Overview

Atropisomerism is an important phenomenon observed in biaryl-containing systems due to restricted rotation. The configurational stability of atropisomeric forms can play an important role in pharmaceutical applications of biaryl motifs, and in asymmetric synthesis, where biaryl systems are also privileged architectures. In the first Section, we look at the electronic modification towards atropisomerism through the formation of a radical cation. By removing a single electron, we predict a lowering of the energy barrier of biaryls towards racemization, which can occur via a two-step mechanism. Although the fundamental steric properties remain unchanged, this electronic effect is general for a series of biaryl systems studied in this section and is understood in terms of the dependence of frontier molecular orbital energies upon the biaryl conformation.[1] In the second Section, we look at the chemical modification towards atropisomerism through alkyl substitution. We show that the stereoselectivity of non-biaryl atropisomers can be achieved by substituting the hydrogen-bond donor with an alkyl

group, hence removing the hydrogen bond in the transition state.[2] The increased barrier to rotation of such *O*-functionalized molecules disallow racemization and facilitate a dynamic kinetic resolution.

[1] **Tan, J. S. J. & Paton, R. S., *Chem. Sci.* 10, 2285–2289 (2019). 'Frontier molecular orbital effects control the hole-catalyzed racemization of atropisomeric biaryls.'**
[2] **Fugard, A. J., Lahdenperä, A. S. K., Tan, J. S. J, Mekareeya, A., Paton, R. S., Smith, M. D., *Angew. Chemie Int. Ed.* 58, 2795–2798 (2019). 'Hydrogen-Bond-Enabled Dynamic Kinetic Resolution of Axially Chiral Amides Mediated by a Chiral Counterion.'**

4.1 Introduction

4.1.1 Overview of atropisomerism

Stereoisomers arising from rotation hindered about one or more sigma bonds are commonly known as atropisomers, and these axially chiral molecules are of vital importance across a range of different fields including materials, catalysis and medicinal chemistry. Owing to the significant importance and demand of these chiral biaryl scaffolds, numerous synthetic procedures, reviews, and concepts have been published in literature,[3,4] and some common examples are given in **Figure 4.1**.

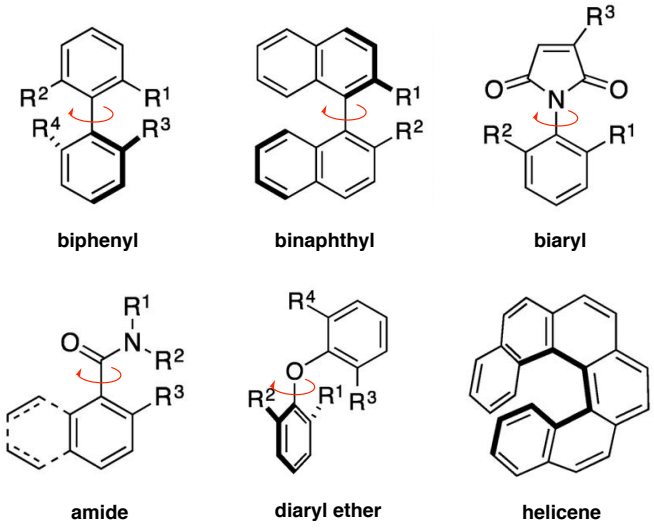

Figure 4.1. Atropisomerism present in common scaffolds of drug discovery

The separation and isolation of atropisomers is possible when the energy barrier for interconversion (which may occur via a hindered rotation) is sufficiently high. It has been suggested that a half-life of ~10^3 s (16.7 min) for interconversion is sufficient for atropisomers to be separable.[5,6] At a temperature of 300 K, according to transition state theory, this corresponds to a rotational energy barrier of 21.9 kcal/mol.[7] Based on this definition, racemization occurs spontaneously for energy barriers lower than those at 300 K, while axial chirality is preserved for higher energy barriers. This also provides a useful 'rule of thumb' in studying whether a particular biaryl system exists

at room temperature as non-interconverting atropisomers, or whether atropisomerization occurs relatively rapidly.

In a pharmaceutical setting, the significance of atropisomerism arises due to the specific binding ability between a drug and its intended protein target, which may vary between the two enantiomeric forms of the small molecule. By correcting for the 30-fold decrease in half-life in going from aqueous solution to plasma, and that the drug should be at least 99.5% homogeneous over 24 hours *in vivo*, this corresponds to a rotational energy barrier of 29.4 kcal/mol.[8,9] Hence, to avoid racemization of a chiral molecule *in vivo*, guidelines have been developed that recommend atropisomeric molecules have half-lives ranging from days to weeks, according to rotational barriers in excess of 29.4 kcal/mol. This has driven the development of better techniques to understand and appreciate atropisomers as drug leads in order to optimize absorption, distribution, metabolism, excretion, and toxicity (ADMET) properties.[10–12]

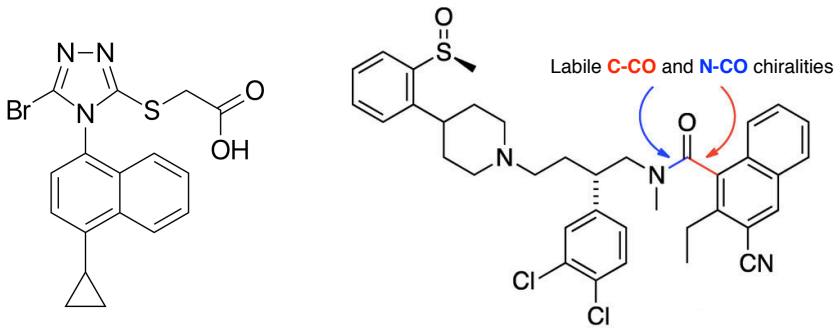

Figure 4.2. Examples of atropisomeric drugs

One example of a stable atropisomer in drug discovery is the FDA-approved drug lesinurad (**Figure 4.2(a)**) that utilises the biaryl scaffold shown in **Figure 4.1**, and is used in the treatment of gout. Another example is the neuropeptide tachykinin

(**Figure 4.2(b)**), a well-known receptor antagonist used for treating depression that featured restricted bond rotation around C–CO and N–CO.[13,14] This led to the presence of multiple diastereomers, which caused complications in drug design. Analysis of the individual atropisomers gave the one with the best potency, which in turn helped to redesign and optimise this drug.

Furthermore, axial chirality can be used as a dynamic means to control reactivity.[15] Biaryl atropisomers such as 1,1′–bi–2–naphthol (BINOL) have gained considerable attention as chemical building blocks for chiral catalysts in asymmetric syntheses.[16] For example, in the asymmetric aldol reaction, Shibasaki and co-workers reported a reaction directly catalysed by their (*S,S*)–Zn–Zn–linked BINOL complex in a highly enantioselective manner (**Figure 4.3**).[17]

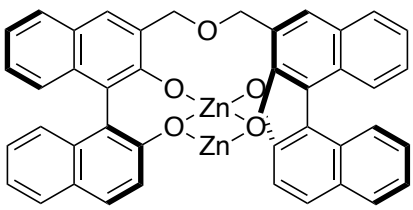

Figure 4.3. (*S,S*)–Zn–Zn–linked BINOL complex reported by Shibasaki et al.

Many biaryl atropisomers are starting materials to active pharmaceutical ingredients due to them having interesting biological activities; and in addition to that, the extended electron systems in naphthalene and its derivatives exhibit unique electronic and optical properties for domains in sensors and batteries.[18,19] Hence, the prevalence of such molecules in many areas has given them the distinction as privileged motifs.

Similarly, helicenes have attracted much attention as simplified models for screw-shaped molecules resembling nucleic acids and proteins.[20] As phosphine ligands have

proven very useful in catalytic asymmetric reactions in the recent years, experimentalists have combined the enantioselective capabilities of phosphines with the chiroptical properties of helicines[21,22]: two examples of helical phosphine molecules are given in **Figure 4.4**.

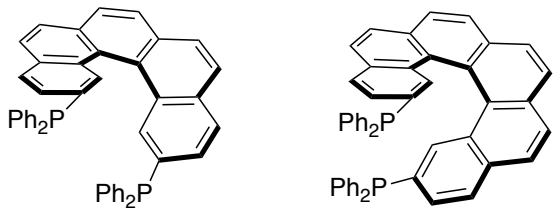

[5]Heliphos **[6]Heliphos**

Figure 4.4. Examples of helical phosphine ligands

In nanomaterial applications, they have recently been recognized as powerful building blocks, leading to an interest in their chemistry and physicochemical properties. The presence of many binding interactions such as π-stacking would position them favorably and efficiently with a large chiral polyaromatic template.[23] Additionally, the use of bigger helicenes (i.e., [6]helicenes or higher) are advantageous for reactions at higher temperatures compared to the lower-energy thermal racemization of binaphthyl ligands.

In nearly all applications of biaryl and helicene containing molecules, the absolute sense of chirality is important. Therefore, understanding the mechanisms and conditions under which this sense of chirality may be lost via interconversion between atropisomeric forms is essential. Conversely, the ability to promote and control this interconversion may also be exploited in the context of e.g., dynamic kinetic resolution.[24]

4.1.2 Implications of electron removal on atropisomerism

Recent experimental results regarding atropisomeric behaviour upon acidic conditions,[25] which proceeds via dearomatized protonated intermediates, and under basic conditions (due to deprotonation and dianion formation) have been highlighted.[26] Photolysis experiments also allow facile racemization by accessing the excited triplet state.[27]

More recently, however, Pappo has reported that optically pure BINOL derivatives can undergo racemization at room temperature using single electron transfer (SET) conditions (**Scheme 4.1**).[28]

Scheme 4.1. BINOL racemization is observed under SET conditions at temperatures for which atropisomers do not interconvert.

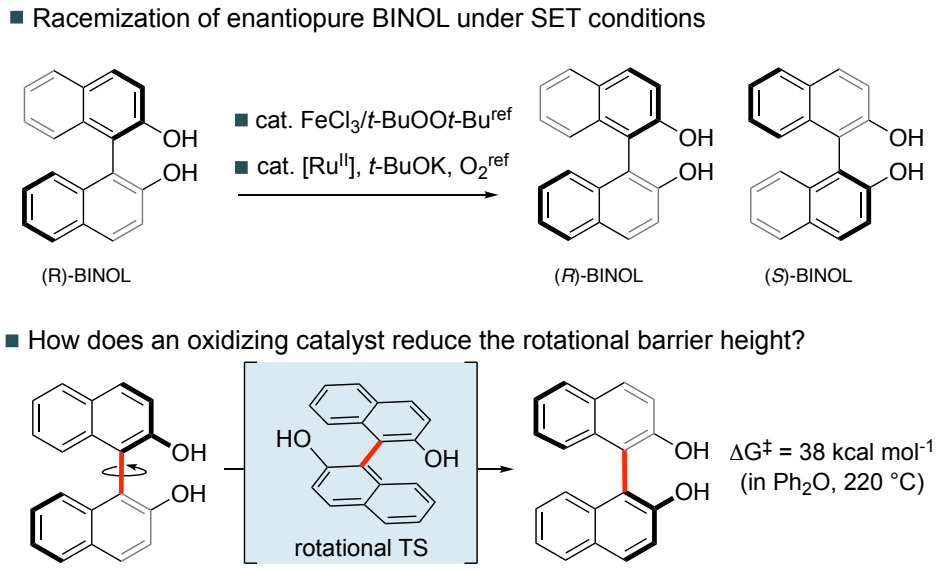

Akai also reported similar SET conditions that promote biaryl racemization at 35-50° C, supporting the development of an enzymatic dynamic kinetic resolution of biaryls in the same laboratory.[29] Likewise, oxidation with a hypervalent iodine reagent promotes BINOL racemization.[30] Pappo also proposed that competing racemization reactions can take place in the radical-anion coupling mechanism, which will reduce product purity, suggesting the importance of quantitative prediction using computational methods to

avoid erosion of enantiomeric excess (*ee*).[31] The racemization mechanism of helicenes have also been studied recently using DFT methods,[32–34] but the exact mechanistic origins in explaining how biaryl oxidation could allow more facile axial rotation, leading to easier racemization, remain unclear.

As seen in **Scheme 4.1**, BINOL shows a typically high resistance towards thermal racemization (the barrier has been determined experimentally as 37-38 kcal/mol hence temperatures above 200 °C are required),[24] but SET clearly promotes a substantial barrier-lowering effect in the rotational transition state. This Chapter therefore set out to understand the origins of this form of catalytic atropisomerization via a computational study.

Often in radical chemistry, the removal of a free election via redox reactions helps promote an entirely different chemical environment within the reactants,[35] as seen in **Chapters 2** and **3**. Therefore, this section provides a computational overview of 5 biaryl systems and 2 helicenes via radical cation means to denote the profound differences invoked by these chemical changes. One key result is the large decrease in atropisomerism energy barrier that has never been reported before.

4.1.3 Implications of chemical substitution on atropisomerism

Primarily, atropisomerization of biaryls is an intramolecular process governed by substituent sterics, and to a lesser extent, by electronic effects.[36–38]

Biphenyl derivatives with restricted rotation have been widely investigated since the seminal report of Kenner[39] and more recently, non-biaryl atropisomers such as anilides, amides, and imides have also been reviewed[3]. Appropriately substituted tertiary amides can possess significant barriers to rotation, and such properties have been exploited for

long-range stereocontrol.[40] The relationship between axial rotation rates and steric hindrance can be simplistically understood in **Figure 4.5**.[12,41] This figure also shows how a set of highly related compounds with incremental changes to steric hindrance (or clashing) around a rotational axis can affect a wide range of rotational energy barriers and subsequently interconversion half-lives ($T_{1/2}$).

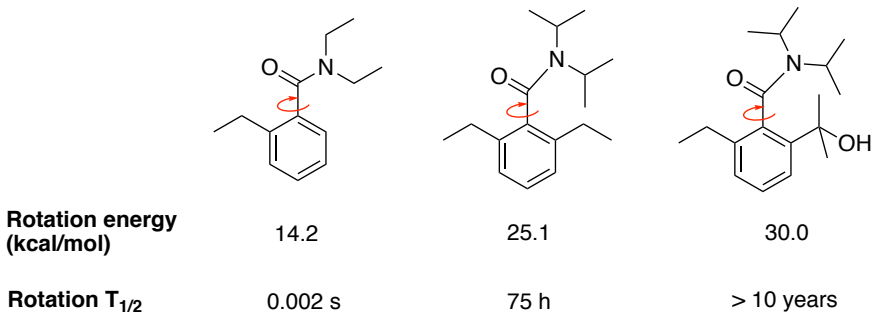

Figure 4.5. Related compounds having increased steric hindrance (or clashing) about a rotational axis (red arrow).

Several methods to the catalytic enantioselective synthesis of atropisomeric amides have been revealed through methods using metal catalysis[42] and organocatalysis[43]. Miller has described a peptide-catalysed atropselective bromination and Walsh's group has demonstrated an enantioselective proline-catalysed aldol reaction with a naphthamide-derived aldehyde.[44] The Sparr group has also described an aldol-elimination procedure for the enantioselective reaction of axially chiral aromatic amides.[45]

Increasingly, research groups are now combining experimental results with computational data to further elucidate key mechanistic details that are useful in designing better and more efficient catalysts. In fact, Diaz was able to demonstrate the existence of a chiral axis in a novel amidinoquinoxaline *N*-oxide using X-ray diffraction

and the ground state geometry using DFT calculations[46]. DFT calculations were also used to locate the transition states for the interconversion of the atropisomers, and identified the interaction of the *ortho* substituent on the ring with the sp^2 nitrogen in the amidine moiety.

One key research objective is to be able to synthesise atropisomers with high enantiomeric ratios (e.r.), and the Smith group at the University of Oxford have been focussed on designing such axially chiral molecules. In a reaction involving certain naphthamides (**Figure 4.6**), it was noticed that naphthamide **1**, with an OH group, has a lower barrier (at a lower temperature) than naphthamide **2**, with an OBn group.

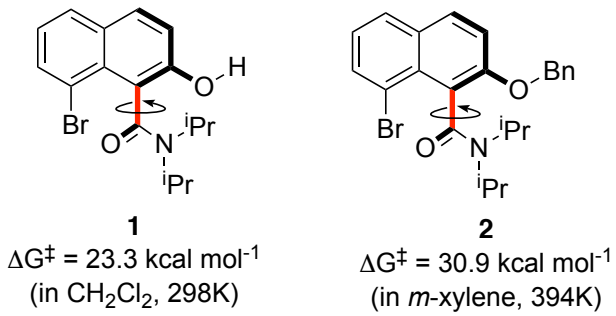

Figure 4.6. Different rotational barriers for atropisomeric naphthamides

In fact, based on the definition provided by Ōki, **1** would atropisomerize at ambient temperature while **2** would not. However, the steric difference between an OH and OBn group is too small to explain this, which led to the postulate that other reasons are in play. Hence, in this section, a collaborative project completed by us demonstrate that, using both experimental and computational efforts, the racemization rate of atropisomeric naphthamides is significantly increased with the presence of an intramolecular hydrogen bond that stabilizes the planar transition state.[2]

4.2 Methodology

Density functional theory (DFT) calculations were performed with Gaussian 09 rev. D.01.[47] All singlet and doublet species were described with unrestricted Kohn-Sham theory; converged densities were checked for their stability (*stable=opt*). Geometry optimisations used the B3LYP[48–50] and M06-2X[51] hybrid meta GGA functionals with 6-31G(d) basis set for all atoms. For the first section, single point energies corrections were done using B3LYP-D3(BJ)[52] with the def2-TZVP basis set,[53–55] and M06-2X with an ultrafine grid.

For the second section, single point calculations were carried out using basis set extrapolation of coupled cluster (CC) methods. CC methods like CCSD(T) have been revealed to be very successful in calculating ground-state energies when using a large basis set, and has been widely acclaimed as the "gold standard" method for its accuracy[56–58]. This was done using the ORCA program 4.0.1[59] with the basis set def2-TZVPD[53] and SMD solvation. Extrapolation to the basis set limit was performed using def2-SVP and def2-TZVP energies, treating the convergence of SCF and correlation energies separately:

(a) The convergence of the HF energy to the basis set limit is calculated as:

$$E_{SCF}^{(X)} = E_{SCF}^{(\infty)} + Ae^{(-\alpha\sqrt{X})}$$

where $E_{SCF}^{(X)}$ is the SCF energy calculated with the basis set having highest angular momentum X, $E_{SCF}^{(\infty)}$ is the basis set limit SCF energy, $\alpha = 10.39$ (empirically optimized for def2), and A is a parameter to be determined.

(b) The correlation energy is assumed to converge as:

$$E_{corr}^{(\infty)} = \frac{X^{\beta}E_{corr}^{(X)} - Y^{\beta}E_{corr}^{(Y)}}{X^{\beta} - Y^{\beta}}$$

where $E_{corr}^{(\infty)}$ is the correlation energy calculated with the basis sets having successive highest angular momentums X and Y, and $\beta = 2.40$ (empirically optimized for def2)[60]. Solvation in dichloromethane and toluene are employed with Solvent Model Based on Density Model (SMD).[61]

Minima and transition structures on the potential energy surface (PES) were confirmed as such by harmonic frequency analysis at the same level of theory. All transition structures were verified with intrinsic reaction coordinate (IRC) calculations.[62] All spin density plots have been generated at 0.15 isovalue using *IQmol*.[63]

The reaction considered is unimolecular and so a standard state correction (from 1 atm to 1 mol/l) has no effect. Gibbs energies were evaluated at 298.15 K, using a quasi-RRHO treatment of vibrational entropies introduced by Grimme.[64] Vibrational entropies of frequencies below 100 cm^{-1} were obtained according to a free rotor description, using a smooth damping function to interpolate between the two limiting descriptions. This was implemented using Goodvibes.[65] All molecular images are produced using Cylview.[66]

4.3 Results

4.3.1 Effects of electron removal to rotational barriers

We have calculated the effects of removing a single electron upon the rotational barriers, and hence racemization/atropisomerization of various biaryl systems. Even though catalyst coordination may play a role in this process,[67] our attention was directed to the fundamental effect of hole-catalysis in forming an oxidized biaryl molecule: and as shown in this Chapter, this effect turns out to be significant and likely an important aspect of this chemistry.

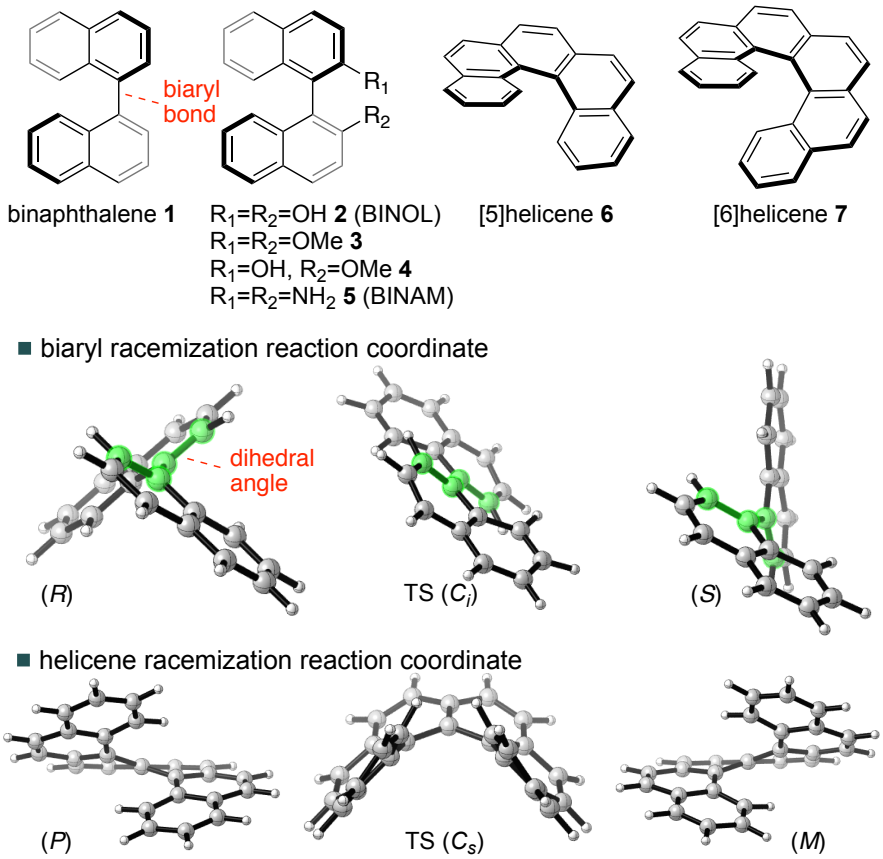

Figure 4.7. Atropisomeric compounds studied computationally (P for clockwise, M for anticlockwise)

Racemization barriers for these radical-cationic systems[35] were compared against those obtained for the parent, neutral system. Helicenes were also included in this study, in addition to the series of binaphthyl and BINOL derivatives, since these display similar

thermal barriers towards atropisomerization, albeit not via the rotation of a single C−C bond (**Figure 4.7**). **Figure 4.7** shows the representative transition structures for the atropisomerism of chiral biaryl and helicene forms for closed-shell systems.[24] Axial rotation from the ground state (**GS**) of the biaryls can proceed in either direction; however, the *anti*-TS shown (in which the 8-positions are as far apart as possible) is favoured for steric reasons.[24] For helicenes, this racemization between (P) and (M) configurations will proceed via a puckered TS.

DFT calculations were used in the investigations, and B3LYP-D3 results were referred to primarily, although there is little qualitative or quantitative difference from using M06-2X. QM calculations has helped understand the chemistry of radical cations considerably.[68–70]

Species			**C−C bond length / Å**	**Dihedral angle / °**
	Neutral	GS	1.50	105
1		TS	1.50	180
	Radical cation	GS	1.46	125
		TS	1.45	180
	Neutral	GS	1.50	95
2		TS	1.49	180
	Radical cation	GS	1.47	115
		TS	1.47	143
	Neutral	GS	1.50	88
3		TS	1.48	180
	Radical cation	GS	1.47	65
		TS	1.43	175
	Neutral	GS	1.50	86
4		TS	1.49	173
	Radical cation	GS	1.47	145
		TS	1.46	180
	Neutral	GS	1.50	88
5		TS	1.48	179
	Radical cation	GS	1.47	111
		TS	1.46	145

Table 4.1. Biaryl bond lengths and dihedral angles in the ground state and in the rotational transition state structure (B3LYP-D3/def2TZVP//B3LYP/6-31G*)

A structural comparison between the ground state (GS) and transition structure (TS)

for neutral and one-electron oxidized biaryl systems showed some obvious differences (**Table 4.1**). A further comparison of these values against M06-2X/def2-TZVP//M06-2X/6-31G(d) calculations is also given in **Table 4.2**, with no noticeable differences.

Species		Energy Level	C−C bond length / Å	Dihedral angle / °
	Neutral	GS	1.49	112
1		TS	1.50	180
	Radical cation	GS	1.45	127
		TS	1.45	168
	Neutral	GS	1.49	112
2		TS	1.49	180
	Radical cation	GS	1.45	119
		TS	1.46	137
	Neutral	GS	1.49	70
3		TS	1.49	174
	Radical cation	GS	1.45	59
		TS	1.43	167
	Neutral	GS	1.49	69
4		TS	1.49	170
	Radical cation	GS	1.47	137
		TS	1.46	168
	Neutral	GS	1.49	71
5		TS	1.48	175
	Radical cation	GS	1.46	64
		TS	1.46	138

Table 4.2. Biaryl bond lengths and dihedral angles in the ground state and in the rotational transition state structure (M062X/def2TZVP//M062X/6-31G*)

Referring to **Table 4.1**, after oxidation, the biaryl C−C bond is shortened 0.03-0.04 Å (in the GS) and by up to 0.05 Å in the TS. This is initially unexpected, as unfavourable H-H steric interactions in the racemization TS should be even more serious for the radical cation, which would lead to a qualitative prediction that racemization is slowed upon oxidation. However, computed activation barriers show that this is not the case, with an enormous barrier-lowering effect of 8-14 kcal/mol due to oxidation (later on in **Table 4.3**).

In the neutral case, the naphthyl rings are almost perpendicular in the GS (dihedral

angles close to 90°), and parallel in the TS (dihedral angles of 180°). For the radical cation case, this is less clear: in fact, the TSs are twisted from planarity with dihedral angles < 180°. Rotation can occur in either direction about the central biaryl axis, which will give rise to two enantiomerization pathways (*anti* and *syn*).

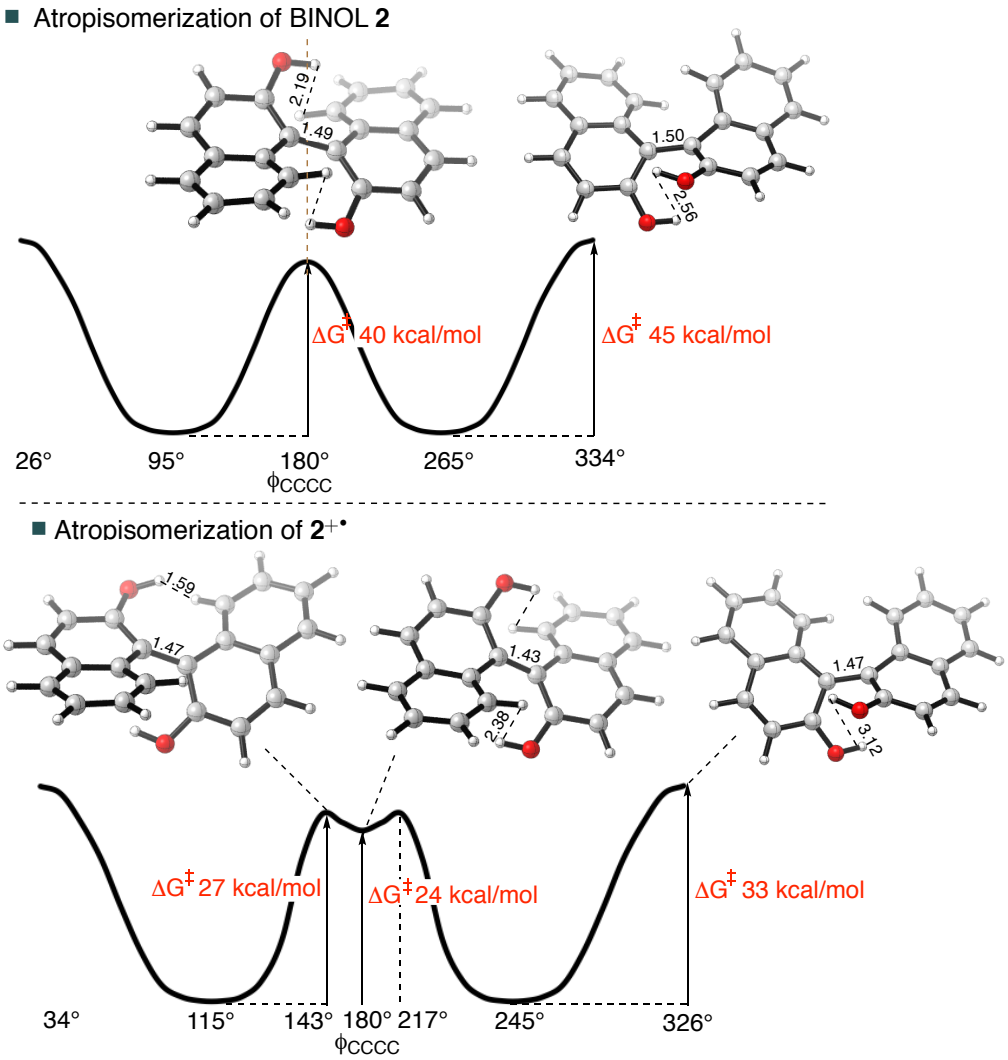

Figure 4.8. The lowest energy thermal racemization of neutral BINOL 2 has a single achiral transition structure (TS); the racemization of $2^{+\bullet}$ proceeds via two TSs with an achiral intermediate that has a much lower overall activation barrier.

As seen in **Figure 4.8**, the *anti*-pathway is favoured by more than ~5 kcal/mol, so attention was focussed on this preferred rotation henceforth. In closed-shell biaryls, the

rotational *anti*-TS is achiral and centrosymmetric. Surprisingly, for radical cation biaryls, this reaction coordinate involves two steps, via two degenerate and chiral rotational TSs. In between lies a shallow intermediate (ca. 2 kcal/mol below these structures), which is the centrosymmetric species that breaks chirality.

Extremely good reproductions of experimentally determined rotational barriers were found for these neutral systems. The solvation effects in dichloromethane were included implicitly with SMD calculations and had a very small influence (typically < 1 kcal/mol) on the rotational barriers. B3LYP-D3(BJ)/def2-TZVP//B3LYP/6-31G(d) (**Table 4.3**) and M06-2X/def2-TZVP//M06-2X/6-31G(d) (**Table 4.4**) calculations gave rotational barrier heights within 2 kcal/mol of experiment.

Molecule	**1**	**2**	**3**	**4**	**5**	**6**	**7**
Neutral:							
Experimental barrier (kcal/mol)	24.1[a]	37.8[a]	-	-	40.9[b]	24.1[c]	36.2[c]
Calculated barrier (kcal/mol)	24.6	39.9	39.6	39.9	42.4	24.4	37.3
Racemization Temp. (K)	336	538	534	538	571	334	504
Half-life $t_{1/2}$ at rt (hours)	69	10^{13}	10^{13}	10^{13}	10^{15}	50	10^{12}
E° Potential/V	0.65[d]	1.18[d]	0.68[e]	-	-	1.14[c]	1.08[c]
Radical cation:	**1**$^{\cdot+}$	**2**$^{\cdot+}$	**3**$^{\cdot+}$	**4**$^{\cdot+}$	**5**$^{\cdot+}$	**6**$^{\cdot+}$	**7**$^{\cdot+}$
Calculated barrier (kcal/mol)	16.9	26.6	25.6	26.1	28.0	19.7	31.7
Racemization Temp. (K)	232	363	349	356	381	271	430
Half-life $t_{1/2}$ at rt (hours)	10^{-4}	2310	379	994	$2x10^4$	0.015	10^7
$\Delta\Delta G^{‡}$ (kcal/mol)	**7.8**	**13.3**	**14.1**	**13.8**	**14.4**	**4.7**	**5.6**
Relative racemization rate, k_{rel}	7 x 10^5	9 x 10^9	3 x 10^{10}	2 x 10^{10}	5 x 10^{10}	2 x10^3	2 x 10^3

[a] Ref. 24 [b] Ref. 6 [c] Ref. 10; E° vs. SHE [d] Ref. 9, E° vs. Ag/AgCl in CH_2Cl_2/$CHCl_3$–BFEE [e] Ref. 8, E° vs. Ag/AgCl in CH_2Cl_2/$CHCl_3$–BFEE

Table 4.3. B3LYP-D3/def2TZVP//B3LYP/6-31G* computed and experimental activation parameters for the racemization of compounds 1-7.

Referring to **Table 4.3**, for a closed-shell biaryl (e.g. BINOL 2), racemization proceeds via a high barrier in a single-step. The reaction coordinate for the $2^{+\bullet}$ however is more complex: the rotational TS (of which there are two mirror image forms) being unsymmetrical and more twisted (the central dihedral is 143° rather than 180°).

Molecule	**1**	**2**	**3**	**4**	**5**	**6**	**7**
Neutral:							
Experimental barrier(kcal/mol)	24.1[a]	37.8[a]	-	-	40.9[b]	24.1[c]	36.2[c]
Calculated barrier (kcal/mol)	25.4	40.3	39.5	40.0	43.1	25.8	38.4
Racemization Temp. (K)	**347**	**543**	**533**	**539**	**580**	**352**	**518**
Half-life $t_{1/2}$ at rt (hours)	*299*	10^{13}	10^{13}	10^{13}	10^{15}	*509*	10^{12}
E° Potential/V	0.65[d]	1.18[d]	0.68[e]	-	-	1.14[c]	1.08[c]
Radical cation:	$\mathbf{1}^{\cdot+}$	$\mathbf{2}^{\cdot+}$	$\mathbf{3}^{\cdot+}$	$\mathbf{4}^{\cdot+}$	$\mathbf{5}^{\cdot+}$	$\mathbf{6}^{\cdot+}$	$\mathbf{7}^{\cdot+}$
Calculated barrier (kcal/mol)	16.6	26.3	24.4	24.6	27.8	21.2	32.6
Racemization Temp. (K)	**229**	**359**	**334**	**336**	**378**	**291**	**442**
Half-life $t_{1/2}$ at rt (hours)	10^{-5}	*1400*	*54.2*	*70.3*	10^{4}	*0.21*	10^{8}
$\Delta\Delta G^{\ddagger}$/kcal/mol	8.8	14.0	15.1	15.4	15.3	4.5	5.8
k_{rel}	10^{6}	10^{10}	10^{11}	10^{11}	10^{11}	10^{3}	10^{4}

[a] Ref. 24 [b] Ref. 6 [c] Ref. 10; E° vs. SHE [d] Ref. 9, E° vs. Ag/AgCl in CH_2Cl_2/$CHCl_3$–BFEE [e] Ref. 8, E° vs. Ag/AgCl in CH_2Cl_2/$CHCl_3$–BFEE

Table 4.4. ΔG values calculated at the M062X/def2TZVP//M062X/6-31G* level of theory, compared with experimental values and E°

The shallow intermediate that is symmetrical actually resembles the closed-shell TS, though with a shorter central bond and closer non-bonding interactions. This intermediate is also surprisingly much more stable than the closed-shell TS by around 15 kcal/mol! As will be explained later, the steric effects caused by the shorter contacts are more than compensated for by the increased bonding interaction of the connecting C−C biaryl bond.

The effects of single-electron oxidation are evident: in every example studied, the racemization barrier height is reduced relative to the neutral compounds. These consequences are significant – as the biaryl rotational barriers are reduced by up to 14 kcal/mol and helicene barrier by 5-6 kcal/mol, this corresponds to an increase in the racemization rate by many orders of magnitude.

This helped to predict that the racemization temperatures for BINOL derivatives and BINAM (2-5) will drop by nearly 200 °C! While the oxidized compounds still have barriers higher than that suggested by Ōki to be considered atropisomeric at r.t.p,[7]

racemization is now accessible in many organic solvents at achievable temperatures (<100 °C), in contrast to their neutral compounds. The measured oxidation potentials listed for several of the compounds studied also suggest that one-electron oxidation is possible with a range of oxidants.

4.3.2 Relevance of Frontier Molecular Theory (FMO)

As the steric properties of each biaryl remain unchanged by oxidation, logically, it is the changes in electronic structure that caused the rate of enantiomerization to increase. Indeed, the reasons are discovered to be embedded in frontier molecular orbital (FMO) theory, and furthermore, will be rationalized with an orbital correlation diagram depicting the two highest occupied molecular orbitals (HOMOs) (**Figure 4.9**). It may seem counterintuitive to focus on frontier orbitals for a reaction where bond-formation is totally absent, but as shown later, our model justifies all energetic and structural observations and even helps postulate good quantitative predictions for barrier height reduction (**Figure 4.10**).

The combination of two HOMOs of the individual naphthalene π-systems forms the biaryl HOMOs. As shown in **Figure 4.9**, in the ground state, the conformation of the two naphthalenes are (or nearly) perpendicular, where there is zero (or very little) interaction between the orthogonal π-systems: hence, there are two degenerate HOMOs. To show one HOMO on each ring system, **Figure 4.9** gives an equivalent representation.

By rotating about the biaryl bond so that racemization can occur, the naphthalene π-systems are now able to interact as the conformation approaches planarity. As a result of the bonding in-phase and anti-bonding out-of-phase overlap across the biaryl C−C

bond, the HOMO and HOMO-1 energies diverge. Hence, by removing an electron from the biaryls, it stabilizes the planar transition state by lessening the impact of a raise in HOMO energy. Since the orbital is singly- rather than doubly-occupied, this energetic cost is essentially halved.

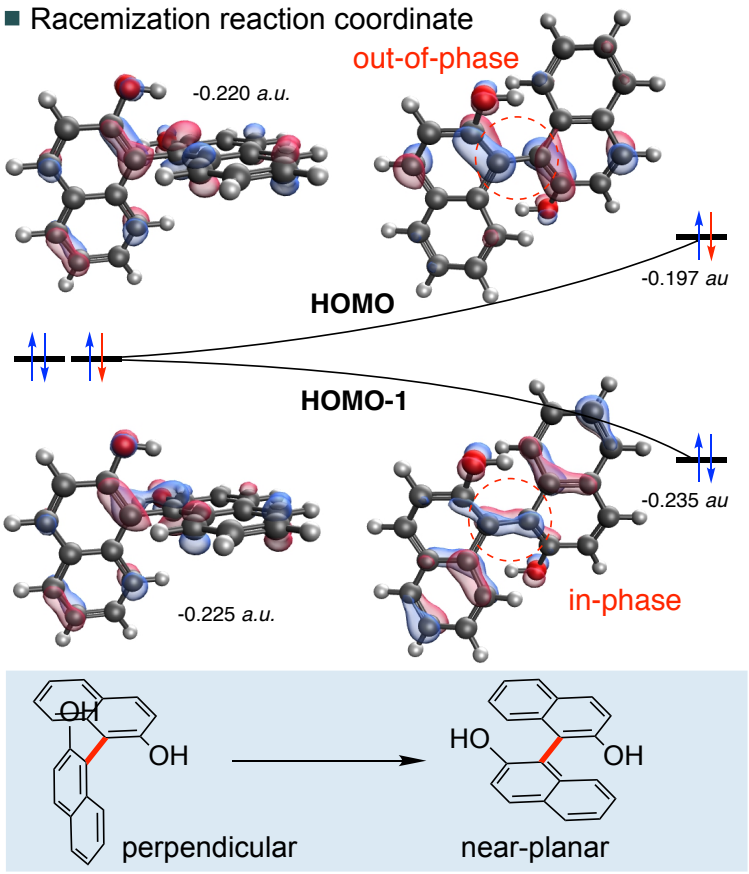

Figure 4.9. Frontier molecular orbitals (FMOs) for biaryl racemization. The orbital correlation diagram shows the B3LYP/def2TZVP energies of the two highest occupied MOs.

This theory clarifies several observations. The removal of an electron from the HOMO stabilizes the planar TS to the extent that it becomes a minimum on the PES (**Figure 4.8**). As seen particularly in the rotational TS and achiral minimum of radical cations, the central biaryl bond is shortened as a result of the greater bonding character

between the two carbon atoms (**Figure 4.9**). The HOMO has anti-bonding overlap between these two atoms: hence by removing an electron, the local bond order is also increased in this region. To bring a similar change in the bond order, this orbital could also be depopulated via photochemical means.[73,74] The two electrons remaining in the HOMO-1 orbital has a bonding interaction here. Additionally, the inclination of radical cations to adopt less orthogonal structures in the GS than the corresponding GS of neutral systems is once again an effect of the extra stabilization gained from the net-bonding interaction between the two naphthalene π-systems when the HOMO is no longer doubly-occupied.

A quantitative relationship was rationalized to exist between the reduction in barrier height from one-electron oxidation and the conformational dependence of the biaryl HOMO energy. The energy change between perpendicular and planar conformations for closed-shell and radical cation systems can be formally related using a thermodynamic cycle (**Figure 4.10**). Recognizing Koopmans' theorem, which connects the negative of the HOMO energies to the ionization energies, the change in activation barrier $\Delta\Delta G^{\ddagger}$ following oxidation is equal to the change in HOMO energy between the GS and TS of closed-shell species.

Molecule	**1**	**2**	**3**	**4**	**5**	**6**	**7**
HOMO/au(GS)	-0.216	-0.220	-0.205	-0.209	-0.202	-0.213	-0.211
HOMO/au(TS)	-0.203	-0.197	-0.183	-0.190	-0.177	-0.206	-0.201
ΔHOMO/kcal/mol	***8.3***	***14.5***	***13.8***	***11.7***	***15.9***	***4.8***	***6.2***
$\Delta\Delta G^{\ddagger}$/kcal/mol	*7.8*	*13.3*	*14.1*	*13.8*	*14.4*	*4.7*	*5.6*
HOMO-1/au(GS)	-0.230	-0.225	-0.206	-0.219	-0.203	-0.218	-0.213
HOMO-1/au(TS)	-0.240	-0.235	-0.217	-0.225	-0.211	-0.224	-0.212
ΔHOMO-1/kcal/mol	-6.118	-6.557	-7.241	-3.916	-4.750	-3.759	1.117

Table 4.5. HOMO and HOMO-1 energy values at B3LYP-D3/def2TZVP//B3LYP/6-31G*, compared with ΔΔG from **Table 4.3**.

These energies were listed in **Table 4.5**, along with the $\Delta\Delta G^{\ddagger}$ values from **Table 4.3**, and the italicized values were also plotted in **Figure 4.10**.

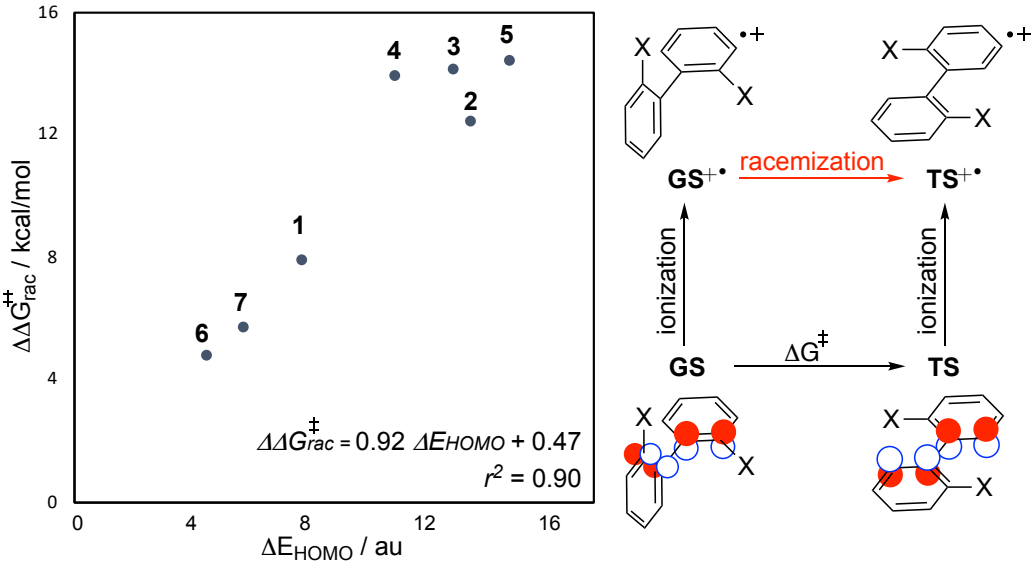

Figure 4.10. The change in HOMO energy level between planar and twisted biaryl conformations is a good postulate of the barrier-lowering effect from SET (note the different energy units for x and y axes).

This predictive model, containing information purely from the closed-shell species, describes the barrier-reducing effect well (**Figure 4.10**, $r^2 = 0.90$) from single-electron oxidation. This offers further support to the above FMO considerations. It is also visible that the helicenes have a smaller energy barrier reduction, due to a smaller ΔHOMO, which is reasonable as the TSs of helicenes are puckered and not coplanar like the biaryls.

4.3.3 Effects of chemical substitution to rotational barriers

As mentioned in **Section 4.1.3**, the steric difference between an OH group and OBn group is too small to explain the differences in rotational barriers; we then postulated that this difference was likely due to the presence of an intramolecular hydrogen bond

between the naphthol OH and the amide nitrogen (**Figure 4.11**).

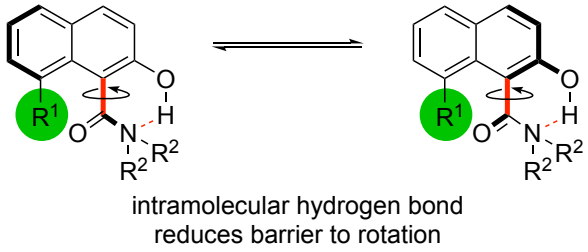

Figure 4.11. H-bond mediated atropisomerism in this work

In principle, the interconversion of the two enantiomeric forms could be stabilized by the planar transition state. Hence, in this setup, increasing the barrier to rotation for *O*-functionalized materials (where this hydrogen bond is removed) will preclude room temperature racemization and enable a dynamic kinetic resolution (e.r. > 95:5). Dr. Alison Fugard in Martin Smith's group primarily carried out the experimental efforts for this work. After optimizing the reaction conditions for *O*-alkylation, a selected scope of the reaction was examined (**Figure 4.12** – only molecules A-F are shown in this chapter). Of the 6 molecules shown in this figure, all of them demonstrated high e.r., therefore demonstrating a highly enantioselective route to axially chiral naphthamides with the catalyst and reaction conditions shown.

To further understand the influence of hydrogen bonding on the rate of racemization, quantum calculations were carried out. Compounds **A1** and **A2** (which bear a dimethyl group rather than a diisopropylamide), are essentially modeled after **A** in **Figure 4.12**, and the effect of *O*-alkylation upon the rotational barrier was quantified (**Figure 4.13**).

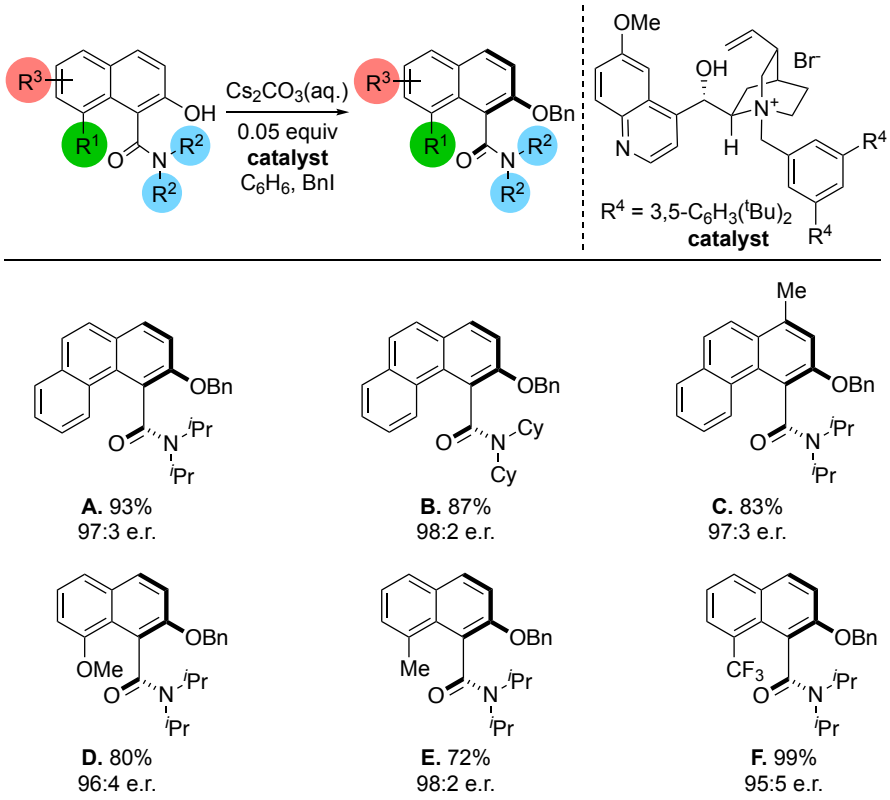

Figure 4.12. Enantioselective *O*-alkylation of axially chiral amides, carried out at r.t. and 48 h

Calculations were executed at the DLPNO-CCSD(T)/def2-TZPD//M062X/6-31G(d) level, with SMD solvation for toluene and CH_2Cl_2. In **Figure 4.13**, the increase in activation energy $\Delta\Delta G^{\ddagger}$, from *O*-alkylation of **A1**, is 39.6 kJ mol^{-1}, which compares favorably with the experimental value of 36.0 kJ mol^{-1}. In **Figure 4.14**, an intramolecular OH–O hydrogen bond (1.85 Å) is seen in the ground-state structure of **A1** that is absent in **A2**. Rotation about the exocyclic C–C bond results in a TS with an almost planar amide (3°). In this TS structure, the pyramidalized nitrogen atom is in very close contact with the hydroxyl proton (1.66 Å).

Entry (R = H/Me)	$\Delta G^{\ddagger}$ (kJ mol^{-1})	$\Delta\Delta G^{\ddagger}$ (kJ mol^{-1})	k_{rel}
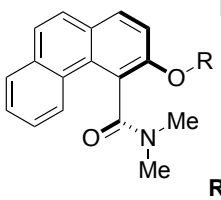 R = H **A1**	72.8 (CH_2Cl_2) 80.2 (Toluene)	42.8 (CH_2Cl_2)	1.08 (CH_2Cl_2) 0.0536 (Toluene)
R = Me **A2**	115.6 (CH_2Cl_2) 119.8 (Toluene)	**39.6 (Toluene)**	3.44×10^{-8} (CH_2Cl_2) 6.27×10^{-9} (Toluene)

Figure 4.13. DLPNO-CCSD(T)/def2-TZPD//M062X/6-31G* with SMD solvation using toluene for closed-shell molecules **A1** and **A2**

As a consequence of the steric demands, the nitrogen atom is in a pyramidalized state, which enhances the hydrogen-bond basicity of the nitrogen atom, therefore leading to a stronger hydrogen bond in the TS than in the ground state, contributing to a pronounced reduction in barrier height.

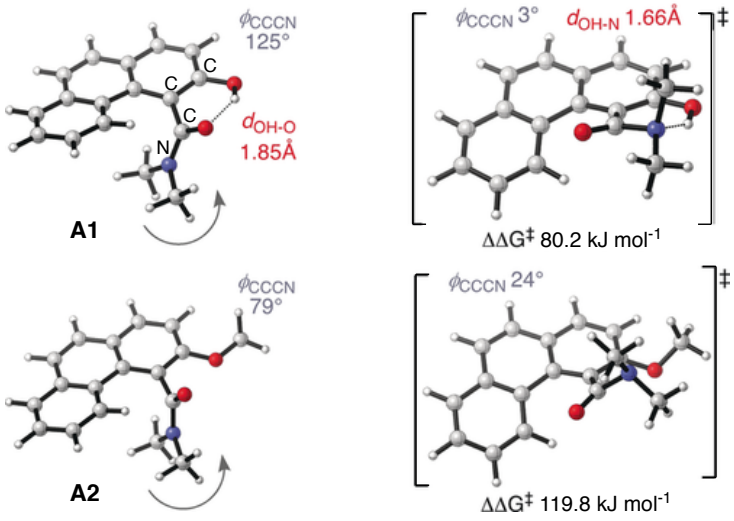

Figure 4.14. Ground and transition state structures for molecules **A1** and **A2**

In the molecule **A2**, with an absence of a free naphthol, the rotational TS cannot be similarly stabilized due to the non-planar amide.

4.4 Conclusion

In the first section, we have explained the first theoretical studies on how biaryl atropisomerism, and consequently, the rate of racemization, is affected by one-electron oxidation. Simply put, the resistance towards biaryl rotation is dramatically reduced via oxidation. The rotational TS of closed-shell biaryls become a stable minimum as the planar conformation of oxidized biaryls experiences preferential stabilization, and the enantiomerization mechanism changes from one, to two-steps. We envisage that singly-oxidized biaryls can undergo atropisomerization at temperatures far below those required for their parent compounds: metal coordination may also assist such racemization. SET from biaryls preferentially stabilizes the planar form over the non-planar ground state, as the HOMO energy is higher in this species, which creates a greater bonding interaction across the connecting biaryl bond. We postulate that this effect may be useful in the development of new approaches for the asymmetric synthesis of biaryls,[5,75–77] particularly if it can be employed in the framework of dynamic kinetic resolution.[29] Moreover, oxidatively-promoted biaryl and helicene atropisomerization may have consequences for the purpose of such compounds in pharmaceutical applications.

In the second section, with the aid of experimental research, we have discovered a highly enantioselective route to synthesise axially chiral napthamides. In this method, a transition-state hydrogen bond is relied on to lower the reaction barrier to rotation and hence promotes substrate racemization. By *O*-alkylation, a dynamic kinetic resolution can be achieved as this removes the free naphthol. Such axially chiral molecules can similarly find applications in catalytic and medicinal chemistry.

References

1. Tan, J. S. J. & Paton, R. S. Frontier molecular orbital effects control the hole-catalyzed racemization of atropisomeric biaryls. *Chem. Sci.* **10**, 2285–2289 (2019).

2. Fugard, A. J. *et al.* Hydrogen-Bond-Enabled Dynamic Kinetic Resolution of Axially Chiral Amides Mediated by a Chiral Counterion. *Angew. Chemie Int. Ed.* **58**, 2795–2798 (2019).

3. Kumarasamy, E., Raghunathan, R., Sibi, M. P. & Sivaguru, J. Nonbiaryl and Heterobiaryl Atropisomers: Molecular Templates with Promise for Atropselective Chemical Transformations. *Chem. Rev.* (2015).

4. Toenjes, S. T. & Gustafson, J. L. Atropisomerism in medicinal chemistry: Challenges and opportunities. *Future Medicinal Chemistry* (2018).

5. Bringmann, G. *et al.* Atroposelective synthesis of axially chiral biaryl compounds. *Angew. Chemie - Int. Ed.* **44**, 5384–5427 (2005).

6. Sanz García, J., Lepetit, C., Canac, Y., Chauvin, R. & Boggio-Pasqua, M. Enantiomerization pathway and atropochiral stability of the BINAP ligand: A density functional theory study. *Chem. - An Asian J.* **9**, 462–465 (2014).

7. Ōki, M. Recent Advances in Atropisomerism. in *Topics in Stereochemistry* **14**, 1–81 (2007).

8. Laplante, S. R., Edwards, P. J., Fader, L. D., Jakalian, A. & Hucke, O. Revealing Atropisomer Axial Chirality in Drug Discovery. *ChemMedChem* **6**, 505–513 (2011).

9. Pivonka, D. E. & Wesolowski, S. S. Vibrational Circular dichroism (VCD) chiral

assignment of atropisomers: Application to γ-aminobutyric acid (GABA) modulators designed as potential anxiolytic drugs. *Appl. Spectrosc.* **67**, 365–370 (2013).

10. Smyth, J. E., Butler, N. M. & Keller, P. A. A twist of nature – the significance of atropisomers in biological systems. *Nat. Prod. Rep.* **32**, 1562–1583 (2015).

11. Glunz, P. W. Recent encounters with atropisomerism in drug discovery. *Bioorg. Med. Chem. Lett.* **28**, 53–60 (2018).

12. Clayden, J., Moran, W. J., Edwards, P. J. & Laplante, S. R. The challenge of atropisomerism in drug discovery. *Angew. Chemie - Int. Ed.* **48**, 6398–6401 (2009).

13. Albert, J. S. *et al.* Design, synthesis, and SAR of tachykinin antagonists: Modulation of balance in NK1/NK2 receptor antagonist activity. *J. Med. Chem.* (2002).

14. Albert, J. S. *et al.* Structural Analysis and Optimization of NK1 Receptor Antagonists through Modulation of Atropisomer Interconversion Properties. *J. Med. Chem.* (2004).

15. Harris, T. *et al.* Twisted Cycloalkynes and Remote Activation of "Click" Reactivity. *Chem* **3**, 629–640 (2017).

16. Patel, D. C. *et al.* Gram scale conversion of R-BINAM to R-NOBIN. *J. Org. Chem.* **81**, 1295–1299 (2016).

17. Yoshikawa, N. *et al.* Direct catalytic asymmetric aldol reaction: Synthesis of either syn-or anti-α,β-dihydroxy ketones. *Journal of the American Chemical*

Society (2001).

18. Lu, B., Liu, C., Li, Y., Xu, J. & Liu, G. Conducting polynaphthalenes from 1,1′-binaphthyl and 1,1′-bi-2-naphthol via electropolymerization. *Synth. Met.* **161**, 188–195 (2011).

19. Lu, B. *et al.* Facile electrosynthesis of novel free-standing electroactive poly((S)-(-)-1,1′-bi-2-naphthol dimethyl ether) films with enhanced main chain axial chirality. *Electrochim. Acta* **55**, 2391–2397 (2010).

20. Rulíšek, L. *et al.* On the convergence of the physicochemical properties of [n]helicenes. *J. Phys. Chem. C* **111**, 14948–14955 (2007).

21. Aloui, F., El Abed, R., Marinetti, A. & Ben Hassine, B. Synthesis and characterization of new hexahelicene derivatives. *Tetrahedron Lett.* **48**, 2017–2020 (2007).

22. El Abed, R., Aloui, F., Genêt, J.-P., Ben Hassine, B. & Marinetti, A. Synthesis and resolution of 2-(diphenylphosphino)heptahelicene. *J. Organomet. Chem.* **692**, 1156–1160 (2007).

23. Gingras, M. One hundred years of helicene chemistry. Part 3: Applications and properties of carbohelicenes. *Chemical Society Reviews* (2013).

24. Meca, L., Řeha, D. & Havlas, Z. Racemization Barriers of 1,1‘-Binaphthyl and 1,1‘-Binaphthalene-2,2‘-diol: A DFT Study. *J. Org. Chem.* **68**, 5677–5680 (2003).

25. Genaev, A. M., Salnikov, G. E., Shernyukov, A. V., Zhu, Z. & Koltunov, K. Y. Protonation Behavior of 1,1′-Bi-2-naphthol and Insights into Its Acid-Catalyzed

Atropisomerization. *Org. Lett.* **19**, 532–535 (2017).

26. Boyd, M. R. *et al.* Anti-HIV Michellamines from Ancistrocladus korupensis. *J. Med. Chem.* **37**, 1740–1745 (1994).

27. Mislow, K. & Gordon, A. J. Photoracemization of Biphenyls. *J. Am. Chem. Soc.* **85**, 3521–3521 (1963).

28. Narute, S., Parnes, R., Toste, F. D. & Pappo, D. Enantioselective Oxidative Homocoupling and Cross-Coupling of 2-Naphthols Catalyzed by Chiral Iron Phosphate Complexes. *J. Am. Chem. Soc.* **138**, 16553–16560 (2016).

29. Moustafa, G. A. I., Ōki, Y. & Akai, S. Lipase-Catalyzed Dynamic Kinetic Resolution of C1- and C2-Symmetric Racemic Axially Chiral 2,2′-Dihydroxy-1,1′-biaryls. *Angew. Chemie - Int. Ed.* **57**, 10278–10282 (2018).

30. Ho (Kenny) Park, K., Chen, R. & Chen, D. Y. K. Programmed serial stereochemical relay and its application in the synthesis of morphinans. *Chem. Sci.* **8**, 7031–7037 (2017).

31. Ballard, A. *et al.* Quantitative Prediction of Rate Constants for Aqueous Racemization To Avoid Pointless Stereoselective Syntheses. *Angew. Chemie - Int. Ed.* **57**, 982–985 (2018).

32. Carreño, M. C. *et al.* Towards Configurationally Stable [4]Helicenes: Enantioselective Synthesis of 12-Substituted 7,8-Dihydro[4]helicene Quinones. *Chem. - A Eur. J.* **14**, 603–620 (2008).

33. Barroso, J. *et al.* Revisiting the racemization mechanism of helicenes. *Chem. Commun.* **54**, 188–191 (2018).

34. Adriaenssens, L. *et al.* [6]Saddlequat: a [6]helquat captured on its racemization pathway. *Chem. Sci.* **2**, 2314–2320 (2011).

35. Sevov, C. S. & Wiest, O. Selectivity in the electron transfer catalyzed Diels-Alder reaction of (R)-alpha-phellandrene and 4-methoxystyrene. *J. Org. Chem.* **73**, 7909–7915 (2008).

36. Patel, D. C., Woods, R. M., Breitbach, Z. S., Berthod, A. & Armstrong, D. W. Thermal racemization of biaryl atropisomers. *Tetrahedron: Asymmetry* **28**, 1557–1561 (2017).

37. Kumarasamy, E. *et al.* Tale of Twisted Molecules. Atropselective Photoreactions: Taming Light Induced Asymmetric Transformations through Non-biaryl Atropisomers. *Acc. Chem. Res.* **49**, 2713–2724 (2016).

38. Zhang, Z., Wang, Y. & Nakano, T. Photo Racemization and Polymerization of (R)-1,1'-Bi(2-naphthol). *Molecules* **21**, 1–10 (2016).

39. Christie, G. H. & Kenner, J. LXXI.—The molecular configurations of polynuclear aromatic compounds. Part I. The resolution of γ-6 : 6′-dinitro- and 4 : 6 : 4′ : 6′-tetranitro-diphenic acids into optically active components. *J. Chem. Soc., Trans.* **121**, 614–620 (1922).

40. Clayden, J., Lund, A., Vallverdú, L. & Helltwell, M. Ultra-remote stereocontrol by conformational communication of information along a carbon chain. *Nature* (2004).

41. Laplante, S. R. *et al.* Assessing atropisomer axial chirality in drug discovery and development. *Journal of Medicinal Chemistry* (2011).

42. Suda, T., Noguchi, K., Hirano, M. & Tanaka, K. Highly enantioselective synthesis of N,N-dialkvlbenzamides with aryl-carbonyl axial chirality by rhodium-catalyzed [2+2+2] cycloaddition. *Chem. - A Eur. J.* (2008).

43. Brandes, S., Bella, M., Kjœrsgaard, A. & Jørgensen, K. A. Chirally aminated 2-naphthols - organocatalytic synthesis of non-biaryl atropisomers by asymmetric friedel-crafts amination. *Angew. Chemie - Int. Ed.* (2006).

44. Barrett, K. T. & Miller, S. J. Enantioselective synthesis of atropisomeric benzamides through peptide-catalyzed bromination. *J. Am. Chem. Soc.* (2013).

45. Fäseke, V. C. & Sparr, C. Stereoselective Arene-Forming Aldol Condensation: Synthesis of Axially Chiral Aromatic Amides. *Angew. Chemie - Int. Ed.* (2016).

46. Díaz, J. E. *et al.* Atropisomerism in amidinoquinoxaline N-oxides: Effect of the ring size and substituents on the enantiomerization barriers. *J. Org. Chem.* (2015).

47. Frisch, M. J. *et al.* Gaussian 09, Revision D.01. *Gaussian Inc Wallingford CT* (2009).

48. Becke, A. D. Density-functional exchange-energy approximation with correct asymptotic behavior. *Phys. Rev. A* **38**, 3098–3100 (1988).

49. Lee, C., Yang, W. & Parr, R. G. Development of the Colle-Salvetti correlation-energy formula into a functional of the electron density. *Phys. Rev. B* **37**, 785–789 (1988).

50. Stephens, P. J., Devlin, F. J., Chabalowski, C. F. & Frisch, M. J. Ab Initio Calculation of Vibrational Absorption and Circular Dichroism Spectra Using

Density Functional Force Fields. *J. Phys. Chem.* **98**, 11623–11627 (1994).

51. Zhao, Y. & Truhlar, D. G. Density functionals with broad applicability in chemistry. *Acc. Chem. Res.* **41**, 157–167 (2008).

52. Grimme, S., Ehrlich, S. & Goerigk, L. Effect of the damping function in dispersion corrected density functional theory. *J. Comput. Chem.* **32**, 1456–1465 (2011).

53. Weigend, F. & Ahlrichs, R. Balanced basis sets of split valence, triple zeta valence and quadruple zeta valence quality for H to Rn: Design and assessment of accuracy. *Phys. Chem. Chem. Phys.* **7**, 3297 (2005).

54. Schäfer, A., Huber, C. & Ahlrichs, R. Fully optimized contracted Gaussian basis sets of triple zeta valence quality for atoms Li to Kr. *J. Chem. Phys.* **100**, 5829–5835 (1994).

55. Schäfer, A., Horn, H. & Ahlrichs, R. Fully optimized contracted Gaussian basis sets for atoms Li to Kr. *J. Chem. Phys.* **97**, 2571–2577 (1992).

56. Řezáč, J., Šimová, L. & Hobza, P. CCSD[T] Describes Noncovalent Interactions Better than the CCSD(T), CCSD(TQ), and CCSDT Methods. *J. Chem. Theory Comput.* **9**, 364–369 (2013).

57. Čížek, J. and J. P. Coupled Cluster Approach. *Phys. Scr.* **21**, 251–254 (1980).

58. Čížek, J. On the Correlation Problem in Atomic and Molecular Systems. Calculation of Wavefunction Components in Ursell-Type Expansion Using Quantum-Field Theoretical Methods. *J. Chem. Phys.* **45**, 4256 (1966).

59. Neese, F. The ORCA program system. *Wiley Interdiscip. Rev. Comput. Mol.*

Sci. **2**, 73–78 (2012).

60. Neese, F., Hansen, A. & Liakos, D. G. Efficient and accurate approximations to the local coupled cluster singles doubles method using a truncated pair natural orbital basis. *J. Chem. Phys.* **131**, (2009).

61. Mennucci, B., Cancès, E. & Tomasi, J. Evaluation of Solvent Effects in Isotropic and Anisotropic Dielectrics and in Ionic Solutions with a Unified Integral Equation Method: Theoretical Bases, Computational Implementation, and Numerical Applications. *J. Phys. Chem. B* **101**, 10506–10517 (1997).

62. Fukui, K. The Path of Chemical Reactions - The IRC Approach. *Acc. Chem. Res.* **14**, 363–368 (1981).

63. Gilbert, A. T. B. IQmol molecular viewer.

64. Grimme, S. Supramolecular Binding Thermodynamics by Dispersion-Corrected Density Functional Theory. *Chem. - A Eur. J.* **18**, 9955–9964 (2012).

65. Paton, R. S. & Funes-Ardoiz, I. GoodVibes v2.0.2.

66. Legault, C. Y. CYLview User Manual. *Comput. Programs Biomed.* **18**, 99–108 (2010).

67. Studer, A. & Curran, D. P. The electron is a catalyst. *Nat. Chem.* **6**, 765–773 (2014).

68. Saettel, N. J., Oxgaard, J. & Wiest, O. Pericyclic Reactions of Radical Cations. *European J. Org. Chem.* **2001**, 1429–1439 (2001).

69. Wiest, O., Oxgaard, J. & Saettel, N. J. Structure and reactivity of hydrocarbon radical cations. in *Advances in Physical Organic Chemistry* 87–109 (2003).

70. Donoghue, P. J. & Wiest, O. Structure and reactivity of radical ions: New twists on old concepts. *Chem. - A Eur. J.* **12**, 7018–7026 (2006).

71. Bally, T. & Sastry, G. N. Incorrect Dissociation Behavior of Radical Ions in Density Functional Calculations. *J. Phys. Chem. A* **101**, 7923–7925 (1997).

72. Johnson, E. R., Otero-de-la-Roza, A. & Dale, S. G. Extreme density-driven delocalization error for a model solvated-electron system. *J. Chem. Phys.* **139**, 184116 (2013).

73. Zimmerman, H. E. & Crumrine, D. S. Duality of Mechanism in Photoracemization of Optically Active Biphenyls. Mechanistic and Exploratory Organic Photochemistry. LXV. *J. Am. Chem. Soc.* **94**, 498–506 (1972).

74. Zimmerman, H. E. & Alabugin, I. V. Excited State Energy Distribution and Redistribution and Chemical Reactivity; Mechanistic and Exploratory Organic Photochemistry *J. Am. Chem. Soc.* **2000** , *122* , 952−953. *J. Am. Chem. Soc.* **122**, 1000–1000 (2000).

75. Zilate, B., Castrogiovanni, A. & Sparr, C. Catalyst-Controlled Stereoselective Synthesis of Atropisomers. *ACS Catal.* **8**, 2981–2988 (2018).

76. Jolliffe, J. D., Armstrong, R. J. & Smith, M. D. Catalytic enantioselective synthesis of atropisomeric biaryls by a cation-directed O-alkylation. *Nat. Chem.* **9**, 558–562 (2017).

77. Chen, Y.-H., Qi, L.-W., Fang, F. & Tan, B. Organocatalytic Atroposelective Arylation of 2-Naphthylamines as a Practical Approach to Axially Chiral Biaryl Amino Alcohols. *Angew. Chemie Int. Ed.* **56**, 16308–16312 (2017).

Appendix
Implications of electron removal on atropisomerism
I. Absolute Contributions to Gibbs Energies

Gas Phase:

		E(au)	ZPE(au)	H(au)	T.qh-S(au)	qh-G(T)(au)	imag. n (cm^{-1})	single point energy (au)
Molecule 1				**B3LYP/6-31G(d)**				**B3LYP-D3(BJ)/def2-TZVP**
Neutral	GS	-770.58763	0.275673	-770.29683	0.055312	-770.35215		-770.943581
	TS	-770.55071	0.276376	-770.26031	0.05267	-770.31298	-39.78	-770.90665
Radical cation	GS	-770.33696	0.276222	-770.04567	0.055464	-770.10113		-770.682671
	TS	-770.31095	0.27651	-770.02033	0.053488	-770.07382	-10.17	-770.657227
Molecule 1				**M06-2X/6-31G(d)**				**M06-2X/def2-TZVP**
Neutral	GS	-770.25958	0.278497	-769.96607	0.054993	-770.02107		-770.533922
	TS	-770.22151	0.279225	-769.92835	0.052517	-769.98087	-37.71	-770.495502
Radical cation	GS	-769.99217	0.278538	-769.69865	0.055287	-769.75394		-770.258795
	TS	-769.96677	0.278836	-769.67387	0.053451	-769.72732	-22.98	-770.233506

Molecule 2				**B3LYP/6-31G(d)**				**B3LYP-D3(BJ)/def2-TZVP**
Neutral	GS	-921.02799	0.284105	-920.72649	0.060005	-920.78649		-921.469161
	TS (anti)	-920.96767	0.28388	-920.66769	0.056405	-920.72409	-3.53	-921.407547
	TS (syn)	-920.96121	0.28420	-920.66096	0.055739	-920.71669	-18.74	-921.400852
Radical cation	GS	-920.77558	0.28443	-920.47385	0.059732	-920.53358		-921.206009
	INT (180°)	-920.73633	0.284339	-920.43481	0.060507	-920.49531		-921.166491
	TS (anti)	-920.73427	0.284262	-920.43358	0.057869	-920.49145	-33.12	-921.164378
	TS (syn)	-920.72449	0.284251	-920.42383	0.057239	-920.48106	-42.46	-920.911118
Molecule 2				**M06-2X/6-31G(d)**				**M06-2X/def2-TZVP**
Neutral	GS	-920.65748	0.287483	-920.35282	0.058874	-920.41169		-921.009693
	TS (anti)	-920.59681	0.287693	-920.29325	0.056004	-920.34926	-5.32	-920.94716
	TS (syn)	-920.59078	0.287903	-920.28702	0.055428	-920.34245	-25.64	-920.941045
Radical cation	GS	-920.39009	0.2874	-920.08559	0.059314	-920.1449		-920.733478
	INT (180°)	-920.35370	0.287743	-920.04903	0.059169	-920.10820		-920.696678
	TS (anti)	-920.34857	0.287004	-920.04507	0.058086	-920.10316	-53.22	-920.691721
	TS (syn)	-920.3386	0.287342	-920.03495	0.057087	-920.09203	-54.02	-920.681921

Molecule 3		**B3LYP/6-31G(d)**						**B3LYP-D3(BJ)/def2-TZVP**
Neutral	GS	-999.62675	0.340808	-999.26541	0.066127	-999.33154		-1000.094059
	TS	-999.56307	0.340176	-999.20364	0.062783	-999.26643	-11.06	-1000.032309
Radical cation	GS	-999.39095	0.341348	-999.02906	0.066359	-999.09542		-999.847882
	TS	-999.34911	0.341049	-998.98862	0.063925	-999.05255	-7.9	-999.808152
Molecule 3		**M06-2X/6-31G(d)**						**M06-2X/def2-TZVP**
Neutral	GS	-999.21144	0.344973	-998.84623	0.065205	-998.91144		-999.581851
	TS	-999.15114	0.344522	-998.78771	0.06211	-998.84982	-16.06	-999.520162
Radical cation	GS	-998.96099	0.344895	-998.59581	0.065776	-998.66158		-999.322468
	TS	-998.92366	0.345035	-998.55945	0.06339	-998.62284	-18.92	-999.284919

Molecule 4		**B3LYP/6-31G(d)**						**B3LYP-D3(BJ)/def2-TZVP**
Neutral	GS	-960.32693	0.312371	-959.99554	0.063032	-960.05857		-960.781292
	TS	-960.26496	0.312056	-959.9352	0.059664	-959.99486	-22.85	-960.719353
Radical cation	GS	-960.08369	0.312872	-959.75188	0.063108	-959.81499		-960.527362
	TS	-960.04214	0.312657	-959.71148	0.061055	-959.77254	-23.65	-960.486599
Molecule 4		**M06-2X/6-31G(d)**						**M06-2X/def2-TZVP**
Neutral	GS	-959.93397	0.316085	-959.59909	0.062239	-959.66133		-960.295308
	TS	-959.87327	0.315869	-959.5399	0.059323	-959.59922	-27.22	-960.233
Radical cation	GS	-959.6759	0.31605	-959.3411	0.062699	-959.4038		-960.026283
	TS	-959.63527	0.31578	-959.30146	0.061158	-959.36261	-47.04	-959.987638

Molecule 5		**B3LYP/6-31G(d)**						**B3LYP-D3(BJ)/def2-TZVP**
Neutral	GS	-881.29642	0.308834	-880.96956	0.060434	-881.02999		-881.720857
	TS	-881.2301	0.308394	-880.90486	0.057528	-880.96239	-2.67	-881.654594
Radical cation	GS	-881.06716	0.309007	-880.73988	0.061378	-880.80126		-881.480627
	TS	-881.02434	0.309626	-880.69774	0.058664	-880.7564	-32.54	-881.437994
Molecule 5		**M06-2X/6-31G(d)**						**M06-2X/def2-TZVP**
Neutral	GS	-880.93108	0.312137	-880.60112	0.059852	-880.66098		-881.261563
	TS	-880.86506	0.312086	-880.53639	0.057095	-880.59349	-9.73	-881.194296
Radical cation	GS	-880.68865	0.312244	-880.35847	0.060666	-880.41914		-881.010044
	TS	-880.64662	0.312871	-880.3169	0.058501	-880.3754	-45.25	-880.967469

Molecule 6		**B3LYP/6-31G(d)**						**B3LYP-D3(BJ)/def2-TZVP**
Neutral	GS	-846.8069	0.288475	-846.50284	0.055681	-846.55852		-847.19783
	TS	-846.76804	0.287776	-846.46522	0.054627	-846.51984	-116.97	-847.158761
Radical cation	GS	-846.55664	0.288201	-846.25259	0.056856	-846.30945		-846.936875
	TS	-846.52539	0.28804	-846.22221	0.05544	-846.27765	-80.03	-846.906087
Molecule 6		**M06-2X/6-31G(d)**						**M06-2X/def2-TZVP**

Neutral	GS	-846.45568	0.291516	-846.14867	0.05551	-846.20418		-846.753729
	TS	-846.41361	0.290869	-846.10779	0.054501	-846.16229	-112.85	-846.712522
Radical cation	GS	-846.18397	0.290127	-845.87798	0.056898	-845.93488		-846.479359
	TS	-846.15499	0.290629	-845.84929	0.055358	-845.90465	-76.33	-846.446811

Molecule 7	**B3LYP/6-31G(d)**							**B3LYP-D3(BJ)/def2-TZVP**
Neutral	GS	-1000.4429	0.33507	-1000.0896	0.060959	-1000.1505		-1000.907726
	TS	-1000.3837	0.333974	-1000.0322	0.059515	-1000.0917	-41.3	-1000.84784
Radical cation	GS	-1000.1967	0.333819	-999.844	0.062889	-999.90689		-1000.651435
	TS	-1000.1477	0.334062	-999.79591	0.06044	-999.85635	-28.18	-1000.602444
Molecule 7	**M06-2X/6-31G(d)**							**M06-2X/def2-TZVP**
Neutral	GS	-1000.0342	0.338669	-999.67738	0.060738	-999.73811		-1000.385148
	TS	-999.97213	0.337709	-999.61697	0.059318	-999.67629	-41.02	-1000.32362
Radical cation	GS	-999.77001	0.337508	-999.414	0.062057	-999.47606		-1000.113934
	TS	-999.71796	0.336872	-999.3634	0.060406	-999.42381	-32.43	-1000.06212

Dichloromethane in SMD:

		E/au	**ZPE/au**	**H/au**	**T.qh-S/au**	**qh-G(T)/au**	**imag. ν**	
Molecule 1	**B3LYP/6-31G(d)**							**B3LYP-D3(BJ)/def2-TZVP**
Neutral	GS	-770.611198	0.275593	-770.320446	0.055582	-770.376029		-770.966937
	TS	-770.57496	0.276131	-770.284746	0.052798	-770.337544	-45.86	-770.930832
Radical cation	GS	-770.414602	0.276134	-770.123431	0.055405	-770.178836		-770.761921
	TS	-770.389323	0.276352	-770.098831	0.053554	-770.152385	-11.31	-770.737209
Molecule 1	**M062X/6-31G(d)**							**M062X/def2-TZVP**
Neutral	GS	-770.284909	0.278464	-769.991438	0.05493	-770.046368		-770.559216
	TS	-770.247491	0.278901	-769.954609	0.052623	-770.007232	-40.79	-770.521473
Radical cation	GS	-770.070908	0.27812	-769.77785	0.055195	-769.833046		-770.338734
	TS	-770.046426	0.278442	-769.753885	0.053501	-769.807386	-33.27	-770.314355

Molecule 2	**B3LYP/6-31G(d)**							**B3LYP-D3(BJ)/def2-TZVP**
Neutral	GS	-921.053312	0.283727	-920.752202	0.059483	-920.811685		-921.494807
	TS	-920.992402	0.283289	-920.692888	0.056629	-920.749517	-14.31	-921.432553
Radical cation	GS	-920.856029	0.284342	-920.554499	0.059434	-920.613933		-921.288277
	TS	-920.815463	0.283872	-920.515163	0.057873	-920.573036	-41.89	-921.247037
Molecule 2	**M062X/6-31G(d)**							**M062X/def2-TZVP**
Neutral	GS	-920.683813	0.286513	-920.379882	0.059615	-920.439497		-921.03632
	TS	-920.623347	0.286844	-920.320513	0.056234	-920.376747	-15.72	-920.97387
Radical cation	GS	-920.471216	0.286775	-920.167334	0.059292	-920.226626		-920.815819
	TS	-920.43145	0.286849	-920.12829	0.057691	-920.185981	-52.22	-920.775211

Molecule 3		B3LYP/6-31G(d)						B3LYP-D3(BJ)/def2-TZVP
Neutral	GS	-999.65366	0.340679	-999.292416	0.066318	-999.358734		-1000.120856
	TS	-999.591247	0.340461	-999.231657	0.062532	-999.294189	-14.62	-1000.060237
Radical cation	GS	-999.465391	0.340534	-999.104095	0.066936	-999.171032		-999.923938
	TS	-999.426186	0.341267	-999.065601	0.063637	-999.129238	-27.15	-999.886602
Molecule 3		**M062X/6-31G(d)**						**M062X/def2-TZVP**
Neutral	GS	-999.239993	0.344724	-998.875045	0.065144	-998.940189		-999.610572
	TS	-999.181041	0.344406	-998.817753	0.062063	-998.879816	-17.00	-999.550071
Radical cation	GS	-999.036873	0.343863	-998.672619	0.066015	-998.738634		-999.399561
	TS	-999.002114	0.344925	-998.638085	0.063226	-998.701311	-35.75	-999.364435

Molecule 4		B3LYP/6-31G(d)						B3LYP-D3(BJ)/def2-TZVP
Neutral	GS	-960.353474	0.3123	-960.022186	0.062896	-960.085082		-960.807929
	TS	-960.291768	0.311895	-959.962146	0.059717	-960.021863	-30.27	-960.746256
Radical cation	GS	-960.161034	0.312589	-959.829568	0.062943	-959.892511		-960.606417
	TS	-960.120496	0.312403	-959.790139	0.060918	-959.851057	-36.81	-960.566364
Molecule 4		**M062X/6-31G(d)**						**M062X/def2-TZVP**
Neutral	GS	-959.962222	0.315708	-959.627661	0.062464	-959.690125		-960.32374
	TS	-959.902011	0.315753	-959.56881	0.059201	-959.628011	-24.02	-960.261851
Radical cation	GS	-959.754217	0.315315	-959.420162	0.062621	-959.482784		-960.107835
	TS	-959.715399	0.315291	-959.382135	0.061029	-959.443164	-72.23	-960.06841
Molecule 5		**B3LYP/6-31G(d)**						**B3LYP-D3(BJ)/def2-TZVP**
Neutral	GS	-881.326498	0.308795	-880.999763	0.060263	-881.060026		-881.750033
	TS	-881.25987	0.307895	-880.935037	0.057715	-880.992751	-9.18	-881.684064
Radical cation	GS	-881.149305	0.308681	-880.822462	0.061138	-880.8836		-881.564246
	TS	-881.108583	0.309265	-880.782339	0.058693	-880.841032	-38.05	-881.523619
Molecule 5		**M062X/6-31G(d)**						**M062X/def2-TZVP**
Neutral	GS	-880.962822	0.311338	-880.633522	0.060308	-880.693829		-881.29251
	TS	-880.896488	0.311194	-880.568552	0.057394	-880.625946	-9.93	-881.225575
Radical cation	GS	-880.772689	0.311736	-880.443109	0.060457	-880.503566		-881.094982
	TS	-880.732952	0.312351	-880.403757	0.058521	-880.462278	-59.30	-881.05448

Molecule 6		B3LYP/6-31G(d)						B3LYP-D3(BJ)/def2-TZVP
Neutral	GS	-846.832556	0.288455	-846.528506	0.055045	-846.583551		-847.222839
	TS	-846.795257	0.287633	-846.492509	0.054774	-846.547284	-153.57	-847.185347
Radical cation	GS	-846.635321	0.288248	-846.331301	0.056701	-846.388002		-847.017212
	TS	-846.605053	0.288198	-846.301741	0.055417	-846.357158	-107.96	-846.987289
Molecule 6		**M062X/6-31G(d)**						**M062X/def2-TZVP**
Neutral	GS	-846.483137	0.291436	-846.176216	0.054857	-846.231073		-846.78113
	TS	-846.442938	0.290852	-846.137115	0.054546	-846.191661	-136.86	-846.741764
Radical cation	GS	-846.268355	0.290474	-845.962159	0.056625	-846.018784		-846.560401
	TS	-846.236001	0.290575	-845.93037	0.055336	-845.985706	-103.00	-846.528909

Molecule 7		B3LYP/6-31G(d)						B3LYP-D3(BJ)/def2-TZVP
Neutral	GS	-1000.472325	0.335089	-1000.118928	0.060981	-1000.179909		-1000.93689
	TS	-1000.414761	0.333685	-1000.063398	0.059758	-1000.123156	-80.48	-1000.878575
Radical cation	GS	-1000.27625	0.333974	-999.923598	0.062411	-999.986009		-1000.732788
	TS	-1000.228103	0.333402	-999.876845	0.060745	-999.93759	-70.87	-1000.684456
Molecule 7		**M062X/6-31G(d)**						**M062X/def2-TZVP**
Neutral	GS	-1000.06577	0.338639	-999.708992	0.060677	-999.769669		-1000.416658
	TS	-1000.005446	0.337419	-999.650521	0.05946	-999.709981	-81.14	-1000.356796
Radical cation	GS	-999.851487	0.337227	-999.495792	0.061973	-999.557764		-1000.196579
	TS	-999.799815	0.335724	-999.44615	0.060981	-999.507131	-77.84	-1000.145102

II. Cartesian Coordinates

Gas Phase:

Molecule 1 (neutral TS b3lyp)

C	-2.36787	1.45731	-0.34768
C	-1.98464	0.11139	-0.06908
C	-0.61766	-0.41468	-0.09673
C	0.61766	0.41468	0.09673
C	1.98464	-0.11139	0.06908
C	2.36787	-1.45731	0.34768
C	3.67454	-1.89080	0.25582
C	4.70499	-1.00512	-0.12002
C	4.40418	0.32640	-0.27818
C	3.07615	0.81082	-0.12851
C	2.85193	2.21029	-0.07324
C	1.60816	2.67513	0.26682
C	0.51991	1.78359	0.35126
C	-0.51991	-1.78359	-0.35126
C	-1.60816	-2.67513	-0.26682
C	-2.85193	-2.21029	0.07324
C	-3.07615	-0.81082	0.12851
C	-4.40418	-0.32640	0.27818
C	-4.70499	1.00512	0.12002
C	-3.67454	1.89080	-0.25582
H	-1.63700	2.15535	-0.72824
H	-3.91074	2.92252	-0.50160
H	-5.72709	1.35905	0.22291
H	-5.19100	-1.05072	0.47723
H	-3.68907	-2.88709	0.22216
H	-1.43478	-3.73464	-0.43417
H	0.43280	-2.20681	-0.62422
H	1.63700	-2.15535	0.72824
H	3.91074	-2.92252	0.50160
H	5.72709	-1.35905	-0.22291
H	5.19100	1.05072	-0.47723
H	3.68907	2.88709	-0.22216
H	1.43478	3.73464	0.43417
H	-0.43280	2.20681	0.62422

Molecule 1 (radical cation TS b3lyp)

C	-2.35324	1.43971	-0.39794
C	-1.96525	0.11442	-0.10146
C	-0.59162	-0.40172	-0.13084
C	0.59162	0.40172	0.13084
C	1.96525	-0.11442	0.10146
C	2.35324	-1.43971	0.39794
C	3.67633	-1.85937	0.28000
C	4.68167	-0.97118	-0.12667
C	4.36098	0.36160	-0.31116
C	3.03009	0.82158	-0.14788
C	2.77544	2.21358	-0.09762
C	1.52629	2.68036	0.29252
C	0.46836	1.78750	0.42545
C	-0.46836	-1.78750	-0.42545
C	-1.52629	-2.68036	-0.29252
C	-2.77544	-2.21358	0.09762
C	-3.03009	-0.82158	0.14788
C	-4.36098	-0.36160	0.31116
C	-4.68167	0.97118	0.12667
C	-3.67633	1.85937	-0.28000
H	-1.63654	2.13689	-0.81132
H	-3.92939	2.88475	-0.53196
H	-5.70559	1.31283	0.23758
H	-5.13574	-1.08691	0.54324
H	-3.59418	-2.90658	0.27023
H	-1.36660	-3.73739	-0.47841
H	0.48477	-2.17396	-0.75507

H	1.63654	-2.13689	0.81132
H	3.92939	-2.88475	0.53196
H	5.70559	-1.31283	-0.23758
H	5.13574	1.08691	-0.54324
H	3.59418	2.90658	-0.27023
H	1.36660	3.73739	0.47841
H	-0.48477	2.17396	0.75507

Molecule 1 (radical cation TS m062x)

C	-2.35140	1.45136	-0.35428
C	-1.97437	0.10700	-0.06252
C	-0.61445	-0.41837	-0.09659
C	0.61445	0.41837	0.09659
C	1.97437	-0.10700	0.06252
C	2.35140	-1.45136	0.35428
C	3.65203	-1.88425	0.26350
C	4.68194	-1.00224	-0.12339
C	4.38402	0.32358	-0.28687
C	3.05708	0.80675	-0.13647
C	2.83506	2.20640	-0.07639
C	1.60054	2.66858	0.27803
C	0.51180	1.77516	0.36460
C	-0.51180	-1.77516	-0.36460
C	-1.60054	-2.66858	-0.27803
C	-2.83506	-2.20640	0.07639
C	-3.05708	-0.80675	0.13647
C	-4.38402	-0.32358	0.28687
C	-4.68194	1.00224	0.12339
C	-3.65203	1.88425	-0.26350
H	-1.61740	2.14019	-0.74663
H	-3.88923	2.91167	-0.52186
H	-5.70187	1.35888	0.22488
H	-5.16902	-1.04693	0.49160
H	-3.67340	-2.88043	0.22869
H	-1.42901	-3.72610	-0.45199
H	0.43995	-2.19373	-0.64907
H	1.61740	-2.14019	0.74663
H	3.88923	-2.91167	0.52186
H	5.70187	-1.35888	-0.22488
H	5.16902	1.04693	-0.49160
H	3.67340	2.88043	-0.22869
H	1.42901	3.72610	0.45199
H	-0.43995	2.19373	0.64907

Molecule 1 (radical cation TS m062x)

C	2.18815	-1.40142	-0.49703
C	1.92585	-0.07797	-0.08951
C	0.59165	0.51211	-0.00167
C	-0.58669	-0.28421	0.26151
C	-1.97443	0.16208	0.11395
C	-2.45280	1.47927	0.26773
C	-3.77813	1.80352	0.01923
C	-4.70038	0.82978	-0.38535
C	-4.29678	-0.48634	-0.42860
C	-2.96128	-0.84563	-0.13217
C	-2.64777	-2.21390	0.05711
C	-1.41436	-2.58755	0.56342
C	-0.41156	-1.63324	0.66976
C	0.52942	1.91762	-0.17885
C	1.64501	2.73222	-0.04059
C	2.88550	2.16632	0.21459
C	3.05726	0.76405	0.13724
C	4.36144	0.21756	0.15305
C	4.57240	-1.11220	-0.14687
C	3.48066	-1.90767	-0.51802
H	1.38308	-2.02197	-0.87218
H	3.64428	-2.92745	-0.85048
H	5.57557	-1.52369	-0.14945
H	5.19869	0.87541	0.36718
H	3.75519	2.79541	0.38184
H	1.53728	3.80816	-0.11754
H	-0.41169	2.38903	-0.41079
H	-1.82127	2.25012	0.68487
H	-4.10586	2.82710	0.16846
H	-5.72811	1.10098	-0.59909
H	-5.00813	-1.27609	-0.65198
H	-3.42452	-2.95517	-0.10871
H	-1.22095	-3.61404	0.85315
H	0.54753	-1.93413	1.07108

Molecule 2 (neutral TS b3lyp - anti)

C	2.36747	1.30469	-0.59078
C	1.98113	0.03037	-0.08535
C	0.58819	-0.44799	-0.07428
C	-0.58819	0.44799	0.07428
C	-1.98113	-0.03037	0.08535
C	-2.36747	-1.30469	0.59078
C	-3.68245	-1.73806	0.56779
C	-4.70200	-0.91814	0.05028
C	-4.38694	0.36970	-0.32916
C	-3.05909	0.85561	-0.25752
C	-2.79475	2.24776	-0.37492
C	-1.57723	2.71876	0.02258
C	-0.51004	1.83495	0.34480
C	3.68245	1.73806	-0.56779
C	4.70200	0.91814	-0.05028
C	4.38694	-0.36970	0.32916
C	3.05909	-0.85561	0.25752

C	2.79475	-2.24776	0.37492
C	1.57723	-2.71876	-0.02258
C	0.51004	-1.83495	-0.34480
O	-0.52916	-2.48893	-0.92758
O	0.52916	2.48893	0.92758
H	1.62570	1.93885	-1.05830
H	-1.62570	-1.93885	1.05830
H	-3.92559	-2.71315	0.98119
H	-5.72791	-1.27257	0.01052
H	-5.16856	1.05977	-0.63870
H	-3.59195	2.92595	-0.66649
H	-1.36976	3.78090	0.10730
H	3.92559	2.71315	-0.98119
H	5.72791	1.27257	-0.01052
H	5.16856	-1.05977	0.63870
H	3.59195	-2.92595	0.66649
H	1.36976	-3.78090	-0.10730
H	-1.26784	-1.88037	-1.09663
H	1.26784	1.88037	1.09663

Molecule 2 (neutral TS b3lyp - syn)

C	-0.55278	-1.35780	1.80031
C	-0.19145	-1.68506	0.46667
C	-0.17108	-0.73056	-0.65141
C	0.17108	0.73056	-0.65141
C	0.19145	1.68506	0.46667
C	0.55278	1.35780	1.80031
C	0.52601	2.28752	2.82375
C	0.14287	3.61977	2.57869
C	-0.08038	4.01054	1.27702
C	0.01016	3.08766	0.20461
C	0.08038	3.56665	-1.13287
C	0.48142	2.71470	-2.12058
C	0.60004	1.32127	-1.86540
C	-0.52601	-2.28752	2.82375
C	-0.14287	-3.61977	2.57869
C	0.08038	-4.01054	1.27702
C	-0.01016	-3.08766	0.20461
C	-0.08038	-3.56665	-1.13287
C	-0.48142	-2.71470	-2.12058
C	-0.60004	-1.32127	-1.86540
O	-1.11802	-0.64169	-2.92619
O	1.11802	0.64169	-2.92619
H	-0.93431	-0.37138	2.01588
H	0.93431	0.37138	2.01588
H	0.83269	1.98583	3.82194
H	0.09390	4.33948	3.39084
H	-0.26948	5.05474	1.03852
H	-0.07158	4.62403	-1.33191
H	0.70641	3.05506	-3.12642
H	-0.83269	-1.98583	3.82194
H	-0.09390	-4.33948	3.39084
H	0.26948	-5.05474	1.03852
H	0.07158	-4.62403	-1.33191
H	-0.70641	-3.05506	-3.12642
H	-1.24467	0.29112	-2.68403
H	1.24467	-0.29112	-2.68403

Molecule 2 (radical cation TS b3lyp - anti)

C	-2.67489	1.42286	0.00945
C	-2.02531	0.16733	0.08251
C	-0.61588	-0.08836	0.43402
C	0.59252	0.68054	0.12138
C	1.80885	-0.06231	-0.25147
C	1.75636	-1.34062	-0.85494
C	2.91382	-2.03173	-1.18951
C	4.17703	-1.47461	-0.94327
C	4.26383	-0.19897	-0.40750
C	3.09950	0.53179	-0.08704
C	3.18487	1.89662	0.31472
C	2.05419	2.66660	0.39273
C	0.77505	2.10387	0.18390
C	-3.97369	1.55940	-0.47300
C	-4.70263	0.44561	-0.90216
C	-4.15271	-0.81206	-0.71561
C	-2.85748	-0.97535	-0.18067
C	-2.43279	-2.28059	0.21500
C	-1.27692	-2.45567	0.92470
C	-0.39298	-1.36701	1.07738
O	0.65693	-1.61810	1.86242
O	-0.20554	3.01360	0.12883
H	-2.25413	2.28944	0.50066
H	0.79577	-1.78139	-1.09616
H	2.83392	-3.00621	-1.66132
H	5.07737	-2.02345	-1.19988
H	5.23255	0.26901	-0.25625
H	4.16214	2.34418	0.47191
H	2.09730	3.73460	0.57811
H	-4.43029	2.54450	-0.48012
H	-5.70350	0.55858	-1.30523
H	-4.73233	-1.70230	-0.94384
H	-3.09426	-3.12206	0.02955
H	-0.99833	-3.40685	1.36449
H	1.24892	-0.84726	1.92029
H	-0.97082	2.66116	-0.35606

Molecule 2 (radical cation TS b3lyp - syn)

C	-0.23695	-1.58462	1.92758

C	-0.13818	-1.76051	0.53176
C	-0.21541	-0.70371	-0.49064
C	0.21541	0.70371	-0.49064
C	0.13818	1.76051	0.53176
C	0.23695	1.58462	1.92758
C	0.05934	2.63483	2.82200
C	-0.23695	3.92502	2.36796
C	-0.23729	4.16196	1.00355
C	0.00129	3.12118	0.08048
C	0.22483	3.45485	-1.28718
C	0.69037	2.51372	-2.16703
C	0.76224	1.16896	-1.75353
C	-0.05934	-2.63483	2.82200
C	0.23695	-3.92502	2.36796
C	0.23729	-4.16196	1.00355
C	-0.00129	-3.12118	0.08048
C	-0.22483	-3.45485	-1.28718
C	-0.69037	-2.51372	-2.16703
C	-0.76224	-1.16896	-1.75353
O	-1.35461	-0.35442	-2.63428
O	1.35461	0.35442	-2.63428
H	-0.55891	-0.63838	2.32530
H	0.55891	0.63838	2.32530
H	0.17466	2.44628	3.88510
H	-0.40569	4.73499	3.06994
H	-0.37989	5.16896	0.62137
H	0.12213	4.49067	-1.59784
H	1.02706	2.76232	-3.16749
H	-0.17466	-2.44628	3.88510
H	0.40569	-4.73499	3.06994
H	0.37989	-5.16896	0.62137
H	-0.12213	-4.49067	-1.59784
H	-1.02706	-2.76232	-3.16749
H	-1.46249	0.54289	-2.27186
H	1.46249	-0.54289	-2.27186

Molecule 2 (neutral TS m062x - anti)

C	2.35008	1.29787	-0.58836
C	1.97328	0.02676	-0.07310
C	0.58688	-0.45155	-0.06537
C	-0.58688	0.45155	0.06537
C	-1.97328	-0.02676	0.07310
C	-2.35008	-1.29787	0.58836
C	-3.65819	-1.73058	0.57376
C	-4.68108	-0.91360	0.05818
C	-4.37175	0.36823	-0.32672
C	-3.04439	0.85139	-0.26458
C	-2.78092	2.24458	-0.38369
C	-1.57021	2.71303	0.01690
C	-0.50463	1.82476	0.34063
C	3.65819	1.73058	-0.57376
C	4.68108	0.91360	-0.05818
C	4.37175	-0.36823	0.32672
C	3.04439	-0.85139	0.26458
C	2.78092	-2.24458	0.38369
C	1.57021	-2.71303	-0.01690
C	0.50463	-1.82476	-0.34063
O	-0.53175	-2.47111	-0.92330
O	0.53175	2.47111	0.92330
H	1.59810	1.92813	-1.04583
H	-1.59810	-1.92813	1.04583
H	-3.89919	-2.70259	0.99263
H	-5.70546	-1.26974	0.02659
H	-5.15333	1.05750	-0.63591
H	-3.57923	2.92041	-0.67562
H	-1.35635	3.77330	0.10178
H	3.89919	2.70259	-0.99263
H	5.70546	1.26974	-0.02659
H	5.15333	-1.05750	0.63591
H	3.57923	-2.92041	0.67562
H	1.35635	-3.77330	-0.10178
H	-1.23269	-1.84727	-1.16611
H	1.23269	1.84727	1.16611

Molecule 2 (neutral TS m062x - syn)

C	-0.46385	-1.40814	1.82419
C	-0.15625	-1.70603	0.47168
C	-0.18076	-0.73027	-0.61901
C	0.18076	0.73027	-0.61901
C	0.15625	1.70603	0.47168
C	0.46385	1.40814	1.82419
C	0.38922	2.35606	2.82039
C	0.01641	3.68095	2.52835
C	-0.13843	4.04122	1.21331
C	-0.00238	3.09258	0.17163
C	0.13843	3.54194	-1.17164
C	0.57241	2.66763	-2.11595
C	0.65358	1.27606	-1.82319
C	-0.38922	-2.35606	2.82039
C	-0.01641	-3.68095	2.52835
C	0.13843	-4.04122	1.21331
C	0.00238	-3.09258	0.17163
C	-0.13843	-3.54194	-1.17164
C	-0.57241	-2.66763	-2.11595
C	-0.65358	-1.27606	-1.82319
O	-1.16163	-0.56285	-2.85586
O	1.16163	0.56285	-2.85586
H	-0.85772	-0.43391	2.07023

H	0.85772	0.43391	2.07023
H	0.65719	2.08013	3.83583
H	-0.06955	4.41784	3.32013
H	-0.31195	5.07876	0.93953
H	0.00633	4.59593	-1.39821
H	0.83744	2.97425	-3.12210
H	-0.65719	-2.08013	3.83583
H	0.06955	-4.41784	3.32013
H	0.31195	-5.07876	0.93953
H	-0.00633	-4.59593	-1.39821
H	-0.83744	-2.97425	-3.12210
H	-1.25177	0.36866	-2.59722
H	1.25177	-0.36866	-2.59722

Molecule 2 (radical cation TS m062x -anti)

C	-2.65034	1.44120	-0.14581
C	-2.01451	0.19830	0.06776
C	-0.61695	-0.02952	0.45323
C	0.59800	0.71082	0.12129
C	1.76956	-0.07406	-0.28303
C	1.64236	-1.35217	-0.86988
C	2.75800	-2.08665	-1.22889
C	4.04831	-1.57514	-1.02836
C	4.20179	-0.30619	-0.50707
C	3.07703	0.46551	-0.15224
C	3.22639	1.81991	0.26839
C	2.13339	2.62503	0.41421
C	0.82852	2.11195	0.23953
C	-3.93356	1.53318	-0.66139
C	-4.66143	0.38666	-0.98846
C	-4.12114	-0.84535	-0.67570
C	-2.83743	-0.95666	-0.11277
C	-2.41533	-2.23556	0.37326
C	-1.26069	-2.37279	1.07824
C	-0.37968	-1.27175	1.15420
O	0.68238	-1.47392	1.91585
O	-0.13114	3.03945	0.29331
H	-2.23644	2.35303	0.25525
H	0.65554	-1.75231	-1.07930
H	2.62897	-3.06153	-1.68700
H	4.91675	-2.16049	-1.30951
H	5.19090	0.12569	-0.38580
H	4.22577	2.22556	0.39730
H	2.21755	3.68318	0.63504
H	-4.38326	2.51358	-0.77823
H	-5.65488	0.46402	-1.41539
H	-4.69691	-1.75313	-0.83122
H	-3.08281	-3.08241	0.24221
H	-0.96872	-3.29450	1.56765
H	1.27525	-0.70231	1.92332
H	-0.85128	2.79718	-0.30669

Molecule 2 (radical cation TS m062x - syn)

C	-0.13208	-1.62651	1.94245
C	-0.11200	-1.77463	0.54331
C	-0.22108	-0.69852	-0.44901
C	0.22108	0.69852	-0.44901
C	0.11200	1.77463	0.54331
C	0.13208	1.62651	1.94245
C	-0.08851	2.69427	2.79725
C	-0.34937	3.97400	2.29849
C	-0.27487	4.17828	0.93551
C	-0.00030	3.11471	0.05535
C	0.27487	3.41764	-1.31321
C	0.75063	2.46019	-2.15820
C	0.79253	1.12433	-1.70774
C	0.08851	-2.69427	2.79725
C	0.34937	-3.97400	2.29849
C	0.27487	-4.17828	0.93551
C	0.00030	-3.11471	0.05535
C	-0.27487	-3.41764	-1.31321
C	-0.75063	-2.46019	-2.15820
C	-0.79253	-1.12433	-1.70774
O	-1.36670	-0.27811	-2.55443
O	1.36670	0.27811	-2.55443
H	-0.43667	-0.69223	2.37724
H	0.43667	0.69223	2.37724
H	-0.03394	2.53089	3.86847
H	-0.54865	4.80027	2.97157
H	-0.39096	5.17540	0.52084
H	0.18944	4.44862	-1.64442
H	1.10956	2.67486	-3.15809
H	0.03394	-2.53089	3.86847
H	0.54865	-4.80027	2.97157
H	0.39096	-5.17540	0.52084
H	-0.18944	-4.44862	-1.64442
H	-1.10956	-2.67486	-3.15809
H	-1.47156	0.60724	-2.16546
H	1.47156	-0.60724	-2.16546

Molecule 3 (neutral TS b3lyp)

C	2.47079	0.98930	0.75656
C	1.96978	-0.17244	0.10583
C	0.54435	-0.50243	0.02487
C	-0.54404	0.50286	-0.02419
C	-1.96927	0.17232	-0.10628
C	-2.46915	-0.98934	-0.75803
C	-3.81779	-1.27258	-0.81825

C	-4.76535	-0.41664	-0.21467
C	-4.33326	0.76928	0.33061
C	-2.95597	1.11802	0.33076
C	-2.55146	2.44012	0.63791
C	-1.28134	2.84091	0.30970
C	-0.31457	1.90046	-0.13184
C	3.81960	1.27208	0.81519
C	4.76622	0.41548	0.21110
C	4.33313	-0.77067	-0.33289
C	2.95570	-1.11888	-0.33141
C	2.55045	-2.44107	-0.63712
C	1.28040	-2.84111	-0.30771
C	0.31426	-1.89987	0.13351
O	-0.84578	-2.31855	0.70757
O	0.84541	2.32017	-0.70525
H	1.78158	1.63304	1.28683
H	-1.77907	-1.63269	-1.28769
H	-4.15447	-2.15385	-1.35880
H	-5.82307	-0.66429	-0.23730
H	-5.04625	1.49301	0.71942
H	-3.27699	3.15308	1.02065
H	-1.00767	3.88612	0.39189
H	4.15717	2.15349	1.35497
H	5.82405	0.66278	0.23242
H	5.04545	-1.49498	-0.72186
H	3.27548	-3.15466	-1.01967
H	1.00628	-3.88628	-0.38884
C	1.16746	3.70045	-0.74474
H	0.42479	4.27053	-1.31692
H	1.25725	4.13021	0.26192
H	2.13559	3.75749	-1.24501
C	-1.16898	-3.69855	0.74775
H	-1.25826	-4.12896	-0.25867
H	-0.42726	-4.26881	1.32098
H	-2.13761	-3.75444	1.24718

Molecule 3 (radical cation TS b3lyp)

C	2.37495	-0.97081	-0.89476
C	1.93528	0.16261	-0.18397
C	0.51070	0.51901	-0.01830
C	-0.53849	-0.44409	0.10430
C	-1.99015	-0.16779	0.12995
C	-2.58049	0.93898	0.76737
C	-3.95539	1.14311	0.73733
C	-4.80163	0.25790	0.05296
C	-4.26249	-0.88601	-0.50874
C	-2.87579	-1.14392	-0.42567
C	-2.37374	-2.43854	-0.74439
C	-1.11815	-2.82220	-0.32729
C	-0.24758	-1.86574	0.23662
C	3.72636	-1.26634	-1.02239
C	4.70124	-0.44802	-0.43025
C	4.30618	0.71450	0.20723
C	2.93861	1.06130	0.28948
C	2.55257	2.36740	0.70533
C	1.28138	2.83102	0.45146
C	0.29350	1.95667	-0.05137
O	-0.84505	2.40071	-0.57449
O	0.84294	-2.19902	0.91950
H	1.65200	-1.60117	-1.40084
H	-1.96733	1.61963	1.34304
H	-4.37751	1.99192	1.26741
H	-5.87049	0.44111	0.01110
H	-4.90543	-1.62856	-0.97327
H	-3.03850	-3.16654	-1.20093
H	-0.81256	-3.85857	-0.40228
H	4.02934	-2.13215	-1.60400
H	5.75367	-0.69904	-0.51515
H	5.04535	1.40239	0.60847
H	3.30292	3.03964	1.11203
H	1.04425	3.87534	0.61246
C	1.21706	-3.57738	1.07741
H	0.41428	-4.13983	1.56302
H	1.46554	-4.02585	0.11003
H	2.10004	-3.55950	1.71460
C	-1.12415	3.80859	-0.64787
H	-1.21404	4.24205	0.35353
H	-0.34542	4.32463	-1.21686
H	-2.07787	3.87942	-1.16918

Molecule 3 (neutral TS m062x)

C	2.59133	0.96481	0.63119
C	1.99083	-0.19111	0.05850
C	0.55816	-0.46186	0.08736
C	-0.52738	0.55360	0.02185
C	-1.92847	0.18524	-0.13928
C	-2.34646	-1.01025	-0.78837
C	-3.67150	-1.33622	-0.93001
C	-4.68283	-0.49070	-0.41966
C	-4.32453	0.71583	0.11826
C	-2.96086	1.10184	0.20730
C	-2.61529	2.43635	0.53109
C	-1.33855	2.86387	0.30463
C	-0.32132	1.94193	-0.05851
C	3.94590	1.18287	0.57722
C	4.80364	0.25786	-0.05811
C	4.27958	-0.92621	-0.50320
C	2.89222	-1.20257	-0.38468

C	2.41329	-2.52299	-0.57102
C	1.16119	-2.84305	-0.12923
C	0.27007	-1.82320	0.29813
O	-0.87509	-2.13848	0.94941
O	0.85681	2.39144	-0.54955
H	1.97405	1.64933	1.19660
H	-1.59588	-1.64805	-1.24287
H	-3.94465	-2.24285	-1.46248
H	-5.72764	-0.77076	-0.50792
H	-5.08018	1.42663	0.44313
H	-3.38738	3.13094	0.84959
H	-1.09223	3.91418	0.40398
H	4.36389	2.06235	1.05871
H	5.86880	0.45418	-0.12662
H	4.92429	-1.70458	-0.90353
H	3.08362	-3.28946	-0.94937
H	0.83642	-3.87644	-0.11600
C	1.23552	3.73604	-0.35815
H	0.60446	4.41658	-0.94063
H	1.19529	4.01989	0.70120
H	2.26536	3.80299	-0.71115
C	-1.36132	-3.46134	0.90484
H	-1.47096	-3.81608	-0.12801
H	-0.70748	-4.14580	1.45749
H	-2.34277	-3.43122	1.37829

Molecule 3 (radical cation TS m062x)

C	2.19612	-1.03275	-0.92924
C	1.87699	0.14848	-0.23094
C	0.49172	0.57539	0.03308
C	-0.57036	-0.37037	0.18810
C	-2.02716	-0.16121	0.09069
C	-2.73498	0.94063	0.60218
C	-4.10536	1.05583	0.43406
C	-4.83326	0.08408	-0.26376
C	-4.18344	-1.05590	-0.68875
C	-2.80194	-1.21882	-0.46537
C	-2.21859	-2.50957	-0.64201
C	-0.99313	-2.80433	-0.10597
C	-0.21961	-1.75469	0.43709
C	3.50877	-1.40441	-1.15249
C	4.56994	-0.61296	-0.68574
C	4.28882	0.58809	-0.07190
C	2.95349	1.00105	0.11880
C	2.67001	2.33288	0.53939
C	1.40695	2.84624	0.42220
C	0.33285	2.00818	0.04170
O	-0.84165	2.50087	-0.30138
O	0.84533	-1.96266	1.18713
H	1.39884	-1.64374	-1.34297
H	-2.22016	1.68606	1.18989
H	-4.62115	1.90608	0.86872
H	-5.90069	0.19971	-0.41535
H	-4.73574	-1.86713	-1.15416
H	-2.81767	-3.29623	-1.09181
H	-0.63130	-3.82439	-0.07964
H	3.71787	-2.30840	-1.71581
H	5.59648	-0.92067	-0.85101
H	5.08993	1.25377	0.23603
H	3.48910	2.97341	0.85368
H	1.22686	3.89693	0.60974
C	1.36822	-3.28173	1.33961
H	0.63185	-3.93203	1.81868
H	1.66394	-3.68639	0.36633
H	2.24288	-3.17273	1.97698
C	-1.08602	3.90681	-0.26867
H	-0.99455	4.29200	0.75098
H	-0.39681	4.42843	-0.93753
H	-2.10921	4.02424	-0.62112

Molecule 4 (neutral TS b3lyp)

C	-2.34464	-1.38989	0.70842
C	-1.99736	-0.15904	0.07574
C	-0.61334	0.31687	-0.04680
C	0.54126	-0.61151	-0.14919
C	1.96253	-0.22557	-0.11500
C	2.46509	1.00085	-0.62503
C	3.80624	1.32969	-0.56408
C	4.74136	0.44838	0.01323
C	4.31442	-0.80161	0.40272
C	2.95463	-1.18411	0.27956
C	2.59073	-2.55455	0.39269
C	1.36199	-2.94991	-0.05085
C	0.37299	-1.99392	-0.40788
C	-3.65296	-1.82133	0.80253
C	-4.70869	-1.05220	0.26926
C	-4.42794	0.18902	-0.25485
C	-3.09906	0.68468	-0.30186
C	-2.84552	2.04531	-0.59817
C	-1.60904	2.56526	-0.31295
C	-0.53120	1.72821	0.07855
O	0.59437	2.26540	0.61592
O	-0.70362	-2.57387	-1.00557
H	-1.56585	-1.98474	1.16821
H	1.79527	1.67297	-1.13988
H	4.14323	2.27002	-0.99356
H	5.78942	0.72527	0.08641
H	5.02646	-1.54466	0.75494

H	3.33023	-3.28203	0.71679
H	1.08780	-3.99631	-0.14096
H	-3.86764	-2.75556	1.31425
H	-5.73207	-1.41249	0.32287
H	-5.23026	0.84074	-0.59331
H	-3.65355	2.68626	-0.93999
H	-1.44493	3.63337	-0.39264
C	0.74453	3.67240	0.71883
H	0.75150	4.15840	-0.26586
H	-0.04554	4.11604	1.33718
H	1.71248	3.82378	1.19945
H	-1.37851	-1.90550	-1.20596

Molecule 4 (radical cation TS b3lyp)

C	2.79873	1.42933	0.20997
C	2.09052	0.21383	0.04440
C	0.66493	-0.02948	0.31492
C	-0.49491	0.83095	0.09445
C	-1.74036	0.21413	-0.38658
C	-1.74521	-0.95893	-1.17324
C	-2.93203	-1.53137	-1.61573
C	-4.16852	-0.95142	-1.29725
C	-4.19422	0.23496	-0.58117
C	-2.99741	0.84690	-0.15046
C	-3.01618	2.14448	0.43942
C	-1.84849	2.83873	0.62104
C	-0.60018	2.24316	0.33700
C	4.11703	1.57730	-0.20804
C	4.80747	0.51824	-0.81171
C	4.19513	-0.72060	-0.86610
C	2.87500	-0.90736	-0.39768
C	2.37104	-2.23150	-0.25211
C	1.19138	-2.47121	0.40680
C	0.36673	-1.37898	0.75505
O	-0.72149	-1.51015	1.50996
O	0.42763	3.10094	0.39124
H	2.39388	2.21865	0.82915
H	-0.80471	-1.40423	-1.47820
H	-2.89553	-2.42407	-2.23321
H	-5.09261	-1.40596	-1.63975
H	-5.13876	0.72841	-0.36929
H	-3.97045	2.61661	0.65548
H	-1.83871	3.87313	0.94770
H	4.62185	2.52194	-0.02899
H	5.82542	0.64953	-1.16326
H	4.73947	-1.58606	-1.23402
H	2.98778	-3.06310	-0.58126
H	0.89007	-3.48383	0.64344
C	-1.17803	-2.80838	1.92470
H	-1.44604	-3.41712	1.05527
H	-0.41684	-3.31195	2.52779
H	-2.06225	-2.61666	2.53086
H	1.18372	2.76179	-0.11740

Molecule 4 (neutral TS m062x)

C	2.29279	-1.40486	-0.69266
C	1.98678	-0.14933	-0.08953
C	0.62059	0.34596	0.06013
C	-0.53583	-0.58476	0.17689
C	-1.95536	-0.22705	0.08408
C	-2.49708	1.00150	0.54614
C	-3.83515	1.30031	0.42948
C	-4.73169	0.38338	-0.15306
C	-4.26997	-0.86661	-0.47872
C	-2.90896	-1.21350	-0.29805
C	-2.51875	-2.58220	-0.33673
C	-1.30621	-2.93182	0.16650
C	-0.34647	-1.93621	0.50397
C	3.58526	-1.85161	-0.81884
C	4.66856	-1.07878	-0.34733
C	4.42268	0.17449	0.14818
C	3.10124	0.68376	0.22776
C	2.87549	2.05280	0.50557
C	1.63956	2.58080	0.26360
C	0.54218	1.74363	-0.07011
O	-0.58999	2.27930	-0.57597
O	0.72960	-2.46025	1.13906
H	1.48636	-2.00379	-1.09805
H	-1.85726	1.69184	1.07616
H	-4.20589	2.24235	0.82339
H	-5.78027	0.63671	-0.27137
H	-4.95274	-1.63754	-0.82685
H	-3.23601	-3.33461	-0.65191
H	-1.00909	-3.96498	0.31182
H	3.77242	-2.80327	-1.30617
H	5.68368	-1.45385	-0.42661
H	5.24087	0.82596	0.44426
H	3.70589	2.68795	0.79972
H	1.48648	3.65136	0.32873
C	-0.83682	3.66298	-0.45626
H	-0.77162	3.99586	0.58723
H	-0.14192	4.24746	-1.06937
H	-1.85455	3.80951	-0.81983
H	1.35972	-1.76067	1.36783

Molecule 4 (radical cation TS m062x)

C	2.79909	1.46480	0.01020
C	2.09255	0.24060	0.04211

C	0.68070	0.03642	0.36563
C	-0.48809	0.86905	0.10050
C	-1.67337	0.20108	-0.43858
C	-1.57716	-0.98383	-1.19885
C	-2.70981	-1.61704	-1.68206
C	-3.98498	-1.08674	-1.43939
C	-4.10222	0.10416	-0.75049
C	-2.95929	0.77117	-0.26651
C	-3.06804	2.05779	0.33965
C	-1.94966	2.78797	0.62391
C	-0.66249	2.24850	0.40935
C	4.09755	1.55054	-0.46056
C	4.77506	0.41759	-0.92643
C	4.16299	-0.81033	-0.79968
C	2.85618	-0.92397	-0.28323
C	2.34468	-2.22580	-0.00519
C	1.15838	-2.40234	0.64671
C	0.34768	-1.27028	0.88299
O	-0.76879	-1.33108	1.58709
O	0.33421	3.11425	0.61843
H	2.42136	2.33753	0.51978
H	-0.59977	-1.38470	-1.44831
H	-2.60454	-2.51957	-2.27557
H	-4.86724	-1.58935	-1.82012
H	-5.07717	0.55606	-0.59187
H	-4.05419	2.48373	0.50128
H	-1.99951	3.80629	0.99262
H	4.60312	2.51021	-0.43340
H	5.78307	0.49805	-1.31706
H	4.69206	-1.72004	-1.06877
H	2.96393	-3.08462	-0.24834
H	0.83790	-3.38700	0.96139
C	-1.33916	-2.59666	1.92043
H	-1.53158	-3.16973	1.00774
H	-0.68283	-3.15071	2.59618
H	-2.27646	-2.36598	2.42191
H	1.06503	2.91838	0.01520

Molecule 5 (neutral TS b3lyp)

C	-2.37970	1.28446	0.61551
C	-1.98106	0.02919	0.07966
C	-0.58374	-0.43734	0.07706
C	0.58218	0.46014	-0.05548
C	1.97279	-0.02546	-0.08635
C	2.34123	-1.28188	-0.64110
C	3.65288	-1.72088	-0.65741
C	4.68734	-0.92873	-0.12246
C	4.38706	0.34343	0.31682
C	3.06044	0.83746	0.27843
C	2.80055	2.22475	0.44541
C	1.58940	2.71359	0.05008
C	0.50731	1.85719	-0.32775
C	-3.69807	1.70411	0.60135
C	-4.71011	0.89023	0.05694
C	-4.38211	-0.38292	-0.35947
C	-3.04923	-0.85595	-0.29089
C	-2.76735	-2.24230	-0.42921
C	-1.55695	-2.70752	-0.00419
C	-0.49317	-1.82854	0.37363
H	-1.64093	1.91819	1.08407
H	1.58310	-1.89906	-1.10160
H	3.88461	-2.68178	-1.10989
H	5.71168	-1.29099	-0.11395
H	5.17690	1.01662	0.64338
H	3.59573	2.89135	0.76878
H	1.40809	3.78619	0.02330
H	-3.95258	2.66614	1.03901
H	-5.73955	1.23630	0.02489
H	-5.15554	-1.07278	-0.69047
H	-3.54796	-2.92531	-0.75381
H	-1.36151	-3.77680	0.04510
N	-0.56409	2.50875	-0.92136
H	-0.31588	3.36091	-1.40640
H	-1.23175	1.94206	-1.42341
N	0.58214	-2.45215	0.98923
H	1.23725	-1.86576	1.48534
H	0.34387	-3.29969	1.48714

Molecule 5 (radical cation TS b3lyp)

C	-2.69930	1.39735	0.09241
C	-2.03111	0.15267	0.08937
C	-0.61129	-0.08460	0.41623
C	0.58157	0.69473	0.09821
C	1.80441	-0.05065	-0.26329
C	1.75139	-1.31614	-0.89194
C	2.90660	-2.01584	-1.21037
C	4.17191	-1.48278	-0.91697
C	4.25962	-0.21990	-0.35603
C	3.09558	0.51957	-0.05654
C	3.17882	1.88025	0.37030
C	2.06018	2.65886	0.39505
C	0.76169	2.12825	0.11389
C	-4.01636	1.52995	-0.33616
C	-4.73766	0.42232	-0.79525
C	-4.15474	-0.83114	-0.70179
C	-2.84246	-0.99238	-0.21488
C	-2.37355	-2.30930	0.09912
C	-1.22772	-2.48604	0.81167

C	-0.37720	-1.36864	1.06770
H	-2.23217	2.25308	0.55571
H	0.79023	-1.73766	-1.16446
H	2.82696	-2.97659	-1.71050
H	5.07145	-2.03866	-1.16166
H	5.22938	0.23406	-0.17061
H	4.15196	2.31498	0.58066
H	2.13686	3.72430	0.59648
H	-4.49236	2.50493	-0.28617
H	-5.75430	0.53361	-1.15788
H	-4.72306	-1.72000	-0.96224
H	-3.00536	-3.15926	-0.14284
H	-0.94366	-3.46293	1.19246
N	-0.22875	3.04133	-0.05533
H	0.04490	4.01550	-0.09620
H	-1.02234	2.80402	-0.63204
N	0.62592	-1.52880	1.94862
H	1.29368	-0.79165	2.12459
H	0.84543	-2.44467	2.31716

Molecule 5 (neutral TS m062x)

C	-2.41700	1.28522	0.56682
C	-1.98333	0.03178	0.05874
C	-0.58516	-0.40645	0.10589
C	0.57871	0.50043	-0.01365
C	1.94929	-0.01728	-0.08635
C	2.25783	-1.27536	-0.67113
C	3.54877	-1.74754	-0.73973
C	4.62301	-0.99290	-0.22934
C	4.37639	0.27450	0.23795
C	3.06384	0.80157	0.25387
C	2.84584	2.19108	0.45774
C	1.64017	2.71352	0.11338
C	0.52565	1.89098	-0.25127
C	-3.73631	1.67816	0.50776
C	-4.71716	0.83476	-0.04661
C	-4.35625	-0.43724	-0.41993
C	-3.01775	-0.87801	-0.30779
C	-2.70835	-2.26382	-0.39030
C	-1.50689	-2.68784	0.07998
C	-0.46772	-1.77167	0.44478
H	-1.70101	1.93659	1.04700
H	1.46067	-1.86200	-1.10811
H	3.73802	-2.70627	-1.21297
H	5.63469	-1.38445	-0.26243
H	5.19296	0.92045	0.55102
H	3.66719	2.82903	0.77136
H	1.47686	3.78844	0.12242
H	-4.02118	2.64040	0.92261
H	-5.75043	1.16003	-0.11254
H	-5.10538	-1.15177	-0.75218
H	-3.46907	-2.96996	-0.71061
H	-1.28443	-3.74857	0.16537
N	-0.53917	2.59166	-0.80052
H	-0.25064	3.42243	-1.30042
H	-1.21822	2.04641	-1.31329
N	0.61489	-2.35843	1.08227
H	1.25391	-1.73337	1.55435
H	0.36442	-3.16327	1.64125

Molecule 5 (radical cation TS m062x)

C	-2.68460	1.42118	-0.06131
C	-2.01991	0.18540	0.08025
C	-0.61394	-0.01593	0.45243
C	0.58874	0.73201	0.10671
C	1.75831	-0.06541	-0.29404
C	1.61582	-1.33391	-0.89815
C	2.71997	-2.08636	-1.25002
C	4.01873	-1.60586	-1.02051
C	4.18737	-0.34708	-0.48300
C	3.07156	0.44212	-0.14039
C	3.23296	1.79376	0.29676
C	2.15629	2.61411	0.39796
C	0.82333	2.14248	0.17131
C	-3.98054	1.50595	-0.54421
C	-4.68487	0.35758	-0.91546
C	-4.10633	-0.87491	-0.68197
C	-2.81226	-0.98050	-0.14592
C	-2.34523	-2.27127	0.27668
C	-1.20848	-2.39605	0.99935
C	-0.36494	-1.25365	1.17067
H	-2.24508	2.31529	0.34949
H	0.62315	-1.71023	-1.12424
H	2.57827	-3.04987	-1.72874
H	4.87960	-2.20493	-1.29636
H	5.18233	0.06520	-0.34110
H	4.23378	2.18121	0.46485
H	2.28543	3.66874	0.62389
H	-4.45834	2.47827	-0.60612
H	-5.68856	0.42969	-1.31905
H	-4.66235	-1.78784	-0.87529
H	-2.97606	-3.13548	0.08953
H	-0.91074	-3.34183	1.44087
N	-0.14549	3.08979	0.11923
H	0.16563	4.05316	0.14920
H	-0.92089	2.93245	-0.50697
N	0.66125	-1.35414	2.01840
H	1.30834	-0.58875	2.15408

H	0.88337	-2.23661	2.45970

Molecule 6 (neutral TS b3lyp)

C	-0.67954	3.22035	-0.49575
C	0.67953	3.22035	-0.49576
C	1.38247	2.01234	-0.26545
C	0.73639	0.73551	-0.34423
C	-0.73639	0.73551	-0.34423
C	-1.38248	2.01234	-0.26544
C	2.72691	2.16144	0.20614
C	1.66394	-0.40824	-0.20779
C	2.91427	-0.21404	0.47501
C	3.41609	1.10336	0.69496
C	3.73961	-1.31462	0.79876
H	4.64852	-1.12049	1.36257
C	3.44843	-2.58822	0.35717
C	2.35181	-2.75500	-0.49928
C	1.50715	-1.69299	-0.77483
H	3.13075	3.16822	0.26606
H	-1.24153	4.14833	-0.55285
H	1.24152	4.14833	-0.55286
H	4.38623	1.22504	1.16858
H	4.09597	-3.42459	0.60313
H	2.17042	-3.71323	-0.97763
H	-0.77122	-1.84256	-1.53803
C	-2.72691	2.16144	0.20615
H	-3.13075	3.16821	0.26608
C	-3.41610	1.10335	0.69497
H	-4.38623	1.22504	1.16858
C	-1.66394	-0.40824	-0.20779
C	-2.91427	-0.21404	0.47501
C	-3.73961	-1.31462	0.79875
H	-4.64853	-1.12050	1.36256
C	-3.44842	-2.58822	0.35716
H	-4.09596	-3.42460	0.60312
C	-2.35180	-2.75500	-0.49929
H	-2.17041	-3.71323	-0.97764
C	-1.50715	-1.69299	-0.77483
H	0.77123	-1.84257	-1.53803

Molecule 6 (radical cation TS b3lyp)

C	-0.67699	3.24700	-0.55427
C	0.67700	3.24700	-0.55428
C	1.37595	2.03230	-0.27531
C	0.72120	0.73776	-0.36689
C	-0.72120	0.73776	-0.36688
C	-1.37594	2.03231	-0.27531
C	2.68008	2.16509	0.24542
C	1.64192	-0.41549	-0.22390
C	2.86011	-0.23057	0.52016
C	3.34854	1.07801	0.76175
C	3.68712	-1.33198	0.84829
H	4.56958	-1.15072	1.45560
C	3.42156	-2.60005	0.35668
C	2.36239	-2.74700	-0.53941
C	1.51056	-1.67421	-0.83018
H	3.10778	3.15979	0.32450
H	-1.24447	4.16834	-0.64186
H	1.24448	4.16834	-0.64187
H	4.29725	1.20494	1.27542
H	4.06393	-3.43860	0.60430
H	2.19981	-3.69608	-1.04133
H	-0.80902	-1.81303	-1.63068
C	-2.68007	2.16510	0.24544
H	-3.10776	3.15980	0.32453
C	-3.34853	1.07801	0.76177
H	-4.29723	1.20495	1.27544
C	-1.64193	-0.41548	-0.22390
C	-2.86010	-0.23056	0.52016
C	-3.68712	-1.33197	0.84830
H	-4.56957	-1.15072	1.45561
C	-3.42157	-2.60004	0.35667
H	-4.06395	-3.43859	0.60429
C	-2.36241	-2.74699	-0.53943
H	-2.19983	-3.69606	-1.04136
C	-1.51058	-1.67420	-0.83019
H	0.80900	-1.81304	-1.63065

Molecule 6 (neutral TS m062x)

C	-0.67774	3.21425	-0.49426
C	0.67783	3.21421	-0.49441
C	1.37803	2.00380	-0.27176
C	0.73559	0.73632	-0.35066
C	-0.73558	0.73637	-0.35058
C	-1.37796	2.00387	-0.27152
C	2.72452	2.15636	0.20422
C	1.66246	-0.40904	-0.20742
C	2.90044	-0.21551	0.47845
C	3.40533	1.10428	0.70120
C	3.72801	-1.31119	0.80387
H	4.63239	-1.11405	1.37346
C	3.44300	-2.58182	0.36152
C	2.35356	-2.74889	-0.50170
C	1.51029	-1.69129	-0.77955
H	3.12610	3.16395	0.26201
H	-1.24124	4.14124	-0.54878
H	1.24137	4.14117	-0.54903
H	4.37287	1.22311	1.18033

H	4.09101	-3.41644	0.60876
H	2.18023	-3.70511	-0.98535
H	-0.78446	-1.83842	-1.55357
C	-2.72440	2.15643	0.20460
H	-3.12593	3.16402	0.26252
C	-3.40525	1.10433	0.70147
H	-4.37276	1.22316	1.18065
C	-1.66250	-0.40895	-0.20740
C	-2.90046	-0.21546	0.47851
C	-3.72806	-1.31117	0.80375
H	-4.63244	-1.11411	1.37338
C	-3.44310	-2.58174	0.36119
H	-4.09116	-3.41637	0.60828
C	-2.35365	-2.74875	-0.50203
H	-2.18036	-3.70492	-0.98580
C	-1.51036	-1.69113	-0.77972
H	0.78451	-1.83876	-1.55349

Molecule 6 (radical cation TS m062x)

C	-0.67434	3.24814	-0.57011
C	0.67434	3.24814	-0.57012
C	1.36926	2.02990	-0.28575
C	0.71518	0.74281	-0.39021
C	-0.71518	0.74281	-0.39021
C	-1.36926	2.02990	-0.28575
C	2.65842	2.15843	0.26214
C	1.62333	-0.41483	-0.23703
C	2.81244	-0.23963	0.53781
C	3.30120	1.06706	0.79545
C	3.62971	-1.33910	0.87467
H	4.49824	-1.16385	1.50296
C	3.37175	-2.59836	0.36610
C	2.33798	-2.73334	-0.55821
C	1.49808	-1.66052	-0.86086
H	3.08797	3.15073	0.35383
H	-1.24609	4.16632	-0.65862
H	1.24609	4.16632	-0.65863
H	4.23543	1.18444	1.33695
H	4.00556	-3.44067	0.61911
H	2.19040	-3.67616	-1.07473
H	-0.81972	-1.78424	-1.68347
C	-2.65841	2.15843	0.26214
H	-3.08797	3.15074	0.35384
C	-3.30120	1.06706	0.79545
H	-4.23543	1.18444	1.33695
C	-1.62333	-0.41483	-0.23703
C	-2.81244	-0.23962	0.53781
C	-3.62971	-1.33910	0.87467
H	-4.49825	-1.16385	1.50295
C	-3.37175	-2.59836	0.36609
H	-4.00556	-3.44066	0.61910
C	-2.33798	-2.73333	-0.55821
H	-2.19040	-3.67615	-1.07473
C	-1.49808	-1.66052	-0.86086
H	0.81972	-1.78424	-1.68347

Molecule 7 (neutral TS b3lyp)

C	1.19903	3.53612	-0.77084
C	2.31110	3.03341	-0.17089
C	2.34410	1.66855	0.22270
C	1.32290	0.76611	-0.19682
C	-0.00001	1.34980	-0.51012
C	-0.00002	2.76490	-0.77213
C	3.40532	1.22846	1.08247
C	1.75167	-0.63564	-0.17304
C	2.75147	-1.05721	0.76493
C	3.51498	-0.07134	1.46493
C	3.11899	-2.42128	0.83815
H	3.83573	-2.72302	1.59837
C	2.66301	-3.33228	-0.09441
C	1.86861	-2.87472	-1.15932
C	1.43024	-1.56232	-1.18780
H	4.08553	1.98412	1.46771
H	1.14733	4.57883	-1.07236
H	3.17591	3.65949	0.03350
H	4.26678	-0.39015	2.18220
H	2.97729	-4.37142	-0.04880
H	1.61056	-3.54543	-1.97431
C	-1.19908	3.53610	-0.77085
H	-1.14740	4.57881	-1.07237
C	-2.31115	3.03337	-0.17090
H	-3.17598	3.65944	0.03348
C	-1.32292	0.76609	-0.19682
C	-2.34413	1.66851	0.22269
C	-3.40535	1.22841	1.08246
H	-4.08557	1.98407	1.46769
C	-3.51499	-0.07139	1.46491
H	-4.26679	-0.39021	2.18219
C	-2.75145	-1.05725	0.76493
C	-1.75165	-0.63566	-0.17304
H	0.90692	-1.20215	-2.05985
C	-3.11895	-2.42133	0.83815
H	-3.83569	-2.72307	1.59837
C	-1.43020	-1.56235	-1.18779
H	-0.90689	-1.20218	-2.05984
C	-2.66295	-3.33232	-0.09440
H	-2.97721	-4.37147	-0.04878
C	-1.86855	-2.87476	-1.15931

H	-1.61048	-3.54547	-1.97429

Molecule 7 (radical cation TS b3lyp)

C	1.20064	3.53153	-0.78792
C	2.31532	3.02672	-0.16935
C	2.33708	1.67858	0.24668
C	1.30522	0.76934	-0.20642
C	0.00000	1.35993	-0.52889
C	0.00000	2.77020	-0.79307
C	3.36501	1.22205	1.12782
C	1.71139	-0.62501	-0.19044
C	2.68529	-1.06105	0.76843
C	3.44530	-0.08811	1.49481
C	3.02529	-2.42380	0.84390
H	3.71755	-2.74747	1.61625
C	2.56165	-3.33571	-0.10348
C	1.79621	-2.87400	-1.17416
C	1.38023	-1.54196	-1.21313
H	4.05258	1.95904	1.53205
H	1.16691	4.56834	-1.10903
H	3.17402	3.65847	0.03757
H	4.17514	-0.42296	2.22596
H	2.86266	-4.37722	-0.04909
H	1.54389	-3.53889	-1.99422
C	-1.20064	3.53153	-0.78792
H	-1.16692	4.56834	-1.10903
C	-2.31532	3.02672	-0.16935
H	-3.17402	3.65846	0.03757
C	-1.30522	0.76934	-0.20642
C	-2.33708	1.67857	0.24668
C	-3.36501	1.22205	1.12782
H	-4.05258	1.95904	1.53205
C	-3.44530	-0.08811	1.49481
H	-4.17514	-0.42296	2.22596
C	-2.68529	-1.06105	0.76843
C	-1.71139	-0.62501	-0.19044
H	0.92435	-1.16112	-2.11398
C	-3.02529	-2.42380	0.84390
H	-3.71755	-2.74747	1.61625
C	-1.38023	-1.54196	-1.21313
H	-0.92434	-1.16112	-2.11398
C	-2.56164	-3.33571	-0.10348
H	-2.86266	-4.37722	-0.04909
C	-1.79621	-2.87401	-1.17416
H	-1.54389	-3.53890	-1.99422

Molecule 7 (neutral TS m062x)

C	1.19907	3.53961	-0.75208
C	2.30483	3.02930	-0.15790
C	2.33216	1.65883	0.21611
C	1.31533	0.77328	-0.20719
C	0.00062	1.36063	-0.52406
C	0.00111	2.76688	-0.76780
C	3.38968	1.20788	1.07878
C	1.72330	-0.63193	-0.17648
C	2.70106	-1.06285	0.76339
C	3.47766	-0.08558	1.46601
C	3.05011	-2.42820	0.84000
H	3.75589	-2.73847	1.60604
C	2.58570	-3.33035	-0.09097
C	1.81220	-2.86165	-1.16428
C	1.40255	-1.54537	-1.19904
H	4.07279	1.95851	1.46695
H	1.14623	4.58542	-1.04013
H	3.17166	3.64814	0.05662
H	4.21937	-0.41586	2.18757
H	2.88157	-4.37349	-0.04143
H	1.55305	-3.52747	-1.98179
C	-1.19636	3.54040	-0.75248
H	-1.14283	4.58608	-1.04086
C	-2.30248	3.03094	-0.15826
H	-3.16896	3.65034	0.05601
C	-1.31456	0.77419	-0.20724
C	-2.33068	1.66056	0.21609
C	-3.38839	1.21055	1.07900
H	-4.07081	1.96177	1.46724
C	-3.47728	-0.08280	1.46640
H	-4.21907	-0.41243	2.18817
C	-2.70166	-1.06074	0.76365
C	-1.72371	-0.63070	-0.17644
H	0.90376	-1.16711	-2.07810
C	-3.05193	-2.42578	0.84036
H	-3.75781	-2.73539	1.60657
C	-1.40416	-1.54443	-1.19912
H	-0.90563	-1.16654	-2.07847
C	-2.58861	-3.32835	-0.09073
H	-2.88543	-4.37122	-0.04112
C	-1.81506	-2.86032	-1.16430
H	-1.55693	-3.52632	-1.98198

Molecule 7 (radical cation TS m062x)

C	1.19677	3.53011	-0.77944
C	2.30551	3.01903	-0.15824
C	2.31949	1.67104	0.24514
C	1.29390	0.77277	-0.21953
C	-0.00019	1.36444	-0.55098
C	-0.00034	2.76815	-0.80152
C	3.33825	1.20621	1.13824

C	1.68412	-0.62134	-0.19836
C	2.63266	-1.06452	0.76998
C	3.39660	-0.09676	1.50732
C	2.95718	-2.42419	0.84896
H	3.63831	-2.75569	1.62733
C	2.49080	-3.32778	-0.10189
C	1.74947	-2.85873	-1.18280
C	1.35760	-1.52436	-1.22907
H	4.02229	1.94058	1.55163
H	1.16391	4.56997	-1.08990
H	3.16328	3.64659	0.06252
H	4.11038	-0.44244	2.24877
H	2.77665	-4.37253	-0.04356
H	1.49966	-3.52089	-2.00514
C	-1.19754	3.52988	-0.77912
H	-1.16491	4.56981	-1.08940
C	-2.30613	3.01851	-0.15783
H	-3.16398	3.64592	0.06308
C	-1.29418	0.77247	-0.21948
C	-2.31990	1.67048	0.24534
C	-3.33879	1.20531	1.13815
H	-4.02303	1.93951	1.55152
C	-3.39700	-0.09772	1.50697
H	-4.11090	-0.44368	2.24817
C	-2.63271	-1.06520	0.76964
C	-1.68408	-0.62170	-0.19847
H	0.92153	-1.12936	-2.13422
C	-2.95668	-2.42501	0.84860
H	-3.63786	-2.75675	1.62682
C	-1.35695	-1.52466	-1.22908
H	-0.92095	-1.12946	-2.13417
C	-2.48971	-3.32844	-0.10209
H	-2.77517	-4.37330	-0.04379
C	-1.74832	-2.85915	-1.18287
H	-1.49813	-3.52124	-2.00515

Dichloromethane in SMD:

Molecule 1 (neutral TS b3lyp)

C	-2.37199	1.46055	-0.34427
C	-1.98738	0.11332	-0.06965
C	-0.61916	-0.41465	-0.09604
C	0.61916	0.41465	0.09604
C	1.98738	-0.11332	0.06965
C	2.37199	-1.46055	0.34427
C	3.68068	-1.89216	0.25201
C	4.71152	-1.00422	-0.12020
C	4.40989	0.32852	-0.27475
C	3.07975	0.81067	-0.12545
C	2.85703	2.21132	-0.07058
C	1.61128	2.67682	0.26340
C	0.52228	1.78480	0.34587
C	-0.52228	-1.78480	-0.34587
C	-1.61128	-2.67682	-0.26340
C	-2.85703	-2.21132	0.07058
C	-3.07975	-0.81067	0.12545
C	-4.40989	-0.32852	0.27475
C	-4.71152	1.00422	0.12020
C	-3.68068	1.89216	-0.25201
H	-1.64409	2.16517	-0.71811
H	-3.91629	2.92513	-0.49427
H	-5.73392	1.35783	0.22159
H	-5.19572	-1.05448	0.46988
H	-3.69567	-2.88655	0.21928
H	-1.43604	-3.73679	-0.42570
H	0.42934	-2.21576	-0.60881
H	1.64409	-2.16517	0.71811
H	3.91629	-2.92513	0.49427
H	5.73392	-1.35783	-0.22159
H	5.19572	1.05448	-0.46988
H	3.69567	2.88655	-0.21928
H	1.43604	3.73679	0.42570
H	-0.42934	2.21576	0.60881

Molecule 1 (radical cation TS b3lyp)

C	-2.35319	1.44296	-0.39378
C	-1.96566	0.11664	-0.10094
C	-0.59179	-0.40053	-0.13191
C	0.59179	0.40053	0.13191
C	1.96566	-0.11664	0.10094
C	2.35319	-1.44296	0.39378
C	3.67688	-1.86053	0.27690
C	4.68292	-0.96983	-0.12284
C	4.36192	0.36340	-0.30582
C	3.03004	0.82026	-0.14616
C	2.77533	2.21360	-0.10107
C	1.52682	2.67942	0.28763
C	0.46952	1.78602	0.42680
C	-0.46952	-1.78602	-0.42680
C	-1.52682	-2.67942	-0.28763
C	-2.77533	-2.21360	0.10107
C	-3.03004	-0.82026	0.14616
C	-4.36192	-0.36340	0.30582
C	-4.68292	0.96983	0.12284
C	-3.67688	1.86053	-0.27690
H	-1.63789	2.14679	-0.79788
H	-3.92824	2.88774	-0.52391
H	-5.70811	1.31012	0.23047

H	-5.13441	-1.09271	0.53302
H	-3.59501	-2.90397	0.27826
H	-1.36345	-3.73702	-0.46705
H	0.48067	-2.17782	-0.75745
H	1.63789	-2.14679	0.79788
H	3.92824	-2.88774	0.52391
H	5.70811	-1.31012	-0.23047
H	5.13441	1.09271	-0.53302
H	3.59501	2.90397	-0.27826
H	1.36345	3.73702	0.46705
H	-0.48067	2.17782	0.75745

Molecule 1 (neutral TS m062x)

C	-2.35588	1.45514	-0.35080
C	-1.97726	0.10925	-0.06361
C	-0.61596	-0.41813	-0.09621
C	0.61596	0.41813	0.09621
C	1.97726	-0.10925	0.06361
C	2.35588	-1.45514	0.35080
C	3.65840	-1.88596	0.26007
C	4.68889	-1.00155	-0.12266
C	4.39017	0.32566	-0.28268
C	3.06097	0.80641	-0.13294
C	2.84066	2.20746	-0.07401
C	1.60396	2.67064	0.27387
C	0.51425	1.77681	0.35841
C	-0.51425	-1.77681	-0.35841
C	-1.60396	-2.67064	-0.27387
C	-2.84066	-2.20746	0.07401
C	-3.06097	-0.80641	0.13294
C	-4.39017	-0.32566	0.28268
C	-4.68889	1.00155	0.12266
C	-3.65840	1.88596	-0.26007
H	-1.62536	2.15173	-0.73585
H	-3.89562	2.91485	-0.51346
H	-5.70940	1.35752	0.22392
H	-5.17393	-1.05145	0.48412
H	-3.68036	-2.87993	0.22629
H	-1.42991	-3.72859	-0.44348
H	0.43643	-2.20359	-0.63369
H	1.62536	-2.15173	0.73585
H	3.89562	-2.91485	0.51346
H	5.70940	-1.35752	-0.22392
H	5.17393	1.05145	-0.48412
H	3.68036	2.87993	-0.22629
H	1.42991	3.72859	0.44348
H	-0.43643	2.20359	0.63369

Molecule 1 (radical cation TS m062x)

C	-2.33558	1.44313	-0.39874
C	-1.95465	0.11936	-0.09925
C	-0.58599	-0.39869	-0.13455
C	0.58599	0.39869	0.13455
C	1.95465	-0.11936	0.09925
C	2.33558	-1.44313	0.39874
C	3.65518	-1.85641	0.28377
C	4.65945	-0.96745	-0.12193
C	4.33981	0.36059	-0.31101
C	3.00931	0.81160	-0.15372
C	2.75316	2.20534	-0.10796
C	1.51291	2.67219	0.29447
C	0.45954	1.77875	0.44074
C	-0.45954	-1.77875	-0.44074
C	-1.51291	-2.67219	-0.29447
C	-2.75316	-2.20534	0.10796
C	-3.00931	-0.81160	0.15372
C	-4.33981	-0.36059	0.31101
C	-4.65945	0.96745	0.12193
C	-3.65518	1.85641	-0.28377
H	-1.61699	2.14347	-0.80500
H	-3.90991	2.88048	-0.53736
H	-5.68382	1.30850	0.22690
H	-5.10968	-1.09138	0.54151
H	-3.57275	-2.89340	0.29395
H	-1.35275	-3.72846	-0.47875
H	0.48930	-2.16348	-0.78607
H	1.61699	-2.14347	0.80500
H	3.90991	-2.88048	0.53736
H	5.68382	-1.30850	-0.22690
H	5.10968	1.09138	-0.54151
H	3.57275	2.89340	-0.29395
H	1.35275	3.72846	0.47875
H	-0.48930	2.16348	0.78607

Molecule 2 (neutral TS b3lyp)

C	2.36875	1.30735	-0.59189
C	1.98268	0.03198	-0.08847
C	0.58899	-0.44742	-0.07580
C	-0.58899	0.44742	0.07580
C	-1.98268	-0.03198	0.08847
C	-2.36875	-1.30735	0.59189
C	-3.68508	-1.73795	0.57262
C	-4.70581	-0.91553	0.05833
C	-4.39062	0.37178	-0.32525
C	-3.05997	0.85440	-0.25804
C	-2.79550	2.24700	-0.38100
C	-1.57712	2.71915	0.01577
C	-0.51173	1.83505	0.34378

C	3.68508	1.73795	-0.57262
C	4.70581	0.91553	-0.05833
C	4.39062	-0.37178	0.32525
C	3.05997	-0.85440	0.25804
C	2.79550	-2.24700	0.38100
C	1.57712	-2.71915	-0.01577
C	0.51173	-1.83505	-0.34378
O	-0.52720	-2.48817	-0.92922
O	0.52720	2.48817	0.92922
H	1.62754	1.94578	-1.05455
H	-1.62754	-1.94578	1.05455
H	-3.92939	-2.71330	0.98524
H	-5.73257	-1.26859	0.02314
H	-5.17099	1.06339	-0.63458
H	-3.59251	2.92395	-0.67545
H	-1.37342	3.78298	0.09565
H	3.92939	2.71330	-0.98524
H	5.73257	1.26859	-0.02314
H	5.17099	-1.06339	0.63458
H	3.59251	-2.92395	0.67545
H	1.37342	-3.78298	-0.09565
H	-1.24360	-1.86947	-1.15465
H	1.24360	1.86947	1.15465

Molecule 2 (radical cation TS b3lyp)

C	-2.67788	1.41538	0.03662
C	-2.02792	0.16084	0.07999
C	-0.61386	-0.09430	0.41366
C	0.58678	0.67817	0.09845
C	1.81323	-0.05831	-0.25449
C	1.77803	-1.33783	-0.85575
C	2.94615	-2.02071	-1.16948
C	4.20224	-1.45444	-0.90378
C	4.27207	-0.17889	-0.36694
C	3.09650	0.54311	-0.06677
C	3.16782	1.90670	0.34020
C	2.03100	2.67013	0.39081
C	0.76042	2.10234	0.15057
C	-3.98784	1.55404	-0.41375
C	-4.72428	0.44365	-0.83944
C	-4.16526	-0.81573	-0.69188
C	-2.85770	-0.98150	-0.18955
C	-2.42037	-2.29280	0.17290
C	-1.25908	-2.47160	0.87252
C	-0.38632	-1.37750	1.04733
O	0.65769	-1.62261	1.84269
O	-0.22269	3.01002	0.05810
H	-2.23179	2.28372	0.49886
H	0.82552	-1.78861	-1.11048
H	2.87974	-2.99705	-1.64026
H	5.11033	-1.99851	-1.14477
H	5.23279	0.29931	-0.19688
H	4.13980	2.35731	0.51935
H	2.06932	3.73868	0.57598
H	-4.44303	2.53985	-0.40303
H	-5.73548	0.55944	-1.21624
H	-4.74242	-1.70639	-0.92463
H	-3.07774	-3.13389	-0.02774
H	-0.97319	-3.43122	1.28965
H	1.21984	-0.83051	1.94970
H	-0.95607	2.66421	-0.48325

Molecule 2 (neutral TS m062x)

C	-2.36748	1.30727	0.57221
C	-1.97824	0.03333	0.07260
C	-0.58895	-0.43891	0.07942
C	0.58770	0.46084	-0.05791
C	1.97061	-0.02980	-0.07933
C	2.33105	-1.30647	-0.59398
C	3.63684	-1.74756	-0.59621
C	4.67311	-0.93686	-0.09389
C	4.37864	0.34685	0.29884
C	3.05211	0.83845	0.25373
C	2.80157	2.23361	0.38649
C	1.58955	2.71477	0.00169
C	0.51522	1.83710	-0.32305
C	-3.67956	1.72987	0.54392
C	-4.69346	0.90045	0.02763
C	-4.37275	-0.38324	-0.34495
C	-3.04069	-0.85507	-0.26887
C	-2.76915	-2.24903	-0.37367
C	-1.55914	-2.70754	0.04355
C	-0.50226	-1.80922	0.36993
O	0.53373	-2.44119	0.96928
O	-0.51879	2.49451	-0.89805
H	-1.62633	1.94773	1.03352
H	1.56999	-1.93436	-1.04024
H	3.86668	-2.72209	-1.01648
H	5.69541	-1.30096	-0.07672
H	5.16783	1.03052	0.60172
H	3.60817	2.90048	0.67650
H	1.38766	3.77901	-0.07075
H	-3.93188	2.70382	0.95246
H	-5.72043	1.24914	-0.01352
H	-5.14606	-1.08204	-0.65428
H	-3.56142	-2.93100	-0.66796
H	-1.34454	-3.76756	0.13781
H	1.20987	-1.80506	1.25570

H	-1.20276	1.87275	-1.19643

Molecule 2 (radical cation TS m062x)

C	-2.66953	1.42701	-0.05945
C	-2.02179	0.18043	0.06753
C	-0.61449	-0.05394	0.42164
C	0.58915	0.69917	0.09709
C	1.78881	-0.06508	-0.27090
C	1.70661	-1.34913	-0.85282
C	2.84786	-2.05850	-1.17969
C	4.12160	-1.51580	-0.95067
C	4.23212	-0.24141	-0.43310
C	3.07952	0.50426	-0.11137
C	3.19052	1.86437	0.30170
C	2.07694	2.64798	0.39780
C	0.78932	2.10785	0.18500
C	-3.97133	1.53239	-0.52607
C	-4.70029	0.39763	-0.88945
C	-4.13873	-0.84546	-0.66722
C	-2.83730	-0.97220	-0.15094
C	-2.39636	-2.26963	0.26700
C	-1.23790	-2.42219	0.96239
C	-0.37386	-1.31283	1.09173
O	0.67707	-1.52053	1.86783
O	-0.18701	3.02168	0.17256
H	-2.22986	2.32322	0.34921
H	0.73630	-1.77765	-1.08235
H	2.75154	-3.03917	-1.63440
H	5.01027	-2.08299	-1.20671
H	5.20518	0.21906	-0.28768
H	4.17810	2.28922	0.45675
H	2.13729	3.71138	0.60257
H	-4.42950	2.51463	-0.57885
H	-5.70898	0.48786	-1.27757
H	-4.70660	-1.75230	-0.85490
H	-3.05624	-3.11608	0.10029
H	-0.93724	-3.36268	1.40985
H	1.23155	-0.72041	1.95408
H	-0.86768	2.76716	-0.47472

Molecule 3 (neutral TS b3lyp)

C	2.54831	0.98878	0.69165
C	1.99120	-0.17094	0.08151
C	0.55558	-0.47390	0.05794
C	-0.53720	0.53044	0.00341
C	-1.95212	0.16783	-0.13695
C	-2.39600	-1.01096	-0.80145
C	-3.73445	-1.32757	-0.91924
C	-4.72854	-0.49156	-0.36227
C	-4.34887	0.70402	0.20405
C	-2.98046	1.08420	0.26809
C	-2.62039	2.41012	0.61870
C	-1.34541	2.84362	0.36076
C	-0.33796	1.93648	-0.06534
C	3.90632	1.24045	0.68672
C	4.80681	0.35088	0.05948
C	4.32287	-0.83634	-0.44158
C	2.93828	-1.15063	-0.37585
C	2.49414	-2.47222	-0.63527
C	1.23090	-2.83839	-0.24602
C	0.30227	-1.86544	0.21183
O	-0.84231	-2.24366	0.83497
O	0.82415	2.40169	-0.58633
H	1.90264	1.66032	1.23895
H	-1.66977	-1.64788	-1.29040
H	-4.02449	-2.22167	-1.46564
H	-5.77813	-0.76476	-0.43121
H	-5.09437	1.40865	0.56615
H	-3.37769	3.09858	0.98426
H	-1.09682	3.89127	0.48262
H	4.28579	2.12458	1.19323
H	5.87002	0.57394	0.03047
H	4.99984	-1.58624	-0.84477
H	3.18936	-3.20829	-1.03035
H	0.93109	-3.87861	-0.29293
C	1.12495	3.79600	-0.55783
H	0.39598	4.37372	-1.13791
H	1.16985	4.18339	0.46699
H	2.10892	3.88930	-1.02136
C	-1.19680	-3.62299	0.91585
H	-1.32937	-4.07072	-0.07621
H	-0.44995	-4.19443	1.47965
H	-2.14831	-3.64680	1.45020

Molecule 3 (radical cation TS b3lyp)

C	2.21503	-1.02508	-0.96325
C	1.89044	0.14135	-0.23906
C	0.49894	0.56662	0.02197
C	-0.56752	-0.38429	0.17054
C	-2.02717	-0.15478	0.08588
C	-2.71158	0.96388	0.60085
C	-4.08605	1.11006	0.44509
C	-4.84227	0.14960	-0.24195
C	-4.21781	-1.00775	-0.67456
C	-2.83457	-1.20256	-0.46563
C	-2.27541	-2.50167	-0.65510
C	-1.04398	-2.81312	-0.13185
C	-0.24103	-1.78399	0.40677

C	3.53422	-1.39441	-1.19069
C	4.59447	-0.61492	-0.69964
C	4.31083	0.57249	-0.04822
C	2.97365	0.98608	0.14701
C	2.68949	2.30433	0.60813
C	1.42475	2.82476	0.48334
C	0.35295	2.00950	0.04993
O	-0.80334	2.53081	-0.33741
O	0.82661	-2.02636	1.15776
H	1.42330	-1.63072	-1.39090
H	-2.17929	1.70555	1.17629
H	-4.57606	1.97727	0.87862
H	-5.90981	0.28721	-0.38478
H	-4.79017	-1.80879	-1.13444
H	-2.88997	-3.27848	-1.10126
H	-0.69816	-3.83901	-0.11187
H	3.74275	-2.28958	-1.76983
H	5.62322	-0.91973	-0.86649
H	5.11085	1.22845	0.28435
H	3.50520	2.93269	0.95451
H	1.24619	3.87190	0.69312
C	1.27929	-3.37709	1.37432
H	0.50177	-3.96666	1.86850
H	1.57199	-3.84445	0.42953
H	2.14711	-3.28176	2.02640
C	-1.03140	3.95331	-0.29103
H	-0.98813	4.32040	0.73850
H	-0.30345	4.47697	-0.91691
H	-2.03524	4.08916	-0.69321

Molecule 3 (neutral TS m062x)

C	2.60001	0.97535	0.62008
C	1.99701	-0.18526	0.05650
C	0.56257	-0.45791	0.09037
C	-0.52809	0.55463	0.02452
C	-1.92873	0.17864	-0.14372
C	-2.34051	-1.02197	-0.78956
C	-3.66536	-1.35204	-0.93826
C	-4.68271	-0.50740	-0.43706
C	-4.33078	0.70120	0.10452
C	-2.96765	1.08990	0.20340
C	-2.62982	2.42565	0.53878
C	-1.35406	2.86059	0.32172
C	-0.33017	1.94650	-0.05037
C	3.95648	1.19128	0.56288
C	4.81329	0.26068	-0.06644
C	4.28696	-0.92610	-0.50658
C	2.89837	-1.19934	-0.38616
C	2.41902	-2.52176	-0.57203
C	1.16740	-2.84146	-0.12867
C	0.27705	-1.82089	0.30462
O	-0.86162	-2.13842	0.96014
O	0.84060	2.40770	-0.53736
H	1.98745	1.67108	1.17626
H	-1.59018	-1.66722	-1.23329
H	-3.93139	-2.26402	-1.46535
H	-5.72634	-0.79121	-0.53118
H	-5.08939	1.40998	0.42747
H	-3.40626	3.11350	0.86164
H	-1.11052	3.91048	0.43468
H	4.37484	2.07655	1.03361
H	5.87883	0.45621	-0.13668
H	4.92919	-1.70799	-0.90430
H	3.08896	-3.28779	-0.95255
H	0.84079	-3.87458	-0.11861
C	1.19927	3.76772	-0.35610
H	0.55214	4.43002	-0.94052
H	1.16510	4.05618	0.70053
H	2.22345	3.85279	-0.72216
C	-1.34484	-3.47071	0.91869
H	-1.46113	-3.82566	-0.11188
H	-0.68453	-4.14940	1.46907
H	-2.32108	-3.44685	1.40412

Molecule 3 (radical cation TS m062x)

C	2.11918	-1.07179	-0.96146
C	1.85513	0.12892	-0.27025
C	0.48988	0.59493	0.03319
C	-0.58678	-0.33778	0.20931
C	-2.04409	-0.14494	0.06366
C	-2.78376	0.97656	0.48573
C	-4.14854	1.06780	0.26178
C	-4.84379	0.04911	-0.40080
C	-4.16769	-1.10723	-0.73298
C	-2.79306	-1.24063	-0.45691
C	-2.19923	-2.53830	-0.55049
C	-0.98634	-2.79388	0.02330
C	-0.22913	-1.70731	0.51934
C	3.41341	-1.48370	-1.22033
C	4.51078	-0.71229	-0.80547
C	4.28281	0.50254	-0.19520
C	2.96654	0.95115	0.04095
C	2.73735	2.28885	0.48234
C	1.48631	2.83345	0.42719
C	0.37400	2.02948	0.07383
O	-0.79591	2.56374	-0.20419
O	0.83436	-1.87240	1.27968
H	1.29517	-1.67396	-1.33248

H	-2.30336	1.76060	1.04918
H	-4.68268	1.94066	0.62420
H	-5.90659	0.14341	-0.59724
H	-4.69207	-1.95361	-1.16754
H	-2.78581	-3.34971	-0.97172
H	-0.61119	-3.80606	0.10746
H	3.57701	-2.40750	-1.76676
H	5.52314	-1.04983	-1.00116
H	5.10855	1.15239	0.08098
H	3.58727	2.90164	0.76877
H	1.33805	3.88388	0.64284
C	1.37884	-3.18178	1.47583
H	0.66488	-3.81281	2.01120
H	1.64394	-3.63275	0.51505
H	2.27374	-3.03280	2.07726
C	-1.01160	3.97378	-0.08073
H	-0.85744	4.29649	0.95203
H	-0.35085	4.51954	-0.75858
H	-2.05062	4.12800	-0.36842

Molecule 4 (neutral TS b3lyp)

C	-2.35523	-1.39593	0.69666
C	-2.00150	-0.15934	0.07870
C	-0.61660	0.31646	-0.04083
C	0.53837	-0.61328	-0.14689
C	1.96089	-0.22867	-0.11634
C	2.46224	0.99919	-0.62848
C	3.80482	1.32685	-0.57202
C	4.74192	0.44433	0.00361
C	4.31578	-0.80515	0.39917
C	2.95376	-1.18701	0.28194
C	2.58940	-2.55743	0.40545
C	1.35897	-2.95205	-0.03739
C	0.37286	-1.99621	-0.40537
C	-3.66679	-1.82227	0.78588
C	-4.71897	-1.04359	0.25839
C	-4.43172	0.20207	-0.25493
C	-3.09958	0.69114	-0.29593
C	-2.84178	2.05498	-0.58272
C	-1.60432	2.57152	-0.29688
C	-0.52800	1.72817	0.09107
O	0.59495	2.25762	0.63135
O	-0.70028	-2.57515	-1.01067
H	-1.58291	-2.00021	1.15559
H	1.79180	1.67484	-1.13791
H	4.14046	2.26829	-1.00009
H	5.79049	0.72123	0.07283
H	5.02710	-1.54827	0.75264
H	3.32725	-3.28302	0.73693
H	1.08610	-4.00024	-0.11820
H	-3.88631	-2.75982	1.29010
H	-5.74419	-1.39967	0.30832
H	-5.22988	0.86100	-0.58927
H	-3.64902	2.69937	-0.92014
H	-1.43725	3.63973	-0.36853
C	0.77243	3.67248	0.69796
H	0.78166	4.13058	-0.29803
H	-0.00326	4.14213	1.31331
H	1.74558	3.81857	1.17045
H	-1.35667	-1.90189	-1.25975

Molecule 4 (radical cation TS b3lyp)

C	2.79909	1.42946	0.21568
C	2.09338	0.21681	0.03443
C	0.66531	-0.02662	0.29469
C	-0.49475	0.83400	0.08160
C	-1.74925	0.21537	-0.38136
C	-1.76712	-0.96814	-1.15340
C	-2.95989	-1.54108	-1.57551
C	-4.19282	-0.95164	-1.25395
C	-4.20765	0.24185	-0.55249
C	-3.00300	0.85348	-0.13876
C	-3.01559	2.15326	0.44434
C	-1.84331	2.84320	0.60975
C	-0.59804	2.24564	0.31490
C	4.12627	1.57564	-0.17551
C	4.82611	0.51602	-0.76555
C	4.20946	-0.72123	-0.84306
C	2.88072	-0.90377	-0.40336
C	2.37051	-2.22995	-0.28198
C	1.18761	-2.47408	0.36552
C	0.36964	-1.38185	0.72894
O	-0.70696	-1.51753	1.49404
O	0.42974	3.11087	0.35448
H	2.37214	2.23123	0.80103
H	-0.83357	-1.42724	-1.45794
H	-2.93126	-2.44611	-2.17559
H	-5.12157	-1.40909	-1.58113
H	-5.14584	0.74489	-0.33452
H	-3.96748	2.62738	0.66656
H	-1.83172	3.87954	0.93135
H	4.62584	2.52192	0.01009
H	5.85250	0.64466	-1.09430
H	4.75436	-1.58823	-1.20625
H	2.98951	-3.05689	-0.61837
H	0.87688	-3.48727	0.58625
C	-1.15322	-2.82443	1.90796
H	-1.41802	-3.43361	1.03880

H	-0.38440	-3.32079	2.50678
H	-2.03746	-2.63935	2.51729
H	1.15720	2.80075	-0.21537

Molecule 4 (neutral TS m062x)

C	2.32970	-1.40293	-0.67839
C	1.99630	-0.15082	-0.08282
C	0.62258	0.33195	0.04360
C	-0.53149	-0.60171	0.15233
C	-1.95008	-0.23174	0.08906
C	-2.46791	0.99905	0.57633
C	-3.80688	1.31004	0.49522
C	-4.72583	0.40671	-0.07738
C	-4.28364	-0.84272	-0.43562
C	-2.92019	-1.20363	-0.29298
C	-2.54135	-2.57469	-0.37193
C	-1.32159	-2.94183	0.10398
C	-0.35222	-1.96030	0.45731
C	3.63195	-1.83097	-0.78581
C	4.69687	-1.04198	-0.29883
C	4.42469	0.20908	0.19321
C	3.09414	0.69788	0.25278
C	2.84606	2.06672	0.52451
C	1.60950	2.58128	0.25801
C	0.52836	1.72907	-0.09863
O	-0.59501	2.24702	-0.63367
O	0.71872	-2.49977	1.08759
H	1.54192	-2.01478	-1.10137
H	-1.80926	1.68332	1.09230
H	-4.15902	2.25289	0.90425
H	-5.77492	0.67141	-0.16634
H	-4.97991	-1.60264	-0.78165
H	-3.26799	-3.31446	-0.69558
H	-1.03264	-3.98208	0.21765
H	3.84063	-2.77892	-1.27272
H	5.71887	-1.40168	-0.36431
H	5.22808	0.87377	0.50086
H	3.66359	2.71109	0.83496
H	1.44115	3.64996	0.32021
C	-0.85989	3.63633	-0.52085
H	-0.82557	3.96944	0.52239
H	-0.15531	4.22360	-1.11875
H	-1.86801	3.77599	-0.91321
H	1.33425	-1.80356	1.37130

Molecule 4 (radical cation TS m062x)

C	2.81758	1.44052	0.08598
C	2.10325	0.22302	0.03887
C	0.68053	0.01532	0.32508
C	-0.47816	0.86179	0.07601
C	-1.70233	0.21590	-0.41185
C	-1.66853	-0.98006	-1.16125
C	-2.83482	-1.58857	-1.58919
C	-4.08773	-1.02362	-1.30142
C	-4.14681	0.17697	-0.62561
C	-2.96621	0.82106	-0.19869
C	-3.02201	2.12011	0.38595
C	-1.87409	2.82873	0.59783
C	-0.61020	2.25451	0.33894
C	4.13595	1.53219	-0.33001
C	4.82050	0.41364	-0.81587
C	4.19116	-0.81371	-0.77160
C	2.86632	-0.93454	-0.31065
C	2.34085	-2.24583	-0.09657
C	1.14902	-2.43777	0.53732
C	0.34608	-1.30767	0.81110
O	-0.76151	-1.38522	1.52108
O	0.41258	3.11212	0.45853
H	2.40923	2.30331	0.58787
H	-0.71403	-1.41716	-1.43758
H	-2.77484	-2.50456	-2.16870
H	-4.99680	-1.51187	-1.63643
H	-5.09967	0.66076	-0.42997
H	-3.99118	2.57034	0.58135
H	-1.88790	3.85863	0.93751
H	4.64463	2.48722	-0.24708
H	5.84472	0.49902	-1.16232
H	4.72016	-1.71771	-1.05915
H	2.95916	-3.09761	-0.36607
H	0.81894	-3.43019	0.81690
C	-1.34554	-2.66181	1.80313
H	-1.50362	-3.21571	0.87300
H	-0.71042	-3.22904	2.48784
H	-2.30100	-2.44164	2.27594
H	1.08516	2.91004	-0.21502

Molecule 5 (neutral TS b3lyp)

C	2.36231	1.28774	-0.62590
C	1.97768	0.02881	-0.08555
C	0.58383	-0.44826	-0.06698
C	-0.58382	0.44828	0.06697
C	-1.97768	-0.02881	0.08555
C	-2.36229	-1.28773	0.62593
C	-3.67880	-1.71632	0.62950
C	-4.70324	-0.91071	0.09320
C	-4.38794	0.36297	-0.33586
C	-3.05644	0.84479	-0.28554
C	-2.78521	2.23317	-0.44516

C	-1.57521	2.71253	-0.03397
C	-0.50321	1.84493	0.35675
C	3.67883	1.71632	-0.62946
C	4.70326	0.91069	-0.09317
C	4.38794	-0.36299	0.33586
C	3.05644	-0.84480	0.28552
C	2.78519	-2.23318	0.44514
C	1.57519	-2.71253	0.03394
C	0.50319	-1.84491	-0.35677
H	1.61516	1.91467	-1.09139
H	-1.61513	-1.91464	1.09143
H	-3.92254	-2.67860	1.07344
H	-5.73087	-1.26379	0.07525
H	-5.16884	1.04547	-0.66507
H	-3.57300	2.90576	-0.77432
H	-1.38778	3.78354	0.00748
H	3.92258	2.67861	-1.07337
H	5.73089	1.26376	-0.07521
H	5.16883	-1.04551	0.66506
H	3.57298	-2.90579	0.77428
H	1.38775	-3.78354	-0.00751
N	0.56169	2.47535	0.96810
H	0.34025	3.36075	1.40778
H	1.19832	1.90764	1.50963
N	-0.56170	-2.47533	-0.96812
H	-1.19838	-1.90761	-1.50960
H	-0.34028	-3.36072	-1.40781

Molecule 5 (radical cation TS b3lyp)

C	-2.69792	1.40148	0.07265
C	-2.03489	0.15409	0.07944
C	-0.61223	-0.08302	0.39997
C	0.58088	0.69448	0.08362
C	1.80757	-0.05179	-0.26703
C	1.76075	-1.31906	-0.89414
C	2.91804	-2.01893	-1.20365
C	4.18196	-1.48306	-0.90530
C	4.26404	-0.21984	-0.34390
C	3.09705	0.51757	-0.04954
C	3.17962	1.87560	0.39142
C	2.06308	2.65368	0.41318
C	0.76415	2.12865	0.10560
C	-4.02096	1.53531	-0.33516
C	-4.75748	0.42338	-0.75938
C	-4.17523	-0.83116	-0.66632
C	-2.85338	-0.99139	-0.20616
C	-2.37900	-2.31297	0.09274
C	-1.22665	-2.49094	0.78820
C	-0.37920	-1.36716	1.05387
H	-2.21266	2.26994	0.48984
H	0.80203	-1.74682	-1.16592
H	2.84048	-2.98368	-1.69730
H	5.08407	-2.03948	-1.14214
H	5.23050	0.23772	-0.14824
H	4.15277	2.30411	0.61493
H	2.13188	3.71789	0.62345
H	-4.48584	2.51658	-0.30022
H	-5.78162	0.53351	-1.10274
H	-4.74789	-1.72254	-0.90853
H	-3.01407	-3.16036	-0.15086
H	-0.92400	-3.46710	1.15596
N	-0.20938	3.04970	-0.07816
H	0.07503	4.02343	-0.09347
H	-0.98671	2.83705	-0.68724
N	0.61918	-1.53209	1.92794
H	1.26180	-0.78399	2.15494
H	0.82436	-2.44915	2.30835

Molecule 5 (neutral TS m062x)

C	-2.34148	-1.28276	-0.62099
C	-1.96806	-0.02566	-0.07165
C	-0.58179	0.45347	-0.05763
C	0.58181	-0.45323	0.05783
C	1.96814	0.02570	0.07158
C	2.34186	1.28278	0.62072
C	3.65096	1.71399	0.63032
C	4.67986	0.91340	0.09597
C	4.37306	-0.35686	-0.33226
C	3.04350	-0.83888	-0.28864
C	2.77696	-2.22963	-0.44008
C	1.57289	-2.70549	-0.02788
C	0.49742	-1.83475	0.35280
C	-3.65051	-1.71416	-0.63089
C	-4.67963	-0.91380	-0.09663
C	-4.37311	0.35645	0.33183
C	-3.04361	0.83868	0.28851
C	-2.77730	2.22945	0.44024
C	-1.57322	2.70555	0.02835
C	-0.49756	1.83505	-0.35233
H	-1.58551	-1.90138	-1.08522
H	1.58609	1.90156	1.08505
H	3.89058	2.67339	1.07996
H	5.70493	1.27067	0.08382
H	5.15533	-1.03834	-0.65841
H	3.56747	-2.90047	-0.76471
H	1.38046	-3.77484	0.01538
H	-3.88989	-2.67355	-1.08068
H	-5.70464	-1.27123	-0.08471

H	-5.15554	1.03776	0.65794
H	-3.56795	2.90012	0.76486
H	-1.38094	3.77494	-0.01467
N	-0.56762	-2.46890	0.95895
H	-0.31853	-3.32629	1.43830
H	-1.20218	-1.89008	1.49350
N	0.56744	2.46949	-0.95825
H	1.20210	1.89088	-1.49290
H	0.31826	3.32694	-1.43743

Molecule 5 (radical cation TS m062x)

C	-2.69138	1.41949	-0.04326
C	-2.02438	0.18257	0.07483
C	-0.61405	-0.02164	0.43851
C	0.58722	0.72693	0.09821
C	1.76783	-0.06466	-0.28727
C	1.64324	-1.33994	-0.88336
C	2.75605	-2.08427	-1.22494
C	4.04941	-1.58757	-0.99509
C	4.20115	-0.32324	-0.46455
C	3.07538	0.45542	-0.12948
C	3.22583	1.80976	0.31009
C	2.14423	2.62100	0.40131
C	0.81315	2.14073	0.15495
C	-3.99509	1.50948	-0.50502
C	-4.70605	0.36418	-0.87414
C	-4.12031	-0.87122	-0.67002
C	-2.81665	-0.98206	-0.15929
C	-2.34099	-2.28355	0.23179
C	-1.20313	-2.41594	0.94618
C	-0.36910	-1.26518	1.15012
H	-2.23793	2.31599	0.34668
H	0.65609	-1.73355	-1.10457
H	2.62446	-3.05540	-1.69211
H	4.91855	-2.18033	-1.26119
H	5.18981	0.10296	-0.31679
H	4.22407	2.20015	0.48708
H	2.25702	3.67717	0.62968
H	-4.46948	2.48453	-0.55464
H	-5.71764	0.43958	-1.25873
H	-4.67406	-1.78487	-0.86809
H	-2.96956	-3.14528	0.02548
H	-0.88724	-3.36616	1.36589
N	-0.14936	3.08407	0.07873
H	0.16091	4.05008	0.10328
H	-0.92478	2.92553	-0.54907
N	0.64199	-1.37271	2.00334
H	1.25589	-0.59217	2.20609
H	0.85143	-2.25945	2.44902

Molecule 6 (neutral TS b3lyp)

C	-0.50036	3.21874	0.68003
C	-0.50036	3.21874	-0.68003
C	-0.26270	2.01026	-1.38403
C	-0.33572	0.72952	-0.73921
C	-0.33572	0.72952	0.73921
C	-0.26270	2.01026	1.38403
C	0.20438	2.16663	-2.73162
C	-0.20508	-0.41293	-1.67745
C	0.47074	-0.21009	-2.93357
C	0.68960	1.11143	-3.43052
C	0.79351	-1.30701	-3.76821
H	1.35197	-1.10611	-4.67940
C	0.35548	-2.58454	-3.48241
C	-0.49475	-2.76010	-2.38063
C	-0.76755	-1.70368	-1.52477
H	0.26005	3.17578	-3.13110
H	-0.56540	4.14652	1.24219
H	-0.56540	4.14652	-1.24219
H	1.16105	1.23869	-4.40151
H	0.59999	-3.41688	-4.13660
H	-0.97052	-3.72084	-2.20246
H	-1.52249	-1.86650	0.78155
C	0.20438	2.16663	2.73162
H	0.26005	3.17578	3.13110
C	0.68960	1.11143	3.43052
H	1.16105	1.23869	4.40151
C	-0.20508	-0.41293	1.67745
C	0.47074	-0.21009	2.93357
C	0.79351	-1.30701	3.76821
H	1.35197	-1.10611	4.67940
C	0.35548	-2.58454	3.48241
H	0.59999	-3.41688	4.13660
C	-0.49475	-2.76010	2.38063
H	-0.97052	-3.72084	2.20246
C	-0.76755	-1.70368	1.52477
H	-1.52249	-1.86650	-0.78155

Molecule 6 (radical cation TS b3lyp)

C	-0.67708	3.24911	-0.54872
C	0.67708	3.24911	-0.54872
C	1.37577	2.03285	-0.27608
C	0.72074	0.73871	-0.37034
C	-0.72074	0.73871	-0.37034
C	-1.37577	2.03285	-0.27607
C	2.68017	2.16590	0.24468
C	1.64092	-0.41524	-0.22929
C	2.85834	-0.23017	0.51593

C	3.34769	1.07837	0.76083
C	3.68214	-1.33218	0.84890
H	4.56524	-1.14802	1.45419
C	3.41138	-2.60168	0.36279
C	2.35373	-2.74918	-0.53563
C	1.50765	-1.67456	-0.83551
H	3.10529	3.16165	0.32485
H	-1.24733	4.16951	-0.62785
H	1.24733	4.16951	-0.62785
H	4.29471	1.20210	1.27842
H	4.04939	-3.44213	0.61685
H	2.18611	-3.69973	-1.03349
H	-0.80954	-1.81491	-1.63842
C	-2.68017	2.16590	0.24468
H	-3.10529	3.16165	0.32486
C	-3.34769	1.07837	0.76084
H	-4.29471	1.20210	1.27843
C	-1.64092	-0.41524	-0.22929
C	-2.85834	-0.23017	0.51593
C	-3.68214	-1.33218	0.84891
H	-4.56524	-1.14803	1.45419
C	-3.41138	-2.60168	0.36279
H	-4.04939	-3.44213	0.61685
C	-2.35373	-2.74918	-0.53563
H	-2.18611	-3.69973	-1.03349
C	-1.50765	-1.67456	-0.83551
H	0.80954	-1.81491	-1.63842

Molecule 6 (neutral TS m062x)

C	-3.21712	-0.49871	0.67842
C	-3.21712	-0.49871	-0.67842
C	-2.00567	-0.27307	-1.37842
C	-0.73776	-0.35359	-0.73567
C	-0.73776	-0.35359	0.73567
C	-2.00567	-0.27307	1.37842
C	-2.15812	0.20827	-2.72437
C	0.40897	-0.21224	-1.66197
C	0.21612	0.48093	-2.89703
C	-1.10411	0.70853	-3.40239
C	1.31428	0.81191	-3.72130
H	1.11840	1.38641	-4.62296
C	2.58493	0.36639	-3.43525
C	2.74967	-0.50636	-2.35147
C	1.69028	-0.78998	-1.51049
H	-3.16584	0.26652	-3.12585
H	-4.14376	-0.55415	1.24267
H	-4.14376	-0.55415	-1.24267
H	-1.22082	1.19523	-4.36667
H	3.42157	0.61774	-4.07961
H	3.70473	-0.99407	-2.18139
H	1.83694	-1.57019	0.79061
C	-2.15812	0.20827	2.72437
H	-3.16584	0.26652	3.12585
C	-1.10411	0.70853	3.40239
H	-1.22082	1.19523	4.36667
C	0.40897	-0.21224	1.66197
C	0.21612	0.48093	2.89703
C	1.31428	0.81191	3.72130
H	1.11840	1.38641	4.62296
C	2.58493	0.36639	3.43525
H	3.42157	0.61774	4.07961
C	2.74967	-0.50636	2.35147
H	3.70473	-0.99407	2.18139
C	1.69028	-0.78998	1.51049
H	1.83694	-1.57019	-0.79061

Molecule 6 (radical cation TS m062x)

C	0.56409	3.24899	-0.67445
C	0.56409	3.24899	0.67445
C	0.28607	2.02935	1.36910
C	0.39108	0.74191	0.71474
C	0.39108	0.74191	-0.71474
C	0.28607	2.02935	-1.36910
C	-0.25945	2.16005	2.65958
C	0.24033	-0.41570	1.62444
C	-0.53162	-0.23803	2.81512
C	-0.79175	1.06962	3.30402
C	-0.87078	-1.33624	3.63247
H	-1.49330	-1.15522	4.50391
C	-0.37008	-2.59817	3.36928
C	0.55114	-2.73705	2.33267
C	0.86101	-1.66374	1.49628
H	-0.35029	3.15419	3.08559
H	0.64354	4.16633	-1.24909
H	0.64354	4.16633	1.24909
H	-1.33500	1.18478	4.23766
H	-0.62763	-3.44102	4.00135
H	1.06080	-3.68282	2.17838
H	1.68166	-1.79212	-0.81660
C	-0.25945	2.16005	-2.65958
H	-0.35029	3.15419	-3.08559
C	-0.79175	1.06962	-3.30402
H	-1.33500	1.18478	-4.23766
C	0.24033	-0.41570	-1.62444
C	-0.53162	-0.23803	-2.81512
C	-0.87078	-1.33624	-3.63247
H	-1.49330	-1.15522	-4.50391
C	-0.37008	-2.59817	-3.36928

H	-0.62763	-3.44102	-4.00135
C	0.55114	-2.73705	-2.33267
H	1.06080	-3.68282	-2.17838
C	0.86101	-1.66374	-1.49628
H	1.68166	-1.79212	0.81660

Molecule 7 (neutral TS b3lyp)

C	1.19880	3.53611	-0.77362
C	2.31137	3.03489	-0.17219
C	2.34493	1.66926	0.22254
C	1.32481	0.76357	-0.19602
C	0.00004	1.34675	-0.50932
C	0.00007	2.76213	-0.77432
C	3.41133	1.23395	1.07992
C	1.75875	-0.63835	-0.17202
C	2.76476	-1.05439	0.76394
C	3.52759	-0.06588	1.46274
C	3.14105	-2.41727	0.83799
H	3.86173	-2.71296	1.59676
C	2.68666	-3.33240	-0.09261
C	1.88411	-2.88043	-1.15520
C	1.43611	-1.56994	-1.18391
H	4.09019	1.99304	1.46060
H	1.14642	4.57764	-1.07863
H	3.17567	3.66118	0.03340
H	4.28211	-0.38319	2.17780
H	3.00708	-4.36983	-0.04725
H	1.62590	-3.55355	-1.96832
C	-1.19861	3.53617	-0.77361
H	-1.14619	4.57770	-1.07862
C	-2.31120	3.03501	-0.17216
H	-3.17547	3.66134	0.03344
C	-1.32476	0.76363	-0.19602
C	-2.34483	1.66938	0.22255
C	-3.41124	1.23412	1.07995
H	-4.09006	1.99325	1.46064
C	-3.52757	-0.06570	1.46276
H	-4.28210	-0.38298	2.17783
C	-2.76480	-1.05425	0.76394
C	-1.75878	-0.63827	-0.17203
H	0.90216	-1.21844	-2.05295
C	-3.14118	-2.41711	0.83799
H	-3.86187	-2.71276	1.59676
C	-1.43621	-1.56987	-1.18393
H	-0.90225	-1.21840	-2.05297
C	-2.68686	-3.33226	-0.09263
H	-3.00734	-4.36967	-0.04728
C	-1.88429	-2.88034	-1.15522
H	-1.62613	-3.55346	-1.96835

Molecule 7 (radical cation TS b3lyp)

C	1.19965	3.53341	-0.78576
C	2.31397	3.02765	-0.16677
C	2.33567	1.67867	0.24580
C	1.30503	0.76868	-0.20899
C	0.00000	1.35932	-0.53085
C	-0.00000	2.76990	-0.79398
C	3.36674	1.22326	1.12505
C	1.71284	-0.62569	-0.19248
C	2.68876	-1.05985	0.76597
C	3.45041	-0.08682	1.49110
C	3.03079	-2.42205	0.84348
H	3.72541	-2.74114	1.61553
C	2.56326	-3.33612	-0.10007
C	1.79365	-2.87742	-1.16933
C	1.37884	-1.54438	-1.21268
H	4.05250	1.96379	1.52634
H	1.16362	4.57085	-1.10434
H	3.17234	3.65802	0.04611
H	4.18168	-0.42491	2.21940
H	2.86234	-4.37834	-0.04258
H	1.53300	-3.54452	-1.98500
C	-1.19965	3.53341	-0.78575
H	-1.16362	4.57085	-1.10434
C	-2.31397	3.02765	-0.16677
H	-3.17235	3.65802	0.04611
C	-1.30503	0.76868	-0.20899
C	-2.33567	1.67867	0.24580
C	-3.36674	1.22326	1.12505
H	-4.05251	1.96379	1.52634
C	-3.45041	-0.08682	1.49111
H	-4.18168	-0.42491	2.21940
C	-2.68876	-1.05986	0.76597
C	-1.71284	-0.62569	-0.19248
H	0.91957	-1.16745	-2.11288
C	-3.03079	-2.42205	0.84348
H	-3.72540	-2.74114	1.61553
C	-1.37884	-1.54438	-1.21268
H	-0.91957	-1.16745	-2.11288
C	-2.56326	-3.33612	-0.10007
H	-2.86234	-4.37834	-0.04258
C	-1.79365	-2.87742	-1.16933
H	-1.53300	-3.54452	-1.98500

Molecule 7 (neutral TS m062x)

C	1.19715	3.54188	-0.75204
C	2.30450	3.03268	-0.15838
C	2.33314	1.66091	0.21528

C	1.31690	0.77222	-0.20659	C	2.64048	-1.06265	0.76742
C	-0.00014	1.35881	-0.52231	C	3.40466	-0.09345	1.50413
C	-0.00027	2.76586	-0.76669	C	2.97008	-2.42113	0.84839
C	3.39741	1.21432	1.07365	H	3.65521	-2.74618	1.62605
C	1.72964	-0.63320	-0.17599	C	2.50073	-3.32764	-0.09819
C	2.71422	-1.05906	0.76118	C	1.75242	-2.86314	-1.17707
C	3.49205	-0.07951	1.46114	C	1.35894	-1.52889	-1.22763
C	3.07004	-2.42393	0.83957	H	4.02238	1.94864	1.54542
H	3.78066	-2.72851	1.60352	H	1.15988	4.57080	-1.08855
C	2.60392	-3.33049	-0.08777	H	3.16107	3.64623	0.07020
C	1.82162	-2.86709	-1.15867	H	4.12005	-0.44178	2.24304
C	1.40520	-1.55160	-1.19504	H	2.78646	-4.37268	-0.03694
H	4.08027	1.96840	1.45590	H	1.49346	-3.52854	-1.99415
H	1.14285	4.58697	-1.04264	C	-1.19593	3.53044	-0.77922
H	3.17121	3.65164	0.05686	H	-1.16091	4.57044	-1.08898
H	4.23738	-0.40895	2.17962	C	-2.30474	3.01899	-0.15634
H	2.90422	-4.37265	-0.03759	H	-3.16167	3.64582	0.07066
H	1.56163	-3.53575	-1.97392	C	-1.29445	0.77086	-0.22158
C	-1.19783	3.54165	-0.75205	C	-2.31869	1.67109	0.24407
H	-1.14372	4.58676	-1.04265	C	-3.34106	1.20852	1.13634
C	-2.30510	3.03226	-0.15841	H	-4.02216	1.94793	1.54645
H	-3.17193	3.65106	0.05680	C	-3.40410	-0.09407	1.50471
C	-1.31707	0.77199	-0.20658	H	-4.11945	-0.44260	2.24356
C	-2.33349	1.66049	0.21526	C	-2.64000	-1.06308	0.76767
C	-3.39770	1.21369	1.07360	C	-1.68842	-0.62322	-0.20023
H	-4.08071	1.96763	1.45582	H	0.91430	-1.13968	-2.13069
C	-3.49210	-0.08015	1.46109	C	-2.96967	-2.42155	0.84815
H	-4.23739	-0.40974	2.17954	H	-3.65470	-2.74690	1.62577
C	-2.71405	-1.05956	0.76117	C	-1.35915	-1.52845	-1.22804
C	-1.72952	-0.63351	-0.17597	H	-0.91514	-1.13875	-2.13123
H	0.89799	-1.18092	-2.07251	C	-2.50048	-3.32772	-0.09890
C	-3.06959	-2.42450	0.83955	H	-2.78619	-4.37279	-0.03796
H	-3.78018	-2.72923	1.60346	C	-1.75244	-2.86284	-1.17776
C	-1.40483	-1.55184	-1.19499	H	-1.49341	-3.52800	-1.99500
H	-0.89766	-1.18104	-2.07243				
C	-2.60323	-3.33097	-0.08776				
H	-2.90330	-4.37320	-0.03758				
C	-1.82097	-2.86742	-1.15863				
H	-1.56079	-3.53603	-1.97386				

Molecule 7 (radical cation TS m062x)

C	1.19517	3.53066	-0.77924
C	2.30425	3.01922	-0.15672
C	2.31856	1.67133	0.24357
C	1.29441	0.77092	-0.22184
C	-0.00012	1.36189	-0.55178
C	-0.00025	2.76603	-0.80305
C	3.34139	1.20901	1.13553
C	1.68856	-0.62313	-0.20032

Implications of chemical substitution on atropisomerism

I. Absolute Contributions to Gibbs Energies

Table 2	M06-2X/6-31g* in toluene (SMD)						DLPNO- CCSD(T)/ def2- TZVPD (SMD)
	E/au	ZPE/au	H/au	T.qh-S/au	qh-G(T)/au	imag .ν	E/au
OH_TS_toluene	-861.709983	0.285263	-861.408626	0.056592	-861.465218	-33.1	-860.8975804
OH_toluene	-861.737922	0.286271	-861.434423	0.058954	-861.493377		-860.9281088
OMe_TS_toluene	-900.968999	0.313652	-900.637333	0.060528	-900.697861	-63.3	-900.1106865
OMe_toluene	-901.010918	0.314648	-900.677193	0.062837	-900.740030		-900.1564912
OH_TS_DCM	-861.714514	0.284846	-861.413567	0.056601	-861.470168	-29.3	-860.9040428
OH_DCM	-861.741787	0.285757	-861.438694	0.059200	-861.497894		-860.9345308
OMe_TS_DCM	-900.974102	0.313648	-900.642558	0.060210	-900.702769	-66.8	-900.1173677
OMe_DCM	-901.017605	0.314547	-900.683996	0.062789	-900.746785		-900.1651021
OH_OMe_TS_toluene	-822.596530	0.271340	-822.308996	0.056721	-822.365717	-66.1	-821.8799457
OH_OMe_toluene	-822.628680	0.272200	-822.339381	0.058640	-822.398022		-821.9139598
OMe_OMe_TS_toluene	-861.853437	0.299315	-861.536207	0.060175	-861.596382	-90.7	-861.0914783
OMe_OMe_toluene	-861.901875	0.299909	-861.582713	0.063298	-861.646011		-861.144060
OH_CF3_TS_toluene	-1045.056302	0.243493	-1044.795686	0.058888	-1044.854574	-45.6	-1044.306627
OH_CF3_toluene	-1045.084009	0.244249	-1044.821994	0.060072	-1044.882066		-1044.333050
OMe_CF3_TS_toluene	-1084.312829	0.271048	-1084.022888	0.062493	-1084.085381	-77.7	-1083.517278
OMe_CF3_toluene	-1084.355593	0.272405	-1084.063315	0.064618	-1084.127933		-1083.560477

II. Cartesian Coordinates

OH_TS_toluene

C	-3.72247	-2.12444	-0.24171
C	-3.91205	-0.86893	0.28241
C	-2.85734	0.07336	0.31353
C	-1.55689	-0.30281	-0.12145
C	-1.41976	-1.57577	-0.72757
C	-2.46904	-2.46329	-0.78588
C	-3.13151	1.43040	0.67927
C	-0.47712	0.67609	-0.06708
C	-0.85547	2.02756	0.09237
C	-2.18328	2.37990	0.49831
C	0.08712	3.05784	-0.15950
H	-0.23570	4.09117	-0.05931
C	1.35613	2.77214	-0.56466
C	1.80379	1.42766	-0.57659
C	0.93024	0.37313	-0.23063
H	-4.13139	1.68964	1.01631
H	-4.54146	-2.83686	-0.27335
H	-4.88780	-0.56278	0.65075
H	-0.47763	-1.84863	-1.18273
H	-2.33013	-3.42746	-1.26524
H	-2.40100	3.43035	0.67323
H	2.07594	3.54483	-0.81197
O	3.09308	1.27292	-0.88395
H	3.29417	0.29222	-0.77393
C	1.49179	-0.93285	0.20055
O	0.86344	-1.85269	0.67278
N	2.94581	-1.05485	0.10982
C	3.54499	-0.61008	1.38338
H	3.24283	-1.26813	2.20845
H	4.63340	-0.62875	1.28588
H	3.23268	0.41251	1.60956
C	3.34961	-2.43049	-0.19347
H	2.87899	-2.75112	-1.12551
H	4.43445	-2.44531	-0.32360
H	3.06721	-3.12608	0.60455

OMe_TS_toluene

C	-4.22160	-1.66490	-0.39409
C	-4.21600	-0.45588	0.26381
C	-3.04346	0.32771	0.32953
C	-1.82660	-0.17347	-0.20803
C	-1.88810	-1.37603	-0.94946
C	-3.05370	-2.10623	-1.03873
C	-3.10940	1.66731	0.83988
C	-0.61867	0.64041	-0.11839

C	-0.79071	2.01271	0.20490
C	-2.04748	2.49388	0.70902
C	0.28193	2.91563	0.05837
H	0.11101	3.96551	0.28254
C	1.50541	2.49798	-0.40271
C	1.72623	1.12246	-0.58373
C	0.72640	0.17464	-0.33186
H	-4.05037	2.02158	1.25181
H	-5.13275	-2.25294	-0.45117
H	-5.12686	-0.06427	0.70941
H	-1.00892	-1.71370	-1.47850
H	-3.06865	-3.02165	-1.62190
H	-2.10933	3.53807	1.00425
H	2.30263	3.20776	-0.59327
O	2.91464	0.67090	-1.04838
C	1.15858	-1.20728	0.08515
O	0.43231	-2.17356	0.13734
N	2.49199	-1.28770	0.65795
C	2.40994	-1.90595	1.98216
H	2.05569	-2.94577	1.95044
H	3.40801	-1.88351	2.43016
H	1.73597	-1.32413	2.61756
C	3.36196	-2.08389	-0.20988
H	3.39203	-1.64428	-1.20867
H	4.37471	-2.07640	0.20625
H	3.02284	-3.12908	-0.28704
C	4.08921	1.19308	-0.44207
H	4.29053	2.21946	-0.76697
H	4.00890	1.14939	0.64828
H	4.91142	0.55615	-0.77363

OH_TS_DCM

C	-3.73975	-2.10532	-0.24279
C	-3.91567	-0.85447	0.29936
C	-2.85401	0.08121	0.32927
C	-1.55974	-0.29984	-0.12098
C	-1.43742	-1.56536	-0.74726
C	-2.49430	-2.44519	-0.80676
C	-3.11715	1.43820	0.70660
C	-0.47209	0.67146	-0.06735
C	-0.84289	2.02513	0.09658
C	-2.16523	2.38355	0.51770
C	0.10110	3.05201	-0.16575
H	-0.21612	4.08672	-0.06245
C	1.36461	2.75787	-0.58451
C	1.80543	1.41106	-0.59455
C	0.93230	0.36071	-0.23773
H	-4.11215	1.70051	1.05574
H	-4.56389	-2.81193	-0.27462
H	-4.88547	-0.54540	0.68089
H	-0.50170	-1.83644	-1.21691
H	-2.36817	-3.40294	-1.30261
H	-2.37416	3.43508	0.69688
H	2.08460	3.52771	-0.84148
O	3.09211	1.24843	-0.91486
H	3.29462	0.26924	-0.79540
C	1.49304	-0.95149	0.18421
O	0.85181	-1.88470	0.61586
N	2.94134	-1.06303	0.12715
C	3.52800	-0.55670	1.38623
H	3.23445	-1.18952	2.23376
H	4.61645	-0.56304	1.29138
H	3.19734	0.46719	1.57497
C	3.37126	-2.44347	-0.11536
H	2.91078	-2.81327	-1.03392
H	4.45668	-2.44109	-0.23911
H	3.10116	-3.10762	0.71324

OMe_TS_DCM

C	-4.23892	-1.61053	-0.44820
C	-4.22147	-0.41237	0.23059
C	-3.03794	0.35386	0.31853
C	-1.82384	-0.15585	-0.21848
C	-1.89699	-1.34397	-0.98350
C	-3.07218	-2.05706	-1.09365
C	-3.08956	1.68604	0.85177
C	-0.60446	0.63878	-0.10597
C	-0.76009	2.00804	0.23875
C	-2.01403	2.49933	0.74131
C	0.33006	2.89524	0.12513
H	0.17543	3.94178	0.37542
C	1.55308	2.46992	-0.33249
C	1.75109	1.09472	-0.54942
C	0.73388	0.15581	-0.31661
H	-4.02887	2.04603	1.26262
H	-5.15784	-2.18466	-0.52214
H	-5.12982	-0.01515	0.67644
H	-1.01837	-1.68271	-1.51337
H	-3.09667	-2.96087	-1.69475
H	-2.06154	3.53963	1.05275
H	2.36395	3.17271	-0.48588
O	2.92058	0.61637	-1.01243
C	1.14305	-1.23307	0.09202
O	0.40759	-2.19611	0.10567
N	2.45404	-1.33229	0.71010
C	2.31571	-1.96552	2.02401
H	1.95754	-3.00324	1.96666
H	3.29570	-1.95627	2.51038

H	1.62061	-1.38657	2.63934
C	3.34825	-2.13175	-0.13184
H	3.43167	-1.67978	-1.12173
H	4.34049	-2.14983	0.32994
H	2.99359	-3.16931	-0.23899
C	4.11835	1.29341	-0.65111
H	4.24850	2.20989	-1.23557
H	4.12429	1.52628	0.41833
H	4.93373	0.60572	-0.88114

OH_OMe_TS_toluene

C	3.66955	-0.28533	0.76563
C	0.96119	-0.29363	-0.10128
C	1.67186	-1.50008	0.15949
C	3.01119	-1.47872	0.61772
C	1.03107	-2.74682	-0.09676
H	1.59400	-3.66267	0.06389
C	-0.23865	-2.79474	-0.57688
C	-1.01699	-1.60549	-0.65338
C	-0.47504	-0.35698	-0.32918
H	4.68877	-0.25448	1.13786
H	3.50003	-2.42291	0.84064
H	-0.73047	-3.72910	-0.82530
O	-2.29635	-1.82553	-1.00190
H	-2.78696	-0.97660	-0.87598
C	-1.39781	0.79243	-0.02446
O	-1.11692	1.96928	0.00461
N	-2.75200	0.40788	0.25590
C	-2.94330	-0.42352	1.45659
H	-2.89914	0.19658	2.36184
H	-3.92307	-0.90593	1.40770
H	-2.17755	-1.19536	1.52869
C	-3.67525	1.53964	0.25941
H	-3.57557	2.10010	-0.67074
H	-4.69257	1.14755	0.33655
H	-3.48563	2.22005	1.09850
C	3.05188	0.90296	0.33552
H	3.62285	1.82491	0.31508
C	1.76095	0.89370	-0.16112
O	1.24993	1.94405	-0.83640
C	1.63589	3.24380	-0.44699
H	1.61665	3.35205	0.64347
H	2.63452	3.50108	-0.82216
H	0.90561	3.92387	-0.88767

OMe_OMe_TS_toluene

C	-3.76021	0.91591	0.71262
C	-1.09043	0.39517	-0.09430
C	-1.52416	1.70703	0.25483
C	-2.85726	1.94348	0.68220
C	-0.61282	2.79104	0.14480
H	-0.96575	3.79005	0.38727
C	0.65784	2.60075	-0.31734
C	1.12379	1.28379	-0.54497
C	0.32176	0.17093	-0.31434
H	-4.77738	1.08236	1.05378
H	-3.13899	2.95017	0.97716
H	1.32180	3.44174	-0.48457
O	2.36795	1.08013	-1.04161
C	1.01443	-1.12545	0.03120
O	0.52653	-2.22852	0.01486
N	2.33743	-0.94153	0.62377
C	2.33594	-1.52364	1.96536
H	2.15916	-2.60929	1.96222
H	3.30712	-1.32438	2.42890
H	1.56208	-1.04403	2.57270
C	3.35175	-1.58895	-0.20621
H	3.33079	-1.15932	-1.21044
H	4.33732	-1.40281	0.23359
H	3.20062	-2.67758	-0.27901
C	-3.39852	-0.35547	0.22075
H	-4.15697	-1.12495	0.13272
C	-2.11686	-0.59819	-0.23270
O	-1.78044	-1.70546	-0.92006
C	-2.59640	-2.84816	-0.80038
H	-2.78767	-3.09178	0.25146
H	-3.55218	-2.71954	-1.32447
H	-2.04176	-3.66403	-1.26535
C	3.44000	1.76510	-0.40950
H	4.35687	1.32757	-0.80890
H	3.43346	2.83505	-0.64435
H	3.40415	1.61222	0.67334

OH_CF3_TS_toluene

C	-3.07846	1.54571	1.18991
C	-0.61765	0.69923	0.00305
C	-0.96215	2.08045	0.14702
C	-2.17344	2.47817	0.75920
C	-0.08122	3.08587	-0.34230
H	-0.39592	4.12366	-0.27261
C	1.11319	2.76342	-0.90438
C	1.56275	1.41900	-0.84132
C	0.75693	0.39838	-0.33709
H	-3.99612	1.83609	1.68959
H	-2.36388	3.54139	0.88067
H	1.78790	3.50811	-1.31201
O	2.83478	1.25068	-1.25026
H	3.12291	0.34331	-1.02064

C	1.40646	-0.90767	0.02927	F	-1.27146	-1.61284	-1.55051
O	0.89224	-1.99924	-0.08929	F	-3.36894	-1.36857	-1.19755
N	2.73056	-0.81274	0.48995	C	3.88851	1.22011	-0.80655
C	3.11173	0.18903	1.49030	H	3.93834	1.22619	0.28673
H	3.01854	-0.23618	2.49759	H	4.66809	0.56787	-1.20316
H	4.15062	0.49256	1.33335	H	4.04061	2.22972	-1.20235
H	2.47500	1.07068	1.43094				
C	3.38451	-2.09796	0.71184				
H	3.22897	-2.74579	-0.15048				
H	4.45416	-1.91980	0.84744				
H	2.98822	-2.60318	1.60141				
C	-2.85359	0.20140	0.85167				
H	-3.65084	-0.51555	1.01389				
C	-1.69529	-0.22706	0.23105				
C	-1.82521	-1.60494	-0.39756				
F	-1.51678	-2.62318	0.41258				
F	-1.14446	-1.71033	-1.54013				
F	-3.12108	-1.81714	-0.73870				

OMe_CF3_TS_toluene

C	-3.17682	1.81468	1.07778
C	-0.76050	0.72252	0.04203
C	-0.91197	2.12348	0.27943
C	-2.11419	2.64012	0.81965
C	0.14757	3.01327	-0.05105
H	-0.00892	4.07752	0.10418
C	1.31152	2.56055	-0.60248
C	1.52420	1.16304	-0.69343
C	0.56956	0.25276	-0.25419
H	-4.09560	2.20092	1.50550
H	-2.17509	3.70713	1.01751
H	2.07919	3.25099	-0.93361
O	2.65371	0.66421	-1.23972
C	1.04938	-1.07387	0.23965
O	0.35315	-2.05026	0.38141
N	2.40482	-1.05057	0.75897
C	2.34272	-1.14810	2.21716
H	1.92006	-2.10364	2.56338
H	3.35561	-1.04301	2.61783
H	1.73166	-0.33070	2.61389
C	3.19326	-2.13893	0.18999
H	3.22395	-2.03128	-0.89799
H	4.21576	-2.06514	0.57382
H	2.79184	-3.13261	0.43977
C	-3.10289	0.47211	0.66559
H	-3.99931	-0.13904	0.70229
C	-1.95099	-0.06894	0.13057
C	-2.16210	-1.39238	-0.58042
F	-2.21054	-2.45582	0.22845

Chapter 5: Quasi-Classical Dynamics of competing pathways in non-Heme enzymes

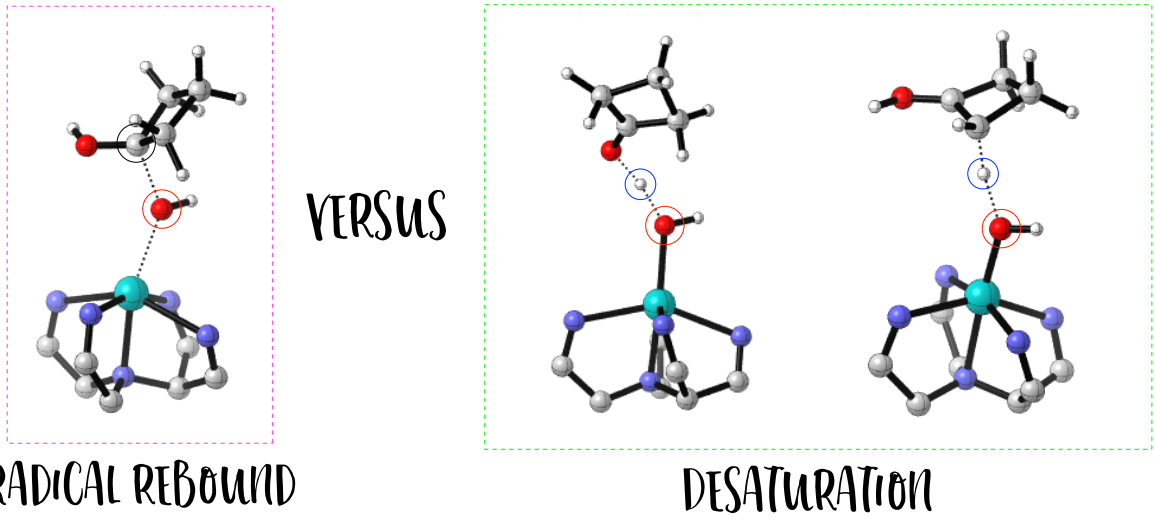

Chapter Overview

Non-heme metal-oxo catalysts are able to hydroxylate organic compounds via the radical rebound (RR) pathway, but the desaturation non-rebound mechanism can be competitive as well. This Chapter explored one such case using quasi-classical dynamics (QCD), as described in Chapters 2 and 3, with the addition of hybrid quantum mechanics/molecular mechanics (QM:MM), which traced both RR and desaturation pathways with unprecedented clarity. These differences in the two pathways are compared for the first time in literature using a combination of dynamics simulations and density functional theory (DFT) calculations. Most importantly, selectivity of these two pathways was observed at different timescales, and RR was found to be almost entirely selective at short timescales. This would lead to better catalytic design that enables controlled selectivity.

5.1 Introduction

5.1.1 Overview of non-heme hydroxylation reactions

Heme and mono-nuclear non-heme catalysts comprise of a large family of enzymes that utilize high-valent iron-sites to initiate a range of regioselective bond formations which are otherwise difficult to construct. Some examples of high-valence iron-oxo species in enzymatic reactions include the hydroxylation reactions of alkanes and olefin epoxidation activated by reactive species of cytochrome P450 enzymes.[1,2] The Jumonji C domain (JMJD) enzymes are able to demethylate mono-, di-, and trimethylated lysine residues located on the tail of histone proteins.[3–8] Non-heme examples like TauD-*J* are also intensely studied upon to mimic such biochemistry.[9]

In the rate determining step of the general mechanism (**Scheme 5.1**),[8,10] non-heme iron(IV/V)–oxo complexes abstract H radical (H•) from the bound substrate in a hydrogen atom transfer (HAT) process to generate a substrate radical R• (usually carbon-centered and either Fe^{IV}–OH or Fe^{III}–OH). This process is followed by either (1) a radical rebound (RR) event, resulting in the formation of an alcohol product and a reduced iron(II)-species, (2) a desaturation mechanism to form the respective C–H oxidation products, or (3) diffusion of the two radicals away from each other.

Scheme 5.1. Different pathways in metal-oxo hydrogen atom transfer (HAT)

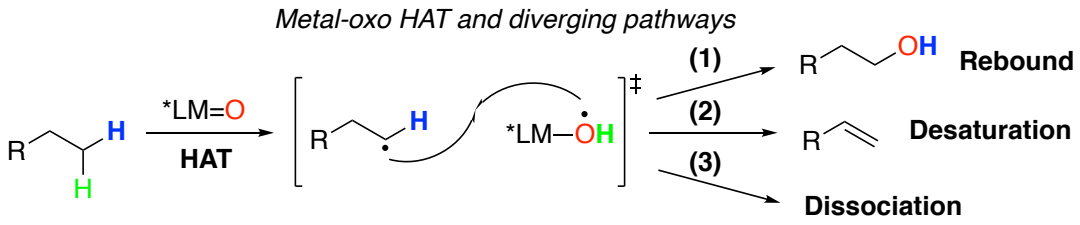

Desaturation is a key mechanism in drug metabolism by P450 chemistry, and altering the catalytic binding pocket can modify the degree of desaturase activity[11,12] which will

also provide for a wide versatility of product patterns. Valproic acid and ethylcarbamate are some important drug molecules that undergo desaturation. The RR pathway is outlined by the loss of hydroxyl radical from the non-heme complex, giving rise to an alcohol product R-OH and a reduced iron(II)-species formed *in situ*. The desaturation mechanism occurs when a second hydrogen atom is abstracted from R• to form water and a 2-electron oxidation product. These two mechanisms have been well studied previously using kinetic isotope experiments[13,14]. However, the differences in selectivity between these paths remain an open question, and continue to be fundamentally important as a matter of biological and chemical interest, as more understanding could lead to designing better catalytic control.

Due to the presence of the radical intermediate, there has been some doubt cast on whether the rebound paradigm is the exclusive pathway occurring in the reaction mechanism.[15,16] As the active site of non-heme substrate system is not as well caged as enzymes, other pathways like dissociation can become prominent. Indeed, there are increasing evidence that different reactivity patterns are observed.[17]

As the enzymes have short-lived intermediates, in order to study reactivity and to make computational modelling tractable, it is not uncommon for chemists to truncate large biological enzymes into chemical structures that resemble active catalytic sites.[17–19] In fact, computational studies have proved invaluable in the understanding of Fe=O mechanisms. In a recent article by Shaik,[20] he purported that MD simulations revealed the chemistry of weak interactions in P540 enzymes, of which many functions are rooted in. Previously, Fang and Cisneros have performed a comprehensive QM/MM study of DNA demethylase AlkB to provide an in-depth discussion of an alternative

OH rebound step coupled with a proton transfer to the OH- ligand that results in a novel zwitterion intermediate.[21] Cossío and co-workers have proposed distinct methylation state dependent mechanisms, following QM calculations of JMJD demethylation, suggesting mono- and dimethylated lysine may proceed via sequential N–H/C–H abstraction to yield an iminium intermediate.[22,23]

5.1.2 Model of interest

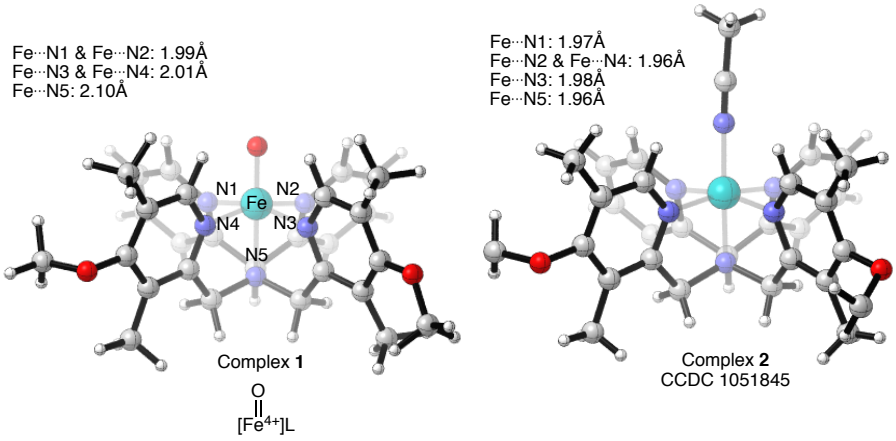

Figure 5.1. ONIOM(uB3LYP/6-31+G(d)/LANL2DZ//GENECP:UFF) optimized geometry of **1** and X-ray structure **2**.

We initiated our study by modeling the cyclam-ligated non-heme iron complex $[(N4Py)^{OMe,Me}Fe^{II}(CH_3CN)]^{2+}$ (Complex **1** in **Figure 5.1**), derived from the X-ray structure complex **2** from Maiti et al[18].

Spin states	ONIOM(uB3LYP/6-31G(d), LANL2DZ:UFF)					
	E/au	**ZPE/au**	**H/au**	**T.qh-S/au**	**qh-G(T)/au**	**ΔG**
Singlet	-746.173	0.619	-977.918	0.102	-978.019	30.9
Triplet	-746.206	0.617	-977.896	0.102	-977.998	***0.0***
Quintet	-746.221	0.619	-977.949	0.105	-978.054	7.4

Table 5.1. Comparison of energies of ONIOM-optimized Complex **1** structures with different spin states

Experimentally, Complex **1** shows paramagnetic character (likely in the S=1 spin state). Computational studies of ONIOM-optimized structures also showed that the

triplet complex is of the lowest energy compared against singlet and quintet complexes (**Table 5.1**).[24]

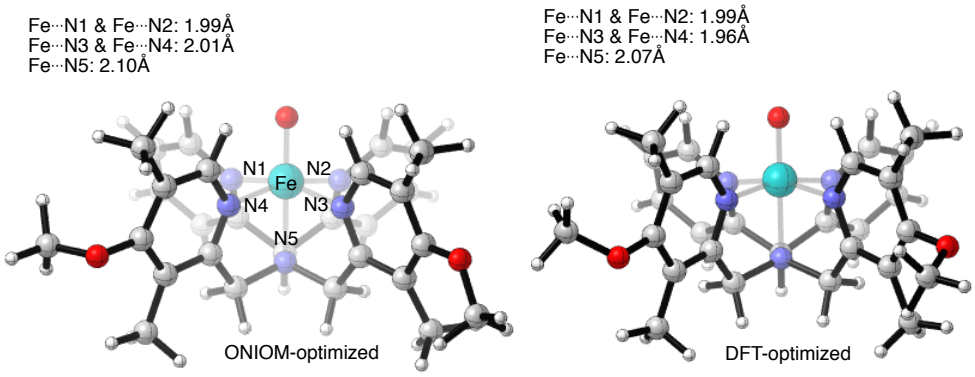

Figure 5.2. Comparison between ONIOM(uB3LYP/6-31+G(D), LanL2DZ:UFF) optimized structure versus uB3LYP-D3/6-31+G(D), LanL2DZ DFT-optimized structure

The DFT-optimized structure is also compared against Complex **1** in **Figure 5.2** to show the similarities of both structures. Previous mechanistic studies revealed that more reactive reaction intermediates could be produced by shortening the Fe–(N4Py) distance, a direct result given by the greater HOMO contribution of the two picolyl moieties.[18] The mechanistic choice between the two eventual pathways after C–H abstraction was suggested to be dependent on the stability of the radical formed from the substrate.[25,26] More stable radicals prefer desaturation while less stable ones underwent RR. In the specific case of R=cyclobutanol, the 2-electron oxidation product cyclobutanone was formed exclusively.

5.1.3 Introducing dynamics into the picture again

We have also employed QCD[27,28] calculations to explore the PES of such reactions with diverging pathways. QCD calculations have become a powerful tool in understanding selectivity for cases that cannot be accurately predicted with transition state theory

(TST),[29] and for small molecule activation around a metal center.[30] In the present study, the PES involving the recombination of two radicals to form several products is especially challenging due to its flatness, highlighting the challenge for statistical rate theories. Studies by Tantillo's group[31–34] and Houk et. al[35,36] revealed that these dynamic studies provided insight into details like bond formation times in bifurcating and ambimodal reactions which aide in influencing product distribution.

The importance of post transition state bifurcations[31] (PTSBs) in C(sp^3)–H insertion by a rhodium-carbene has been demonstrated by Tantillo[32]. From a single TS, DFT quasi-classical dynamics trajectories have produced two distinct products without any intervening intermediates.[37] Analysis of the intrinsic reaction coordinate (IRC) alone fails to describe for the formation of both products. Efficiency in this catalytic C–H functionalization is explained only by considering non-statistical dynamic effects. As the product determining steps involve small activation barriers (or in some cases, barrierless) from an intermediate carrying an excess of internal energy, the assumption of internal redistribution of energy among vibrational modes hence breaks down, such that non-statistical dynamic tendencies to move along the PES will influence the route taken by the intermediate. In this case, a quantitative failure in the estimation of product selectivity is remedied through the use of trajectory calculations.

By assuming a PES shape qualitatively similar to that shown in **Figure 5.3(a)**, in which there is only a single TS between starting materials and products, the dynamics of radical/diradicaloid recombination are able to play an important, but hitherto, hidden role in these mechanisms.

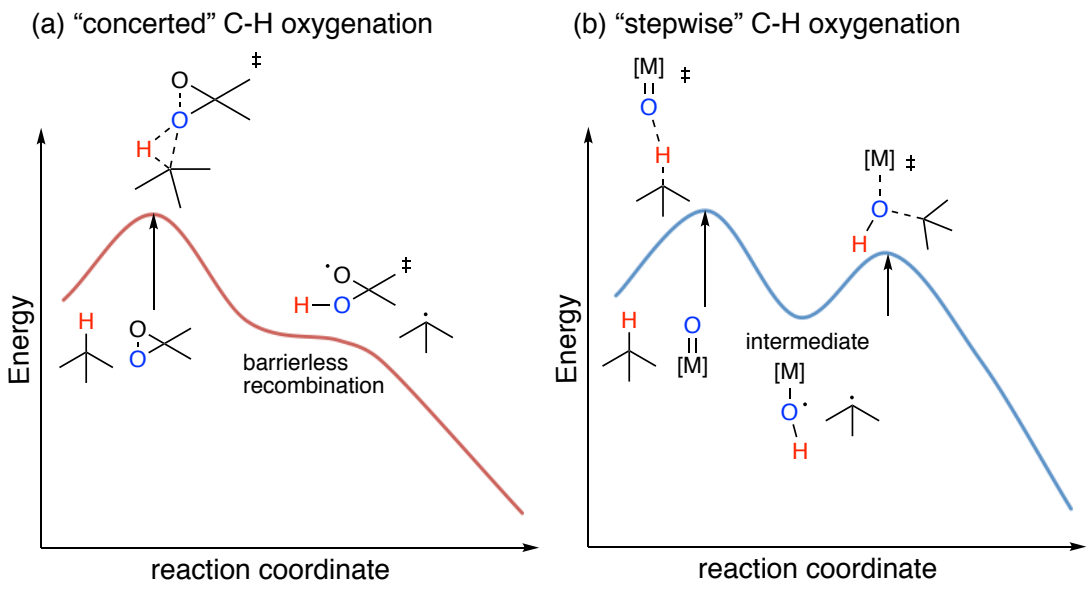

Figure 5.3. The mechanistic dichotomy classically proposed to explain C–H oxygenation in terms of distinct “concerted” and “stepwise” processes.

Carpenter’s seminal contributions to reaction dynamics have demonstrated the dynamic origins of stereoselectivity in [1,3]-shifts proceeding via singlet diradical intermediates.[38] The potential for dynamic effects to play a role in the chemistry of radical-cations has previously been suggested, due to their relatively flat PES.[39] Dynamic effects have also been reported in cyclizations for which diradicaloid products are formed from neutral precursors.[40]

At the other end of the mechanistic spectrum of C(sp^3)–H oxyfunctionalizations lie metal-oxo species, since oxygen insertion is typically viewed to occur in a fully stepwise fashion via a radical pair,[41] as summarized by the PES in **Figure 5.3(b)**. Prior to this research, we are aware of only two examples, one which is focused on reaction dynamics, where Car-Parinello (CP) MD simulations have been used to study propane hydroxylation by iron-porphyrin complex,[2] and the second focused on the PES of FeO^+ and hydrogen, where different reaction spin states energies contribute to previously

unexpected pathways.[42] Recent work has identified the existence of barrierless oxygen rebound steps in the case of iridium-oxo[43] and iron-oxo catalysts,[23] such that these oxygen-insertions occur in a single step. Correspondingly to the chemistry of organic oxidants such as dioxiranes, we anticipate that dynamic effects must also play a key role in metal-oxo C(sp^3)–H insertions, given the presence of a flat PES around the radical pair, from which barrierless exit can occur. It is particularly important to understand if non-statistical effects play a role in forming the desaturated product, since despite biological precedent, this transformation has proven challenging to control synthetically.[12]

5.2 Methodology

5.2.1 QM/MM

Geometry optimizations were performed using hybrid QM/MM optimizations, by adopting our own N-layered integrated molecular orbital and molecular mechanics (ONIOM) implementation.[44] Optimized TSs, which are required to perform QCD calculations, were obtained at the ONIOM(uB3LYP/6-31+G(d)/LANL2DZ //GENECP:UFF) level of theory. The QM layer was used to describe the active site region at the DFT level of theory. The remaining atoms were described using the Universal Force Field (UFF).[45] Previous computational studies have demonstrated that the use of UFF to describe the MM region led to greater accuracy than the use of uncorrected DFT (e.g. B3LYP) calculations when studying systems with a rigid catalyst backbone.[46–49] The area highlighted in green in **Figure 5.4** is obtained from QM calculations while the rest of the system is modeled in the MM region. The highlighted area captures the key reaction site while the area outside this cavity can be well described by forcefield parameters (i.e. ether groups and hydrocarbons).

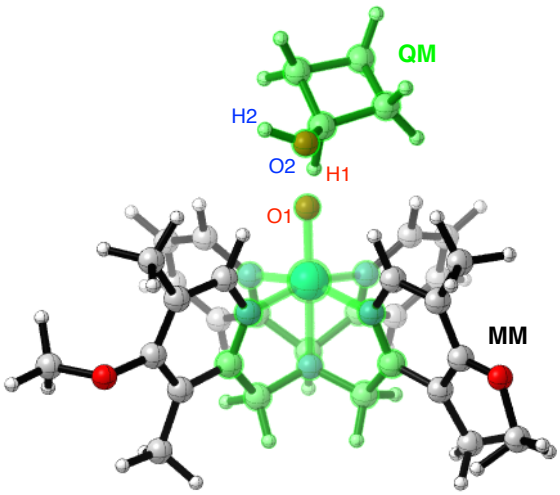

Figure 5.4. QM region highlighted in green and the rest of the structure is in the MM region.

5.2.2 DFT and QCD

DFT calculations are carried out separately with *Gaussian09*[50] using Becke's unrestricted three-parameter exchange functional in combination with the Lee, Yang and Parr correlation functional (uB3LYP) and Pople's 6-31+G(d),[51,52,53] and LANL2DZ mixed basis set on the metal Fe. Structures were optimized with default optimization criteria, ultrafine grid and acc2e=14 for the numerical integration used in DFT calculations. Additionally, high-precision frequencies for vibrational modes were calculated for the simulations. All transition states were verified with intrinsic reaction coordinate (IRC) calculations. Energies in the report are zero-point corrected electronic energies, unless otherwise stated. All molecular images were produced using *Cylview*.[54]

The frequencies taken from the transition state optimizations were processed by Progdyn, an external script by Singleton,[27] at 298.15K, to give a randomized set of 50 starting structures with initial velocities, where the displacements represent that of a Boltzmann distribution. These structures were then calculated using the Born-Oppenheimer molecular dynamics[55,56] (BOMD) model in Gaussian09 to give 100 forward and reverse trajectories. These trajectories were set to run at a stepsize of about 1.5 fs for 5000 steps (step lengths of 0.7 amu½ · Bohr), with force constants updated every 97 steps, alongside the ReadStop option to stop the run as soon as a C-C bond formation criterion is reached (bond lengths <1.6A). All preparation and analysis was automated through Python and Bash scripts.

5.3 Results

5.3.1 DFT calculations

We investigated the hydrogen atom abstraction and radical recombination steps for cyclobutanol reacting with complex **1**. Generally in the mechanism, the reactants first form a reactant cluster ***CPX***, which is followed by a transition state ***TS1*** (the highest activation barrier in the entire energy profile) for C–H abstraction that gives an intermediate ***INT***. [57] Following C–H abstraction, the PES is extremely flat in the region of the intermediate radical pair.

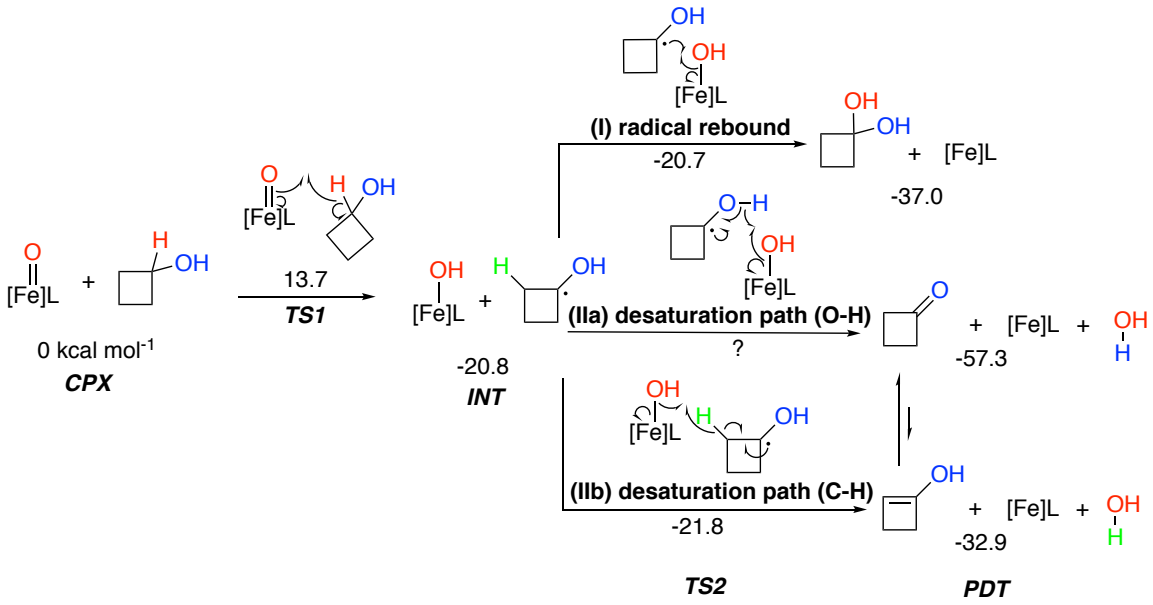

Figure 5.5. Competitive reaction pathways for RR and desaturation. Zero-point energy inclusive electronic energies (kcal/mol) were obtained at the ONIOM(uB3LYP/6-31+G(d)/LANL2DZ //GENECP:UFF) level of theory, full structures are shown in **Figure 5.6**

The subsequent recombination or desaturation steps are barrierless (0.1 kcal/mol). In addition to pathway **I**, we considered the possibility of desaturation in two distinct ways; **IIa** has the hydrogen abstracted from oxygen – H colored in blue, while **IIb** has the hydrogen abstracted from one of the neighboring carbons – H colored in green. In

fact, for **IIa** no saddle point on the PES could be found, although evolution to product along this pathway is possible (**Figure 5.7**).

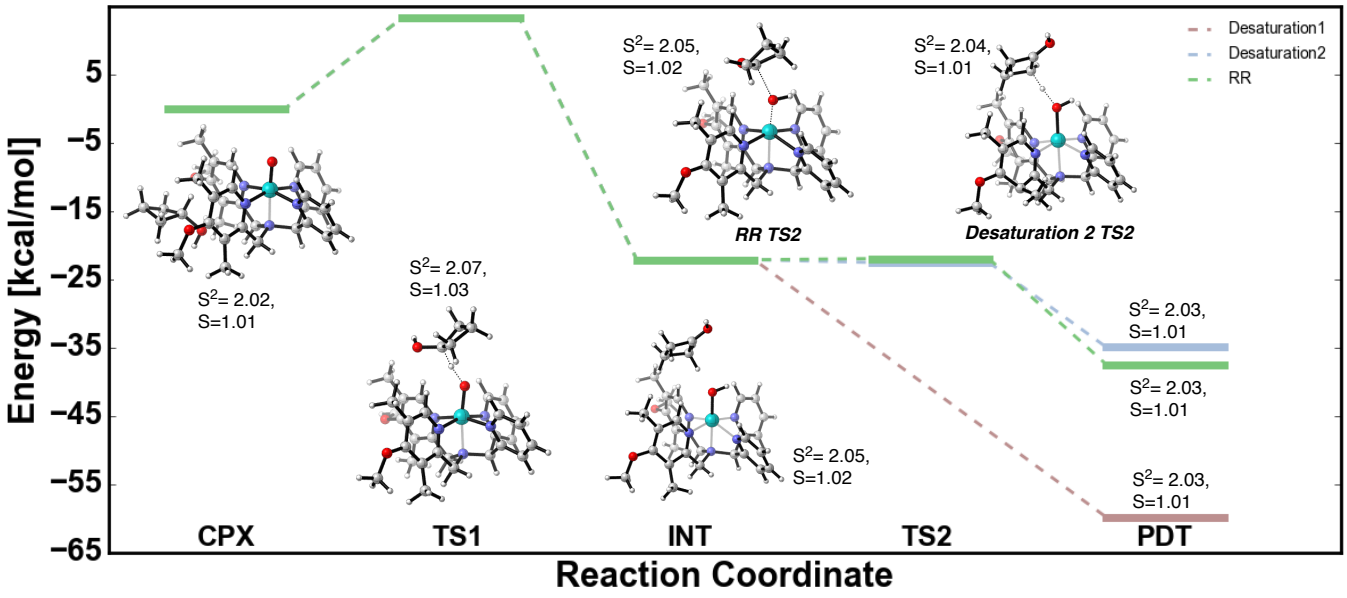

Figure 5.6. Gibbs Free energy values and full structures at the ONIOM(uB3LYP/6-31+G(d)/LANL2DZ//GENECP:UFF) level of theory for **Figure 5.5**

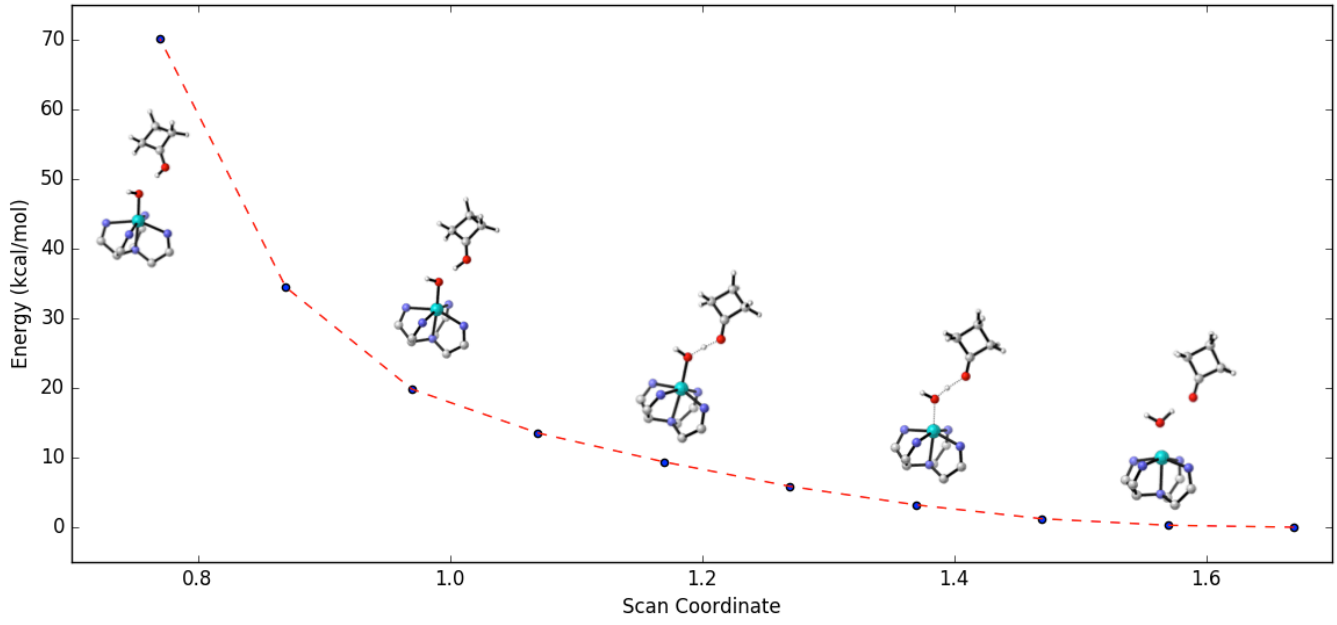

Figure 5.7. PES Scan of **(IIa)** pathway at ONIOM(uB3LYP/6-31+G(d)/LANL2DZ//GENECP:UFF) level of theory (only QM region shown).

For **I**, ***TS2*** is actually 0.1 kcal/mol lower in energy than ***INT***. For **IIb**, ***TS2*** is actually only 1.1 kcal/mol higher in energy than that of the RR pathway, which suggests that the two paths are very energetically similar. This raises the possibility of non-TST behavior.

5.3.2 QCD simulations

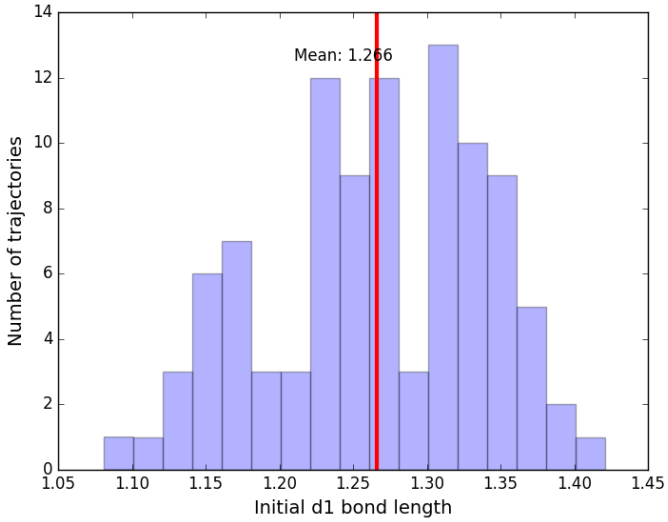

Figure 5.8. Boltzmann distribution of the 100 trajectories

To address nonstatistical dynamic effects QCD[25] trajectories were propagated from ***TS1***, 100 initial coordinates and momenta were generated using Singleton's *Progdyn*[27] to represent a Boltzmann distribution in **Figure 5.8** and simulated using Born-Oppenheimer Molecular Dynamics (BOMD). These trajectories were propagated in forward and reverse directions in steps of 1.5 fs, until the reactants are either separated by >5 Å or until cyclobutanediol (C–O forming bond <1.5 Å for **I**) or water is formed (O–H forming bond <1.1 Å for **IIa** and **IIb**). Of the 100 trajectories, 28 achieved hydrogen abstraction but none of them passed beyond this stage to form products; 6 trajectories recrossed for both forward and reverse directions; 29 continued on to form RR and 34 gave water and cyclobutanone via **IIa** while 3 formed via **IIb** (numbers are tabulated in **Figure 5.9**).

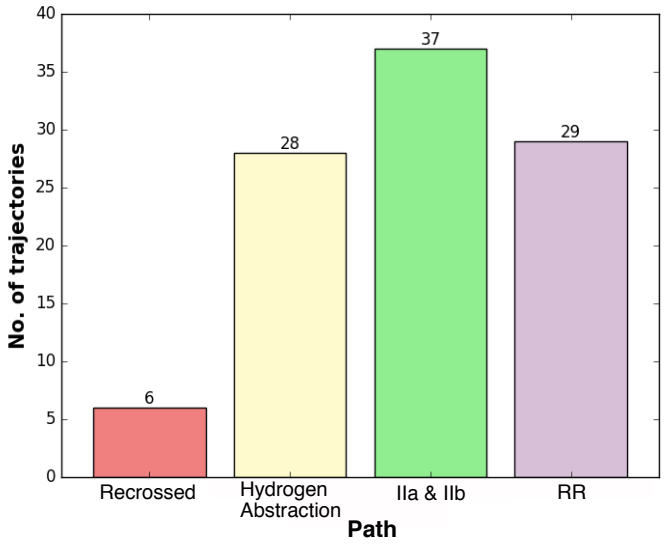

Figure 5.9. Tabulated statistics of various pathways for the 100 trajectories

The relatively small amount of recrossing shows that the transition structure provides a good estimate for the position of the dividing surface in phase space (i.e. the transition state). A competition between the RR and desaturation pathways is evident from the distribution of trajectories after the TS.

The average formation times for both RR and **IIa** are analysed in **Figure 5.10**. The cut-off bond distance of C1–O1 for RR pathway is set at 1.45 Å, as the standard C–O bond length is 1.43 Å. The cut-off of O1–H2 and O1–H3 for **IIa** is 1 Å as the standard O–H bond length is 0.97 Å. These trajectories are shown in **Figure 5.10** and the images of the two pathways are pictured clearly with only the QM region being shown. For the 29 trajectories of RR, the formation time is split twoways. At the shorter timescale (<200 fs) for 10 trajectories, the radical rebound is 100% selective, with an average formation time of 146 fs. At the longer timescale however, other pathways become more competitive.[48] For the 34 trajectories of **IIa**, the trajectories are represented as a continuum along the longer timescale (>200 fs), and this average is 446 fs. At the short timescale, with the **TS1** structure being in the right configuration

for this C–O bond formation, the RR pathway can occur quickly, hence the reaction path could be more coupled. This can be observed by looking at an example path from each timescale.

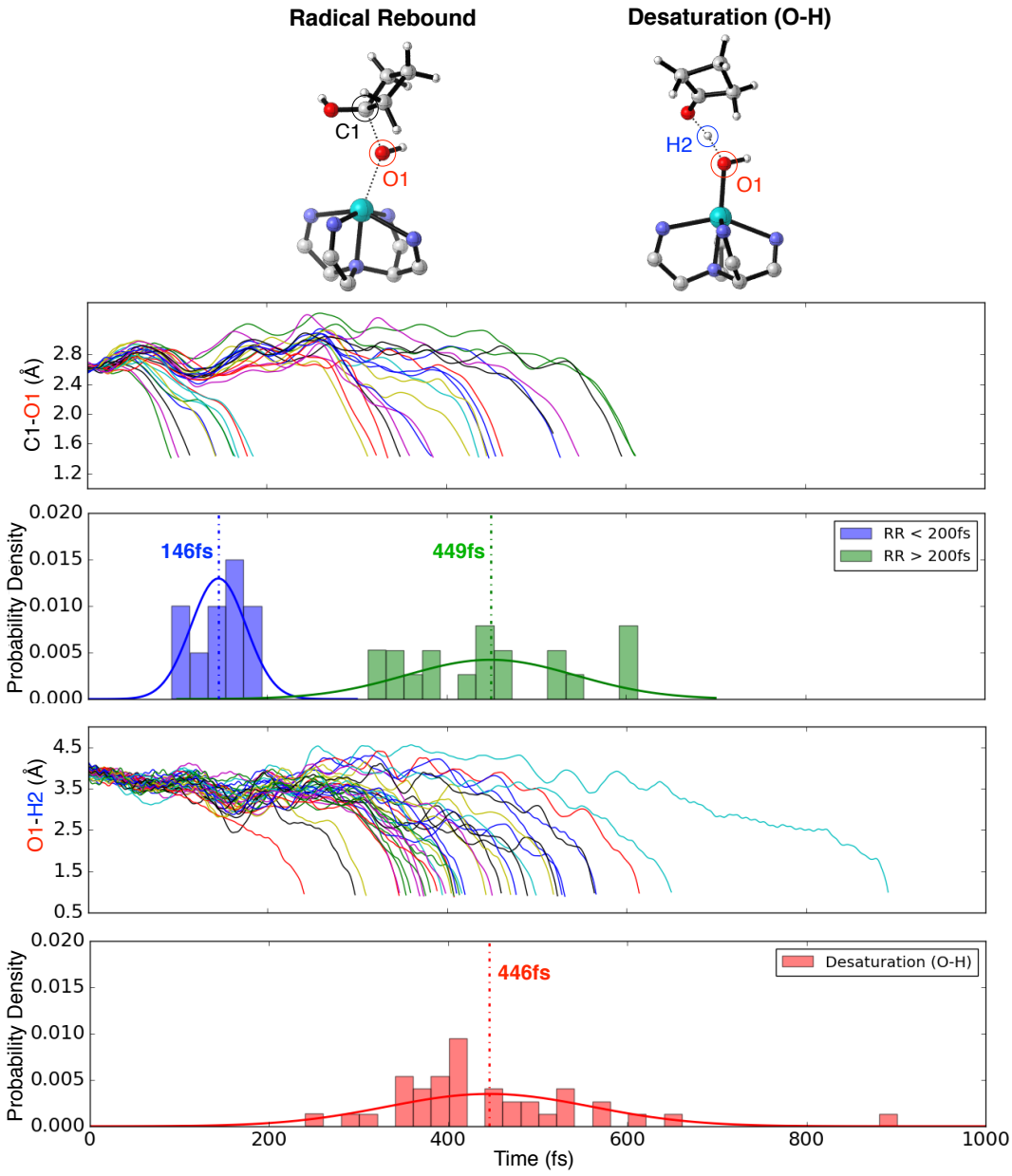

Figure 5.10. Average formation times for RR (top) and **IIa** (bottom)

Examples of each path (OH rebound and the 2 desaturation paths) are described in detail in **Figures 5.11**, **5.12** and **5.13** respectively (only the QM region is shown). In **Figure 5.11**, a comparison of the two RR paths from different timescales is examined.

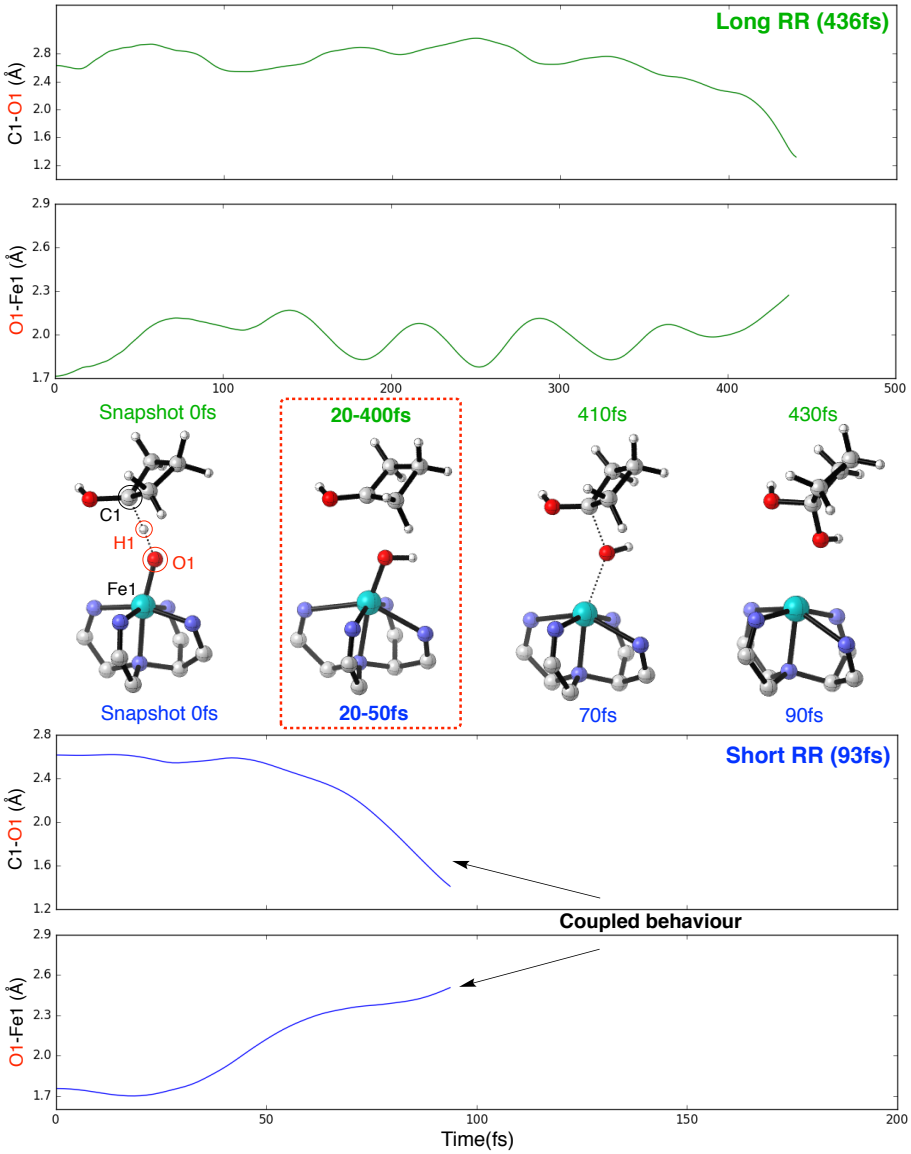

Figure 5.11. Comparison of RR pathways of 2 model trajectories from long and short timescales

Two bond distances are drawn (C1–O1 and O1–Fe1) to outline the RR mechanism. At the start (0 fs), both trajectories start moving from TS1 and began to form the first O–H bond. Around 20 fs, the intermediary structure circled in red exists for only a short time in the short RR path while it exists as an intermediate[29] for the long RR path (~400 fs). For the short path, the C1–O1 bond distance decreases simultaneously as the O1–Fe1 distance increases, revealing a coupled behaviour between these two bond

lengths as the RR product is formed very quickly. This correlation is not observed for the long RR path.

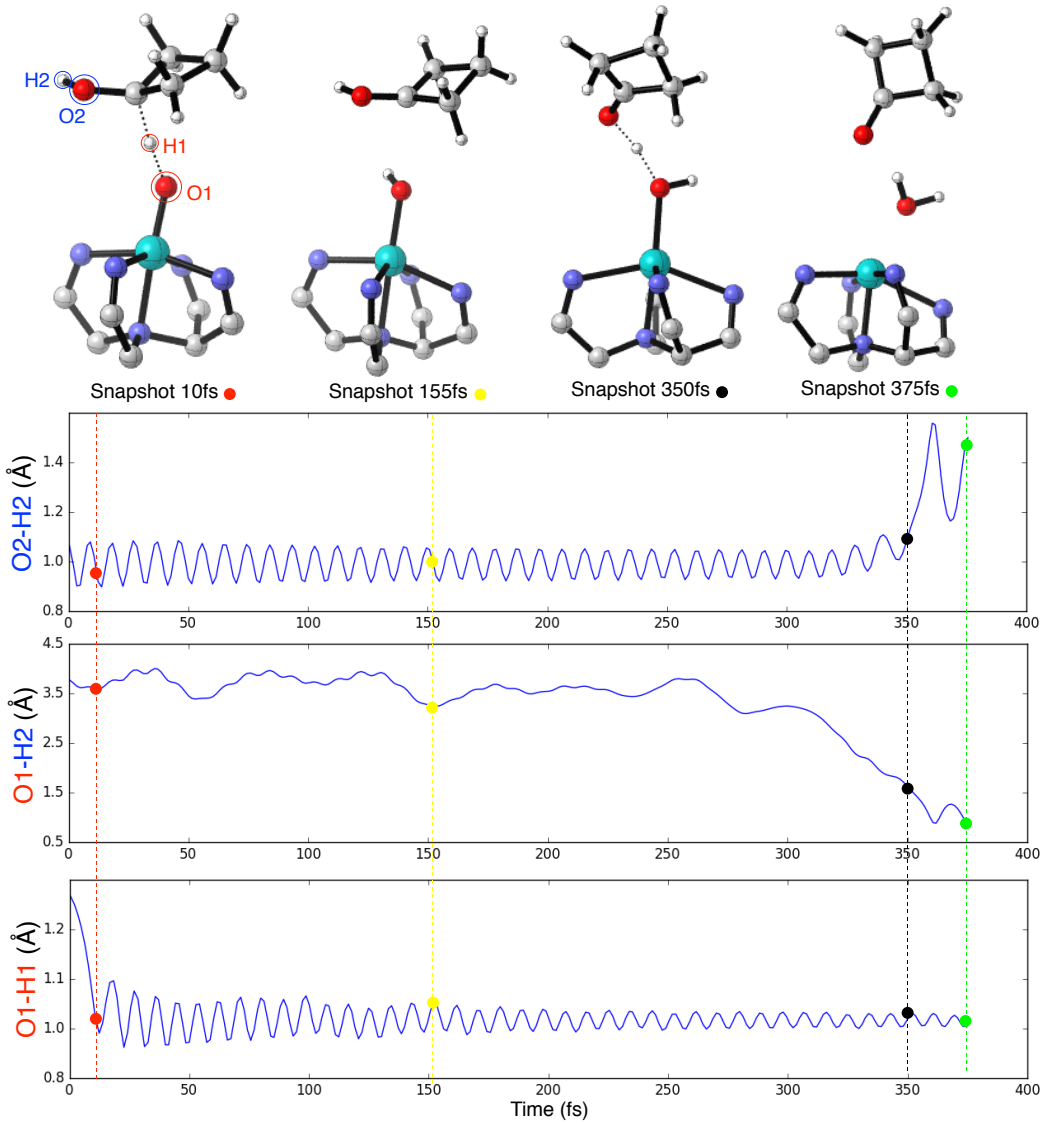

Figure 5.12. Model trajectory of **IIa**

In **Figure 5.12**, three bond distances are similarly drawn (O2–H2, O1–H2, O1–H1) to demonstrate **IIa**. Likewise at 10 fs, the trajectory moves from TS1 and forms the first O–H bond. At 200 fs, the O1–H2 bond distance is slowly decreasing as the hydrogen (H2) on the cycloalkane is approaching the oxygen (O1) on the non-heme catalyst for the second hydrogen atom abstraction. This is seen occurring at 350 fs where the O2–H2 bond distance is increasing simultaneously since the same hydrogen is now leaving

the oxygen (O2) on the cycloalkane. Nearing the end of the trajectory at 440 fs, cyclobutanone is formed and a water molecule is released.

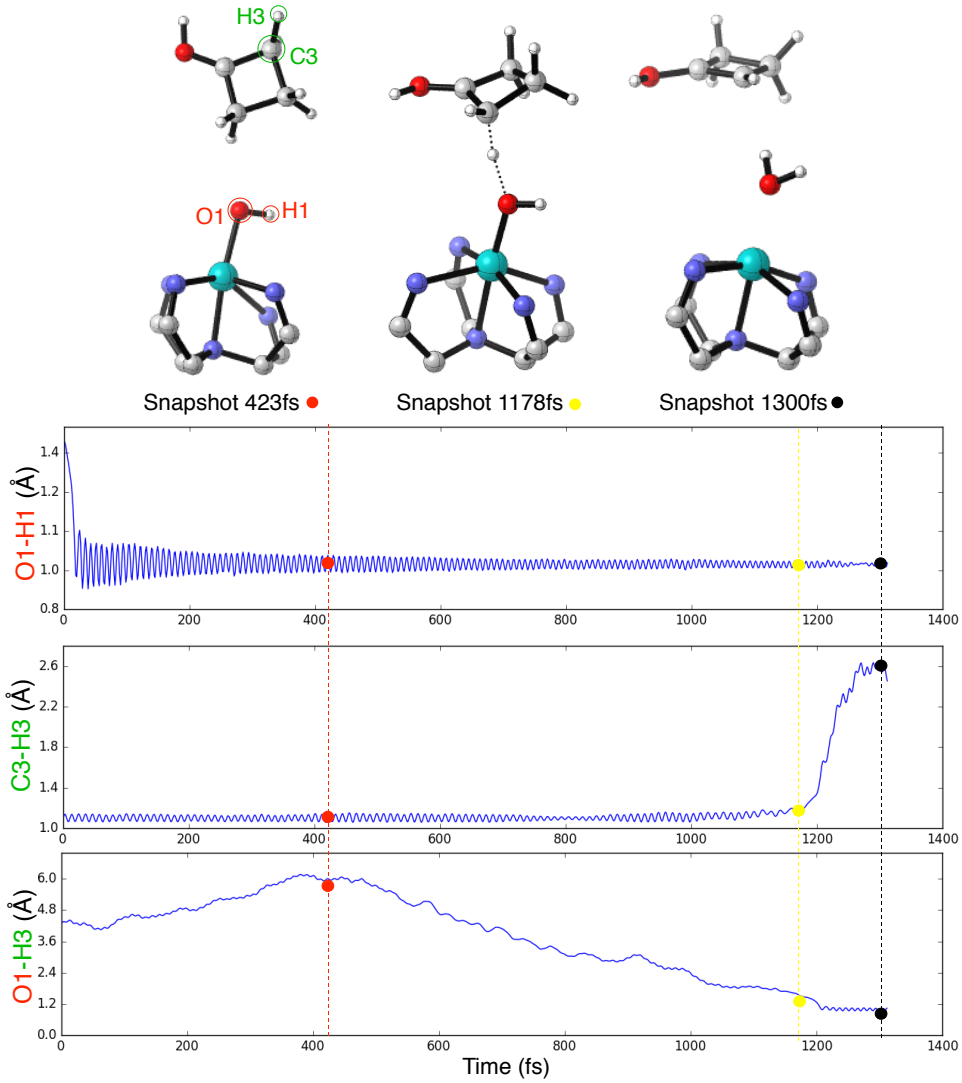

Figure 5.13. Model trajectory of **IIb**

For **Figure 5.13**, three bond distances (C3–H3, O1–H3, O1–H1) are chosen to show **IIb**. Similarly, a second hydrogen atom is leaving from the cycloalkane to the oxygen on the catalyst, but this time it is taken from C3 instead of O2. Water is subsequently formed but with cyclobutene-1-ol, which could tautomerise to cyclobutanone.

O–H bond cleavage generally requires more energy than C–H bond cleavage,[59,60] and the carbon radical tends to be more stabilised than the oxygen radical. However, less

trajectories are seen for this C–H bond cleavage, which suggests that the formation of the more stable ketone is favored compared to the enol form. This is evident in **Figure 5.5** where the energies of the products from **IIa** are almost 30 kcal/mol lower than that of **IIb**. Furthermore, C=O bond formation is more energetically stable than C=C bond formation, and less strain and repulsion occurring within the ring for ketone as the C–C bonds are spaced further apart as compared to the C=C bond in the enol.

The RR and desaturation pathways are entirely explored using a combination of DFT and QCD methods, providing a convincing look of the power of computation for metal-oxo complexes, enabling us to predict selectivity based on the different timescales observed.

5.4 Conclusion

The role of diradicaloid and diradical-pair intermediates is explored computationally, providing new insights into their role upon stereospecificity and product selectivity in the reaction class of iron-oxo catalysis. Despite the RR pathway occurring faster, fewer trajectories are observed for this pathway. Perhaps this could be alluded to the fact that the products from the desaturation pathways are more thermodynamically stable, with C=O formation and lesser ring strain. The important observation of the RR pathway being strongly selective at short timescales could lead to new catalytic design which enables controlled selectivity based on different timescales. The QCD results are very accurate in describing the mechanistic details for this reaction, and the research to fine tune the selectivity between these different pathways is the subject of ongoing investigation. The role of non-statistical dynamic effects upon the reactivity and selectivity of transient intermediates is rapidly gaining recognition, however, these effects are only beginning to be explored in the context of the activation of $C(sp^3)$–H bonds, which are of paramount importance. The novel insights gained from our work provided mechanistic knowledge, from which we, and others, will explore further aspects of dynamic effects upon the fate of diradicaloid and diradical-pair intermediates.

References

1. Rittle, J. & Green, M. T. Cytochrome P450 compound I: Capture, characterization, and C-H bond activation kinetics. *Science* **330**, 933–937 (2010).

2. Elenewski, J. E. & Hackett, J. C. Ab initio dynamics of the cytochrome P450 hydroxylation reaction. *J. Chem. Phys.* **142**, 064307 (2015).

3. Chang, B., Chen, Y., Zhao, Y. & Bruick, R. K. JMJD6 Is a Histone Arginine Demethylase. *Science* **318**, 444–447 (2007).

4. Mantri, M. *et al.* The 2-Oxoglutarate-Dependent Oxygenase JMJD6 Catalyses Oxidation of Lysine Residues to give 5S-Hydroxylysine Residues. *ChemBioChem* **12**, 531–534 (2011).

5. Han, G. *et al.* The hydroxylation activity of JMJD6 is required for its homo-oligomerization. *J. Cell. Biochem.* **113**, 1663–1670 (2012).

6. Webby, C. J. *et al.* JMJD6 Catalyses Lysyl-Hydroxylation of U2AF65, a Protein Associated with RNA Splicing. *Science* **325**, 90–93 (2009).

7. Walport, L. J. *et al.* Arginine demethylation is catalysed by a subset of JmjC histone lysine demethylases. *Nat. Commun.* **7**, 11974 (2016).

8. Milan, M., Bietti, M. & Costas, M. Enantioselective aliphatic C–H bond oxidation catalyzed by bioinspired complexes. *Chem. Commun.* **54**, 9559–9570 (2018).

9. Biswas, A. N. *et al.* Modeling TauD- J: A high-spin nonheme oxoiron(IV) complex with high reactivity toward C-H bonds. *J. Am. Chem. Soc.* **137**, 2428–2431 (2015).

10. Lai, W., Li, C., Chen, H. & Shaik, S. Hydrogen-Abstraction Reactivity Patterns from A to Y: The Valence Bond Way. *Angew. Chemie Int. Ed.* **51**, 5556–5578 (2012).

11. Ji, L. *et al.* Drug Metabolism by Cytochrome P450 Enzymes: What Distinguishes the Pathways Leading to Substrate Hydroxylation Over Desaturation? *Chem. - A Eur. J.* **21**, 9083–9092 (2015).

12. Bigi, M. A., Reed, S. A. & White, M. C. Diverting non-haem iron catalysed aliphatic C-H hydroxylations towards desaturations. *Nat. Chem.* **3**, 216–222 (2011).

13. Groves, J. T., McClusky, G. A., White, R. E. & Coon, M. J. Aliphatic hydroxylation by highly purified liver microsomal cytochrome P-450. Evidence for a carbon radical intermediate. *Biochem. Biophys. Res. Commun.* **81**, 154–160 (1978).

14. Auclair, K., Hu, Z., Little, D. M., Ortiz de Montellano, P. R. & Groves, J. T. Revisiting the Mechanism of P450 Enzymes with the Radical Clocks Norcarane and Spiro[2,5]octane. *J. Am. Chem. Soc.* **124**, 6020–6027 (2002).

15. Cho, K.-B., Hirao, H., Shaik, S. & Nam, W. To rebound or dissociate? This is the mechanistic question in C–H hydroxylation by heme and nonheme metal–oxo complexes. *Chem. Soc. Rev.* **45**, 1197–1210 (2016).

16. Solomon, E. I., Decker, A. & Lehnert, N. Non-heme iron enzymes: contrasts to heme catalysis. *Proc. Natl. Acad. Sci. U. S. A.* **100**, 3589–3594 (2003).

17. Zaragoza, J. P. T. *et al.* Direct observation of oxygen rebound with an iron-

hydroxide complex. *J. Am. Chem. Soc.* **139**, 13640–13643 (2017).

18. Rana, S., Dey, A. & Maiti, D. Mechanistic elucidation of C–H oxidation by electron rich non-heme iron(IV)–oxo at room temperature. *Chem. Commun.* **51**, 14469–14472 (2015).

19. Alberro, N., Torrent-Sucarrat, M., Arrieta, A., Rubiales, G. & Cossío, F. P. Density Functional Theory Study on the Demethylation Reaction between Methylamine, Dimethylamine, Trimethylamine, and Tamoxifen Catalyzed by a Fe(IV)–Oxo Porphyrin Complex. *J. Phys. Chem. A* **122**, 1658–1671 (2018).

20. Dubey, K. D. & Shaik, S. Cytochrome P450 - The Wonderful Nanomachine Revealed through Dynamic Simulations of the Catalytic Cycle. *Acc. Chem. Res.* **52**, 389–399 (2019).

21. Fang, D. & Cisneros, G. A. Alternative pathway for the reaction catalyzed by DNA dealkylase AlkB from Ab initio QM/MM calculations. *J. Chem. Theory Comput.* **10**, 5136–5148 (2014).

22. Alberro, N., Torrent-Sucarrat, M., Arrastia, I., Arrieta, A. & Cossío, F. P. Two-State Reactivity of Histone Demethylases Containing Jumonji-C Active Sites: Different Mechanisms for Different Methylation Degrees. *Chem. - A Eur. J.* **23**, 137–148 (2017).

23. Alberro, N., Torrent-Sucarrat, M., Arrieta, A., Rubiales, G. & Cossío, F. P. Density Functional Theory Study on the Demethylation Reaction between Methylamine, Dimethylamine, Trimethylamine, and Tamoxifen Catalyzed by a Fe(IV)-Oxo Porphyrin Complex. *J. Phys. Chem. A* **122**, 1658–1671 (2018).

24. Verma, P. *et al.* Assessment of electronic structure methods for the determination of the ground spin states of Fe(II), Fe(III) and Fe(IV) complexes. *Phys. Chem. Chem. Phys.* **19**, 13049–13069 (2017).

25. Kumar, S. *et al.* Long-Range Electron Transfer Triggers Mechanistic Differences between Iron(IV)-Oxo and Iron(IV)-Imido Oxidants. *J. Am. Chem. Soc.* **136**, 17102–17115 (2014).

26. Na, Y. O. *et al.* Mechanistic insight into alcohol oxidation by high-valent iron-oxo complexes of heme and nonheme ligands. *Angew. Chemie - Int. Ed.* **44**, 4235–4239 (2005).

27. Ussing, B. R., Hang, C. & Singleton, D. A. Dynamic effects on the periselectivity, rate, isotope effects, and mechanism of cycloadditions of ketenes with cyclopentadiene. *J. Am. Chem. Soc.* **128**, 7594–7607 (2006).

28. Paranjothy, M., Sun, R., Zhuang, Y. & Hase, W. L. Direct chemical dynamics simulations: Coupling of classical and quasiclassical trajectories with electronic structure theory. *Wiley Interdiscip. Rev. Comput. Mol. Sci.* **3**, 296–316 (2013).

29. Tan, J. S. J., Hirvonen, V. & Paton, R. S. Dynamic Intermediates in the Radical Cation Diels-Alder Cycloaddition: Lifetime and Suprafacial Stereoselectivity. *Org. Lett.* **20**, 2821–2825 (2018).

30. Carlsen, R., Wohlgemuth, N., Carlson, L. & Ess, D. H. Dynamical Mechanism May Avoid High-Oxidation State Ir(V)–H Intermediate and Coordination Complex in Alkane and Arene C–H Activation by Cationic Ir(III) Phosphine. *J. Am. Chem. Soc.* **140**, 11039–11045 (2018).

31. Hare, S. R. & Tantillo, D. J. Post-transition state bifurcations gain momentum – current state of the field. *Pure Appl. Chem.* **89**, 679–698 (2017).

32. Hare, S. R. & Tantillo, D. J. Cryptic post-transition state bifurcations that reduce the efficiency of lactone-forming Rh-carbenoid C–H insertions. *Chem. Sci.* **8**, 1442–1449 (2017).

33. Hare, S. R., Pemberton, R. P. & Tantillo, D. J. Navigating Past a Fork in the Road: Carbocation-π Interactions Can Manipulate Dynamic Behavior of Reactions Facing Post-Transition-State Bifurcations. *J. Am. Chem. Soc.* **139**, 7485–7493 (2017).

34. Hong, Y. J. & Tantillo, D. J. Biosynthetic consequences of multiple sequential post-transition-state bifurcations. *Nat. Chem.* **6**, 104–111 (2014).

35. Yang, Z., Yu, P. & Houk, K. N. Molecular Dynamics of Dimethyldioxirane C-H Oxidation. *J. Am. Chem. Soc.* **138**, 4237–4242 (2016).

36. Yu, P. *et al.* Mechanisms and Origins of Periselectivity of the Ambimodal [6 + 4] Cycloadditions of Tropone to Dimethylfulvene. *J. Am. Chem. Soc.* **139**, 8251–8258 (2017).

37. Fructos, M. R. *et al.* Mechanistic studies on gold-catalyzed direct arene C-H bond functionalization by carbene insertion: The coinage-metal effect. *Organometallics* **36**, 172–179 (2017).

38. Carpenter, B. K. Dynamic Matching: The Cause of Inversion of Configuration in the [1,3] Sigmatropic Migration? *J. Am. Chem. Soc.* **117**, 6336–6344 (1995).

39. Haberl, U., Wiest, O. & Steckhan, E. Ab initio studies of the radical cation

Diels-Alder reaction. *J. Am. Chem. Soc.* **121**, 6730–6736 (1999).

40. Mohamed, R. K., Peterson, P. W. & Alabugin, I. V. Concerted Reactions That Produce Diradicals and Zwitterions: Electronic, Steric, Conformational, and Kinetic Control of Cycloaromatization Processes. *Chem. Rev.* **113**, 7089–7129 (2013).

41. Saint-Denis, T. G., Zhu, R.-Y., Chen, G., Wu, Q.-F. & Yu, J.-Q. Enantioselective C(sp 3)–H bond activation by chiral transition metal catalysts. *Science* **359**, 759 (2018).

42. Essafi, S., Tew, D. P. & Harvey, J. N. The Dynamics of the Reaction of FeO + and H 2 : A Model for Inorganic Oxidation. *Angew. Chemie Int. Ed.* **56**, 5790–5794 (2017).

43. Zhou, M., Balcells, D., Parent, A. R., Crabtree, R. H. & Eisenstein, O. Cp* Iridium Precatalysts for Selective C–H Oxidation via Direct Oxygen Insertion: A Joint Experimental/Computational Study. *ACS Catal.* **2**, 208–218 (2012).

44. Vreven, T. *et al.* Combining Quantum Mechanics Methods with Molecular Mechanics Methods in ONIOM. *J. Chem. Theory Comput.* **2**, 815–826 (2006).

45. Rappe, A. K., Casewit, C. J., Colwell, K. S., Goddard, W. A. & Skiff, W. M. UFF, a full periodic table force field for molecular mechanics and molecular dynamics simulations. *J. Am. Chem. Soc.* **114**, 10024–10035 (1992).

46. Simón, L. & Goodman, J. M. Theoretical study of the mechanism of Hantzsch ester hydrogenation of imines catalyzed by chiral BINOL-phosphoric acids. *J. Am. Chem. Soc.* **130**, 8741–8747 (2008).

47. Peng, Q., Duarte, F. & Paton, R. S. Computing organic stereoselectivity – from concepts to quantitative calculations and predictions. *Chem. Soc. Rev.* **45**, 6093–6107 (2016).

48. Shaik, S., Kumar, D. & de Visser, S. P. A Valence Bond Modeling of Trends in Hydrogen Abstraction Barriers and Transition States of Hydroxylation Reactions Catalyzed by Cytochrome P450 Enzymes. *J. Am. Chem. Soc.* **130**, 10128–10140 (2008).

49. Cortopassi, W. A., Simion, R., Honsby, C. E., França, T. C. C. & Paton, R. S. Dioxygen Binding in the Active Site of Histone Demethylase JMJD2A and the Role of the Protein Environment. *Chem. - A Eur. J.* **21**, 18983–18992 (2015).

50. Vinet, L. & Zhedanov, A. A 'missing' family of classical orthogonal polynomials. *Gaussian 09 Revis. C.01* Gaussian Inc., Wallingford CT (2010).

51. Hehre, W. J., Ditchfield, R. & Pople, J. A. Self-Consistent Molecular Orbital Methods. 12. Further extensions of Gaussian-type basis sets for use in molecular-orbital studies of organic-molecules. *J. Chem. Phys.* **56**, 2257–2261 (1972).

52. Becke, A. D. Density-functional exchange-energy approximation with correct asymptotic behavior. *Phys. Rev. A* **38**, 3098–3100 (1988).

53. Lee, C., Yang, W. & Parr, R. G. Development of the Colle-Salvetti correlation-energy formula into a functional of the electron density. *Phys. Rev. B* **37**, 785–789 (1988).

54. Legault, C. Y. CYLview User Manual. *Comput. Programs Biomed.* **18**, 99–108

(2010).

55. Helgaker, T., Uggerud, E. & Jensen, H. J. A. Integration of the classical equations of motion on ab initio molecular potential energy surfaces using gradients and Hessians: application to translational energy release upon fragmentation. *Chem. Phys. Lett.* **173**, 145–150 (1990).

56. Uggerud, E. & Helgaker, T. Dynamics of the reaction CH2OH+ -> CHO+ + H2. Translational energy release from ab initio trajectory calculations. *J. Am. Chem. Soc.* **114**, 4265–4268 (1992).

57. Hirao, H., Kumar, D., Que, L. & Shaik, S. Two-state reactivity in alkane hydroxylation by non-heme iron-oxo comolexes. *J. Am. Chem. Soc.* **128**, 8590–8606 (2006).

58. Oyola, Y. & Singleton, D. A. Dynamics and the failure of transition state theory in alkene hydroboration. *J. Am. Chem. Soc.* **131**, 3130–3131 (2009).

59. Sun, X., Sun, X., Geng, C., Zhao, H. & Li, J. Benchmark study on methanol C-H and O-H bond activation by bare [Fe(IV)O]2+. *J. Phys. Chem. A* **118**, 7146–7158 (2014).

60. Deng, L. & Ziegler, T. Density Functional Study of C−H and O−H Bond Activation by Transition Metal d0−Oxo Complexes: 1. Thermodynamic Considerations. *Organometallics* **15**, 3011–3021 (1996).

Appendix

I. Absolute energies and Cartesian coordinates of transition structures

Fig. 5.5	ONIOM(uB3LYP/6-31+G(D),LANL2DZ:UFF)					
	E/au	ZPE/au	H/au	T.qh-S/au	qh-G(T)/au	imag. v
CPX	-978.69279	0.736685	-977.91756	0.101562	-978.01912	-
TS1	-978.66261	0.728291	-977.89567	0.102268	-977.99794	-689.02
INT	-978.71984	0.73062	-977.94927	0.105091	-978.05436	-
TS2 (RR)	-978.7206	0.731529	-977.94954	0.104559	-978.05409	-141.1
PRD (RR)	-978.75079	0.735702	-977.97613	0.10265	-978.07878	-
PRD (HAT 1)	-978.77954	0.732075	-978.00684	0.107589	-978.11443	-
TS2 (HAT 2)	-978.71856	0.727772	-977.95154	0.103356	-978.0549	-566.89
PRD (HAT 2)	-978.74045	0.731889	-977.96796	0.106765	-978.07472	-

Table S1. Energies of ONIOM-optimized structures for **Figure 5.5**

freq=hpmodes oniom(ub3lyp/genecp:uff) opt(QuadMac,TS,CalcFC) geom=connectivity iop(2/9=1000,3/33=0,3/36=1,3/160=2,4/33=0,5/33=0,6/7=2,6/9=2,6/10=2,6/12=2,7/8=10,215=3)

TS1

Fe	-0.05040	0.75626	0.14956	C	-2.56378	2.32136	0.91135
N	1.16578	2.31557	-0.20713	H	-2.56521	1.78667	1.85168
N	-1.37535	-0.71060	-0.11016	C	1.81211	-0.57675	-1.56201
N	-1.55500	2.09165	-0.00812	C	2.91958	-1.44135	-1.97964
N	1.42842	-0.51584	-0.33288	C	3.48618	-2.31682	-0.99333
C	0.86877	2.92448	-1.30091	C	3.05358	-2.17161	0.33868
C	1.63142	4.05400	-1.77612	C	2.02959	-1.27460	0.64441
H	1.37024	4.55605	-2.69856	H	1.67573	-1.19382	1.65719
C	2.71536	4.48248	-1.01136	C	-0.34682	2.35407	-2.03816
H	3.31233	5.32562	-1.33369	H	-0.45090	2.73251	-3.06103
C	3.02196	3.81331	0.17556	C	-1.40914	0.07622	-2.38122
H	3.85955	4.13132	0.78261	H	-2.22246	0.75363	-2.67042
C	2.23428	2.72560	0.57056	H	-1.17593	-0.49848	-3.28426
H	2.46609	2.19689	1.48539	C	1.05978	0.31466	-2.54598
C	-1.90592	-0.84293	-1.27866	H	1.71466	1.14295	-2.84077
C	-2.96138	-1.81643	-1.52147	H	0.83218	-0.23136	-3.46884
C	-3.40475	-2.59743	-0.43613	N	-0.20312	0.85268	-1.95100
C	-2.77373	-2.45920	0.81041	O	0.02996	0.92300	1.86327
C	-1.76522	-1.49908	0.95401	H	0.32193	0.16958	2.97341
H	-1.28006	-1.36714	1.90858	C	3.65237	-3.01019	1.43836
C	-1.53264	2.71105	-1.13551	H	3.47716	-4.08622	1.22747
C	-2.55063	3.66649	-1.50179	H	4.74524	-2.82295	1.49743
H	-2.51818	4.18000	-2.45387	H	3.20712	-2.77364	2.42865
C	-3.57900	3.91072	-0.59311	C	3.50903	-1.25652	-3.36248
H	-4.36172	4.61921	-0.83093	H	3.27786	-2.12032	-4.01525
C	-3.58804	3.23240	0.62749	H	3.12140	-0.36357	-3.88606
H	-4.37838	3.40831	1.34555	H	4.60016	-1.07764	-3.28402
				C	-3.16193	-3.32925	1.97337

H	-4.22039	-3.14512	2.24877
H	-3.03630	-4.39777	1.69910
H	-2.53242	-3.12353	2.86530
C	-3.54564	-1.98292	-2.90143
H	-4.31210	-2.78256	-2.94615
H	-4.01588	-1.03105	-3.22520
H	-2.74284	-2.25724	-3.61665
O	-4.42610	-3.54293	-0.59915
O	4.38392	-3.29180	-1.19752
C	-5.73066	-2.98596	-0.43627
H	-6.48386	-3.78749	-0.57901
H	-5.85605	-2.56586	0.58430
H	-5.92000	-2.19014	-1.18829
C	4.69156	-3.79867	-2.49425
H	5.35552	-3.11325	-3.05377
H	5.26980	-4.73622	-2.36468
H	3.76725	-4.07168	-3.04541
C	0.07991	0.60377	5.16584
C	0.62317	-0.33776	4.07543
C	2.07918	0.08615	4.35187
C	1.50220	1.24003	5.22473
H	-0.74890	1.26272	4.89191
H	-0.18856	0.05247	6.07549
H	2.70160	0.36945	3.49802
H	2.59742	-0.68927	4.92600
H	1.54751	2.21407	4.73186
H	1.93104	1.32266	6.22597
O	0.33330	-1.68125	4.03338
H	-0.52948	-1.86695	4.44555

TS2 (RR)

Fe	0.04795	0.71598	0.33323
N	1.34749	2.46529	-0.44228
N	-1.59028	-0.73579	0.10757
N	-1.31578	2.13517	0.60249
N	1.28413	-0.59589	-0.54951
C	0.68534	3.07713	-1.35550
C	1.20589	4.24229	-2.03367
H	0.63423	4.74519	-2.80288
C	2.46890	4.70312	-1.66857
H	2.89529	5.57251	-2.15182
C	3.17730	4.03021	-0.67198
H	4.15986	4.37150	-0.37314
C	2.60190	2.90807	-0.06366
H	3.14294	2.37801	0.70887
C	-2.30674	-0.66663	-0.95495
C	-3.49483	-1.49158	-1.12695
C	-3.85259	-2.35766	-0.07487
C	-3.02296	-2.44069	1.05551
C	-1.89778	-1.60966	1.12938
H	-1.25096	-1.64355	1.99576
C	-1.56849	2.80919	-0.47619
C	-2.62987	3.78683	-0.53046
H	-2.83140	4.34190	-1.43748
C	-3.39551	3.99514	0.61384
H	-4.20074	4.71818	0.60891
C	-3.11600	3.25890	1.76486
H	-3.70245	3.40425	2.66275
C	-2.07005	2.32976	1.74641
H	-1.85262	1.75228	2.63471
C	1.39667	-0.57193	-1.83605
C	2.32411	-1.46071	-2.54205
C	3.00517	-2.45878	-1.76884
C	2.87196	-2.40790	-0.36839
C	2.01271	-1.47625	0.21622
H	1.88461	-1.46484	1.28722
C	-0.68906	2.48913	-1.68753
H	-1.09762	2.90831	-2.61558
C	-1.88253	0.33451	-2.02136
H	-2.66912	1.09394	-2.11709
H	-1.83812	-0.15752	-2.99986
C	0.52673	0.44093	-2.58155
H	1.16990	1.25588	-2.92945
H	0.10218	-0.01614	-3.48379
N	-0.57256	0.98691	-1.73397
O	0.73286	0.62648	2.15806
H	0.68488	1.52885	2.51296
C	3.61176	-3.38373	0.50988
H	3.31104	-4.42163	0.25421
H	4.70533	-3.27144	0.35381
H	3.39680	-3.21698	1.58675
C	2.64436	-1.18019	-3.99560
H	2.20347	-1.94996	-4.65834
H	2.25500	-0.20717	-4.34727
H	3.74191	-1.10000	-4.12898
C	-3.32508	-3.40775	2.16594
H	-4.29925	-3.15707	2.63320
H	-3.36936	-4.44046	1.76057
H	-2.54504	-3.37788	2.95634
C	-4.30066	-1.42192	-2.39937
H	-5.15009	-2.13422	-2.40460
H	-4.70502	-0.39656	-2.52993
H	-3.65471	-1.67457	-3.26549
O	-4.99035	-3.17055	-0.16619
O	3.75257	-3.46970	-2.23520
C	-6.17987	-2.51344	0.27174
H	-7.03458	-3.21308	0.17116
H	-6.09601	-2.21472	1.33830

H	-6.38876	-1.61480	-0.34754
C	3.72391	-3.88049	-3.60062
H	4.31896	-3.20425	-4.24289
H	4.21884	-4.87073	-3.66859
H	2.68073	-4.02374	-3.95309
C	2.25841	0.59690	4.82817
C	1.99882	-0.61930	4.00289
C	3.39870	-1.10569	3.96868
C	3.57026	-0.17836	5.23388
H	2.50125	1.47446	4.22502
H	1.50981	0.84797	5.58474
H	3.95891	-0.70244	3.11853
H	3.54243	-2.18614	4.04161
H	4.47756	0.42585	5.24637
H	3.45622	-0.73024	6.16763
O	0.97549	-1.38435	3.93477
H	0.14635	-0.86598	4.02739

TS2 (HAT 2)

Fe	-0.00122	0.64628	0.64170
N	1.15645	2.45950	0.89824
N	-1.44368	-0.55803	-0.39935
N	-1.51188	1.76327	1.26386
N	1.44706	-0.07595	-0.53860
C	0.64599	3.45203	0.26752
C	1.25279	4.76182	0.29143
H	0.81373	5.59227	-0.24591
C	2.42561	4.92581	1.02902
H	2.91283	5.89114	1.07266
C	2.96520	3.83123	1.71089
H	3.87447	3.93938	2.28769
C	2.31561	2.59283	1.63814
H	2.72189	1.73536	2.15771
C	-2.03507	-0.08461	-1.43790
C	-3.07883	-0.83501	-2.12404
C	-3.43270	-2.09722	-1.60747
C	-2.73263	-2.60448	-0.50111
C	-1.75073	-1.80723	0.09839
H	-1.22171	-2.16276	0.97102
C	-1.68252	2.85166	0.58612
C	-2.79065	3.73848	0.85001
H	-2.92523	4.64827	0.27953
C	-3.68461	3.39473	1.86267
H	-4.52624	4.03626	2.08915
C	-3.48770	2.21168	2.57721
H	-4.17804	1.92360	3.35930
C	-2.39591	1.39540	2.26170
H	-2.25154	0.46299	2.79030
C	1.68337	0.50043	-1.67101
C	2.75439	0.03208	-2.55593
C	3.44570	-1.16936	-2.18887
C	3.19762	-1.70130	-0.90725
C	2.20541	-1.13919	-0.10509
H	2.00679	-1.56594	0.86631
C	-0.63770	3.12862	-0.50453
H	-0.93833	3.94599	-1.17121
C	-1.62651	1.30814	-1.90958
H	-2.47670	1.98533	-1.75458
H	-1.45737	1.30496	-2.99291
C	0.80915	1.70436	-2.04451
H	1.41899	2.60908	-1.94024
H	0.53525	1.65104	-3.10579
N	-0.41995	1.82351	-1.22002
O	0.41231	-0.34134	2.34736
H	0.26355	0.20066	3.13977
C	3.93443	-2.90449	-0.37374
H	4.71384	-3.27959	-1.06767
H	4.43197	-2.63874	0.58288
H	3.21322	-3.72764	-0.18426
C	3.20058	0.91580	-3.70224
H	2.86398	0.50745	-4.67534
H	2.80228	1.94503	-3.63675
H	4.30115	1.04610	-3.66976
C	-3.02272	-3.97863	0.03511
H	-4.06711	-4.02967	0.40478
H	-2.88248	-4.73095	-0.76927
H	-2.34523	-4.23968	0.87623
C	-3.74036	-0.27673	-3.35873
H	-4.49187	-0.96850	-3.78940
H	-4.24854	0.67840	-3.11087
H	-2.97636	-0.09377	-4.14231
O	-4.43245	-2.86944	-2.21395
O	4.29882	-1.86451	-2.95370
C	-5.74102	-2.56330	-1.73170
H	-6.47647	-3.20847	-2.25420
H	-5.81606	-2.75979	-0.64108
H	-6.00104	-1.50202	-1.93367
C	4.37055	-1.69022	-4.36809
H	4.97360	-0.80283	-4.63899
H	4.91066	-2.56139	-4.79176
H	3.35813	-1.69241	-4.82494
C	2.15375	-3.93098	3.29005
C	1.49620	-2.97511	4.24292
C	0.33054	-2.75900	3.47246
C	0.78812	-3.90603	2.51988
H	3.02276	-3.52711	2.75720
H	2.43586	-4.89164	3.73825
H	0.45764	-1.62539	2.89843

H	-0.66094	-2.66247	3.92227
H	0.84936	-3.66014	1.45753
H	0.22653	-4.83422	2.64562
O	1.81625	-2.51811	5.41518
H	2.69710	-2.81381	5.72139

II. Sample input BOMD calculation

oniom(ub3lyp/genecp:uff) BOMD=(readstop, maxpoints=5000,recalcfc=99,rtemp=300,stepsize=7000,readmwvelocity, update=97) geom=connectivity scf(yqc) int=(ultrafine,acc2e=14)

Cartesian coordinates from Progdyn

0 1 2 3 2 3

Fe-Fe6+2	0	-0.0860182	0.6971922	0.1715743	H			
N-N_R	0	1.1005207	2.3451298	0.0418187	H			
N-N_R	0	-1.2918028	-0.7979188	-0.3264327	H			
N-N_R	0	-1.6439009	1.9623756	0.0504761	H			
N-N_R	0	1.4739982	-0.4765856	-0.3441450	H			
C-C_R	0	0.8564638	3.0733162	-0.9329974	H			
C-C_R	0	1.5595925	4.3758889	-1.2113133	L	H-H_	6	0.0000
H-H_	0	1.3470097	4.9235706	-2.0902142	L			
C-C_R	0	2.5822616	4.7596582	-0.3422271	L			
H-H_	0	3.2855764	5.6555661	-0.5444536	L			
C-C_R	0	2.7929692	3.9413946	0.8600507	L			
H-H_	0	3.5673712	4.0876768	1.5109595	L			
C-C_R	0	2.0530009	2.7371034	0.9982394	L	H-H_	2	0.0000
H-H_	0	2.2901756	2.0294788	1.8332850	L			
C-C_R	0	-1.7664342	-0.7649267	-1.5205804	H			
C-C_R	0	-2.8386973	-1.7160610	-1.8528893	L	H-H_	15	0.0000
C-C_R	0	-3.2758221	-2.6369468	-0.9087687	L			
C-C_R	0	-2.7619332	-2.6379357	0.3394719	L			
C-C_R	0	-1.7624060	-1.6771287	0.5937610	L	H-H_	3	0.0000
H-H_	0	-1.3898460	-1.5310191	1.6483956	L			
C-C_R	0	-1.5050235	2.7423979	-0.9769253	H			
C-C_R	0	-2.5023174	3.7233941	-1.2782080	L	H-H_	21	0.0000
H-H_	0	-2.5091609	4.3039283	-2.1641254	L			
C-C_R	0	-3.5904853	3.8084419	-0.4926151	L			
H-H_	0	-4.2978055	4.6695109	-0.5448852	L			
C-C_R	0	-3.7007441	3.0395045	0.6788708	L			
H-H_	0	-4.5656016	2.9822934	1.3901500	L			
C-C_R	0	-2.7050600	2.0612758	0.8960039	L	H-H_	4	0.0000
H-H_	0	-2.7181459	1.3926366	1.6844001	L			
C-C_R	0	1.9164231	-0.4240535	-1.5120195	H			
C-C_R	0	3.0726795	-1.1980029	-1.9469862	L	H-H_	30	0.0000
C-C_R	0	3.6687414	-2.1205883	-1.0072818	L			
C-C_R	0	3.1042591	-2.0687737	0.2788911	L			
C-C_R	0	2.0401367	-1.2434257	0.6106385	L	H-H_	5	0.0000
H-H_	0	1.5354118	-1.2428475	1.6489127	L			
C-C_3	0	-0.2527287	2.5526614	-1.8710635	H			

H-H_	0	-0.3124885	2.9576248	-2.8049231	H
C-C_3	0	-1.2568193	0.2555548	-2.4443515	H
H-H_	0	-2.1922526	0.9411605	-2.7526749	H
H-H_	0	-0.9216988	-0.1490750	-3.4030212	H
C-C_3	0	1.2394691	0.5303903	-2.5357395	H
H-H_	0	1.9270272	1.3946026	-2.6623800	H
H-H_	0	1.0977198	0.2354149	-3.4912971	H
N-N_3	0	-0.0590805	1.0101376	-1.9002640	H
O-O_3	0	-0.0933389	0.7158112	1.9135911	H
H-H_	0	0.1119073	-0.1412559	2.8530196	H
C-C_3	0	3.7105246	-2.9847877	1.4132222	L
H-H_	0	3.4028499	-4.0635457	1.1731713	L
H-H_	0	4.8715889	-2.8196624	1.6089111	L
H-H_	0	3.1713936	-2.6968896	2.3065547	L
C-C_3	0	3.7010634	-0.9198196	-3.2735241	L
H-H_	0	3.4165755	-1.7186515	-4.1304291	L
H-H_	0	3.4561742	0.0896670	-3.7580125	L
H-H_	0	4.7590898	-0.7097547	-3.1462243	L
C-C_3	0	-3.1537191	-3.5747020	1.4147573	L
H-H_	0	-4.2819674	-3.4523723	1.6879393	L
H-H_	0	-2.8839675	-4.5767229	1.1896537	L
H-H_	0	-2.6194100	-3.3978852	2.4397623	L
C-C_3	0	-3.2414897	-1.7590995	-3.2637154	L
H-H_	0	-3.8454831	-2.4848654	-3.5779629	L
H-H_	0	-3.7010389	-0.8148395	-3.5716450	L
H-H_	0	-2.4002476	-1.9338364	-3.9126845	L
O-O_R	0	-4.2312458	-3.5984361	-1.3270098	L
O-O_R	0	4.6591573	-3.0537759	-1.1874182	L
C-C_3	0	-5.6393214	-3.2071819	-1.1967989	L
H-H_	0	-6.3516953	-4.1462909	-1.4221761	L
H-H_	0	-5.8712294	-2.6533112	-0.1543926	L
H-H_	0	-5.8254839	-2.4372881	-1.8640558	L
C-C_3	0	4.9185029	-3.4763481	-2.5363047	L
H-H_	0	5.7131902	-2.7901163	-2.9886379	L
H-H_	0	5.4719048	-4.4803469	-2.5322711	L
H-H_	0	4.0861899	-3.8006111	-3.1080387	L
C-C_3	0	-0.4220709	-0.0926011	5.1461002	H
C-C_3	0	0.3441854	-0.8253097	4.0011380	H
C-C_3	0	1.7281038	-0.2930049	4.5469295	H
C-C_3	0	0.9202056	0.7154491	5.3732594	H
H-H_	0	-1.3180791	0.4140211	5.1086611	H
H-H_	0	-0.5852137	-0.9095878	5.9329890	H
H-H_	0	2.4938648	0.0216141	3.8823652	H
H-H_	0	2.1815941	-1.0724976	5.0519047	H
H-H_	0	0.9971344	1.6843714	4.9735085	H

```
H-H_             0     1.1472224   0.8442254   6.5312781   H
O-O_3            0     0.1322033  -2.1678337   3.7827513   H
H-H_             0    -0.6967643  -2.4130130   4.2034585   H

1 45 1.0 3 1.0 4 1.0 2 1.0 44 1.0 5 1.0
2 6 1.5 13 1.5
3 15 1.5 19 1.5
4 21 1.5 28 1.5
5 30 1.5 34 1.5
6 7 1.5 36 1.0
7 8 1.0 9 1.5
8
9 10 1.0 11 1.5
10
11 12 1.0 13 1.5
12
13 14 1.0
14
15 16 1.5 38 1.0
16 17 1.5 59 1.0
17 18 1.5 63 1.0
18 19 1.5 55 1.0
19 20 1.0
20
21 22 1.5 36 1.0
22 23 1.0 24 1.5
23
24 25 1.0 26 1.5
25
26 27 1.0 28 1.5
27
28 29 1.0
29
30 31 1.5 41 1.0
31 32 1.5 51 1.0
32 33 1.5 64 1.5
33 34 1.5 47 1.0
34 35 1.0
35
36 37 1.0 44 1.0
37
38 39 1.0 40 1.0 44 1.0
39
40
41 42 1.0 43 1.0 44 1.0
```

42
43
44
45
46
47 48 1.0 49 1.0 50 1.0
48
49
50
51 52 1.0 53 1.0 54 1.0
52
53
54
55 56 1.0 57 1.0 58 1.0
56
57
58
59 60 1.0 61 1.0 62 1.0
60
61
62
63 65 1.0
64 69 1.0
65 66 1.0 67 1.0 68 1.0
66
67
68
69 70 1.0 71 1.0 72 1.0
70
71
72
73 74 1.0 76 1.0 77 1.0 78 1.0
74 75 1.0 83 1.0
75 76 1.0 79 1.0 80 1.0
76 81 1.0 82 1.0
77
78
79
80
81
82
83 84 1.0
84

3 #stopping conditions for reaction

1, 1, 1, 1, 1, 1, 1, 1, 1, 1, 1, 1, 1, 1, 1, 1, 1, 1, 1, 1, 1, 1, 1, 1, 1, 1, 1, 1, 1, 1, 1, 1, 1, 1, 1,
1, 1, 1, 1, 1, 1, 1, 1, 1, 1, 1, 1, 1, 1, 1, 1, 1, 1, 1, 1, 1, 1, 1, 1, 1, 1, 1, 1, 1, 1, 1, 1, 1, 1, 1,
1, 2, 2, 2, 2, 2, 2, 2, 2, 2, 2, 2, 2, 2
1, 1, 1, 1, 1, 1, 1, 1, 1, 1, 1, 1, 1, 1, 1, 1, 1, 1, 1, 1, 1, 1, 1, 1, 1, 1, 1, 1, 1, 1, 1, 1, 1, 1, 1,
1, 1, 1, 1, 1, 1, 1, 1, 1, 1, 1, 1, 1, 1, 1, 1, 1, 1, 1, 1, 1, 1, 1, 1, 1, 1, 1, 1, 1, 1, 1, 1, 1, 1, 1,
1, 1, 2, 2, 2, 2, 2, 2, 2, 2, 2, 2, 2, 2
1, 1, 1, 1, 1, 1, 1, 1, 1, 1, 1, 1, 1, 1, 1, 1, 1, 1, 1, 1, 1, 1, 1, 1, 1, 1, 1, 1, 1, 1, 1, 1, 1, 1, 1,
1, 1, 1, 1, 1, 1, 1, 1, 1, 1, 1, 1, 1, 1, 1, 1, 1, 1, 1, 1, 1, 1, 1, 1, 1, 1, 1, 1, 1, 1, 1, 1, 1, 1, 1,
1, 1, 1, 2, 2, 2, 2, 2, 2, 2, 2, 2, 2, 2
0, 0, 0, 0, 0, 0, 46, 74, 2.01
0, 0, 0, 0, 0, 1, 46, 74, 11.34
0, 0, 0, 0, 0, 1, 1, 45, 7.00

-467410608000.000000 -53840808000.000000 -2311990128000.000000
1524101292000.000000 -2422111356000.000000 -3338362944000.000000
674364852000.000000 920617488000.000000 766308060000.000000
-2710641780000.000000 442543500000.000000 -5087887560000.000000
3177703116000.000000 -4720606884000.000000 8653859424000.000977
3925854324000.000000 4168153836000.000488 -2578251816000.000000
1981769328000.000000 5817389760000.000000 -422391564000.000000
16784387676000.000000 -17815258692000.000000 17043510456000.000000
-2470977684000.000000 -168216804000.000000 -3004379532000.000000
4231133928000.000000 -15141412188000.000000 -15720161184000.000000
-4976538588000.000000 -501046560000.000000 -1647976428000.000000
24649522128000.000000 15295197708000.000000 41101789176000.000000
-8145875052000.000000 -1710554328000.000000 2497035492000.000000
32894643348000.000000 13004391456000.000000 1661931432000.000000
-7405815312000.000000 -5898754260000.000000 1527789816000.000000
5652824436000.000000 5572539504000.000000 1945984824000.000000
-1365272496000.000000 7086347856000.000000 -3759373296000.000000
2833188624000.000000 -2833315632000.000000 -480333672000.000000
-4858765128000.000000 -2826335484000.000000 -4984963452000.000000
33586873992000.000000 22323651084000.000000 2067886044000.000000
3052928340000.000000 -4390407251999.999512 122880240000.000000
-14131354608000.000000 392952168000.000000 6953550408000.000000
8239845096000.000000 40480481916000.000000 -24425898084000.000000
5153937012000.000000 1761696216000.000000 -8058578220000.000000
40749453108000.000000 -11153265732000.000000 -7306272792000.000000
4510302804000.000000 -5859524664000.000000 1615086648000.000000
11284126308000.000000 297611496000.000000 -30779388612000.000000
-89720568000.000000 -1782223884000.000000 7991750844000.000000
-20322597708000.000000 -2941716960000.000000 14509272204000.000000
6405262164000.000000 515292624000.000000 -10550750364000.000000
5482803060000.000000 6712176996000.000000 4206018095999.999512
-6978010032000.000000 -2514779568000.000000 1656930492000.000000

758825172000.000000 -736646400000.000000 8998929576000.000000
-3727912356000.000000 6396170508000.000000 5736030552000.000000
-22222007640000.000000 -5256146700000.000000 -14805481320000.000000
-5143723452000.000000 -691637940000.000000 -3240074628000.000000
32978987244000.000000 10232076708000.000000 22387567860000.000000
-1725599484000.000000 -4305597660000.000488 1952885592000.000000
-8147351520000.000000 11400777864000.000000 3880380168000.000000
15372259812000.000000 4124494836000.000000 16034632992000.000000
-3269212380000.000000 1164546936000.000000 6332671800000.000000
2798563068000.000000 -7898108904000.000000 -6737028228000.000000
5096518812000.000000 -10032753528000.000000 -46674466272000.000000
6194936916000.000000 4199254920000.000488 5603217228000.000000
1493656416000.000000 -767461716000.000000 -2307312000.000000
-14934394440000.000000 -20480320476000.000000 6680710764000.000000
-1237031460000.000000 58937004000.000000 -5001167556000.000000
6674503248000.000000 -48234108636000.000000 -33866339220000.003906
2506264740000.000000 8076285252000.000000 -18421393788000.000000
5425130844000.000000 38649190608000.000000 -15851889648000.000000
23533524000.000000 -8426160540000.000977 4801542732000.000000
14158259136000.000000 -22988823732000.000000 -21732836328000.000000
670919760000.000000 44799018516000.000000 -34750515996000.000000
-9072483084000.000000 -2700989172000.000000 -3698081352000.000000
1884126636000.000000 1044048096000.000122 -1657417356000.000000
-19081390860000.000000 -22655888136000.000000 -31075989336000.000000
-18954478116000.000000 -21359919672000.000000 11546032680000.000000
29689532964000.000000 -10198440756000.000000 29900710224000.000000
4769044560000.000000 -6162258816000.000000 1591955316000.000000
-1985875920000.000000 803240928000.000000 -9993195828000.000000
-23299998624000.000000 20997555264000.000000 9858577932000.000000
-14023043244000.000000 -1510940088000.000000 5479114536000.000000
1727224128000.000000 -1696340016000.000000 -950051592000.000000
197195796000.000000 -963138708000.000000 -700507332000.000000
2589036912000.000000 1686893796000.000000 2732592996000.000000
-7067868192000.000000 48067532352000.000000 -11560358124000.000000
-8305153668000.000000 2171868551999.999756 13207154436000.000000
-36030624336000.000000 17003481768000.000000 -27781121340000.000000
1041354468000.000000 236499480000.000000 -2155902588000.000000
-12788578404000.000000 10336450824000.000000 29081873772000.000000
-14193482688000.000000 4378378536000.000488 12456658872000.000000
-5942407968000.000000 -2179377900000.000244 -33767902728000.003906
4550162148000.000000 4229869140000.000000 -486657612000.000000
-8394689015999.999023 -6699703752000.000000 -174016836000.000000
2770621308000.000000 -2444327172000.000000 2763932220000.000000
-876476916000.000000 7299541368000.000000 3479188356000.000000
-35698302612000.000000 -1595045844000.000000 -3805376652000.000000

-14163323580000.000000 5689201644000.000000 26687910564000.000000
20254277988000.000000 169587432000.000000 -41635619676000.000000
-14655331404000.000000 -17341058448000.001953 -15574715856000.000000
10454742900000.000000 32066868708000.000000 -16256992248000.000000
8261034264000.000000 -24178158396000.000000 18334536192000.000000
-62858376000.000000 2087487612000.000244 2316932856000.000000
32470590096000.000000 6129697140000.000000 -12905907336000.000000

C H N O 0
6-31+g*
****
Fe 0
LANL2DZ
****

Fe 0
LANL2DZ

III. Usage of Progdyn script

First step: Python extractout.py. Run this command in the "out.txt" directory, which contains all the Gaussian output files.
Second step: ./sampling.sh

extractout.py:

```
import glob

lookup1 = 'Input orientation:'
lookup2 = 'Harmonic frequencies (cm**-1), IR intensities (KM/Mole), Raman scattering'

filename= ' *.out'
for out in glob.glob(filename):
        NUM_1=1
        NUM_2=1

        with open(out) as myFile:
         for num, line in enumerate(myFile, 1):
                if lookup1 in line: NUM_1=num
                if lookup2 in line: NUM_2=num

        fileout=open(out+'.txt','w')
        with open(out) as myFile:
         for num, line in enumerate(myFile, 1):
                if num >= NUM_1 and num <= NUM_2 : fileout.write(line)
                if num > NUM_2 : break
```

sampling.sh:

```
mkdir g09_NC
for i in {1..150}       #to generate 160 geoPlusVel files
do
        if (test -f ./out.txt/TS_NC.out.txt) then
         sh g09.sh ./out.txt/TS_NC.out.txt
         mv geoPlusVel ./g09_NC/geoPlusVel_1$i
        fi
done
```

g09.sh:

```
mkdir used
origdir=./
randdir=~/bin
proggramdir=~/program/
#freqfile=$1
```

```
# B1B1B1B1B1B1B1B1B1B1B1B1B1B1B1B1B1B1B1B1B1B1B1B1B1B1B1B1B1B1B1B1B1B1
        generate geoPlusVel and first input file
echo 3 > runpointnumber
$randdir/randgen > temp811
# the next 8 lines would have to be changed to use low-precision modes
awk '/A         A         A         A         A/,/Harmonic frequencies/ {print}' $freqfile >
        temp401
awk '/Frequencies --/ {print $3;print $4;print $5;print $6;print $7}' temp401 >
        tempfreqs
awk '/Reduced masses/ {print $4;print $5;print $6;print $7;print $8}' temp401 >
        tempredmass
awk '/Force constants/ {print $4;print $5;print $6;print $7;print $8}' temp401 >
        tempfrc
mv tempfreqs tempfreqs_1
mv tempfrc tempfrc_1
python revisefreq.py
awk '/0/ && ((length($1) < 2) && ($1 < 4)) {print}' temp401 > tempmodes
awk '/has atomic number/ {print}' $freqfile > tempmasses
awk '/Input orientation:/,/tional const/ {if ( $2 < 50 && $2 > 0) print}' $freqfile >
        tempstangeos
awk -f $proggramdir/proggenHP ' $freqfile > geoPlusVel

if (test -f isomernumber) then
        cp isomernumber temp533
        awk 'BEGIN {getline;i=$1+1;print i,"----trajectory isomer number----"}'
        temp533 > isomernumber
        rm temp533
else
        echo "1 ----trajectory isomer number----" > isomernumber
fi

revisefreq.py:
import sys
import os
from numpy import *
import numpy as np
datain=np.genfromtxt('tempfreqs_1')
datain1=np.genfromtxt('tempfrc_1')
fileout=open('./tempfreqs','w')
fileout1=open('./tempfrc','w')
num=len(datain)
for i in range(0,num):
        if datain[i]<100 and datain[i]>0 :
         datain1[i]=datain1[i]*(100/datain[i])*(100/datain[i])
         datain[i]=100
```

```
        fileout1.write(str(datain1[i])+'\n')
        fileout.write(str(datain[i])+'\n')
fileout.close()
fileout1.close()
```

Concluding Remarks

This thesis discusses the use of state-of-the-art computational chemistry techniques to understand and elucidate mechanistic details from a variety of radical cation DA reactions. With a combination of QM, MM, and QCD techniques, a thorough investigation of important chemical reactions could be seen over the previous 4 chapters.

In Chapter 1, the history of DA reactions was established to lay the foundation upon where this research was built on, and the principles of computational chemistry was described to aid in the study of such chemical phenomena.

In Chapter 2, the limitations of TST were illustrated, and the direct dynamics approach was shown to be promising in tackling difficult tasks where post-TS dynamics, recrossing and timescales of each step of a particular reaction of interest (in this case, Cp and ethylene) are important. Furthermore, recrossing can contribute substantially to the overall frequency of asynchronous and stepwise cycloadditions, and direct dynamics demonstrated the importance of this effect.

Further investigation of a larger system; anethole as the dienophile, using this computational technique was examined in Chapter 3. In this Chapter, the product stereoselectivity from this DA radical cation reaction was understood with the combinatorial employment of DFT and kinetics rate theory as well. As this reaction lacked a 'dynamic intermediate', QCD was limited in drawing any insight, but did reveal that rotation could exist. Coupled with kinetic theory, the reversibility of the neutral products helped to explain this product ratio.

In Chapter 4, while taking a break from QCD, DFT calculations were used to explain the first theoretical studies on how biaryl atropisomerism, and consequently, the rate of racemization, is affected by one-electron oxidation. This effect would be useful in the development of new approaches for the asymmetric synthesis of biaryls, particularly if it can be employed in the framework of dynamic kinetic resolution. This was further explored in a collaborative project where chemical modifications towards atropisomerism were performed via alkyl substitution. By substituting the hydrogen bond with an alkyl group, we effectively remove the hydrogen bond in the transition state and increase the barrier for rotation to such an extent that precludes racemization in atropisomeric amides.

Lastly in Chapter 5, QCD was used once again to investigate the competing pathways in non-heme enzymes in the radical environment. With the addition of QM:MM, a key observation that different pathways are selective at different timescales was made, which would lead to new catalytic design that enables controlled selectivity based on these different timescales.

The role of non-statistical dynamic effects upon the reactivity and selectivity of 'dynamic intermediates' is rapidly gaining recognition, and the novel insights gained from this work provided mechanistic knowledge, from which others could explore further aspects of dynamic effects upon the fate of radical cation systems and diradical-pair intermediates.